Abstract

Biophysical Studies of Cytokine Receptor Interactions

Jiejin Li
St. John's College
Submitted for the degree of Doctor of Philosophy, Trinity 2000

The IL-6 family of cytokines includes IL-6, ciliary neurotrophic factor (CNTF), leukemia inhibitory factor (LIF), oncostatin M (OSM), cardiotrophin-1, and IL-11. Functioning in a pleiotropic and redundant manner, these cytokines play an important role in the regulation of complex cellular processes such as gene activation, proliferation and differentiation, by signalling through homo- or heterodimers of gp130.

This thesis describes the characterization of the interactions between the cytokine oncostatin M (OSM) and the cytokine-binding homology region (CHR) of its receptor gp130. Three forms of OSM were expressed, the native form and two truncated forms. Both mutations were obtained by C-terminal truncation. The first, OSM185, has an 11 amino residue deletion and the second, OSM187, has a 9-residue deletion. A variety of biophysical techniques were applied to investigate the complex.

Analytical ultra-centrifugation (AUC), surface Plasma Resonance (SPR) and isothermal titration calorimetry (ITC) studies indicated that the purified proteins were stable in monomeric form and can form a 1:1 complex with affinity in the 0.1 μM range. One of the C-terminal truncated forms, the 187 residues version, showed higher stability than the native OSM (196 residues), but still demonstrated similar binding properties to the gp130-CHR.

A ^{15}N and ^{13}C double-labelled OSM187 sample was produced for NMR studies. Due to the size of these two proteins, OSM187 (21.5 kDa) and gp130-CHR (25.2 kDa), the NMR studies of the complex are challenging. Applying the TROSY technique, data were obtained from the labelled OSM187 when it is in complex with gp130-CHR. The data could be compared with the free form OSM187 and several shifted peaks were detected. The binding site mapping work has just begun. The characterized binding properties and methods established for sample preparation provide a solid starting point for later studies.

The thesis also contains an exploratory study of interactions between interleukin-2 (IL-2) and the IL-2 receptor β chain.

Biophysical Studies of Cytokine Receptor Interactions

Thesis submitted in partial fulfilment of the requirements for the degree of Doctor of Philosophy

by

Jiejin Li

St. John's College

Trinity 2000

Department of Biochemistry

University of Oxford

South Parks Road

Oxford OX1 3QU

ENGLAND

To my parents

Acknowledgements

It is a very difficult task to adequately express my gratefulness to everyone who has generously provided me with all forms of help during my years in Oxford. They are the ones who made this thesis possible.

Firstly, I would like to thank Professor Iain Campbell for providing me this invaluable opportunity to study in his group. It was his support and encouragement that has kept this project moving. In spite of his busy schedule, he always has time for me when help was needed.

I was fortunate enough to have Dr. David Staunton as my supervisor on molecular biology and biophysical studies, which are the corner stone of this thesis. He taught me hand by hand from how to setup a cell culture to analyzing the final data from biophysical studies. His enthusiasm in research and ability to solve problems from multiple approaches has always been a great inspiration to me. Above all, he showed me how to research, which I consider to be one of the most valuable skills to acquire.

It has also been a great pleasure to have Dr. Jörn M. Werner helping me on the NMR studies. His extensive knowledge on the quantum mechanics nature of NMR spectroscopy made the mighty NMR experiments not that difficult to grasp even for a novice. He also helped me with the ITC and AUC studies, which brought this project into new dimensions and depths.

I would like to thank Dr. Jeremy Bright, who helped me to get everything started and always has an ear for my questions big or small. My most sincere thanks also go to Dr. Klas Arvidsson who helped me with the NMR studies for IL-2Rβ. Their friendship has been an "Energizer" in times when my project was between a rock and the hard place.

Many thanks to all the current and previous members of the IDC group who had offered me a kind hand on numerous occasions. Their kindness has made Oxford a place not too far from home.

I owe a lot of gratitude to my family, whose love and encouragement has given me the strength to push all the way through. Particularly I would like to thank my mother, who taught me how to study when I was at a young age. This great gift no doubt will benefit me for the rest of my life.

Table of content

1 INTRODUCTION 1

1.1 THE CLASS I CYTOKINE RECEPTOR FAMILY 5
1.1.1 Structural features of cell surface receptors 5
1.1.2 The signalling mechanism 6
1.1.3 Nuclear Responses 8
1.2 CURRENT STUDIES ON OSM AND GP130 INTERACTIONS 10
1.2.1 Biophysical properties of OSM and gp130 12
1.2.2 Signalling of OSM 15
1.2.2.1 Structure and functions of Jaks 16
1.2.2.2 Structure and functions of STATs 17
1.2.2.3 Jaks and STATs involved in OSM signalling 19
1.2.2.4 Receptor sequences important for Jak association 19
1.2.2.5 Nuclear translocation of STATs and gene regulation by STATs 20
1.2.2.6 Other signalling pathways for OSM signalling 21
1.2.2.7 Regulation of the gp130/Jak/STAT pathway 23
1.2.3 Biological responses to OSM 24
1.3 UNDERSTANDING THE PLEIOTROPY AND REDUNDANCY OF IL-6 FAMILY CYTOKINES 26

2 QUANTITATIVE TECHNIQUES IN PROTEIN/PROTEIN INTERACTIONS 30

2.1 A BRIEF OVERVIEW OF THE DIFFERENT TECHNIQUES USED 30
2.2 ANALYTICAL ULTRACENTRIFUGATION (AUC) 33
2.2.1 Sedimentation equilibrium of a single ideal solute 34
2.2.2 Sample nonideality 37
2.2.3 Instrumentation 39
2.2.3.1 Rotors 40
2.2.3.2 Cells 41
2.2.3.3 Optical system 42
2.2.4 General methodology 43
2.2.4.1 Sample preparation 43
2.2.4.2 Selection of operation speed 44
2.3 ISOTHERMAL TITRATION CALORIMETRY (ITC) 45
2.3.1 Theory of ITC 45
2.3.1.1 Wiseman isotherm theory 45
2.3.1.2 Instrumentation 48
2.3.1.3 General methodology 50
2.3.1.4 Data analysis 53
2.3.2 Applications of ITC 55
2.4 SURFACE PLASMON RESONANCE (SPR) 56
2.4.1 Basic Principle of SPR 56
2.4.2 SPR for real-time Biomolecular Interaction Analysis (BIA) 57
2.4.3 General methodology 60
2.4.3.1 Basic concepts 60
2.4.3.2 Ligand immobilization 61
2.4.3.3 Detection of the interaction between analyte and surface immobilized ligand 63
2.4.3.4 Surface regeneration 64
2.4.4 Interpreting experimental data 65
2.4.4.1 Basic kinetic measurements 65
2.4.4.2 Equilibrium measurements 67
2.4.4.3 Competitive kinetics 69
2.4.4.4 Complex models and artifacts 70
2.4.5 BIA application areas 73
2.5 NUCLEAR MAGNETIC RESONANCE (NMR) 75
2.5.1 The principle of NMR 76
2.5.1.1 Chemical shift 76
2.5.1.2 Scalar coupling 77
2.5.1.3 Dipolar coupling and nuclear Overhauser effect (NOE) 78
2.5.2 NMR of protein 78
2.5.3 NMR spectroscopy of ligand receptor binding site mapping in solution 80

3 METHODS 83

3.1 CLONING OF OSM 83
3.1.1 Ethanol precipitation 83
3.1.2 Phenol-chloroform extraction 83
3.1.3 Agarose gel electrophoresis 84
3.1.4 Oligonucleotides 84
3.1.5 PCR amplification 84
3.1.6 Restriction enzyme digestion 85
3.1.7 5'-dephosphorylation of double-stranded DNA 85
3.1.8 Ligations 85
3.1.9 Preparation of $CaCl_2$-competent JM109 86
3.1.10 Transformation 86
3.1.11 Miniprep and Maxprep of plasmid DNA 87
3.1.12 Sequencing the constructs 87
3.2 EXPRESSION OF OSM AND GP130-CHR 87
3.2.1 Host strains and expression media 87
3.2.2 Small scale protein expression 88
3.2.2.1 Small scale expression of OSM 88
3.2.2.2 Small scale expression of gp130-CHR 88
3.2.3 Fermentation 89
3.2.3.1 Large scale expression of OSM 89
3.2.3.2 Large scale expression of gp130-CHR 89
3.2.4 Isotope labelling of OSM187 90
3.3 PURIFICATION OF OSM AND GP130-CHR 90
3.3.1 Periplasmic purification of MBP-gp130-CHR 90
3.3.2 Purification of the GST-OSM fusion protein 90
3.3.3 Cleavage of the fusion proteins 91
3.3.4 Ion-exchange chromatography 91
3.3.4.1 Ion-exchange purification of OSM 91
3.3.4.2 Ion-exchange purification of gp130-CHR 92
3.3.5 Gel-filtration chromatography 92
3.3.5.1 Purification of OSM 93
3.3.5.2 Purification of gp130-CHR 93
3.4 DETERMINATION OF SAMPLE QUALITY 93
3.4.1 Analysis of protein by SDS-PAGE 93
3.4.2 Electrospray mass spectrometry 94
3.4.3 N-terminal sequencing and amino acid analysis 94
3.4.4 Sample screening by activity 94
3.4.5 Sample folding status 95
3.5 CHARACTERIZATION OF BINDING 95
3.5.1 Analytical ultracentrifugation 95
3.5.2 Isothermal titration calorimetry 96
3.5.3 Surface plasmon resonance 97
3.6 NUCLEAR MAGNETIC RESONANCE (NMR) STUDIES ON THE INTERACTION 98
3.6.1 Sample preparation 98
3.6.2 Experiments 99
3.6.2.1 One dimensional NMR spectroscopy 99
3.6.2.2 2D spectra (HSQC, 2D-NOESY, TROSY) 99
3.6.3 Data processing 99

4 EXPRESSION AND PURIFICATION OF OSM AND GP130-CHR 100

4.1 DNA SEQUENCING OF THE CONSTRUCTS 100
4.2 EXPRESSION AND PURIFICATION OF OSM 100
4.2.1 Analysis the OSM proteins by SDS-PAGE 101
4.2.2 Electrospray mass spectrometry 102
4.2.3 N-terminal sequencing and amino acid analysis 102
4.2.4 Sample activity and folding status 102

4.3 EXPRESSION AND PURIFICATION OF GP130-CHR 103
4.3.1 Analysis gp130-CHR by SDS-PAGE 103
4.3.2 Electrospray mass spectrometry 103
4.3.3 N-terminal sequencing and amino acid analysis 104
4.3.4 Sample activity and folding status 104
4.4 1D-^{1}H NMR STUDY ON THE 1:1 COMPLEX 104

5 INTERACTIONS BETWEEN THE OSM AND GP130-CHR 106

5.1 ANALYTICAL ULTRACENTRIFUGATION 106
5.1.1 Solution behaviour of OSM187 106
5.1.2 Solution behaviour of gp130-CHR 107
5.1.3 The stoichiometry of binding 107
5.2 ISOTHERMAL TITRATION CALORIMETRY 108
5.3 SURFACE PLASMON RESONANCE 111
5.3.1 The kinetic rate constants 111
5.3.2 The equilibrium binding constants 112
5.3.3 The OSM187 and OSM196 bind gp130-CHR in similar manners 113
5.4 PRELIMINARY NMR STUDIES ON A 1:1 COMPLEX OF ^{15}N OSM187 AND GP130-CHR 114

6 INTERACTIONS BETWEEN THE IL-2 AND IL-2 RECEPTOR BETA CHAIN 115

6.1 INTRODUCTION 115
6.2 METHODS 117
6.2.1 Cloning IL-2Rβ 117
6.2.2 Expression and purification 118
6.2.2.1 Western blotting 118
6.2.2.2 Purification of IL-2Rβ with anion exchange chromatography 119
6.2.2.3 Affinity chromatography 119
6.2.3 One dimensional NMR spectroscopy 120
6.3 RESULTS 120
6.3.1 PCR screening for positive clones 120
6.3.2 DNA sequencing of the IL-2Rβ constructs 121
6.3.3 Expression and purification of IL-2Rβ from MBP fusion system 121
6.3.3.1 Analysis the IL-2Rβ proteins by SDS-PAGE 121
6.3.3.2 Electrospray mass spectrometry 121
6.3.3.3 N-terminal sequencing 122
6.3.3.4 Sample folding status 122
6.3.4 Expression IL-2Rβ in other expression systems 122
6.3.4.1 Express IL-2Rβ in GST fusion systems 122
6.3.4.2 Expression of IL-2Rβ in yeast *Pichia pastoris* 123
6.4 A SHORT SUMMARY FOR IL-2Rβ EXPRESSION 124

7 CONCLUSIONS 127

7.1 COMPARISON OF THE RESULTS OBTAINED FROM DIFFERENT TECHNIQUES. 127
7.2 USE THE RIGHT TOOL FOR THE RIGHT TASK 129
7.3 OUTLOOK 132

8 INDEXES 134

8.1 INDEXES OF FIGURES 134
8.2 INDEXES OF TABLES 136

9 REFERENCES 137

APPENDIXES 157

APPENDIX I: THE HUMAN OSM 157
APPENDIX II: THE HUMAN GP130-CHR 158
APPENDIX III: THE HUMAN IL-2Rβ 159

Abbreviations

AMP	Adenosine Monophosphate
AP-1	Activator protein-1
APP	Acute phase protein
APRF	Acute phase response factor
AUC	Analytical ultracentrifugation
B_{max}	Maximum binding
CBM	Cytokine binding homology module
CHR	Cytokine binding homology region
CIS	Cytokine inducible SH2 containing protein
CNTF	Ciliary neurotrophic factor
CREB	Cyclic AMP response element binding protein
CSA	Chemical shift anisotropy
ΔG_b^0	Free energy of binding
ΔH_b^0	Enthalpy of binding
ΔS_b^0	Entropy of binding
F3	Fibronectin Type III
gp130	Glycoprotein 130
HSQC	heteronuclear single-quantum correlation
IFC	Integrated micro-fluidic cartridge
IFN	Interferon
Ig	Immunoglobulin
ITC	Isothermal titration calorimetry
Jak	Janus kinase
JH	Jak homology
K_A	Equilibrium association constant
K_D	Equilibrium dissociation constant
k_{on}	Association rate constant
k_{off}	Dissociation rate constant
LIF	Leukemia inhibitory factor
MAPK	Mitogen-activated protein kinase
M_{app}	Apparent molecular weight
M_{calc}	Calculated molecular weight
MMP	Matrix metalloproteinase
M_{tot}	Total macromolecule concentration in the reaction cell of ITC
M_w	Weight-averaged molecular weight
NLS	Nuclear localization sequence

OMRE	OSM-responsive element
OSM	Oncostatin M
PIAS	Protein inhibitor of activated STAT
PMA	Phorbol ester phorbol 12-myristate 13-acetate
PTK	Protein tyrosine kinase
R_{eq}	Response at equilibrium
R_{max}	Maximum response
SHP2	SH2 domain-containing tyrosine phosphatase 2
SOCS	Suppressor of cytokine signalling
SPR	Surface plasmon resonance
STAT	Signal transducers and activators of transcription
TIMP	Tissue inhibitors of metalloproteinases
TROSY	Transverse relaxation-optimized spectroscopy
X_{tot}	Total ligand concentration (free and bound)

1 Introduction

Although it seems as a "given" that cells use specific receptors to interpret outside signals carried by biological substance such as cytokines and drugs, this dogma was not always self-evident but evolved during years of research. Much of the conceptual framework regarding how to study receptor function originated from pharmacological investigation of drug action.

During his study of the mechanism of arrow poison curare, Claude Bernard (1813-1878) pioneered a pattern of scientific research that permitted the understanding of the specificity and selectivity of drug action. Although he never used the term receptor, Claude demonstrated that the functional efficacy of a drug depends on its access to a particular location. The receptor concept is generally attributed to Paul Ehrlich (1854-1915), although the actual word 'receptor' (receptive substance) was first introduced by one of Ehrlich's contemporaries, J.N. Langley.

Ehrlich's earliest work on distribution of lead in the body demonstrated differential uptake of lead in various organs of animals. He subsequently revealed that the antigen-antibody interactions are chemical encounters and developed the "side chain theory", which won him the Nobel Prize in Medicine in 1908. Ehrlich pointed out that there are two active areas on an antigen: the haptophore (the anchorer) and the toxophile (the poisoner). He believed that the specificity of an antigen on certain mammalian cells is the result of the existence of specific "side chains", on the cells, which are complementary to the chemical groups on the haptophore domain of the antigen. His studies on the lethal effects of arsenicals also

proved that the agent needed to first "bind" to the target cells and the arsenicals-resistant strains were those that lost their "binding" abilities. Ehrlich's studies on the basis of selectivity are often distilled into his often-quoted dictum: " *Corpora non agunt nisi fixata*" (agents cannot act unless they are bound).

J.N. Langley (1852-1926), of Cambridge University, was interested in the chemical basis for autonomic transmission and neuromuscular communication. He found that nicotine could chemically stimulate the frog gastrocnemius muscle and the effect could be blocked by curare. The mutually antagonistic effects of nicotine and curare, as well as the ability of direct electrical stimulation of the muscle to bypass the effects of curare, implied that nicotine and curare act on the same substance, which is neither nerve nor muscle. Langley called this postulated substance the "receptive substance" and believed the drugs were effective by forming "compounds" with the receptive substance. Further, he stated that these compounds (complexes) are formed according to some law by which the relative concentration of the drugs and their affinity for the receptive substance are critical factors. Thus, Langley first introduced the drug-receptor interaction concept and predated the mathematical description of these interactions as reflecting a consequence of mass action law.

In 1926, A. J. Clark (1885-1941) found that drugs combine with their receptors at a rate dependent on the concentration of drug and receptor, and that the resulting drug-receptor complex breaks down at a rate proportional to the number of complexes formed. These findings indicated that drug-receptor interactions obey the principles of the mass action law. Thus, the same isotherms from Langmuir's studies

on the adsorption of gases onto metal surfaces can be applied to describe the drug-receptor interaction.

Evolved over about 150 years, the receptor concept is widely accepted as an important mechanism for signal transduction. Cells of multi-cellular organisms need to communicate with each other in order to co-ordinate their growth and differentiation. The mechanisms for such communication include secretion of soluble signalling molecules, as well as direct contacts between cells. Generally, extracellular signalling molecules interact with a receptor embedded within the plasma membrane or presented in the cytoplasm. Then distinct intracellular signal transduction pathways are initiated that directly affect different kinds of cytoplasmic machinery or the cell nucleus, where the activities of specific genes are regulated.

Cytokines are soluble signalling molecules that participate in extra-cellular communication. Unlike hormones, which are carried from the source to the target cell some distance away by the circulatory system, the majority of cytokines act locally. Released by cells in response to a particular stimulus, cytokines can stimulates target cells that bear the appropriate cytokine receptor. The receptor transduces the signal to target genes via intracellular signalling cascades that cause one or more changes in cell activity. Cytokines rarely operate in isolation and generally exhibit a high degree of redundancy and pleiotropy. A particular activity in a target cell is normally the net result of several cytokines operating simultaneously. The well-studied growth factors, interleukins, lymphokines, monokines, interferons and the colony stimulating factors all demonstrates the above characteristics (1,2).

There are more than 100 cytokines that have been characterized since the discovery of the first cytokine, nerve growth factor (3). The number is still growing. Based on structural similarity, cytokines can be grouped into several families (Table 1.1). The revealed evolutionary relationships were not instantly inferred from the limited sequence homology (4).

Many cytokine receptors were discovered through co-immunoprecipitation experiments, such as gp130 (a 130 kDa glycoprotein, which co-precipitates with IL-6R) (5). The molecular cloning of most of the receptors for cytokines regulating the immune and hematopoietic systems has allowed us to characterize these receptors in greater detail than previously possible. Currently, there are four major families of cytokine receptors. They are the receptor kinase family (6), the haematopoietin receptor family (7), the tumor necrosis factor/nerve growth factor family (8), and the family of G-protein-coupled receptors (9).

Signal transduction is usually initiated by ligand induced receptor association (10). In many cases, the receptor association leads to an increased phosphorylation of cytoplasmic proteins on tyrosine residues, which is the starting point of signalling pathways downstream. This kinase activity can either reside in the receptor (as for protein tyrosine kinase family) or in an associated protein (such as the haematopoietin family). Many signalling pathways have been determined with detailed structural characterization of key regulatory components such as the regulation of G-proteins and the detailed description of the Src signalling pathway (9,11,12).

In the haematopoietin receptor family a number of cytoplasmic signalling molecules have been identified. Among which, there are two families of proteins: the

Family	Subclass	Examples
Four-helix bundle	Short chain	IL-2, IL-3, IL-4, IL-5*, M-CSF*, GM-CSF (IL-7, IL-9, IL-13, IL-15)
	Long chain	GH, LIF, G-CSF, IL-6, CNTF, EPO, Leptin (OSM, IL-11, IL-12, TPO)
	Interferon	INFα, INFβ, IFNγ*, IFN-tau, IL-10*
EGF-like		EGF, TGFα, heregulin,
Insulin-like		Insulin, IGF1, IGF2
β-trefoil		FGF, IL-1
Cysteine knot		NGF, PDGF, TGFB

* The cytokine is a dimer.

Table 1.1: Structural classification of cytokines. The structures of the cytokines shown in brackets have not been determined but they are putative members of the respective families.

Jaks (Janus kinase) and the STATs (signal transducers and activators of transcription). The Jaks associate with the receptors and are activated by ligand binding. The activated Jaks phosphorylate both themselves and the receptor subunits, creating docking sites for downstream components in the Ras pathway (13,14). In addition, the Jaks phosphorylate STATs. The phosphorylation of STATs initiates their nuclear translocation and DNA-binding activity. Activation of STATs represents a novel signalling pathway correlated with mitogenesis.

The haematopoietin receptor family can be further divided into Class I and Class II cytokine receptor family base on structural alignments. Gp130 belongs to the Class I cytokine receptor family (Figure 1.1).

1.1 The class I cytokine receptor family

1.1.1 Structural features of cell surface receptors

Members of this family contain a conserved domain of around 200 amino acid residues in their extracellular domains as well as two or three short conserved motifs in the cytoplasmic region (15,16). The conserved extracellular domain is composed of two fibronectin type III (F3) modules, with an L-shaped quaternary structure (17-19). The fibronectin type III domains are composed of two β sheets that fold to form a sandwich of seven antiparallel β-strands. Loops from the F3 domains form the binding pocket at the elbow position of this L-shaped structure. Four positionally conserved cysteine residues in the N-terminal half and a WSXWS motif in the C-terminal end are considered to be important to keep this ternary structure, since mutations in them abolish the binding capability of the receptors (20). In the

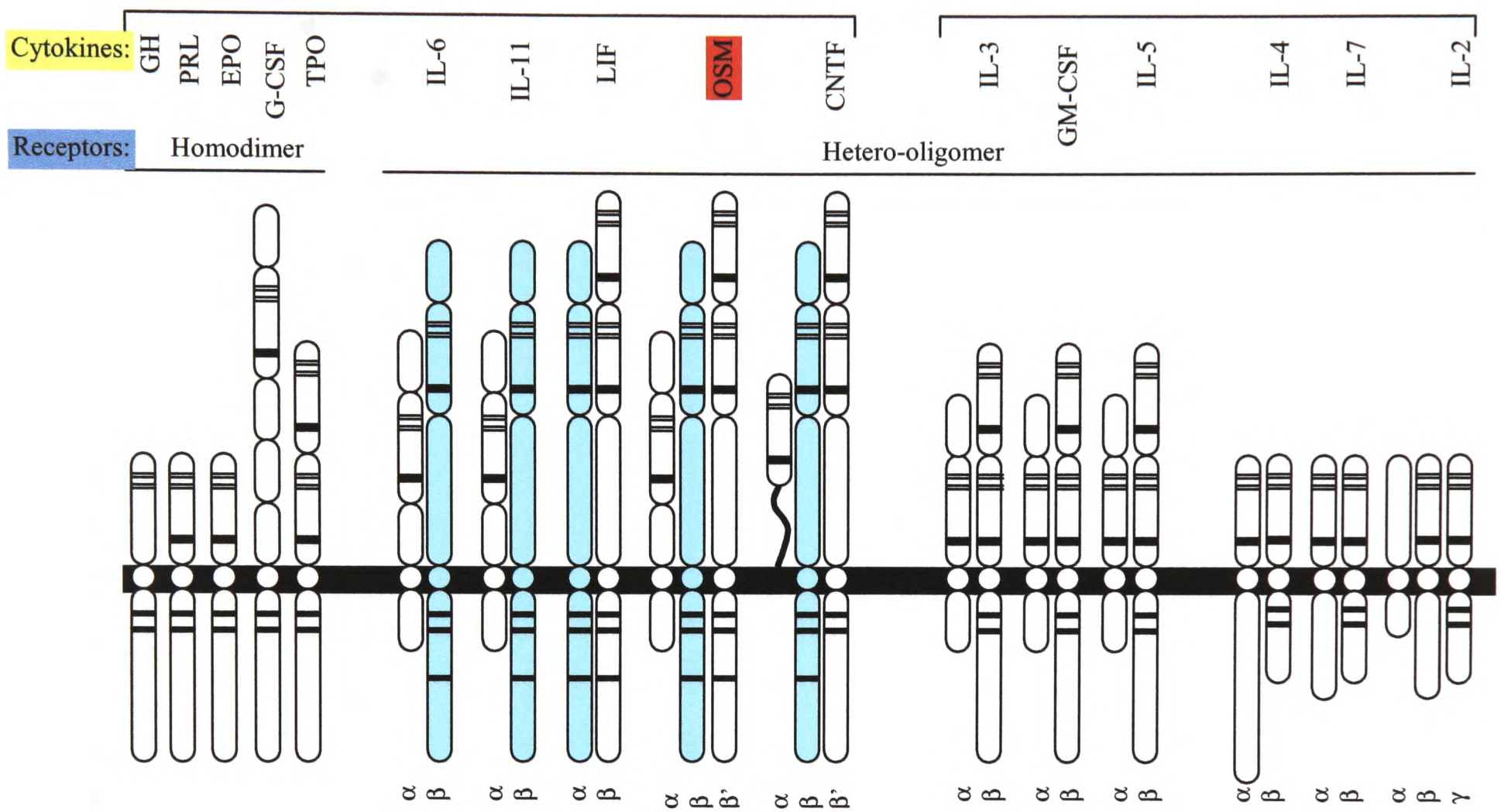

Figure 1.1: Class I cytokine receptor family. Members of the family have conserved extra-cellular domain of about 200 amino acid residues. Four conserved cysteine (set of four horizontal bars) residues and a WSXWS (thick horizontal bar) motif characterize this domain. The box1, box2 and box3 motifs in cytoplasmic region marked as thick horizontal bars. The common signal transducing chain of IL-6 family (gp130) is coloured blue.

cytoplasmic domain, there are usually two short motifs named box1 and box2 close to the membrane (16,21). LIF-R, gp130 and G-CSFR also contain another conserved motif (box3) in the middle of the cytoplasmic region (21,22) (Figure 1.2).

1.1.2 The signalling mechanism

All known class I cytokine receptors are believed to form homo- or heterodimers (or, in a few cases, trimers) upon binding of their ligand. One partner of the complex is generally a signal-transducing component. There are three common signal-transducing subunits, gp130, βc and γc. Based on their ability to form complexes with the common signal transducers, the family can be divided into three subsets (Table 1.2). The common signal-transducing components explain the functional redundancy of the family. Apart from the signal-transducing unit, there are also ligand specific receptor components in the complex. They have limited expression in different tissues. This leads to the apparent distinct effects of this family of cytokines as well as their functional redundancy. Receptors like IL-6R, CNTFR and IL-11R can still retain binding capabilities in extracellular soluble form (sIL-6R, sCNTFR and sIL-11R) (5,23-25) and induce homo- or heterodimers of gp130 (Figure 1.3). Combined with the appropriate cytokine, they can mimic all

Common signal transducer	Class I cytokine receptor
gp130	IL-6, IL-11, LIF, CNTF, CT-1, OSM
βc	GM-CSF, IL-3, IL-5
γc	IL-2, IL-4, IL-7, IL-9, IL-15

Table 1.2: The three groups of class I cytokine receptors. Class I cytokine receptors employ common receptor subunits for signal transduction. Based on the different common signal transducer involved, the family can be divided into three groups. Ligand induced dimerization between their specific receptor and the respective signal transducer is a critical step for signal transduction.

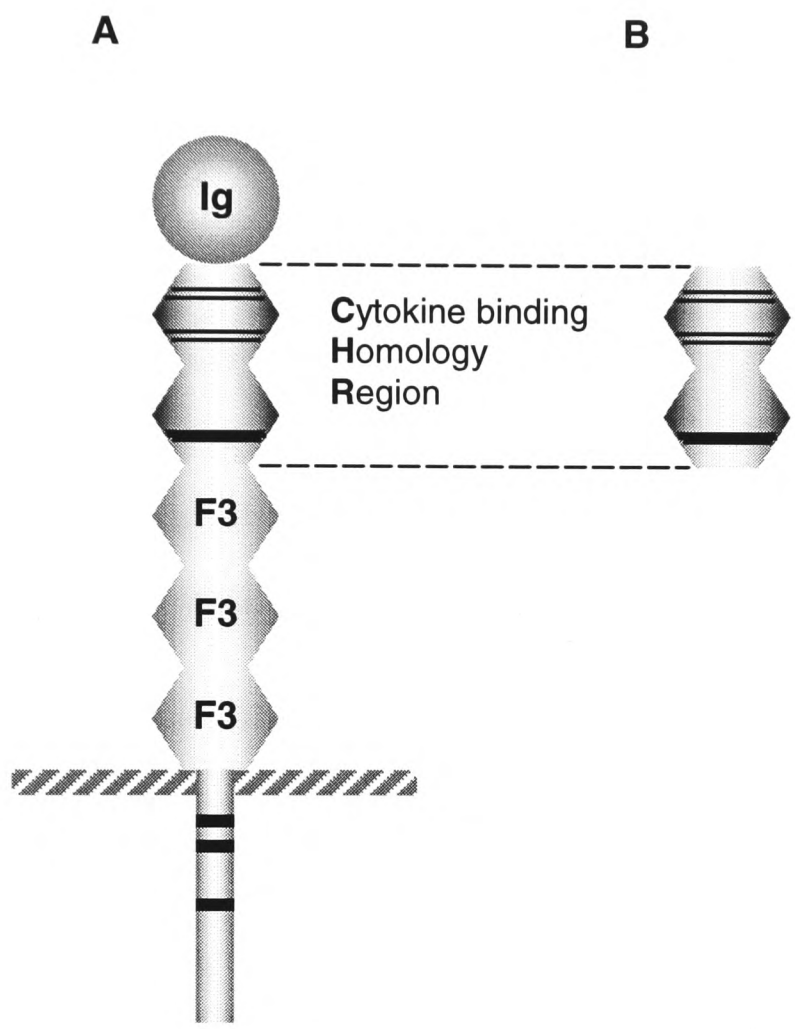

Figure 1.2: Schematic diagram of the signal transducing chain gp130. A) The gp130 features the Class I cytokine receptor family's conserved extra-cellular domain of about 200 amino acid residues (marked as cytokine binding homology region (CHR)). B) gp130-CHR is the module used in the following studies. The conservative domains follow the same convention as in figure 1.1.

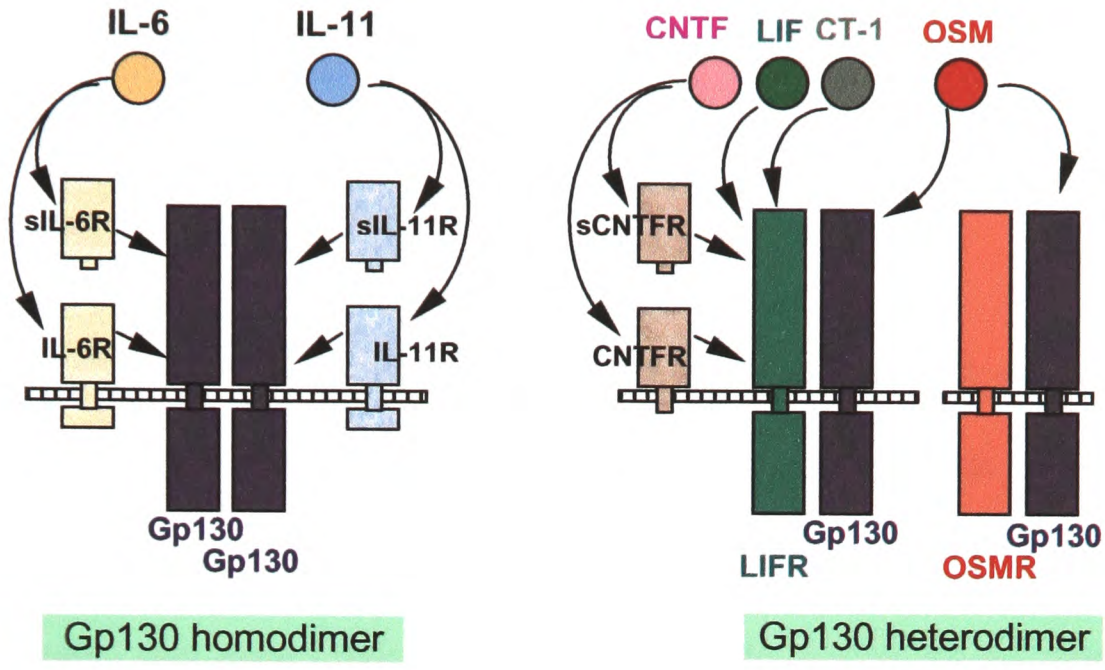

Figure 1.3: Receptor systems sharing gp130 as a common signal transducer. IL-6, when bound to either a membrane-anchored or a soluble form of its receptor (IL-6R or sIL-6R), induces homodimerization of gp130. The IL-11/IL-11R or sIL-11R complexes are suggested to induce the same type of homodimer. Hetero-dimerization of LIFR and gp130 is induced by the CNTF/CNTFR or sCNTFR complex, the LIF, CT-1 and OSM. OSM also induces another type of heterodimer composed of OSMR and gp130. Attention also should be drawn to the fact the OSM can bind directly to gp130 and induce hetero-dimerization between gp130 and LIFR or OSMR. Although it was reported that LIF is able to bind directly to soluble gp130, the events after that are not clear.

other gp130-stimulatory cytokines in cells expressing gp130 (26,27) by triggering gp130-mediated signalling pathways through the formation of gp130 homo- or heterodimers. Physiological agonistic functions of these soluble receptors have been reported (25,28).

Members of the class I cytokine receptor family do not possess obvious enzymatic motifs in their structure. By juxtaposition upon ligand-induced dimerization, they activate associated cytoplasmic protein tyrosine kinases. A line of research revealed that even GHR, EPOR and G-CSFR, which are not considered to require an additional receptor chain for signalling, form homodimers after binding of their respective ligand (15,21,29,30). As mentioned above, Jaks have a well-established role for the signal-transducing event. They bind with the cytoplasmic domains of the receptors and are activated by ligand-stimulated dimerization. The increase in local concentration, or the juxtaposition, of Jaks may allow them to phosphorylate each other in addition to the receptor components. Receptor oligomerization has now been firmly established as the mechanism for cytokine receptor signal transduction (reviewed in (31,32)). New structure information on the interaction between erythropoietin with its receptor suggests that the orientation of receptor dimers is critical to intracellular activation (33). This provides cells with a safeguard against receptor non-specific dimerization. There are four different members of the Jak family, Jak1, Jak2, Jak3 and Tyk2 that are known to be involved in class I cytokine receptor signalling (34). The nature of their involvement may differ in individual receptor complexes (reviewed in (38-40)) (Table 1.3). Unlike the other two subsets of the family, in the γc-receptor complexes, two different Jaks are required. For example, in the functional IL-2 receptor complex, Jak1 binds to IL-2Rβ

	Jaks				STATs					
Ligands	Jak1	Jak2	Jak3	Tyk2	1	2	3	4	5	6
gp130 family										
IL-6	+	+	+		+/-	-	+	-		
IL-11		+			+/-	-	+	-		
OSM	+	+		+	+/-	-	+	-		
LIF		+	+		+/-	-	+	-		
CNTF	+/-	+	+		+/-	-	+	-		
G-CSF		+			+/-	-	+	-		
CT-1	+	+		+			+			
γc family										
IL-2	-	+	-	+	+/-		+		+	
IL-4	-	+	-	+						+
IL-7	-	+	-	+					+	
IL-9	-	+	-	+					+	
IL-15		+		+					+	
βc family										
IL-3	-	-	+	-					+	
IL-5	-	-	+	-					+	
GM-CSF	-	-	+	-					+	
Growth Hormone family										
EPO	-	+	-		-	-	-	-		
GH	-	+	-		+/-	-	+	-	+	
PRL	+/-	+	-		+/-	-	-	-	+	

Table 1.3: Activation of Jaks and STATs by various ligands (39). The table indicates which Jaks and STATs are the main targets (+) of activation for the ligand listed on left. Minor targets are indicated as (+/-).

chain and Jak3 to the γc component (34,35). Mutagenesis studies have shown that the box1 motif is important for the association of Jak (36,37).

Gene transcription is initiated by activation of transcription factors. Many recent studies focus on the STAT family members. Examples of their involvement in the class I cytokine receptor signalling are shown in Table 1.3. Generally, cytokine stimulation triggers the tyrosine phosphorylation of the SH2 domain on STATs and allows them to form stable homodimers. The dimerized STATs can bind to a target DNA sequence. The resident Jak kinases on the γ receptor chain are responsible for STAT's phosphorylation. Other downstream signalling molecules containing an SH2 domain can also be recruited by the tyrosine-phosphorylated class I cytokine receptors (41). The Ras/MAP kinase pathway is one of the best-studied (42,43). Different receptors may contain different kinds of docking motifs. In a specific receptor, different sites of the cytoplasmic region may be able to recruit different molecules from distinct intracellular signal pathways. The presence of different signalling pathways, transmitted from distinct sites of the cytoplasmic region of the receptors may partly account for the functional pleiotropy.

1.1.3 Nuclear Responses

Most signal transduction pathways ultimately act on gene transcription and alter the expression of genes in response to extracellular and intracellular signals. The response may lead to cell division in the case of mitogenic stimuli but more often involves subtle changes in the capacity of a cell to react to its environment. Thus, changes in gene expression play a role in a vast number of cell responses from mast

cell secretion to nerve depolarization. Advances in molecular cloning and protein expression techniques have allowed studies of a variety of gene transcription regulators. The mechanisms controlling gene expression are beginning to be understood.

Protein phosphorylation is a repeating theme in most of the signalling pathways. Many transcription factors need to be phosphorylated or dephosphorylated to become active. One example is the negative and positive regulation of c-jun protein by phosphorylation (44,45). Many resting cell types contain a dormant form of c-Jun protein that is highly phosphorylated at sites just amino-terminal to the DNA binding domain. The presence of phosphate groups at these residues interferes with DNA binding. Upon cell stimulation, these sites are dephosphorylated and binding is no longer blocked. There is a transactivation domain in human c-Jun. By forming an interaction interface with the other proteins, the transactivation domain passes the stimulation to the next protein in the signalling pathway. The activation of the transactivation domain is achieved by phosphorylation of two serine residues (Ser63 and Ser73) proximal to the domain.

Signalling pathways can be divided into two groups based on where the transcription factors are activated. The first one involves a spectrum of cytoplasmic mediators such as activator protein-1 (AP-1) (46,47), cyclic AMP response element binding protein (CREB) (48,49), serum response element binding protein (50) and NF-κB (51,52). Transcription factors in the second group are activated at the plasma membrane and directly translocated to the nucleus. These signalling pathways,

utilizing Jaks and STATs as their mediators, are demonstrated by a variety of cytokines.

Signalling pathways can also crosstalk to one another. Human primary astrocytes can be stimulated by OSM to express matrix metalloproteinases (MMPs), a family of enzymes directly involved in extracellular matrix breakdown. Analysis of the signal transduction leading to activation of the MMP-1 gene revealed the presence of an OSM-responsive element (OMRE) encompassing the AP-1 binding site and the STAT binding element, which mediate activation by OSM. Cross-talk between the mitogen-activated protein kinase and Jak-STAT pathways is required to achieve maximal induction of the OMRE-driven transcription by OSM (53). STAT3 has an additional requirement for serine phosphorylation to provide a further level of co-ordinate control.

In summary, stimulation of cells induces a complex wave of events leading to contextual changes in gene expression. The consequences of this depend on the cell type, be it proliferation, secretion, cell death, differentiation or a myriad of other responses. The molecular dissection of the regulatory pathways promises to allow intelligent manipulation of gene expression.

1.2 Current studies on OSM and gp130 interactions

Oncostatin M was discovered and named by J.M. Zarling in 1986 (54). PMA (Phorbol ester phorbol 12-myristate 13-acetate) treated U-937 cells were reported to release a polypeptide that inhibits the growth of A375 melanoma and other tumor cells, but augments the growth of normal fibroblasts. This factor, termed oncostatin

M, appears to be a distinct cell growth regulator based on its amino-terminal amino acid sequence and its biological activities. The ability to inhibit cancer cells selectively and not the surrounding normal tissue cell made OSM a potential cancer therapeutic agent. Much interest has been centered on the studies of OSM and its receptors and their downstream signalling pathways.

Subsequent studies have revealed that OSM belongs to the IL-6 cytokine family (55) and is most closely related to LIF in both structural and functional terms. The first discovered functional OSM receptor complex included the LIF receptor (LIFR) (56). As with all the members of the IL-6 family of cytokines, OSM uses gp130 as a signal-transducing component in its functional receptor complex (57). In 1994 Thoma *et. al.* (58) observed that OSM is a potent inducer of both mitogen-activated protein kinase activity and biological response, both of which correlate with the expression of a second OSM receptor that does not bind LIF. In addition, different patterns of tyrosine- phosphorylated proteins were stimulated by OSM and LIF. This led to the discovery of the type II OSM receptor, which is composed of OSM specific receptor and gp130 (59,60).

OSM participates in a broad spectrum of events, spanning the hematopoietic system, immune system and the nervous system. This is partially due to the wide expression of its signal transducer gp130. From this aspect, the biophysical characterization of the binding between OSM and gp130 is of huge interest. Apart from LIF, OSM is the only IL-6 family member that can bind directly to gp130. (61,62). The OSM/gp130 complex is expected to be a simple one to one system that serves as a building block toward higher order complexes.

1.2.1 Biophysical properties of OSM and gp130

The tertiary structures of LIF (63), CNTF (64) and IL-6 (65,66) have been solved by X-ray crystallography or NMR spectroscopy (Figure 1.4). All structures have a four-helix-bundle topology. Helix A is connected, by a long loop, to helix B in such a way that helix B lies parallel with helix A. Helix B is separated from helix C by a very short loop, allowing only antiparallel packing. Helix C is again joined by a long loop with helix D, resulting in parallel packing of the C-terminal helices. The overall folding shows an 'up-up-down-down' topology of the four long helices. While the 3D structure of OSM has not been solved, the NMR backbone assignment of a double-labelled OSM confirmed that it has the four-helix-bundle topology of the IL-6 family cytokines (67).

Gp130 shows the classic features of a class I cytokine receptor as described above (Figure 1.2). The extra-cellular region of gp130 is composed of three fibronectin type III domains, two cytokine binding homology modules (CBM) and one Ig domain. The cytoplasmic region of gp130 is 277 residues long and contains the Box 1, 2 and 3 motif for signal transduction.

Ligand-induced homo- or hetero-dimerization of signal transducing receptor component is the major theme behind many cytokine receptor signalling pathways. The functional IL-6 family receptor complex is usually composed of ligand specific α-receptor subunits (IL-6R (68), IL-11R (69) and CNTFR (70)) and the signal transducing subunits (gp130). OSM has two types of receptor complexes. The type I OSM receptor complex contains LIFR and gp130. The type II OSM receptor complex is composed of OSMR and gp130. OSM directly binds to gp130 and

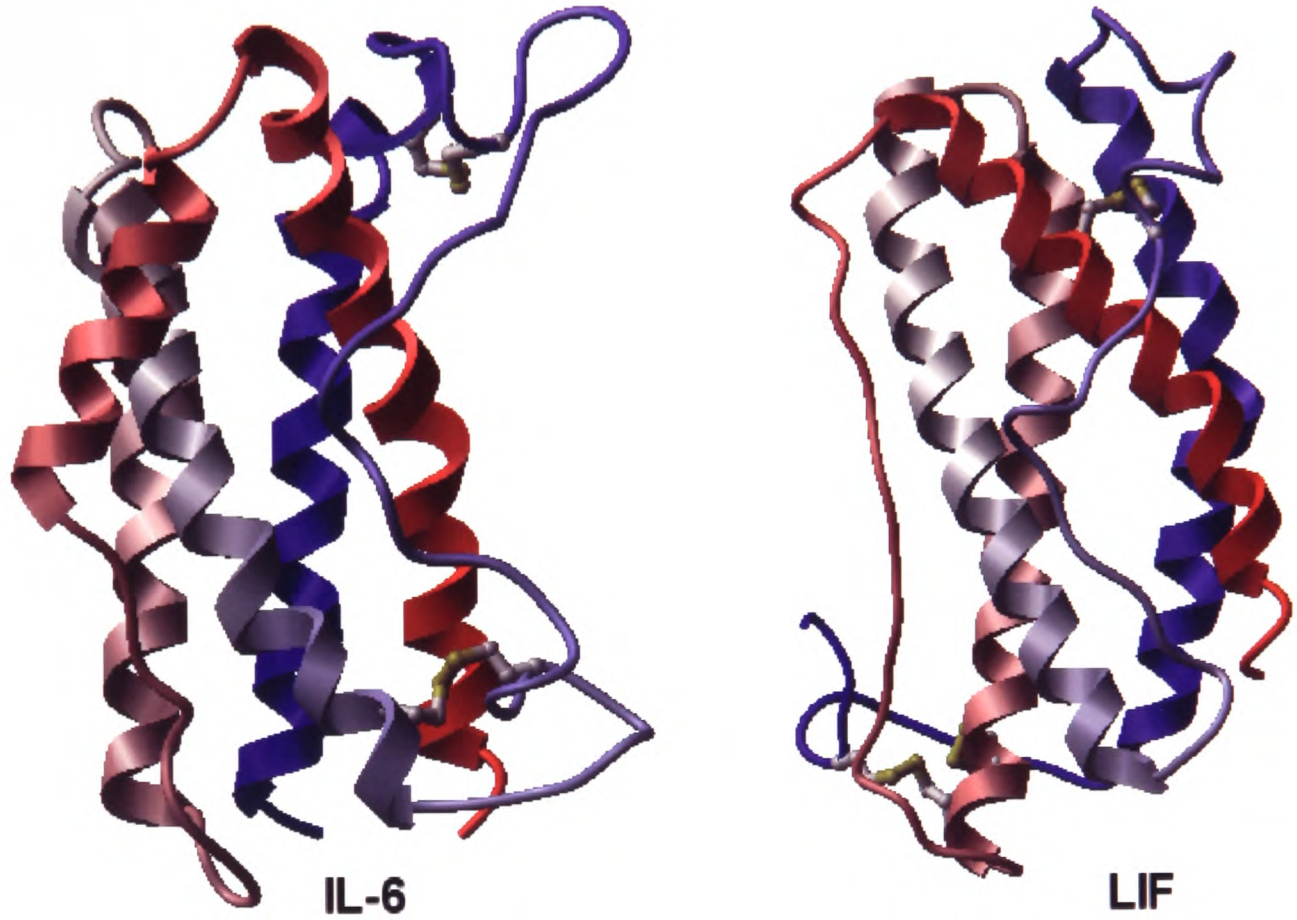

Figure 1.4: Structures of IL-6 and LIF. The four α-helices are coloured as A (red), B (pink), C (sliver grey) and D (blue). The overall fold shows an "up-up-down-down" topology of the four helices. The Brookhaven Databank accession numbers are 1IL6 and 1LK1 for IL-6 and LIF respectively.

induces hetero-dimerization of the gp130 with LIFR (Type I) or OSMR (Type II). Unlike the other non-signal transducing α-receptor subunits, LIFR and OSMR are both able to activate downstream signalling molecules. The type I receptor complex also can exist as a functional LIF receptor complex and this explains the apparent signal overlapping between OSM and LIF. The responsiveness of a given cell type to these cytokines is usually determined by expression of respective ligand specific subunits.

There are also soluble forms of some of the receptors, such as soluble IL-6 (sIL-6), soluble IL-11 (sIL-11), soluble CNTF (sCNTF) and soluble gp130 (sgp130). The presence of soluble receptors gives added complexity for cell responsiveness. The IL-6-sIL-6R complex can be introduced to cells to mimic signals from other IL-6 family cytokines. Soluble gp130 can also neutralize the IL-6-sIL-6R complex, thereby acting as an antagonist (28). The antagonist effect of sgp130 on LIF and OSM were also demonstrated by its ability to prevent the biological activities of LIF and OSM in the TF-1 erythroleukemia cell line. This property suggests that sgp130 may have therapeutic value in the specific prevention of LIF or OSM mediated pathologies (61).

The binding stoichiometry between OSM and gp130 is one of the questions this project is trying to answer and will be discussed in detail later. Up to now, the interaction between IL-6/IL-6R/gp130 has been studied in most detail among the IL-6 family cytokine/receptor complexes. Although the Ig domain of gp130 is required for signalling by IL-6 (71), it is not essential for ligand binding between gp130 and IL-6 or OSM (72). There is also evidence that the three membrane proximal fibronectin-

type-III domains are also dispensable for IL-6 and OSM binding (73). The two cytokine binding homology modules of gp130, termed the cytokine binding homology region (CHR), are responsible for the interaction of the IL-6/IL-6R complex as well as specific recognition of the related cytokines LIF, OSM, and probably also of CNTF and IL-11.

Mutagenesis studies on gp130 revealed that the hot spot of binding is resident in the loops near the hinge region between the two domains of cytokine binding homology module (20,74-76). This binding mode is comparable to the one observed from the well-studied growth hormone-growth hormone receptor complex. Recent studies indicated that the residues Y73, F74 and V135 of gp130 are crucial for ligand binding of class I cytokine/receptor family (Figure 1.5) (77). Compared with growth hormone receptor (GHR), these residues are in positions analogous to W104 (for Y72, F73) and W169 (for V134), which are essential for GHR ligand binding (78).

IL-6 family cytokines have three distinct receptor-binding sites referred to as sites 1, 2 and 3. Site 1 is formed by the C-terminal residues of helix D and the C-terminal part of the AB-loop and determines the specificity of α-receptor binding. Site 2 consists of residues located near the middle of helices A and C and seems to be the universal gp130-binding site of the family. Depending on the cytokine, site 3 is most probably used for recruitment of LIFR, OSMR or a second gp130 molecule (76,79). Further studies on the stoichiometry of functional IL-6 receptor complex indicated a 2:2:2 ratio between IL-6, IL-6R and gp130 (80,81). This hexameric complex is also likely in the CNTF receptor complex, which consists of two

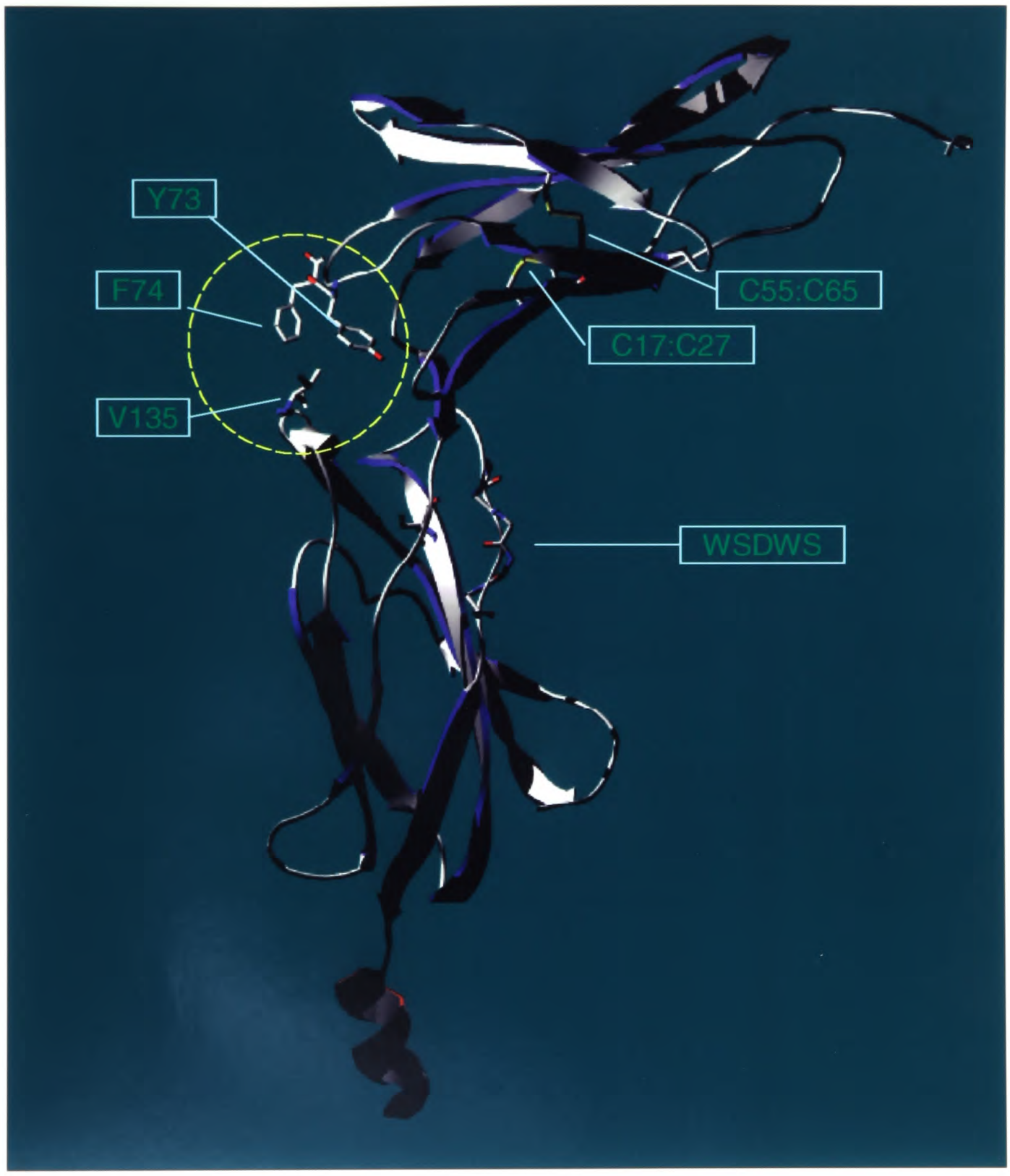

Figure 1.5: A ribbon diagram of human gp130-CHR. The cytokine-binding region is located at the interface between the two fibronectin type III domains and marked with a yellow circle. The characteristic features of the class I cytokine receptor family (four conserved cysteine residues and WSXWS motif) are labeled. The side chains critical for binding are shown. Residues Y73 and F74 are located in the E-F loop of D2 and V135 is situated in the B-C loop of D3. The numbering system is based on the construct employed in this study (see methods).

molecules each of CNTF and CNTFR and one molecule each of gp130 and LIFR (82).

1.2.2 Signalling of OSM

Members of the IL-6 cytokine family utilize tyrosine kinases of the Jak family and transcription factors of the STAT family as major mediators of signal transduction (83,84). The gp130 associated kinases Jak1, Jak2 and Tyk2 become activated upon stimulation, and the cytoplasmic region of gp130 is phosphorylated (85). Several phospho-tyrosine residues of gp130 are docking sites for STATs with matching SH2 domains, mainly STAT3 and STAT1 (83,86). The STATs are activated by phosphorylation and form dimers. Subsequently, the dimers are translocated to the nucleus, where they regulate transcription of target genes.

Signalling mediators involved in other pathways can also bind to phosphorylated gp130 such as the tyrosine phosphatase SHP2 and Shc (87,88). Their existence explains the cross talk between Jak-STAT pathways and the mitogen-activated protein kinase (MAPK) pathway. Owing to the OSM specific receptor, the type II OSM receptor can also active STAT5b. This might explain some of the activities specifically displayed by OSM.

The key players in the mechanism of the OSM signalling pathways will be discussed in the following sections.

1.2.2.1 Structure and functions of Jaks

Jaks are intracellular tyrosine kinases with molecular masses around 130 kDa. Currently there are four members known in mammalian cells: Jak1, Jak2 and Tyk2, which are widely expressed, and Jak3, which is mainly found in cells of haematopoietic origin. The structural organization of Jaks is shown in Figure 1.6. A typical kinase domain, also called the Jak homology (JH)-1 domain, is located at the C-terminus. A kinase-like domain (JH2) precedes it. The N-terminal half of the Jaks contains five additional regions with high sequence similarity between the different Jaks (JH3-JH7) (reviewed by (89,90)).

The role of the JH-1 domain is to provide tyrosine kinase activity. Two tyrosine residues 1007 and 1008 of Jak2 were found to be phosphorylated, and a single mutation of tyrosine-1007 abolished essentially all tyrosine kinase activity (91). Ligand-induced receptor dimerization is thought to bring the associated Jaks into close proximity, leading to their activation via inter- or intra-molecular phosphorylation at sites necessary for catalytic activity (Figure 1.7) (89,90,92). Moreover, when Jaks are highly over-expressed in insect or mammalian cells, they become tyrosine-phosphorylated and display kinase activity even in the absence of an exogenous stimulus (93-95). This indicates that close contact between these enzymes may be sufficient to trigger their activation. However, the recent description of the influence of redox state on kinase activity points to a further level of regulation imposed on the Jaks (90).

The N-terminal half of the Jaks (regions JH7-JH3, Figure 1.6) is involved in receptor association. The receptor interaction is complex, possibly involving multiple

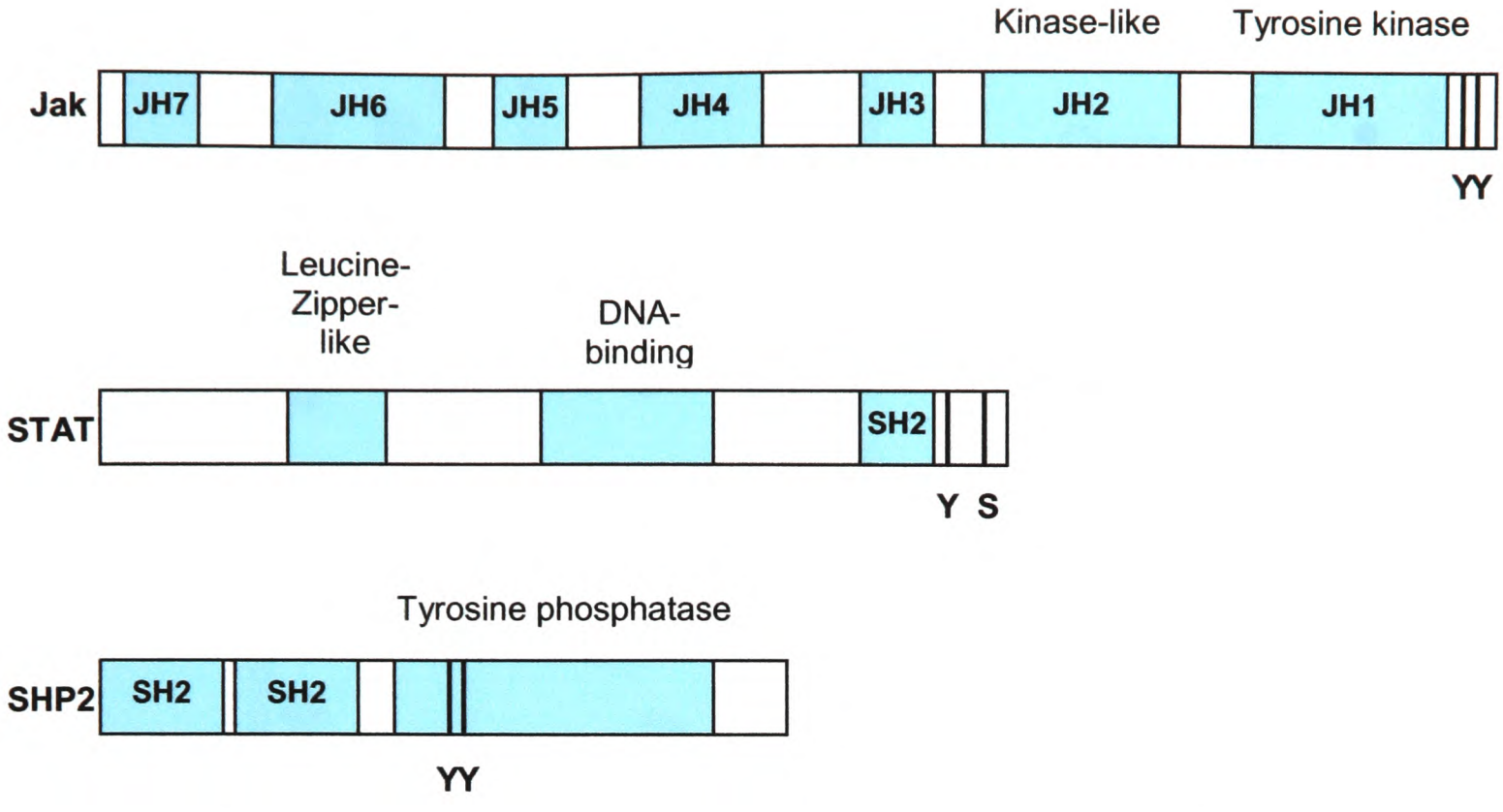

Figure 1.6: Structural organisation of Jaks, STATs and SHP2. The important tyrosine residues, phosphorylated upon activation, are shown as black bars.

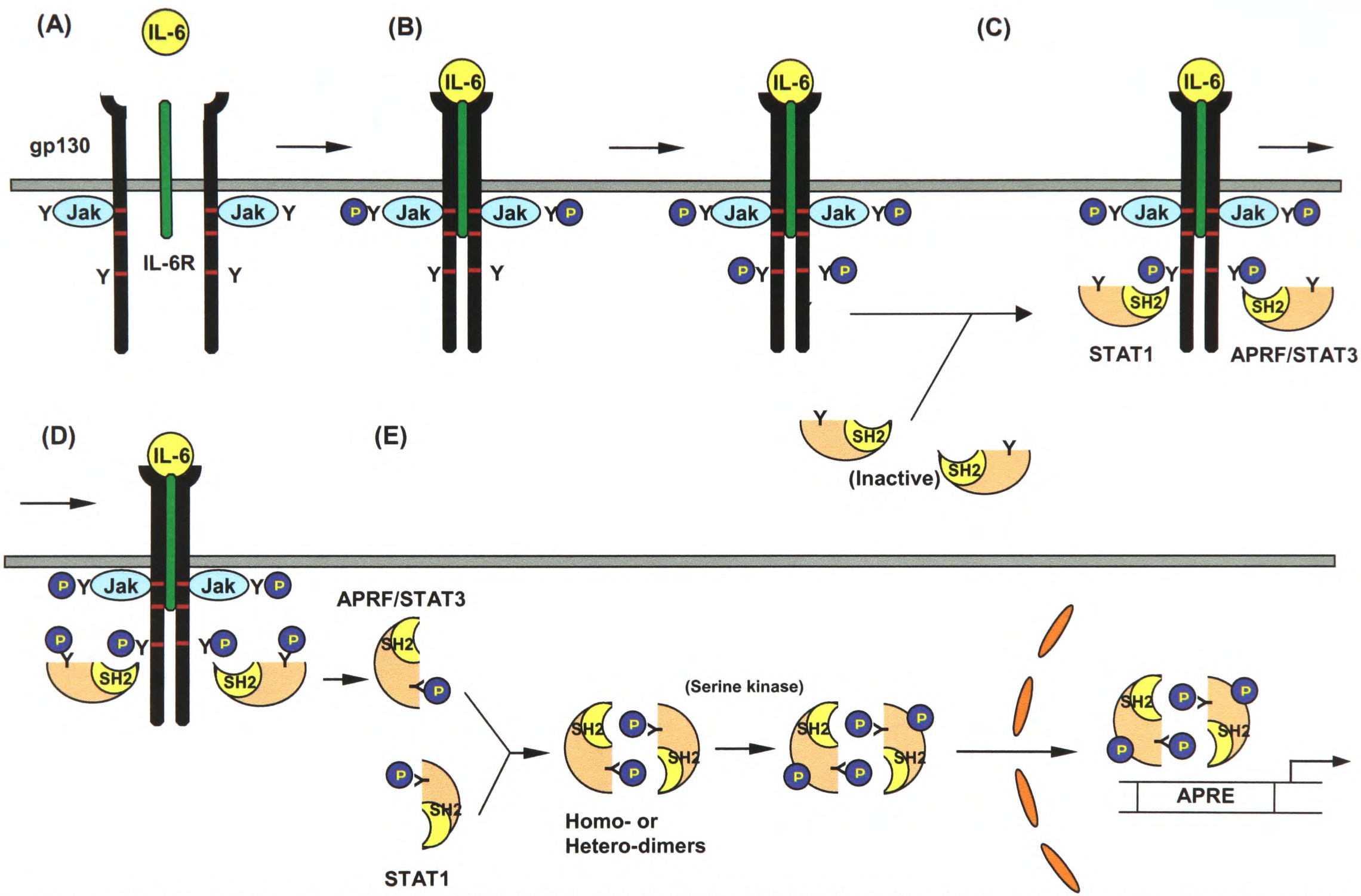

Figure 1.7: Signalling through gp130/Jak/STAT pathways. The IL-6 induced gp130 homodimer is taken as an example. The three red bars are box1, box2 and box3 motif from top to bottom. (A) Prior to stimulation, Jaks are associated with gp130 at its box1 motif. (B) Upon binding to IL-6, gp130 form homodimer. The dimerization triggers the activation of associated Jaks, leading to tyrosine phosphorylation of the distal part of gp130 including the box3 motif. (C) STATs are recruited to the phosphotyrosine-containing motif via their SH2 domains, and (D) tyrosine phosphorylated by the juxtaposed Jaks. (E) Tyrosine phosphorylated STATs then form homo or hetero-dimers via intermolecular SH2-phosphotyrosine interactions. The dimers are then fully activated by serine kinase (presumably by MAP kinase) and translocated to the nucleus, resulting in the transcriptional activation of the target genes. Although the box2 motif does not seem to be directly involved in these steps, it is critical for transmission of the signals required for growth regulation, in co-ordination with box1.

and discontinuous regions, and the structural requirements for interaction may vary between the different Jaks. Whereas the JH7-6 domains of Jak 3 were necessary and sufficient for association with the IL-2R γ chain (96), the binding of Tyk2 to IFNαR1 requires the JH7-JH3 domains (97). Moreover, the way a given Jak associates with cytoplasmic regions of cytokine receptors may depend on the respective receptor complex. The finding that Jak1, with a point mutation within its JH5 domain, lost its ability to transmit signals via gp130, but still was capable of sustaining IFN responses added credence to the claim.

Apart from being receptor-associated enzymes, Jaks may fulfill additional functions. For Tyk2, a structural role has been reported: it is necessary for surface expression of the IFNαRI receptor as well as for high-affinity binding of IFNα (98-100). Jaks also have adapter functions, since several proteins (such as Tec, Btk, Raf, SHP1, SHP2, STAM, SH2-Bb) were discovered to be associated with Jaks (101-106).

1.2.2.2 Structure and functions of STATs

STATs are proteins with a conserved structural organization (Figure 1.6). They consist of 750-850 amino acids and various domains within the STAT molecules have been defined: a tetramerization domain and a leucine-zipper-like domain at the N-terminus, a DNA-binding domain in the middle, an SH2 domain and a transactivation domain at the C-terminal end.

The SH2 domain is responsible for binding of the STATs to the tyrosine-phosphorylated receptor motifs (87,107,108) and also for homo- and hetro-dimerization with other tyrosine-phosphorylated STAT molecules (Figure 1.7) (109).

The STAT1 and STAT3 bind to pYXPQ and pYXXQ motif respectively. The SH2 domain determines the specificity of the correspondent STAT. By recombinant methods, the SH2 domain from STAT1 was inserted into STAT3. The chimaera shows the same pattern of activation through gp130 phosphotyrosine motifs as wild-type STAT1 (pYXPQ) (110). Both STAT1 and STAT3 are activated via a common signal transducer (gp130) of IL-6 family of cytokines (111). The tyrosine phosphorylation site which is essential for dimerization of STATs is located around amino acid position 700 (STAT1, tyrosine-701; STAT3, tyrosine-705) (112,113).

The dimerization of STAT is a prerequisite for DNA binding (109). The DNA binding domain of STAT is located almost in the middle of the molecule (amino acids 300-480), and its primary structure is not related to any other known protein sequence (114). Due to the highly conserved DNA binding domains, various STATs are able to bind to similar DNA elements (TTN_5AA) (115,116). The composition of the STAT dimer complex determines the sequences of the preferred DNA elements. For example, the STAT1/STAT3 dimer preferentially binds to $TTCN_3GAA$ present in the promoter regions of acute-phase-protein (APP) genes (116,117).

The activation of the C-terminal transactivation domain of STATs is at least partially regulated by a serine phosphorylation (serine-727 in STAT1 and STAT3) (Figure 1.7) (118-121). The kinase responsible for this serine phosphorylation depends on the signalling pathway and the cellular context. After growth-hormone stimulation, STAT3 is MAPK-dependently serine-phosphorylated; in contrast, after stimulation with IL-6, STAT3 is phosphorylated at the same amino acid independently from MAPK activation (122,123).

In addition to being a transcription factor, STAT1 alpha also works as a protein that may function to provide a scaffold for signaling components required for activation of the distinct Raf/MEK/MAPK signaling cascade (124). Whether this also holds true for other STATs remains to be determined.

1.2.2.3 Jaks and STATs involved in OSM signalling

Both type I and type II OSM receptors activate Jak1, Jak2, and Tyk2 receptor-associated tyrosine kinases (125,126). Which kinases are involved and to what extent a certain kinase is activated varies among cells and possibly reflects different expression levels of Jaks. In cultured human and mouse osteoblastic cells OSM induces a rapid but transient tyrosine phosphorylation of the three JAK family members tested (Jak1, Jak2, and Tyk2) (125). Whereas in U266B1 human multiple myeloma cells, OSM induces tyrosine phosphorylation and activation of Jak2, but not Jak1 or Tyk2, kinases (127).

Two members of the STAT family, STAT1 and STAT3, are the most common transcription factors for OSM signalling. Stimulated by OSM, tyrosine phosphorylated STAT1 and STAT3 could be found in the osteoblast-like human osteosarcoma cell line MG63 (128) as well as the human and mouse osteoblastic cells (125). In certain cell types, for example the A375 melanoma cell line, the type II OSM receptor can also stimulate the activation of STAT5b (126).

1.2.2.4 Receptor sequences important for Jak association

Receptor association of Jaks is thought to be mediated by the membrane-proximal box1/box2 regions that are conserved among many cytokine (Figure 1.7)

(16,89). Box1 is a proline-rich motif of eight amino acid residues essential for Jak association, whereas box2, a cluster of hydrophobic amino acid residues followed by positively charged amino acids, is necessary for Jak association only with some receptors. In the case of LIFR, the box1 region of the cytoplasmic domain is sufficient for hemopoietic cell proliferation and differentiation (129). Also, the region between the two boxes is variably important, depending on the receptor investigated.

The gp130 chain also contains box1 and box2 sequences within the membrane proximal part of the cytoplasmic region. Mutations within the box1 region reduced the ability of gp130 to associate with Jaks (36), abolished ligand-induced activation of Jak1 and Jak2 (130) and further receptor functions (16,95). The box2 also contributes to Jak-binding: studies with progressive gp130 truncations revealed a reduction of Jak2 binding (95) and abrogation of certain biological effects upon deletion of box2 (16,95). There is also a box3 motif in the cytoplasmic region of gp130 (22). Recent reports indicate that box3-derived and box3-independent signals cooperate in the control of hepatic APP genes and that box3 may be involved in the modulation of MAPK activity in gp130 signaling (131).

The LIFR and OSMR also contain box1, box2 and box3 motifs. Unlike the LIFR, the box3 motif is required for signal transduction by the OSM-specific receptor (132).

1.2.2.5 Nuclear translocation of STATs and gene regulation by STATs

STATs are activated in the cytoplasm, but they exert their function in the nucleus (Figure 1.7). Thus, after tyrosine phosphorylation, they have to be transported into the nuclear compartment. This translocation can be followed by

indirect immunofluorescence. In untreated cells both STAT1 and STAT3 are distributed evenly in the cytoplasm and the nucleus and within minutes after IL-6 stimulation both transcription factors are found preferentially in the nucleus. This translocation is transient, since after 2 hours the staining pattern is comparable with the one obtained for untreated cells (119).

The mechanism by with STATs enter the nucleus is unknown. Transport of macromolecules in and out of the nucleus is a signal-mediated and energy-dependent process (133). Proteins to be transported to the nucleus contain a so-called nuclear localization sequence (NLS), which usually is a short motif characterized by a cluster of basic amino acids. This NLS is recognized by the NLS receptor importin-α, which, together with importin-β, mediates the docking of the transported protein to cytoplasmic face of the nuclear-pore complex. The NLS-containing protein, together with the importins, is then translocated across the pore, a step that requires the GTPase Ran and GTP hydrolysis (133). Up to now only STAT1 was reported to enter the nucleus via the pattern above (134,135). All cloned STATs do not reveal a conventional NLS sequence. Thus, nuclear translocation of STATs is achieved either via an untypical NLS or via a shuttle protein that binds to activated STATs and carries an NLS. The findings about activated STAT5b (136), as well as STAT3 (137) forming a complex with NLS contained glucocorticoid receptor, seem to agree with the latter hypothesis.

1.2.2.6 Other signalling pathways for OSM signalling

Upon activation, not only Jaks and STATs, but also other downstream signalling molecules containing an SH2 domain could be recruited to gp130. These

cytoplasmic signalling molecules can themselves be activated through tyrosine phosphorylation by the juxtaposed kinase or might serve as adapters, attracting further downstream molecules. Stimulated by OSM, gp130 demonstrates the ability to recruit Shc (88), Grb2 (127) and tyrosine phosphatase 2 (SHP2) (138,139). Some of these molecules are suggested as adapters that link tyrosine-phosphorylated receptors and activation of Ras. The Ras/MAPK kinase signalling pathway is often activated following stimulation of class I cytokine receptors (Figure 1.8). The ratio of GTP-bound Ras to GDP-bound Ras has been reported to increase (140). Tyrosine phosphorylation and activation of c-Raf-1, a serine/threonine kinase that interacts with Ras-GTP, has been observed (141). Hyperphosphorylation of MAPK and up-regulation of its Ser/Thr kinase activity has also been noted (142).

SHP2 is a ubiquitously expressed tyrosine phosphatase of a molecular mass about 65 kDa. It binds to phosphotyrosine-759 of gp130 (87,143). The SHP2 can be phosphorylated by tyrosine receptor kinases as well as by cytoplasmic kinases like Src (144), bcr-abl (145) and Jaks. A Jak-SHP2 interaction and the phosphorylation of SHP2 by Jaks have been demonstrated (104). Jak1 and Jak2, but not Jak3, associate with SHP2 after overexpression in co-transfected COS-1 cells. Tyrosine residues 304 and 327 in SHP2 are phosphorylated by Jaks, and phosphorylated SHP2 can associate with the downstream adapter protein Grb2. The recruitment of Grb2 to gp130 via SHP2 enables the cross talk between the Jak/STAT pathway and the MAPK pathway. Functional analysis of gp130 in rat hepatoma cells demonstrates that SHP2 acts as a negative regulator of the Jak/STAT signaling in part by downregulating Jak activity. Overexpression of truncated SHP2 that lacks Grb2-interacting sites, but not the full-length catalytically-inactive SHP2, reduces ERK activation by IL-6, confirming the

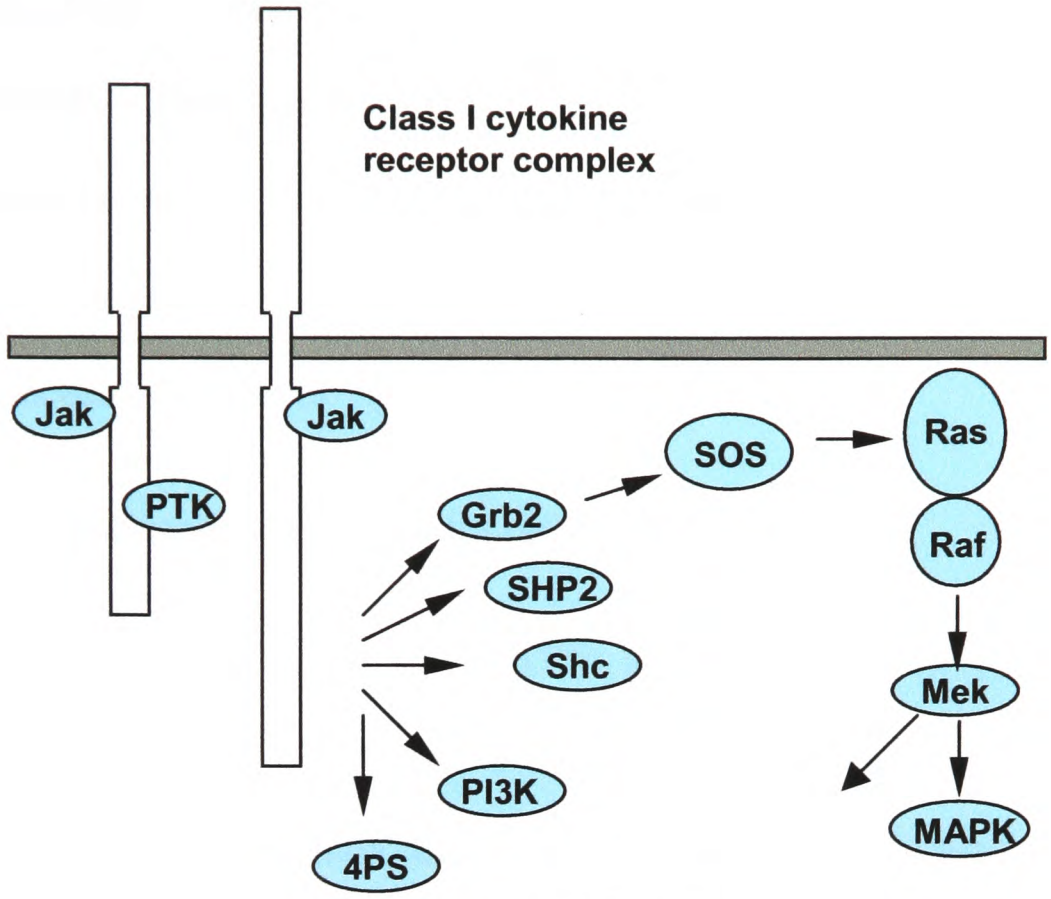

Figure 1.8: Signal pathways for class I cytokine receptors. The STAT pathway is omitted (see figure 1.7). Relevant transcription factors for this figure include NF-IL6 and c-Fos. A C-terminal part of class I cytokine receptors is suggested to be important for the activation of the Ras/MAP kinase cascade. Abbreviations: MAPK, MAP kinase; Mek, MAP kinase kinase; PTK, protein tyrosine kinase; PI3K, phosphoinositide 3'-kinase; SHP2, SH2-containing protein tyrosine phosphatase 2; Grb2, growth factor receptor bound protein 2; 4PS, insulin receptor kinase substrate 1-related protein.

signal-mediating role of SHP2. Stimulation of the c-fos, c-jun, and egr-1 genes is essentially absent in cells expressing gp130 with a Y759F mutation, which is unable to recruit SHP2. These results suggesting a dual signalling role with SHP2 acting as a phosphatase on the Jak/STAT pathway and serving as linker to the MAP kinase pathway, to regulate expression of acute-phase plasma proteins by interleukin-6 cytokine receptors in hepatic cells (139).

1.2.2.7 Regulation of the gp130/Jak/STAT pathway

Although the activation of STAT is generally transient, the mechanisms for STAT inactivation are still under investigation. Monitoring ^{35}S-labelled STAT1 illustrated that activated molecules promptly enter the nucleus and later return quantitatively to the cytoplasm as non-phosphorylated molecules (146). The finding argues for dephosphorylation as being the means of inactivating STATs. Currently, there are three groups of molecules found to be involved in the regulation of the Jak/STAT pathway. They are the protein inhibitor of activated STAT (PIAS1 and PIAS3 for STAT1 and STAT3 respectively), the suppressor-of-cytokine-signalling (SOCS) proteins and the SH2 domain-containing tyrosine phosphatase (SHP1 and SHP2) (reviewed in (147-149)). The three groups of proteins all function as negative regulators in the Jak/STAT pathway (Figure 1.9).

The studies of pituitary proopiomelanocortin (POMC) induction by LIF demonstrated the inhibitory role of SHP1 and SOCS-3. Activated by LIF, SHP1 is constitutively associated with Jak2, and LIF induces recruitment of phosphorylated STAT3 to this complex. Overexpression of wild type or dominant negative forms of SHP1 shows decreased or increased LIF-induced proopiomelanocortin promoter

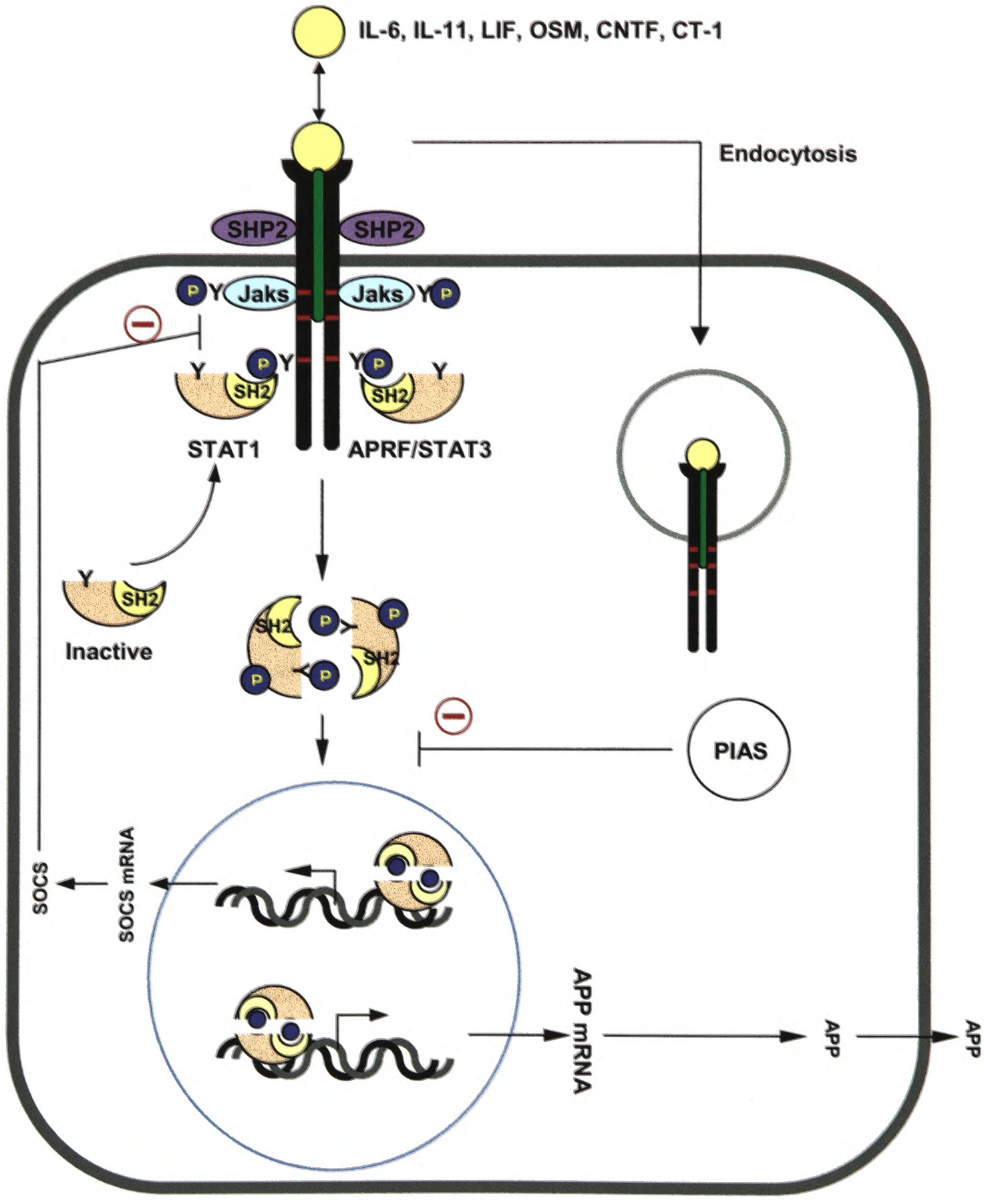

Figure 1.9: Negative regulation of the IL-6 family cytokine signal-transduction. The scheme highlights several mechanisms possibly responsible for negative regulation of signals from IL-6 family cytokines. They are receptor endocytosis, induction of feedback inhibitors (SOCS) or further inhibitory proteins like PIAS. The negative regulation of SHP2 is also included.

activity, respectively. LIF-induced Jak2 and STAT3 dephosphorylation is delayed until after 60 minutes in cells that overexpresses the mutant SHP1. SOCS-3 overexpression blocks LIF-induced Jak2 tyrosine phosphorylation, confirming a role for SOCS-3 in deactivating Jak2 by direct association (150).

PIAS3 has been discovered in various human tissues (151). This 68 kDa protein co-immunoprecipitates with tyrosine phosphorylated STAT3, but not STAT1. It also blocks DNA binding of activated STAT3 and inhibits STAT3-mediated gene activation (Figure 1.9). A similar protein (PIAS1) has been isolated for STAT1 (152). The discovery led to the speculation that there may exist specific PIAS for every STAT factor.

Cytokine receptors are not permanently located at the cell surface, but also undergo endocytosis. Mutagenesis studies of gp130 revealed that the cytoplasmic domain of gp130 contains a dileucine internalization motif that is crucial for efficient endocytosis and receptor down-regulation (153). The endocytosis is constitutive. The process is uncoupled from the Jak/STAT pathway and is not ligand-mediated (154,155). The fate of internalized gp130 is still unclear. Complexed with IL-6 and IL-6R it could be targeted to lysosomes (156).

1.2.3 Biological responses to OSM

OSM is a pleiotropic cytokine produced late in the activation cycle of T cells and macrophages. The expression of OSM can be induced by a subset of cytokines including interleukin-2 (IL-2), IL-3, and erythropoietin (EPO). Studies in HEK293 cells demonstrated that STAT5 works as a mediator for the induction of OSM. They

also revealed, in HEK293 cell, that there is a feedback modulator of STAT5, CIS (Cytokine Inducible SH2 containing protein), its expression is induced by STAT5 and it negatively modulates STAT5 activation (157). These findings indicate that CIS acts as an inhibitor for OSM expression through its ability to down-regulate STAT5 activation.

Originally discovered as an inhibitor for A375 melanoma cell growth, OSM's role in tumour cell proliferation and differentiation has been studied intensively. It is known that OSM can modulate tumour cell capacity to adhere to the matrix component (158) and up-regulate ICAM-1 expression on the melanoma cell surface which suggested a potential role for these cytokines in human immune surveillance during tumor progression (159). Apart from being an inhibitor for proliferation of breast cancer cells, OSM promotes differentiation (160,161). The response is mediated through the MEK/ERK signaling pathway (162). The same role was also assumed by OSM on anaplastic glioma cell lines (163). Studies of the H3922 breast cancer cell line suggested that the inhibitory activity is mediated predominantly through the OSM specific receptor (164). Although these reports imply a potential usage for OSM in tumour treatment, cell responses to OSM are far more complex *in vivo*. There are reports indicating that OSM has the potential to stimulate tumour growth in some instances (165). OSM also functions as a potent growth factor for AIDS-associated Kaposi's sarcoma-derived cells.

OSM's function in inflammation regulation has also drawn huge attention from many researchers. The *in vivo* effects correlate with endothelial cell expression of inflammatory cytokines and adhesion molecules, demonstrating OSM's role as a

proinflammatory mediator (166). As a proinflammatory cytokine, OSM also regulates tissue inhibitors of metalloproteinase (TIMP) expression, thus providing an important mechanism for controlling the activity of matrix metalloproteinases (167). On the other hand, studies on tissue destruction in murine models of rheumatoid arthritis and multiple sclerosis gave evidence that the *in vivo* activity of OSM is anti-inflammatory (168). OSM also reduced inflammation in animal models of human disease, including inflammatory bowel disease, antibody-induced arthritis, and experimental autoimmune encephalomyelitis (169). Taken together, the role of OSM in inflammation is still not clear. The effects may be different among different cell types.

OSM also has many other biological functions such as: bone remodelling (170), inhibition of endothelial cell growth (171), modulation of neuronal cell damage in HN-l-infected individuals (172), regulation of lymphoid tissue function and morphogenesis (173) and regulation of connective tissue collagen turnover and its localization within the rheumatoid joint (174).

1.3 Understanding the pleiotropy and redundancy of IL-6 family cytokines

The redundancy of IL6 family cytokines arises from the fact that they use gp130 as their common signalling transducer. In the case of LIF and OSM, they also use the same LIFR. Many overlapping functions between LIF and OSM, as discussed above, were the result of this receptor-sharing scheme. The fact that IL6 family cytokines use the same downstream signalling mediator also confirms the functional redundancy. The discovery that cytokine gene knock-outs in mice are not always

fatal while mice without gp130 die in embryonic stage is a good example of the benefit of functional redundancy.

Due to their ligand specific receptors, IL6 family cytokines can also exert distinct functions. Many OSM induced cell responses are mediated by an OSM specific receptor, which does not respond to LIF; for example, the proliferation and morphology of human aortic smooth muscle cells (175). The restricted expression of receptor components in different cell types also ensures the specificity of cell responses. The CNTFR alpha expression is largely limited to cells of the nervous system. This enables CNTF to utilize identical signal transducing receptor components (LIFR/gp130) in neurons that its relatives use on non-neuronal cells to elicit strikingly dissimilar responses (176). Studies on murine embryonic fibroblasts (EF), revealed that IL-6 or IL-11 in combination with their soluble receptors (sIL-6R or sIL-11R) increased dose-dependently the number of alkaline phosphatase (AP)-positive cells in 3-6-day-long cultures, which are not responsive to LIF or OSM. Unlike IL-6/slL-6R, LIF, OSM, and CNTF did not promote osteoblastic differentiation of EF cells. This pattern of specificity was accounted for by the finding that EF cells express gp130, but not the ligand-binding subunits of the IL-6 receptor nor the LIF receptor beta (177). Different receptor repertoires may be expressed at different stages of differentiation of a cell lineage (178).

Different signalling pathways can also cross talk to each other. Analysis of the signal transduction leading to activation of the MMP-1 gene revealed the presence of an OSM-responsive element (OMRE) encompassing the AP-1 binding site and the signal transducer and activator of transcription (STAT) binding element, which

mediate activation by OSM. The study indicated that cross talk between the mitogen-activated protein kinase and Jak-STAT pathways is required to achieve maximal induction of the OMRE-driven transcription by OSM (53). The discovery that different signalling pathways employ common transcription regulators such as APRF (acute phase response factor) (179) and STAT5 (180) also adds credence on the cross-talking mechanism. The cross-talk is not only limited to the signals from same family members, the response of certain stimulation is usually the integrated effect across a variety of signals.

One should keep in mind that many reported responses are from *in vitro* studies. They do not always hold up in *in vivo* conditions. More credibility should be given to results that show consistency between *in vitro* and *in vivo* studies (181). Attention also should be drawn to the fact that responses from animal models may be different from that of human cell origin. In mouse cells, only mouse OSM is capable of activating the mouse OSM receptor; human OSM instead activates the LIF receptor. Therefore, these data suggest that previous studies with human OSM in mouse systems did not elucidate the biology of OSM but, rather, reflected the biological actions of LIF (182).

Signal integration is the major theme behind cell responses to stimulation. Many signalling pathways and dozens of signalling mediators are involved in the process. Although it all seems very complicated, one can always put things into categories. Any signalling pathway can be described as three sections: the stimulator, the receptor complex and downstream mediators. The diversity of these three sections leads to the differences between different signalling pathways. As long as

this framework is kept in mind one can always find the root from all these "leaves" and "branches" of the "knowledge tree". Also we should be aware of the collaboration among signalling pathways. Then we can have a better view of the "forest".

Due to the broad involvement of OSM and its signal transduction chain gp130 in the signalling events in a variety of systems, the signalling mechanism between OSM and its receptors is of huge interest. This project is aiming to characterize the interactions between OSM and the cytokine homology region of gp130, which will serve as a starting point for studies of the multimeric functional cytokine receptor complex.

2 Quantitative techniques in protein/protein interactions

2.1 A brief overview of the different techniques used

With the recognition of the importance of large molecules such as proteins and nucleic acids in biology new tools for their study and analysis were developed. One of the most influential developments in the study of macromolecules was that of the analytical ultracentrifuge by Svedberg and his colleagues in the 1920s (183). After 75 years of refinement of the theory, as well as the instrument, the method provides a powerful and robust tool for the physicochemical characterization of biological macromolecules and of the interactions between them. This technique allows one to determine the molecular mass, density and size of polymeric substances and, in the case of heterogeneous substances, their distributions. Techniques for estimating the sedimentation or diffusion behavior have been widely used for the study of synthetic polymers, as well as biological macromolecules, with size varying between several hundreds to tens of millions of Daltons. Moreover, researchers can obtain a wide range of information about the shape, gross conformation and conformational changes of biopolymers in solution or other parameters such as subunit stoichiometry, the mechanism of assembly and disassembly of macromolecular complexes, the equilibrium constants or thermodynamic data of association reactions.

The most widely used analytical ultracentrifugation (AUC) instruments are the Beckman analytical ultracentrifuges XL-A and XL-I (Beckman Coulter, Inc.

California, USA). The XL-I has integrated Rayleigh interference and absorption optics and can offer some advantages over the pure absorption optics of the XL-A. The Rayleigh system can be applied to molecular species that do not provide a significant absorbance in the UV-visible range. The methods for quantitative characterization of the heterogeneous protein interactions include sedimentation equilibrium, tracer sedimentation equilibrium, sedimentation velocity and analytical band sedimentation. Among these methods, sedimentation equilibrium will be described in a later section (section 2.2).

The understanding of protein recognition requires information about the nature of the forces that stabilize the interaction. The thermodynamics of association can be characterized by the stoichiometry of the interaction (n), the binding constant (K), the free energy (ΔG_b^0), enthalpy (ΔH_b^0), entropy (ΔS_b^0) and heat capacity of binding (ΔC_p). Combined with structural information, the thermodynamic properties of binding can provide a complete characterization of the interaction. Isothermal titration calorimetry (ITC) provides a quantitative means for measuring the thermodynamic properties of protein/protein interactions. Currently, the most commonly used instrument is the VP-ITC MicroCalorimeter from MicroCal Inc. (Northhampton MA. USA). Based on the Wiseman isotherm theory (184), the values of the binding constant, the stoichiometry and enthalpy of binding can be determined in a single experiment. The free energy and entropy of binding are determined from the association constant. The heat capacity of binding can be measured by performing the titration at varying temperatures. Unlike other methods ITC measures the heat evolved on association of a ligand with its binding partner directly. The VP-ITC can

accurately measure heat change as low as 3-5 μCal in its 1.3ml reaction cell. A more detailed description of the technique can be found in section 2.3.

The development of Surface Plasmon Resonance (SPR) has provided an alternative technique for the studies of protein interactions. The major advantage of SPR over other interaction technologies is that the formation and breakdown of complexes can be monitored in real time, which offers the possibility of determining the mechanism and kinetic rate constants associated with a binding event. Briefly, SPR transduces the accumulation of mass at a surface into an optical signal. The ligand binding properties are quantified by first coating a sensor chip surface with the ligand and then passing one or more analyte over this surface. Anchoring ligand on a sensor chip surface enables affinity purification of the analytes and bypasses the need for complete purification of analytes in some experiments, such as activity screening during protein purification. Provided that the complex between analyte and ligand on the surface is stable, SPR can also be used to study association and dissociation of multi-molecular complexes. The studies in the thesis are performed on the BIAcore 2000 (Biacore AB, Uppsala, Sweden). The ability to measure interaction properties of biological macromolecules quantitatively across a wide range of affinities, sizes and purity makes SPR an important tool for structure-function studies.

The techniques described above can provide information about stoichiometry, kinetic rate constants, equilibrium constants and the free energy of binding. To investigate the molecular basis of an interaction, one needs structural information about the interacting system. Both NMR (nuclear magnetic resonance) and X-ray

crystallography are the main prime tools for protein structure determination. Here we describe experiments using NMR.

NMR measures the energy transitions of nuclear spins in a static magnetic field that are induced by the application of an electro-magnetic field. The energy transitions are registered as the absorbance of radiation and have characteristic frequencies depending on the nucleus. Because these frequencies are modulated by the electronic environment of the nuclei, NMR allows the monitoring of binding events with atomic resolution.

In this thesis, four techniques are applied to characterize different aspects of the biophysical properties of a protein or a protein/protein interaction. Each one of them brings particular strengths to the analysis and they are highly complementary. A brief comparison of the AUC, ITC and SPR can be found in Figure 2.1. Detailed descriptions of the techniques used are provided in following sections.

2.2 Analytical Ultracentrifugation (AUC)

As introduced above, different experimental techniques were developed for AUC studies. The following sections will concentrate on sedimentation equilibrium experiments, because it is relevant to the studies of the interactions of OSM with gp130-CHR. The theory introduced below was based on the Beckman's Introduction to Analytical Ultracentrifugation (185) and the Training guide for Optima XL-A.

More complete and fundamental description of the technique can be found in the following textbooks (186-188) and articles (189,190). A broad overview of possible applications of AUC can be found in recent reviews (191-193).

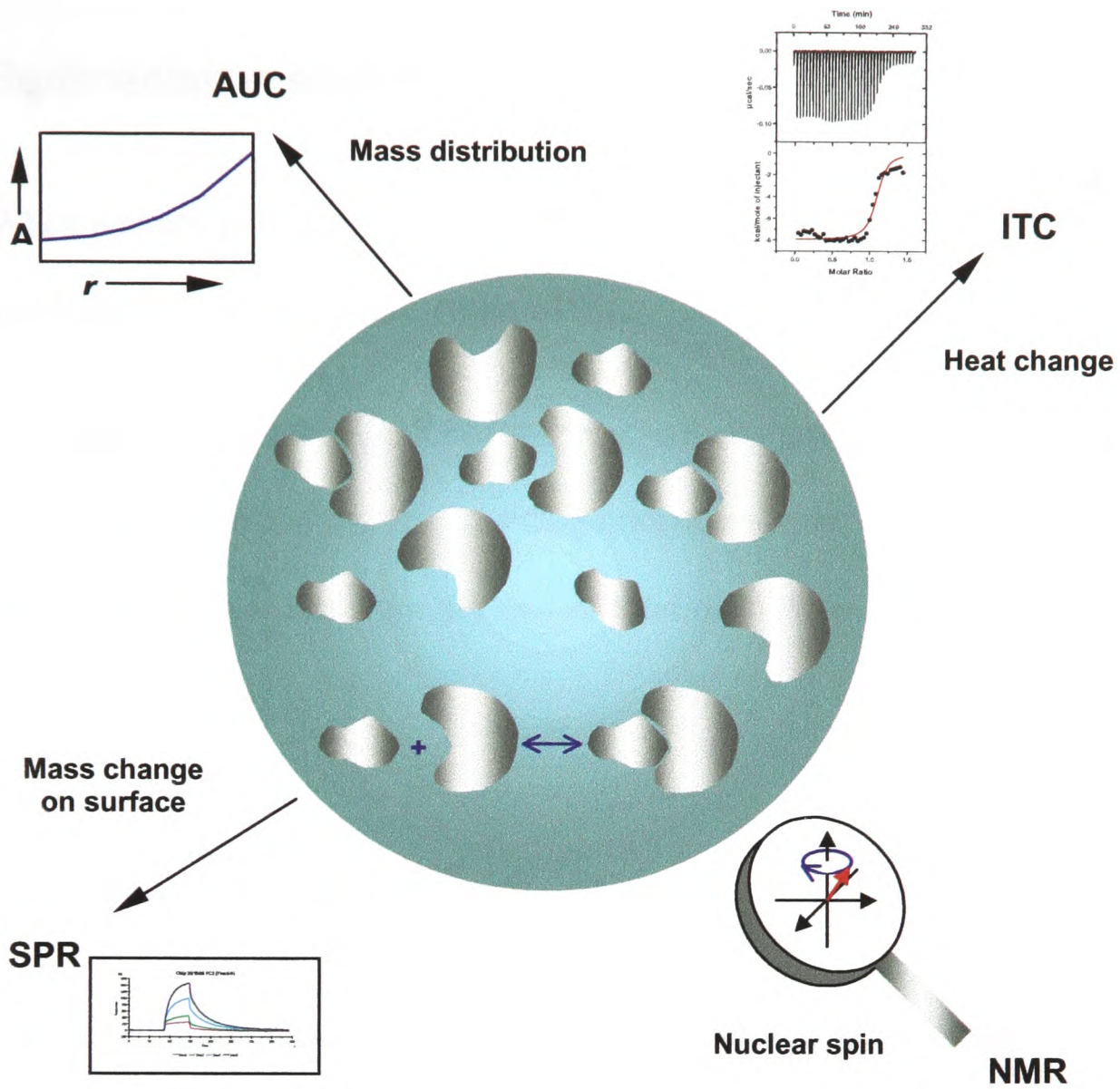

	AUC	ITC	SPR
Measured Quantity	Apparent molecular mass	Heat change upon binding	Mass change
Environment	Solution	Solution	Solution at a surface
Directly determined	M_{app},	ΔH_b^0, n, K_D	K_D, k_{on}, k_{off}
Derived Quantities	n, K_D	ΔS_b^0, ΔG_b^0, ΔC_p	ΔG_b^0
Measuring range (K_D)	10^{-3}-10^{-8} M	10^{-6}-10^{-11} M	10^{-4}-10^{-11} M
Typical experimental time	3-4 days	2-3 hours	2-3 hours
Maximum Number of samples	9	1	192

Figure 2.1: Biophysical techniques used in this work. Different aspects of the AUC, ITC and SPR are compared. The NMR studies protein or protein/protein interactions in atomic detail. Abbreviations are M_{app} (apparent molecular weight, n (binding stoichiometry), K_D (dissociation constant), k_{on} (association rate constant), k_{off} (dissociation rate constant), ΔH_b^0 (enthalpy of binding), ΔS_b^0 (entropy of binding), ΔG_b^0 (free energy of binding) and ΔC_p (heat capacity of binding)

2.2.1 Sedimentation equilibrium of a single ideal solute

When a solute particle is suspended in a solvent and subjected to a centrifugal field, three forces act on the particle (Figure 2.2).

The centrifugal force (F_s), or sedimenting force, is proportional to the mass of the particle and the acceleration. In a spinning rotor, the acceleration is determined by the distance (r) of the particle from the axis of rotation and the square of the angular velocity (ω).

$$F_s = m\omega^2 r = \frac{M}{N}\omega^2 r \qquad (1)$$

Where, m is the mass in grams of a single particle, M is the molar weight (numerically equal to the molecular weight) of the solute in g/mol and N is Avogadro's number.

The buoyant force (F_b) is equal to the weight of fluid displaced:

$$F_b = -m_0\omega^2 r \qquad (2)$$

where, m_0 is the mass of fluid displaced by the particle:

$$m_0 = mv\rho = \frac{M}{N}v\rho \qquad (3)$$

Here, v is the partial specific volume (the volume in ml that each gram of the solute occupies in solution) and ρ is the density of the solvent (g/ml). The particles will sediment as long as their density is greater than that of the solvent. As the

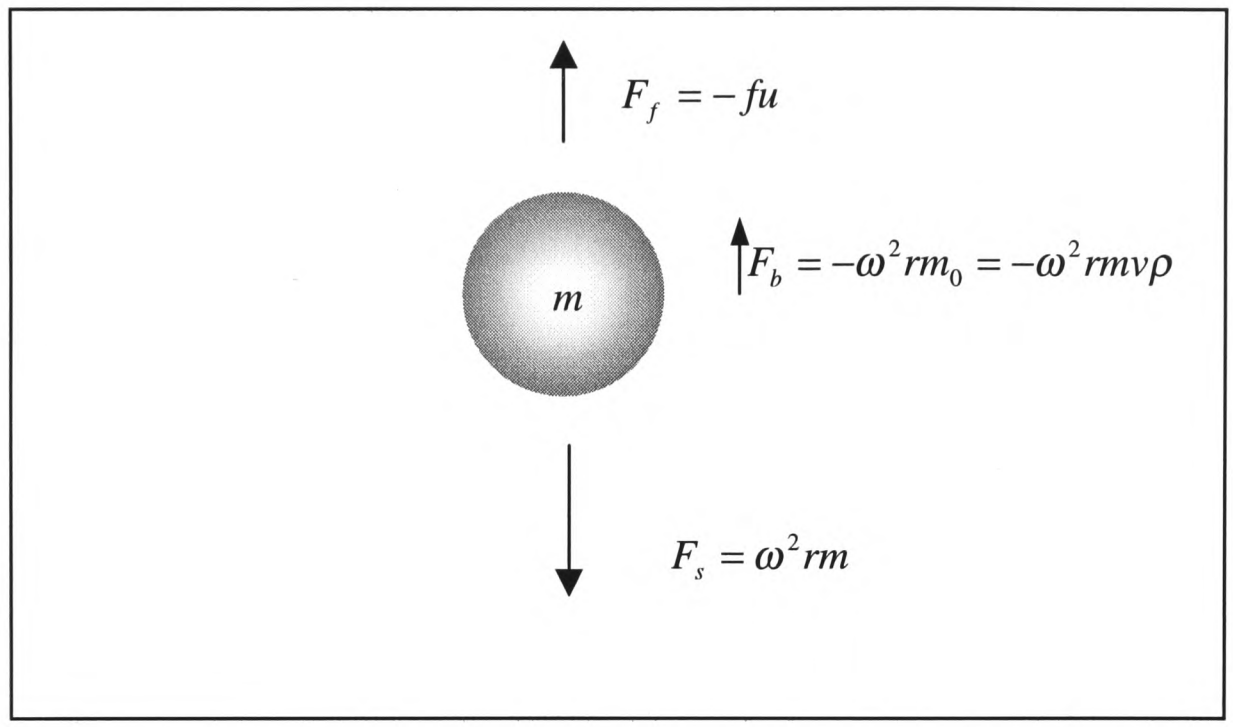

Figure 2.2: The forces acting on a solute particle in a centrifugal field.

There are three forces acting on a solute particle in a gravitational field: the centrifugal force (F_s), the buoyant force (F_b) and the frictional force (F_f). Within a very short time (usually less than 10^{-6} s) the forces come into balance. Depending on their sedimentation coefficient, different particles will move with different velocities in a given centrifugal field.

particle begins to move along a radial path towards the bottom of the sample cell, its velocity (u) will increase because of the increasing radial distance. Since particles moving through a viscous fluid experience a frictional drag that is proportional to the velocity, the particle will experience a frictional force:

$$F_f = -fu \tag{4}$$

Here, f is the frictional coefficient, which depends on the shape and size of the particle. Bulky or elongated particles experience more frictional drag than compact, smooth spherical ones. The negative signs in equations (2) and (4) indicate that these two forces act in the opposite direction to sedimentation.

The three forces come into balance within a very short time (usually less than 10^{-6} s). When the forces come into balance:

$$F_s + F_b + F_f = 0 \tag{5}$$

using equations (1), (2), (3) and (4), this gives:

$$\frac{M}{N}\omega^2 r - \frac{M}{N}v\rho\omega^2 r - fu = 0 \tag{6}$$

rearranging equation (6) gives:

$$\frac{M}{N}(1 - v\rho)\omega^2 r - fu = 0 \tag{7}$$

Collecting the terms that relate to the particle on one side, and those terms that relate to experimental conditions on the other, we obtain:

$$\frac{M(1 - v\rho)}{Nf} = \frac{u}{\omega^2 r} \equiv s \tag{8}$$

The term $u/\omega^2 r$, the velocity of the particle per unit acceleration, is called the *sedimentation coefficient*, and can be seen to depend only on the properties of the particle. In particular, it is proportional to the buoyant effective molar weight of the particle (the molar weight corrected for the effects of buoyancy) and it is inversely proportional to the frictional coefficient. Molecules with different molecular weights, or different shapes and sizes, will, in general, move with different velocities in a given centrifugal field.

The sedimentation coefficient has dimensions of seconds. For many substances, the value of s lies between 1 and 100 x 10^{-13} seconds. The Svedberg unit (abbreviation S) is defined as 10^{-13} seconds, in honour of Svedberg. For example, serum albumin has a sedimentation coefficient of 4.5 x 10^{-13} seconds or 4.5 S.

As the process of sedimentation continues, the solute begins to move toward the bottom of the centrifuge cell. As the concentration at the bottom begins to increase, the process of *diffusion* opposes that of sedimentation. After an appropriate period of time, the two opposing processes attain equilibrium in all parts of the solution column and, for a single, ideal solute component, the concentration of the solute increases exponentially towards the cell bottom. At sedimentation equilibrium, the processes of sedimentation and diffusion are balanced, the concentration distribution in the cell no longer changes with time and the distribution is a function of molecular weight. This can be described by the Lamm equation:

$$\frac{\partial C}{\partial t} = \frac{1}{r}\frac{\partial}{\partial r}\left[r \bullet D \bullet \frac{\partial C}{\partial r} - s\omega^2 r^2 C \right] = 0 \qquad \textbf{(9)}$$

Where, C is the solute concentration, t is time, r is radial distance from the center of rotation, D is the diffusion coefficient, s is the sedimentation coefficient and ω is the angular velocity of the rotor in radians/second.

Based on the Lamm equation, the distribution of a single ideal solute at sedimentation equilibrium can be described as:

$$C_r = C_F \exp[M(1-v\rho)\omega^2(r^2 - F^2)/2RT] \quad \textbf{(10)}$$

Here, C_r is the solute concentration at radius r, C_F is the solute concentration at a reference distance F, R is the gas constant (R=8.314 x 107 erg/molK) and T is the temperature in Kelvin.

Equation (10) relates the solute concentration to radial distance. Provided C_r is known in equilibrium, the buoyant molecular weight, $M(1\text{-}v\rho)$, can be estimated by least squares minimization of equation (10).

2.2.2 Sample nonideality

Rearranging Equation (10) yields:

$$\frac{d\ln(C_r)}{dr^2} = \frac{M(1-v\rho)\omega^2}{2RT} \quad \textbf{(11)}$$

Plotting $\ln(C_r)$ versus r^2 will give a line with a slope that equals $M(1\text{-}v\rho)$, the buoyant molecular weight of the sample.

Complications arise, when this plot is not a straight line. A downward curving plot, indicating that the molecular weight decreases with increasing concentration,

indicates that the solution is non-ideal, and that the molecular weight exhibits concentration dependence. An upward curving plot, on the other hand, is an indication that the sample is polydisperse. It is a mixture of molecular weights either because it is impure or because sample material has aggregated. In this case $d\ln(C_r)/dr^2$ yields an average molecular weight that, providing all the species have the same partial specific volume, gives the weight-averaged molecular weight, M_w.

If the polydispersity is caused by self-association, where aggregates are in reversible equilibrium with monomers, a weight-average molecular weight at any point in the cell will depend only on the concentration of the macrosolute at that point. Plots of M_w versus solute concentration, under different rotor speed, should all overlap within experimental errors. If, on the other hand, the polydispersity is not due to a self-association, plots of M_w and C_r at different rotor speeds will not overlap.

Nonideality can arise from the finite size of macromolecules and the charge they carry. With real solutions of a single solute, the measured molecular weight obtained from the slope of ln$c$ versus r^2 is an apparent molar weight, M_{app}:

$$M_{app} = \frac{2RT}{(1-v\rho)\omega^2} \times \frac{d(\ln c)}{dr^2} = \frac{M}{(1+cd\ln y/dc)} \qquad \textbf{(12)}$$

Where, M is the true molar weight. If the logarithm of the activity coefficient (y) is expressed as a polynomial in c (weight concentration of the sample):

$$\ln y = BMc + CMc^2 + \ldots \qquad \textbf{(13)}$$

Over a limited concentration range, such that higher order terms can be neglected, the apparent molecular weight can be approximated as follows:

$$M_{app} \approx \frac{M}{(1+BMc)} \qquad (14)$$

where, B is termed the *second virial coefficient.*

The B factor is the sum of two effects: the excluded volume which depends on the size and shape of the molecule and the charge which depends on the charge of the molecule and on the salt molarity of the solvent.

The product BM, with units of L/g of solute, is a measure of the volume of solution from which each gram of solute excludes other solute molecules. For globular proteins, the value of BM is smallest. The value of B is increased for expanded molecules that contain solvent (such as unfolded proteins), and for elongated, rod-like molecules, such as double-stranded DNA, and rigid rod-like proteins, such as myosin (194).

From equation (14) it is clear that, as the concentration approaches zero, M_{app} approaches M, the true molecular weight. The higher the concentration at which the measurement is made, the lower will be the apparent molecular weight.

2.2.3 Instrumentation

In an analytical ultracentrifuge one must be able to record the concentration distribution of the sample in the rotor cell during operation. The rotor speed and temperature also have to be accurately controlled. This ability to measure the distribution of the sample while it is spinning sets the analytical ultracentrifuge apart from preparative centrifuges.

In order to achieve rapid sedimentation and to minimize diffusion, high angular velocities may be necessary. Commercially available rotors for analytical ultracentrifuges are typically capable of rotating at speeds of 60,000 rpm. An evacuated chamber is needed to minimize frictional heating, and to minimize aerodynamic turbulence. It is important that the spinning rotor is stable and free from wobble or precession. Instability can cause convection and stirring of the cell contents, which lead to uncertainty in the concentration distribution, particularly when the concentration and concentration gradient of the solute are low.

2.2.3.1 Rotors

Rotors for analytical ultracentrifugation are capable of withstanding enormous gravitational stresses. At 60,000 rpm, a typical ultracentrifuge rotor generates a centrifugal field in the cell of about 250,000 g. Under these conditions, a mass of 1 g experiences an apparent weight of 250 Kg. The rotor should also allow the passage of light through the spinning sample, and some mechanism must be available for temperature measurement.

The Optima™ XL-A Analytical Ultracentrifuge is equipped with a four-hole rotor. One of the holes is required for the counter-balance and its reference holes provide calibration of radial distance. This leaves three positions available for sample cells. Operation with multiple cells in each position increases the number of samples that can be examined in a single experiment. This is particularly useful, for example, when several different concentration ratios of a protein ligand mixture are required for the determination of the stoichiometry of binding.

2.2.3.2 Cells

Cells for ultracentrifugation must also withstand the stresses caused by the extremely high gravitational fields, must not leak or distort, and yet must allow the passage of light through the sample so that the concentration distribution can be measured. The sample is usually contained within a cavity sandwiched between two thick windows of optical-grade quartz or sapphire. The cavity is produced in a *centerpiece* of aluminum alloy, reinforced epoxy, or a polymer known as Kel-F™. Although the double-sector centerpieces can be used for sedimentation equilibrium experiments, the six-hole centerpieces are used more frequently. User-manufactured centerpieces for special applications have also been reported (195-197). A wide range of sample concentrations can be examined through combination of various optical path-lengths and selectable wavelengths.

The six holes in a centerpiece hold three samples and their respective solvent. In sedimentation equilibrium experiments, the time required to attain equilibrium within a specified tolerance is decreased for shorter column lengths and this is one of the reasons for the preference of six-hole centerpieces over double-sector ones. For even more rapid attainment of equilibrium, shorter solution length may be used (198). Centerpieces that can hold both the solute and the solvent are essential for the measurement of absorbing components in the solvent, because they allow the user to correct redistribution of solvent components, particularly at high g values. Samples of the solution are placed in the upper three holes, and samples of the solvent in dialysis equilibrium with the solution are placed in the lower holes (Figure 2.3). The optical

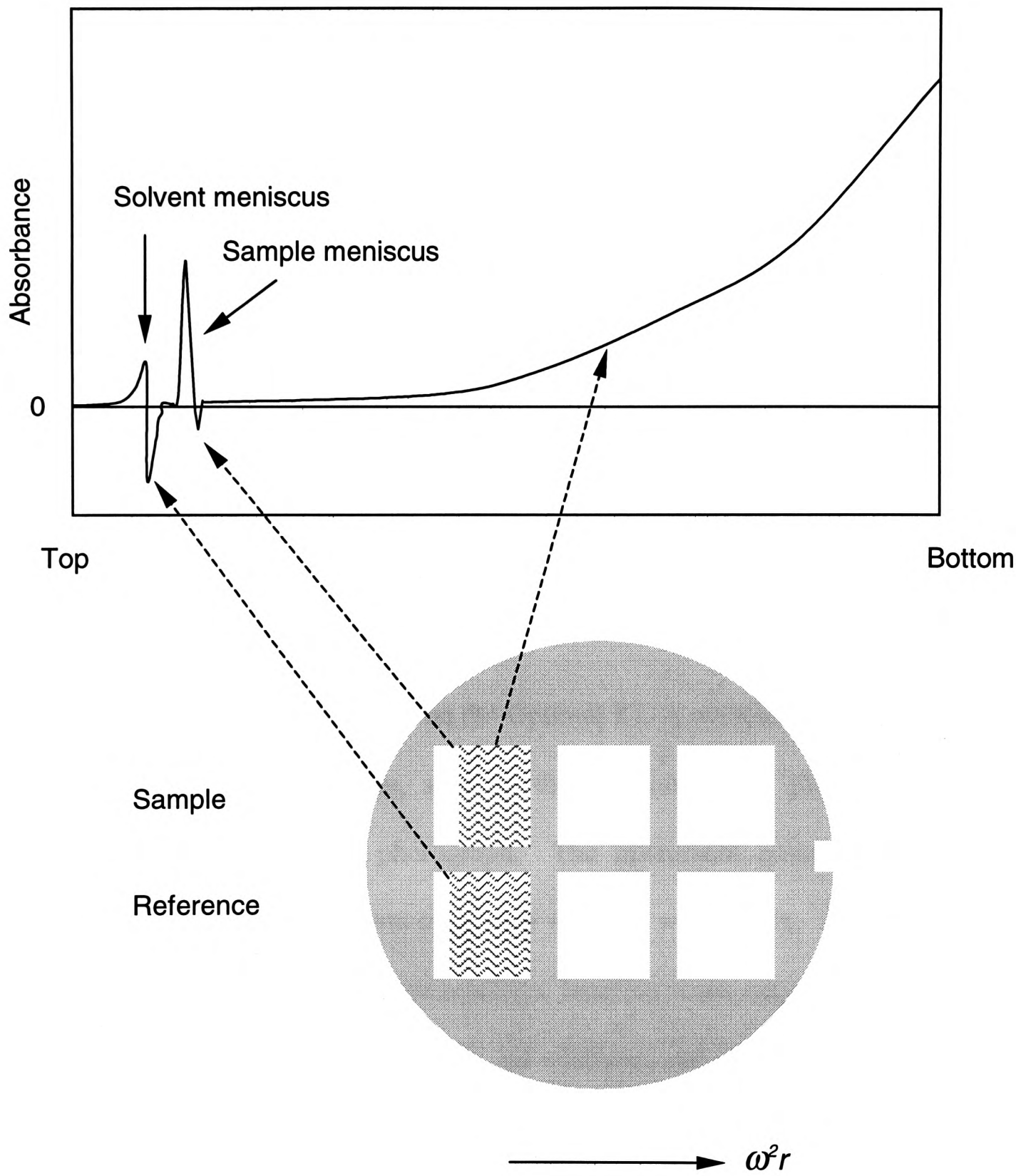

Figure 2.3: Schematic diagram of a six-hole centerpiece. The six-hole centerpiece has three sample compartments and three reference compartments. The reference compartments hold solvent in dialysis equilibrium with the sample. The reference compartments are usually filled slightly more than the sample compartments, so that the reference meniscus does not obscure the sample profile.

system measures the difference in absorbance between the sample and reference chambers in a manner similar to the operation of a double-beam spectrophotometer.

2.2.3.3 Optical system

The essential data obtained from an experiment with the analytical ultracentrifuge is a record of the concentration distribution in the sample cell. There are two means of data collection: the refractometric methods and the absorption methods. Although refractometric methods have the advantage of being able to study materials with little optical absorbance, the following text will describe the absorption optics of the Optima XL-A system.

The absorption optical system on the Optimal XL-A overcame many problems suffered by earlier optical system, such as the requirement of photography and subsequent densitometry of the photograph. The instrument possesses increased sensitivity and allows measurements on a wide range of wavelength. Because of the high reproducibility of the absorbance readings, baseline scans may be subtracted to remove the effects of oil droplets on lenses and windows, and of optical imperfections in the windows and lenses. With the absorption optics, the absolute concentration is available in principle at any point. Hence one is not restricted to a concentration difference with respect to reference points as it is the case for the refractometric optics.

The optical system of the Optima XL-A is shown in Figure 2.4. A high-intensity xenon flash lamp allows the use of wavelengths between 190 and 800 nm. The lamp is fired briefly as the selected sector passes the detector. Cells and individual sectors may be examined, with the aid of timing information from a

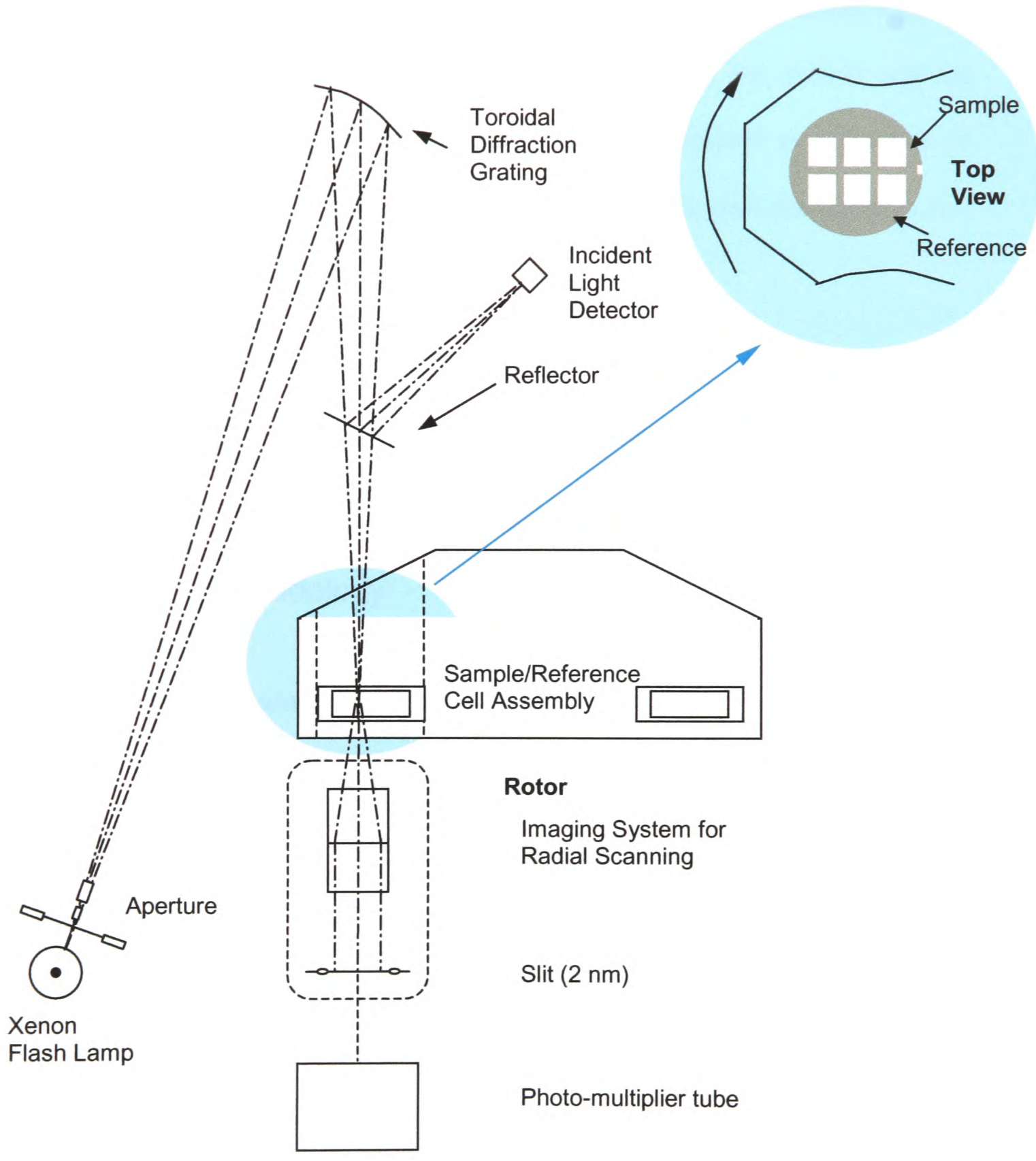

Figure 2.4: Schematic diagram of the optical system of Optima XL-A analytical ultracentrifuge.

reference magnet in the base of the rotor. The intensity of the incident light is normalized by sampling a small fraction of the incident light reflected onto a photo-multiply. The main fraction of the light is passed through the sample and the reference cell. The intensity of the transmitted light is measured as a function of radial position by using a movable slit. To minimize noise, multiple readings at a single position may be collected and averaged.

The sensitivity of the absorbance optics of Optima XL-A allows measurements at low sample concentration. This makes the examination of strong interaction ($K_A > 10^7\ M^{-1}$) possible.

2.2.4 General methodology

2.2.4.1 Sample preparation

For charged samples, a buffer and a supporting electrolyte are added to maintain a constant pH as well as to reduce nonideality effects caused by charges on the macromolecule. The presence of salts implies that the solution no longer a simple two-component system, for which most theoretical relationships have been derived. Taking the additional components into account can be a daunting task. Fortunately, Casassa and Eisenberg (199) have shown that if the macromolecular solution is dialyzed against a large excess of the buffer/salt solution, a difference measurement of the sample and the buffer may be treated as a simple two-component system. Hence, the dialyzate is required as a reference.

In choosing a buffer, preference should be given to those whose densities are near that of water, and for which the anions and cations are of comparable molecular

weight, in order to avoid excessive redistribution of buffer components. The optical absorbance of buffers should also be considered, in order to reduce background readings.

2.2.4.2 Selection of operation speed

The rotor speed of a sedimentation experiment need to be sufficiently low so that the solute concentration at the meniscus is not zero, and that the entire contents of the cell reach sedimentation equilibrium. In order to compute molecular weights, the concentration of the solute throughout the cell must be determined when equilibrium is reached. It is therefore important to know at least an approximate time to reach equilibrium, and an appropriate rotor speed. Whether equilibrium has been reached is determined experimentally. For this purpose the profiles of scans taken several hours apart are compared. If the difference between the profiles is within the noise of the data, equilibrium has been reached.

Selection of the rotor speed is based on the desired concentration difference at the meniscus and the bottom of the cell. For a 3-mm solution column and a homogeneous ideal solute, the speeds shown in Figure 2.5 shall give a concentration ratio for the meniscus and bottom of the cell of about 4. Figure 2.5 (based on the Participant's guide for AUC training from Backman) can be used to estimate an appropriate operating speed as a function of approximate molecular weight.

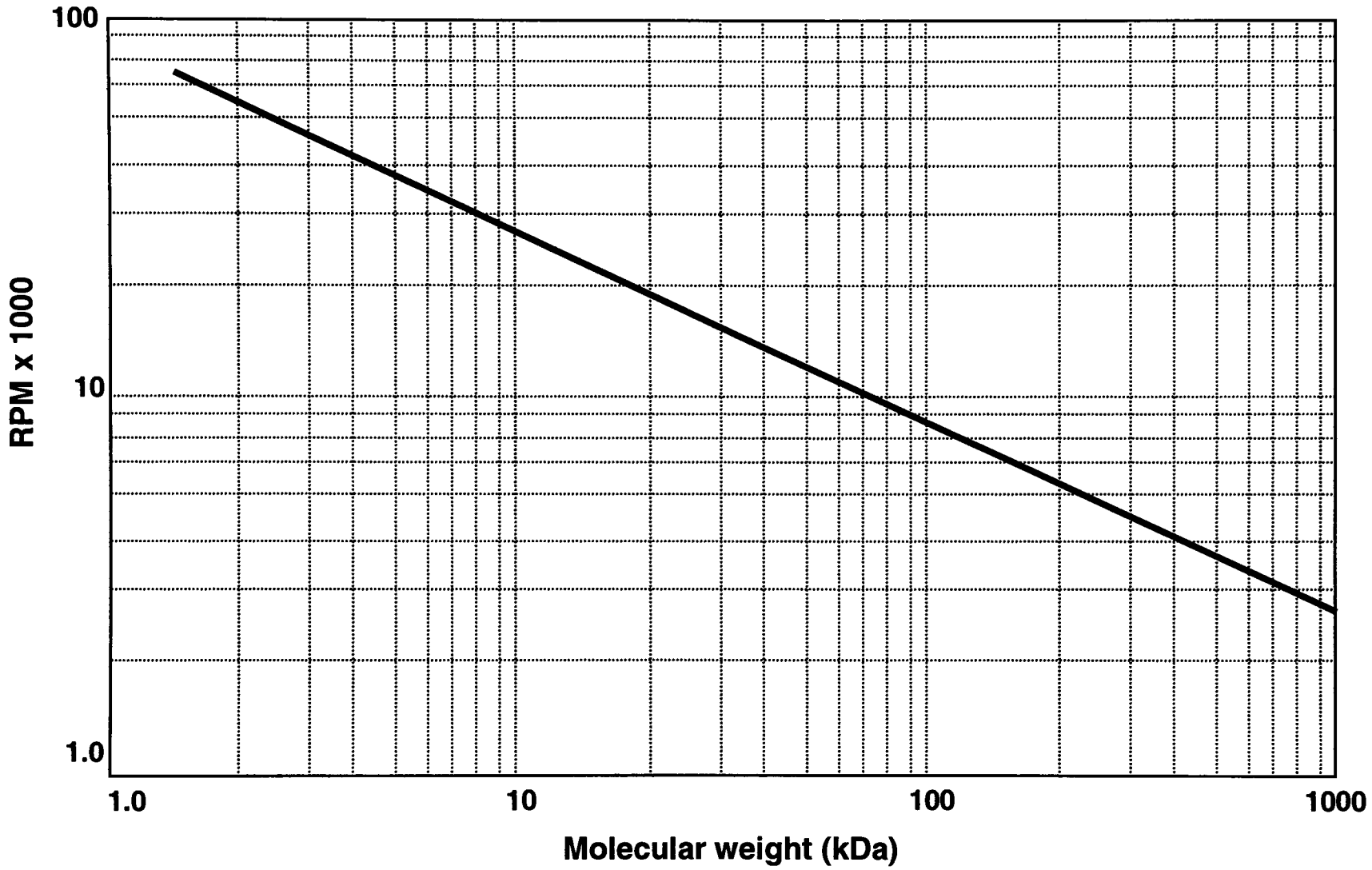

Figure 2.5: Nomogram for selecting an operating speed for a sedimentation equilibrium experiment.

2.3 Isothermal Titration Calorimetry (ITC)

2.3.1 Theory of ITC

The equations used in the following sections are based on the studies of Wiseman *et al* (184) and the user guide accompany the VP-ITC machine. A more thorough and fundamental introduction of the field can be found in the following textbook (200) and articles (184,201).

2.3.1.1 Wiseman isotherm theory

The binding of a ligand X to a single set of n identical sites on a macromolecule M, is described by the following set of equations:

$$\begin{aligned} M + X &= MX \\ MX + X &= MX_2 \\ \vdots \quad &\quad \vdots \\ MX_{n-1} + X &= MX_n \end{aligned} \tag{15}$$

The single-site binding constant, K_A, the enthalpy, ΔH_b^0, and the number of sites, n, in the set are the independent variables of thermodynamic interest. The entropy ΔS_b^0 and free energy ΔG_b^0 of binding are dependent variables, obtained from the equation below:

$$\Delta G_b^0 = -RT \ln K_A = \Delta H_b^0 - T\Delta S_b^0 \tag{16}$$

Based on the studies of Wiseman *et al* (184), a binding reaction with 1:1 stoichiometry can be described by the binding equilibrium $M + X = MX$:

with

$$K_A = \frac{[MX]}{[M][X]} \tag{17}$$

and

$$X_{tot} = [X] + [MX] \tag{18}$$

and

$$M_{tot} = [M] + [MX] = \frac{[MX]}{K_A[X]} + [MX] \tag{19}$$

where K_A is the equilibrium association constant, X_{tot} is the total (free and bound) ligand concentration, free and bound, M_{tot} is the total macromolecule concentration in the reaction cell. Equation (18) can be solved for the ligand concentration, [X] and this can then be substituted into the right hand side of equation (19), which can then be rearranged to give the quadratic equation:

$$[MX]^2 + [MX](-M_{tot} - X_{tot} - 1/K_A) + M_{tot}X_{tot} \tag{20}$$

The real root of the above equation is:

$$[MX] = \frac{-b - \sqrt{b^2 - 4c}}{2} \tag{21}$$

where

$$\begin{aligned} b &= -M_{tot} - X_{tot} - 1/K_A \\ c &= M_{tot}X_{tot} \end{aligned} \tag{22}$$

differentiation and rearrangement of equation (21) then gives:

$$\frac{d[MX]}{dX_{tot}} = \frac{1}{2} + \frac{1-(1+r)/2-X_r/2}{\sqrt{X_r^2 - 2X_r(1-r)+(1+r)^2}} \quad \textbf{(23)}$$

where r is equal to $1/(K_A M_{tot})$ and X_r is equal to X_{tot}/M_{tot}. The change in the concentration of MX can be related to the heat change by

$$dQ = d[MX] \bullet \Delta H_b^0 \bullet V_0 \quad \textbf{(24)}$$

where ΔH_b^0 is the enthalpy of binding, V_0 is the reaction cell volume and Q is the heat absorbed or evolved. Substitution of equation (24) into equation (23) then yields the final equation:

$$\frac{1}{V_0(dQ/dX_{tot})} = \Delta H_b^0 \left(\frac{1}{2} + \frac{1-(1+r)/2-X_r/2}{\sqrt{X_r^2 - 2X_r(1-r)+(1+r)^2}}\right) \quad \textbf{(25)}$$

The experimental parameter that is determined in the titration calorimeter is a finite differential heat dQ/dX_{tot}. It is clear from the equations above that this depends not on the absolute value of M_{tot} but only on its value relative to K_A and to X_{tot}.

By studying the shape of the binding curves simulated from equation (25) (Figure 2.6), it is clear that a rectangular curve of height ΔH_b^0 represents very tight binding ($K_A M_{tot} = \infty$). For moderately tight binding the product $K_A M_{tot}$, designated as c, values between 1 and 1000. The shapes of the binding isotherms are very sensitive to small changes in c values. The intercept of these curves on the ordinate is no longer exactly equal to ΔH_b^0 but this parameter is still easily obtained from the total area under the curve and its shape. Very weak binding ($c \leq 0.1$) yields a nearly

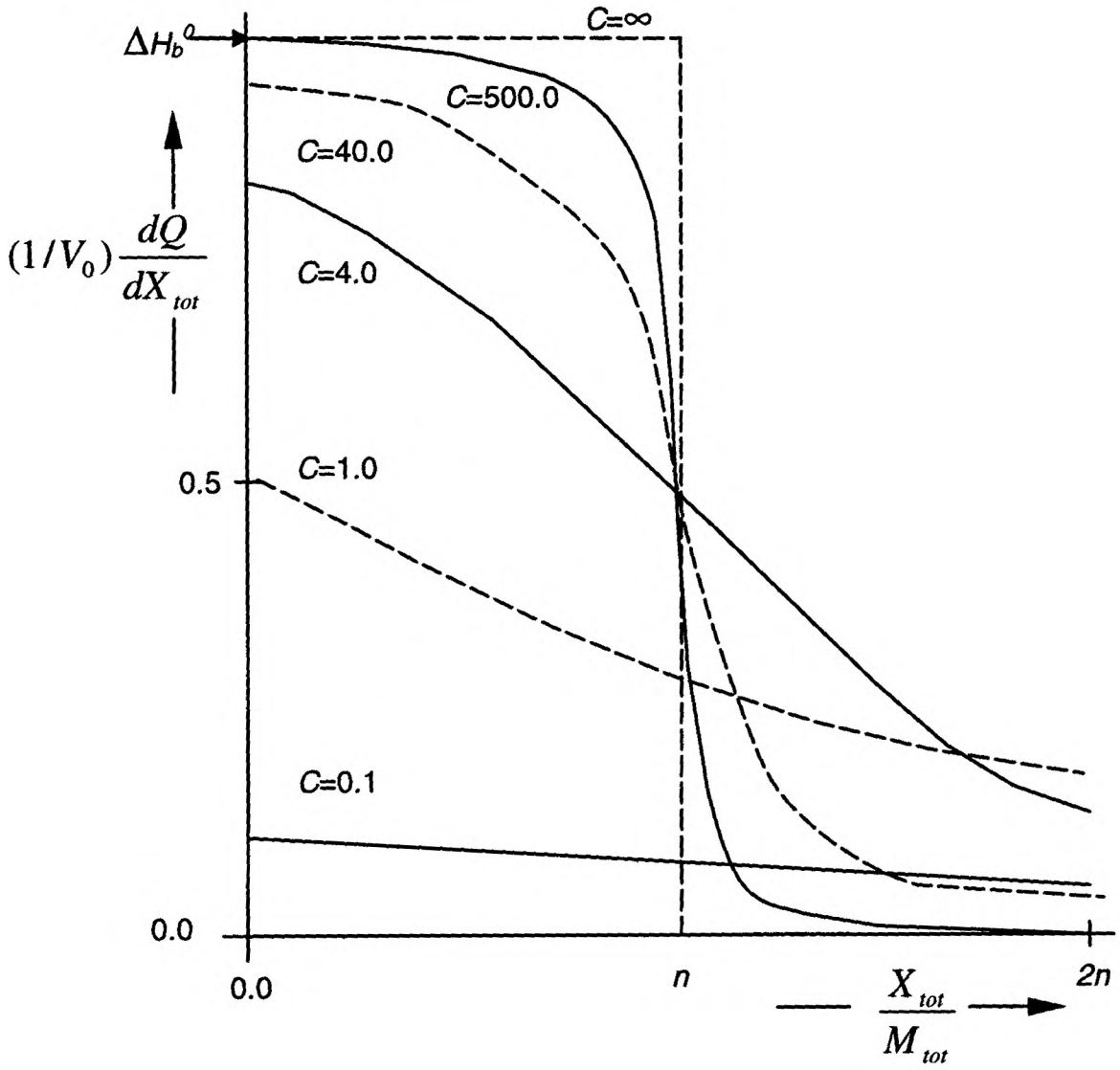

Figure 2.6: Simulated binding isotherms for a single-site interaction. The isotherms are simulated for various values of the parameter *c* (equal to $K_A M_{tot}$). It is obvious that for the *c* values between 1 and 1000 (experimental *K* window) the shape of the binding isotherms are very sensitive to small changes in *c*. For binding constant studies a value for *c* between 10 and 100 is most desirable.

horizontal trace which again, like very tight binding, provides little information of the precise value of equilibrium association constant, K_A.

In order to measure the equilibrium association constant from an isotherm, the c value needs to be in the range of 1 to 1000. This range is referred as the *experimental K window* and it is obvious that reactions with large equilibrium association constants must be studies at low macromolecule concentrations and those with small equilibrium association constants at high concentrations in order to fall within this widow. For interactions with very high K, the point will eventually be reached where the detection limit of the calorimeter precludes studying the interaction. The condition under which this occurs depends on the volume-normalized-sensitivity of the calorimeter and the enthalpy (ΔH_b^0) of the interaction.

2.3.1.2 Instrumentation

In this study, the measurements were preformed using the VP MicroCalorimetry system (abbreviated as VP-ITC) from MicrocCal Inc.

A schematic of the calorimeter cells, adiabatic shield and injector/stirrer assembly of the VP-ITC is shown in Figure 2.7. The cells are of the total-fill type, with a lollipop shape and long narrow access tubes through which samples are introduced or removed using long-needled syringes. Each cell has two heaters distributed uniformly over the outer flat surface with a special thermoelectric device (not shown) sandwiched between the two inner surfaces to measure the temperature difference ΔT_1. The temperature difference between the adiabatic shield and the outer

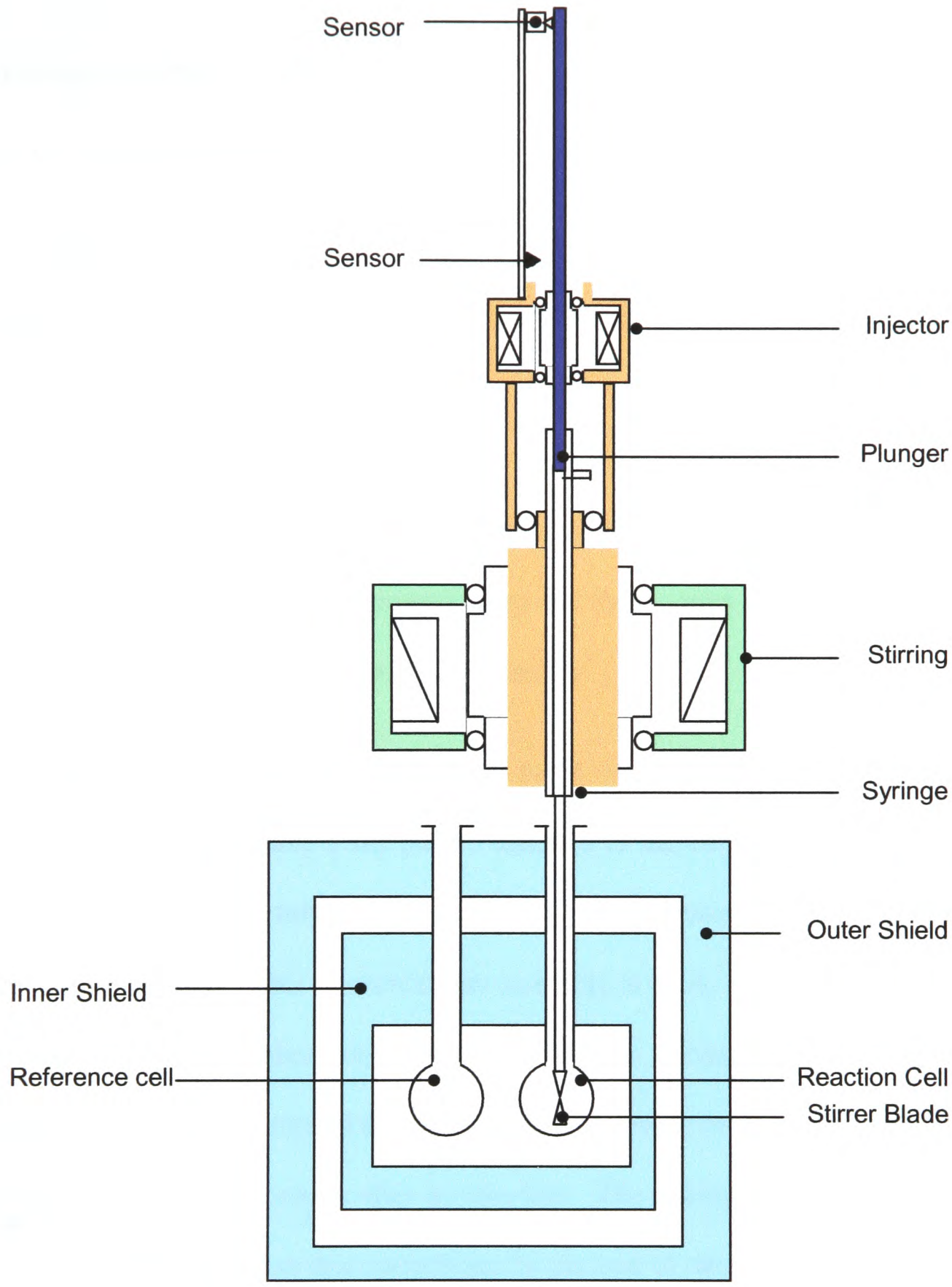

Figure 2.7: Diagram of the VP-ITC cells, adiabatic shield and injector/stirrer assembly. The adiabatic shield consists of an inner shield and an outer shield (blue colour). The injector/stirrer assembly is coloured green and brown. A stirrer blade is attached on the tip of injection needle, which helps to produce complete mixing in the cell within a few seconds after an injection.

circumference of the two cells, ΔT_2, is measured and fed to the feedback heater on the jacket to maintain its temperature very close to that of the cells.

During an experiment, a small, constant power of less that a milliwatt is dissipated in the heater of the reference cell, which activates the cell feedback circuit to maintain ΔT_1 at zero. In the absence of an interaction, the feedback power will be a constant that is resting at the baseline value. Exothermic interactions will temporarily decrease and endothermic interactions temporarily increase the feedback power. A computer is used to register experimental data and the reaction heats are obtained by integrating the deflections from the resting baseline.

The injection syringe (25-250 µl) is made of precision-bore glass and long stainless needles which have a stir paddle attached to the extreme end (Figure 2.7). The syringe is seated firmly in a low friction bearing assembly that contains an attached timing wheel. This injector/stirrer assembly is easily engaged into a loading barrel and the timing wheel coupled to a precision stirring motor. The entire assembly is continuously rotated during an experiment and produces complete mixing in the cell within a few seconds after an injection. The resting baseline is monitored while the needle is stirred so that corrections for the heat of stirring are not necessary.

The syringe plunger is coupled to a precise digital stepping motor. An injection schedule is set up with interactive software, and this schedule is carried out automatically during the experiment. All data are stored on disk for later analysis.

2.3.1.3 General methodology

2.3.1.3.1 Experimental design

In order to measure the binding constant of an interaction, the *c* value for the interaction should be kept between 10 to 100. When considering the starting concentration of the sample in reaction cell, the detection limit for the calorimeter must be taken into account. The sensitivity of VP-ITC is about 0.1 μCal. For a reliable measurement, each injection should absorb or evolve an average of at least 3-5 μ in the 1.3-ml reaction cell. The number of injections that are needed to define the total binding isotherms can be estimated from the total heat, Q, required in the reaction. If the enthalpy of binding is known, the minimum total macromolecule concentration in the reaction cell required can be estimated from the equation below

$$Q = \left|\Delta H_b^0\right| \times M_{tot} \times V \qquad \textbf{(26)}$$

Here V is the reaction cell volume (1.3 ml for VP-ITC). It should be noted that for this equation the absolute value of binding enthalpy is used. The sample concentration should be adjusted such that the product of $K_A M_{tot}$ is between 1-1000. Although any value within the range is acceptable, sample concentrations that have a *c* value between 10 and 100 are most desirable for the estimation of equilibrium binding constants.

The injection schedules are based on the consideration that complete saturation of the binding site is only achieved in the last few injections and that the

peaks are well separated by stable baseline segments. Usually, the interval between successive injections should be about several minutes.

If the stoichiometry of the interaction is not known, two injection series with the samples in the reaction cell and the syringe interchanged should be performed. A consistent result from both injection series indicates there is only one binding site (p60-61, ITC Tutorial Guide). An example of a 2:1 complex between EPOR and EPO could be found in the study of Philo *et al* (202).

2.3.1.3.2 Sample preparation

ITC sample solutions must not contain any undissolved solutes or extraneous solid material of other types. Samples are adjusted for pH and concentration and must be degassed before they are introduced into the reaction cell. This is particularly important for samples that were kept at refrigerator temperatures, because the increase of temperature could introduce air bubbles in the sample. The sample should be warmed to the preferred experimental temperature before degassing. For a typical aqueous macromolecule solution, a period of 10 minutes of degassing in the degassing station provided with the VP-ITC should be sufficient.

When running experiments at a fixed temperature, the temperature of the sample should be such that, after loading into the cell, it is at or below the experimental temperature. This will prevent a long equilibration period before the experiment can start. The temperature of the sample in the syringe has little effect on the equilibration period.

If experiments are to be carried out at different temperatures in the course of the day, it is always a good practice to start from the lowest intended temperature first.

2.3.1.3.3 Cell loading

Cell loading must be carried out with utmost care to avoid introducing air bubbles into the sample cell. The reference cell is usually filled with degassed water. The cells are filled using a long needled 2.5-ml syringe, filling the cell from the bottom of to the top. Sample should be introduced gradually. One or two rapid spurts of the last 0.25 ml of sample ensure the removal of air bubbles from the bottom of reaction cell. A small pool of sample solution must be visible over the top of the access tube to guarantee complete filling of the cell. The reference cell does not have to be refilled with each experiment.

Filled with one of the reactants, the tip of the injection syringe is immersed into the reaction cell. After stirring starts, the solutions in the cell and the syringe are allowed to equilibrate for about 30 minutes. The length of the equilibration period is determined by monitoring the temperature difference between the cell and the jacket. The injection schedule, as designed earlier based on the particular interaction, is programmed into the Origin (MicroCal, Inc. East Northampton, MA, USA) data acquisition software. It is always useful to precede the injection schedule with a small initial injection in order to clear denatured protein from the syringe tip.

2.3.1.3.4 Control experiments

Depending on the specific experiments, one or both of the following control experiments may have to be performed. First, the reaction cell filled with buffer is titrated with the ligand solution in the syringe, using the same injection schedule as used for the actual titration. This provides the heat of dilution of the ligand for each injection. In a second control experiment, the reaction cell filled with the original protein solution is titrated by the buffer or the solvent in the syringe. This control run corresponds to the heat of dilution of the protein solution.

2.3.1.4 Data analysis

In the first step of data analysis the heats of dilution are subtracted from the raw data. This can be done by the data analysis software that accompanies the VP-ITC. If the whole series of heats of dilution data is not available, the raw data can be a line that is estimated from those heats of dilution data points that were measured.

Knowledge of the precise initial concentrations of the macromolecule and the ligand is required for concentration normalization. These initial or total concentrations determine the free and bound concentrations of both the macromolecule and the ligand in the reaction cell after each injection and are also used to convert the integrated heat signal to standard molar units.

In the case of one binding site, the total ligand concentration, X_{tot} and the total macrosolute concentration, M_{tot} can be described by equation (18) and equation (19). Taking equation (17) into consideration, the concentration of the bound ligand ($[MX]$) can be written as:

$$[MX]=[M_{tot}]\times\frac{K_A[X]}{1+K_A[X]} \quad (27)$$

In an isothermal calorimetric binding experiment, the heat, Q, absorbed or evolved is proportional to the concentration of the bound ligand.

$$Q=V\Delta H_b^0[M_{tot}]\times\frac{K_A[X]}{1+K_A[X]} \quad (28)$$

The initial estimates of the equilibrium binding constant, K_A and enthalpy of binding, ΔH_b^0 can be made by fitting equation (28) to Q as function of ligand concentration, [X] data as a first approximation (203). Using the obtained equilibrium binding constant, the concentration of ligand is calculated at each point and equation (28) refitted to Q as a function of [X] and refined values of K_A and ΔH_b^0 are calculated. The iteration is continued until constant values of K_A and ΔH_b^0 are obtained.

The data analysis software utilizes the dependence of the incremental heat signal on X_{tot} / M_{tot} as described by Wiseman *et al* (184). It should be noted that the fitted curve represents the derivative of the heat, Q with respect to the ligand concentration, [X]. The ability of the method to provide incremental data points with a high signal-to-noise ratio forms the basis of its sensitivity. This rather unconventional method of data presentation provides a facile method of fitting and comparing complex binding schemes to experimental data. The determination of a binding constant requires a complete titration curve starting from zero ligand concentration to a saturating value. The protein concentration should be close to the dissociation constant (K_D=1/K_A), and the total ligand concentration at the end of each

injection should cover a large range of concentration around the dissociation constant. However, for the determination of the binding enthalpy, a single injection of a ligand concentration below the K_D value is sufficient. The isotherm curve clearly displays the upper and lower limits corresponding to the saturation of protein by ligand and vice versa. This correspondence of the upper and lower plateaus to the two saturation levels depends on whether the heat is absorbed or evolved. The enthalpy of binding can be calculated from the difference between the initial and end points of the isotherm.

2.3.2 Applications of ITC

ITC has been extensively used for obtaining association constants and measuring the thermodynamic parameters for binding reactions. In recent years, due to the development of ultra-sensitive micro-calorimeters, the thermodynamics of a variety of protein-ligand systems have been studied. Such studies have contributed a great deal to our understanding of interactions of proteins with either small molecules (204-206), DNA (207-209) and other proteins (210-213). A broad overview of the application areas of ITC can be found in following reviews (214,215).

Owing to its ability to measure the binding equilibrium directly by determining the heat evolved, ITC can be easily applied to investigate the nature of the forces that govern the interaction (216,217).

Combined with structural information, ITC can be used to identify the most important regions of the interface and the energetic contributions of binding (218-221). The relationship between the energetic and the structure has been explored for

drug design. But the complexity of this relationship does not allow in general to calculate free energy of binding for a given structure.

2.4 Surface Plasmon Resonance (SPR)

The sections below give an introduction to surface plasmon resonance (SPR) relevent to the studies in this thesis. It is based on textbooks from Biacore AB (222-224). In depth discussion of modern experiments and their analysis can also be found in some recent articles (225-229).

2.4.1 Basic Principle of SPR

At an interface between two transparent media of different refractive index, light coming from the side of higher refractive index is partly reflected and partly refracted. Above a critical angle of incidence no light is refracted across the interface and total internal reflection is observed (230). Although the incident light is totally reflected, an electromagnetic field component called the evanescent wave penetrates a short distance (of the order of one wavelength) into the medium of lower refractive index (Figure 2.8).

If the interface between the media is coated with a thin layer of metal, and the light is monochromatic polarized such that the electric vector is parallel to the plane of incidence, the intensity of the reflected light is markedly reduced at a specific incident angle (Figure 2.9). This phenomenon is caused by surface charge oscillation in the metal (plasmon) and is therefore called surface plasmon resonance (SPR). The

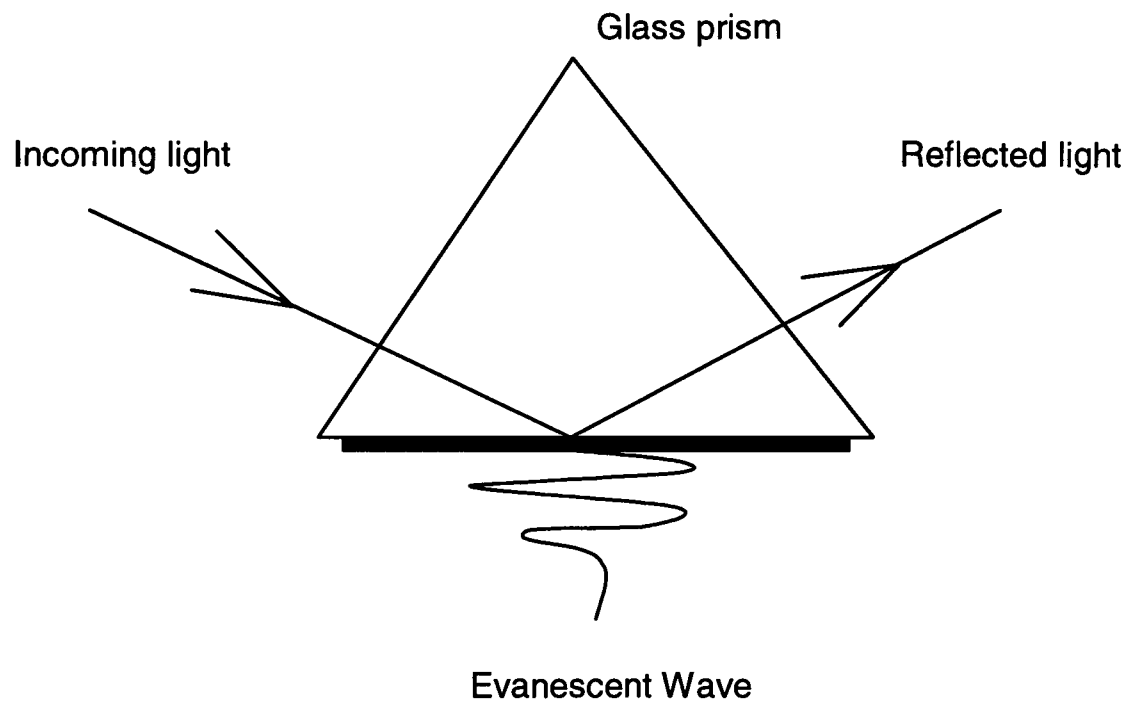

Figure 2.8: Creation of the evanescent wave. Under conditions of total internal reflection at a metal-coated interface, an evanescent wave propagates into the medium of lower refractive index on the non-illuminated side.

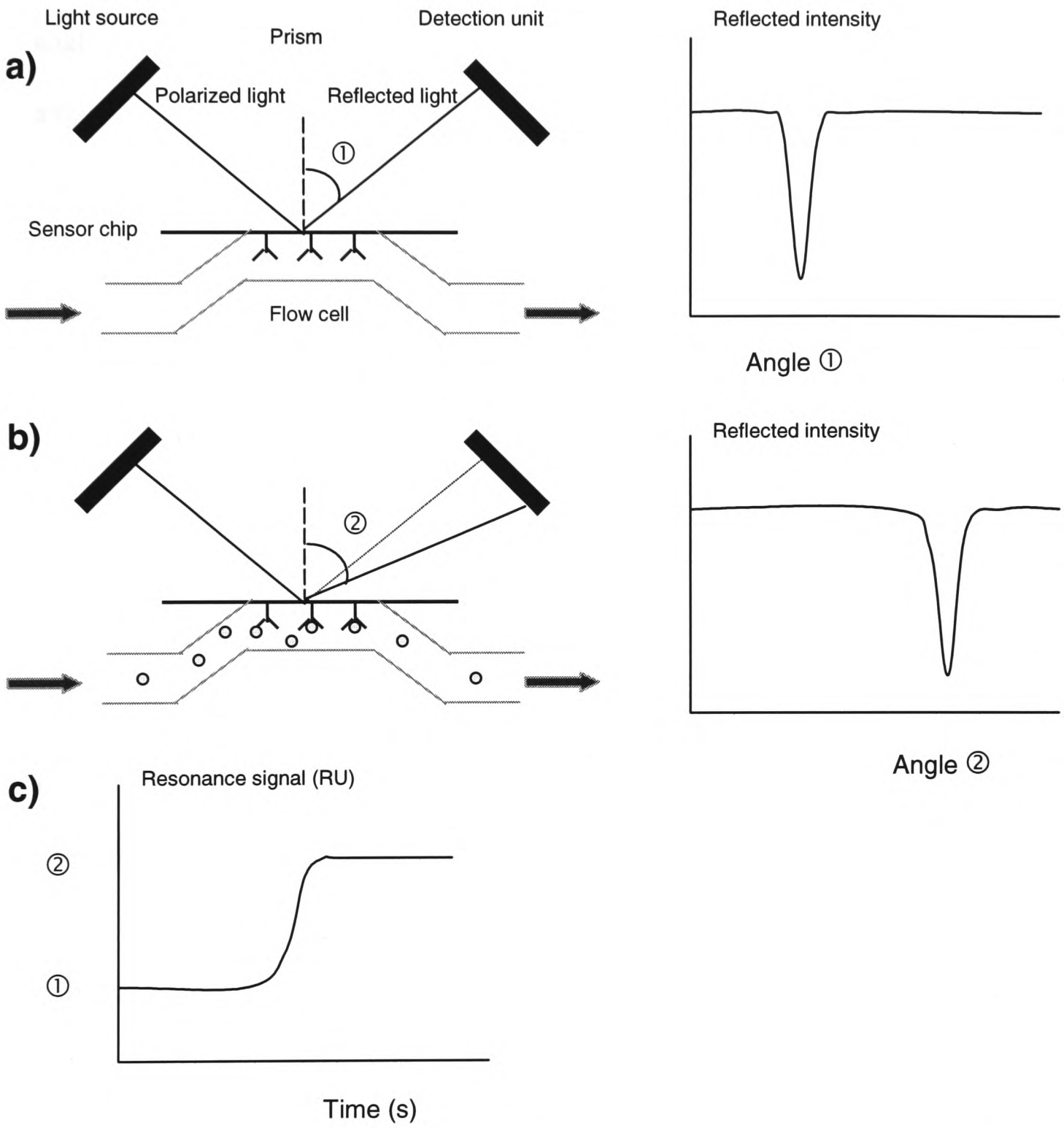

Figure 2.9: BIA detects changes in the refractive index of the surface layer of a solution in contact with the sensor chip. (a) SPR is observed as a sharp dip in reflected intensity at an angle which depends on the refractive index of the medium on the non-illuminated side of the surface. (b) The SPR angle shifts when biomolecules bind to the surface and change the refractive index of the surface layer. (c) The sensorgram is a plot of the SPR angle against time, and displays the progress of the interaction at the sensor surface.

angle of incident light at which the reduction of the intensity is observed is the SPR angle.

The SPR angle depends on three factors: the properties of the metal film, the wavelength of the incident light and the refractive index of the medium into which the evanescent wave propagates. The BIAcore instrument from Biacore AB utilizes the SPR phenomenon to monitor biomolecular interactions in real time. In the BIAcore instrument the first two factors are kept constant. Since the refractive index of the medium is affected by the surface concentration of solutes, the BIAcore instrument monitors the change of SPR angle to register the changes in surface concentration. This is illustrated in Figure 2.9, where binding of analyte shifts the SPR angle from position 1 to position 2. The distance probed from the metal film is determined by how far the evanescent wave penetrates into the solution. The wave decays exponentially with distance from the metal film, and the penetration depth is usually defined as the distance over which the wave decays to $1/e$, or about 37%, of its strength at the surface (e is the base of the natural logarithm). The BIAcore instrument has a penetration depth of about 300 nm.

2.4.2 SPR for real-time Biomolecular Interaction Analysis (BIA)

BIAcore measures changes in the concentration of molecules in a surface layer of solution in contact with the sensor surface in real time. The measurements are carried out under continuous flow of analytes over the sensor surface. As the analyte binds to the immobilized ligand, the changes of resonance angle are measured. The BIAcore has three essential components:

1. The sensor chip with a bio-specific surface where the interaction takes place.

2. The optical system responsible for generation and detection of the SPR signal.

3. The liquid handling system with precision pumps and an integrated micro-fluidic cartridge (IFC) for controlled transport of samples to the sensor surface.

The sensor chip is a glass slide coated on one side with a thin gold film, to which a flexible surface matrix is covalently attached. Bio-molecules can be immobilized to the matrix using well-defined chemistry. For sensor chip CM5 (Biacore AB, Uppsala, Sweden) the matrix consists of carboxymethylated dextran. This matrix provides a hydrophilic environment suitable for studies of molecular interactions. The linear dextran matrix behaves as a homogeneous layer of approximate thickness of 100 nm (231). The noncrosslinked nature of the dextran matrix allows minimal conformational distortion of immobilized ligand and maximum accessibility of binding epitopes. The net negative charge on the dextran at physiological pH can attract positively charged biomolecules at low ionic strength. This concentrates biomolecules in the matrix and allows effective covalent immobilization of samples even at low concentration. After immobilization, the modified matrix still carries a negative charge, which might cause non-specific binding of analyte. Using relatively high ionic strength buffers minimizes the electrostatic attraction between matrix and the biomolecules in solute, therefore physiological salt concentration (0.15 M) or higher are recommended. The dextran

matrix is chemically stable in most buffers used in biomolecular interaction studies and can be exposed to extremes of pH for short periods without deterioration (232). However, oxidizing agents and dextran hydrolyzing enzymes should be avoided. The bio-specified sensor chip can be regenerated by exposing it to conditions which dissociate the surface-bound complex without damaging the covalently attached ligand, so that one sensor chip can be used for repeated series of measurements.

The light source in BIAcore is a high-efficiency light emitting diode with a wavelength in the near infrared region (233). The light is focused on the glass-gold interface of the sensor chip in a wedge-shaped beam, giving a fixed range of incident angles. Reflected light is monitored by a fixed array of diode detectors to monitor the position of the resonance angle. The change of resonance angle is caused by the refractive index change at the interface of the sensor and the bulk phase, which is the direct consequence of the change of mass at sensor chip surface. The processed resonance angle or signal, referred to as response, R, is expressed in resonance units, RU. For proteins, a response of 1000 RU corresponds to a change in the sensor chip's surface concentration of about 1 ng/mm^2. The interpolation algorithms in the instrument software determine the resonance angle to a resolution of 0.1 RU. The sensitivity of the optical system allows measuring a mass change of about 10 pg/mm^2 (234). The high signal-to-noise ratio achieved by SPR permits detection of binding molecules as small as 200 Da. Kinetic models have been applied successfully to molecules as small as 1500 Da (235).

The integrated micro-fluidic cartridge (IFC) controls delivery of sample and buffer to the sensor chip surface. It consists of flow channels, sample loops and

pneumatic valves and flow-cells formed by pressing the IFC against the sensor chip. The rapid exchange of sample and buffer at the sensor surface and the ability to control the contact time of the sample with the surface are the advantages of the continuous flow technology used in the IFC design (233).

The BIAcore has a thermally insulated housing covering the sensor chip and most part of the IFC (including sample loops), since refractive index, reaction kinetics and mass transport of the interacting molecules from bulk solution in the flow cell to the sensor chip surface are sensitive to temperature. The temperature at the sensor chip surface can be set by the operator.

The results of a measurement using the BIAcore instrument are presented as plots of changes in the resonance signal as a function of time, termed sensorgrams. A typical sensorgram is shown in Figure 2.10. The ordinate is marked in RU. Every sensor chip has a baseline reading. The plot in the figure has already been zeroed to this baseline. The response after zeroing the baseline is called real response. The progress of the interaction is followed by observing the changes of the resonance signal, and kinetic data are extracted from the rate of change of the signal.

2.4.3 General methodology

2.4.3.1 Basic concepts

In real-time biological interaction analysis (BIA), the surface immobilized molecule is referred to as the ligand, and the molecule in free solution as the analyte. In some cases, the ligand is attached indirectly to the surface through binding to

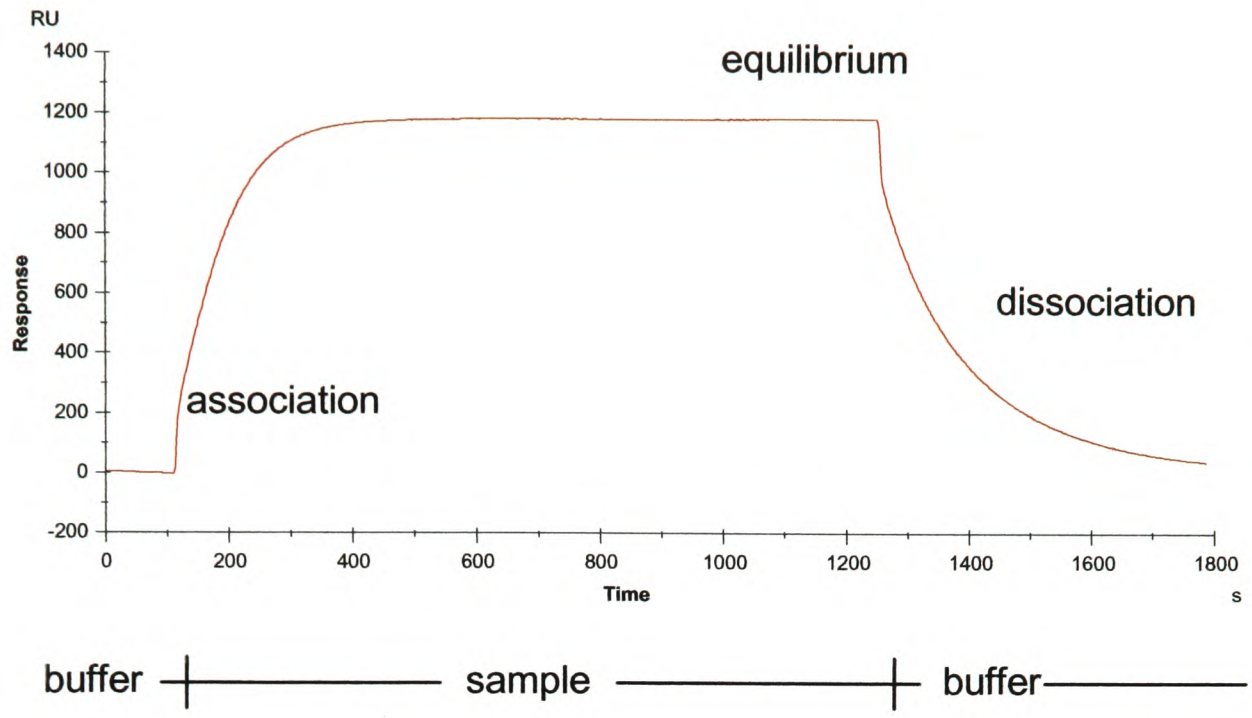

Figure 2.10: A typical sensorgram. The diagram shows association, equilibrium and dissociation phases, corresponding to an injection cycle consisting of buffer, sample and buffer

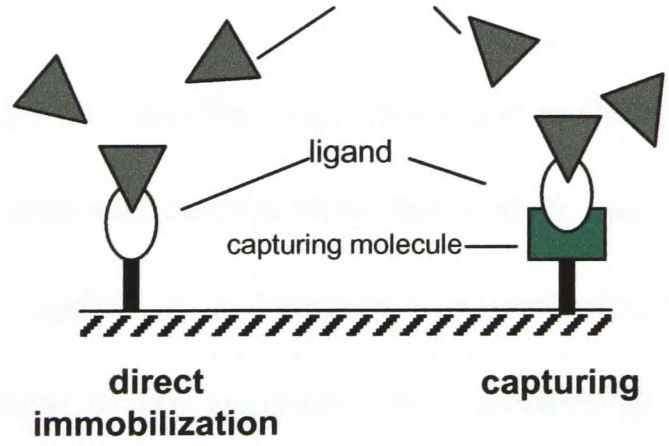

Figure 2.11: Two methods of immobilization. For a interacting system with two components, the immobilized reactant is named ligand and the other is called analyte. There are two mehtods of ligand immobilization: direct immobilization and capturing. Capturing techniques usually provide a homogenous chip surface with all the captured ligand in a well defined orientation.

another immobilized molecule. This technique is called capturing, and the immobilized molecule is the capturing molecule (Figure 2.11).

Depending on how many steps are involved in the interaction of interest, BIA methods can be divided into single- or multi-step methods. Single step methods analyze the interaction assuming one binding step. Such methods may be used in kinetic analyses and for concentration measurement of biomolecules. Multi-step methods rely on a series of binding steps to analyze the interaction. In this respect, real-time BIA has a marked advantage over many other surface interaction techniques (222,223). Each stage in the binding process can be recorded by a sensorgram. This gives unique control over intermediate binding stages. Multi-step methods are typically used to study multi-molecular complex formation in sequential binding experiments.

BIA methods can be classified into direct and indirect methods. In the direct method, the measured response derives from the analyte itself. The indirect methods rely on binding of the analyte to a competing macromolecule in the bulk solution, followed by determination of the remaining free competing molecule. Competitive binding studies using indirect methods provide an opportunity to monitor binding events in solution, since both interaction-parties are free in solution.

2.4.3.2 Ligand immobilization

Although the design of a real-time BIA experiment is dictated primarily by the purpose of the investigation, a number of properties of the system are desirable:

1. Specificity: high specificity of the ligand ensures a selective BIA method even when the bulk solution is a complex mixture.

2. Regeneration stability: the ligand should withstand conditions for regenerating the surface, so that one sensor chip flow cell can be re-used in a series of measurements.

3. Purity: the ligand should be as pure as possible to avoid non-specific binding and to provide reproducible immobilization.

4. Size: since the response is proportional to the mass of analyte bound to the surface, it is advantageous to immobilize the smaller component if possible.

Among the available immobilization methods, amine coupling is the most generally used (223,232). Amine coupling introduces N-hydroxysuccinimide esters into the surface matrix by modification of the carboxymethyl groups with a mixture of N-hydroxysuccinimide (NHS) and N-ethyl-N`-(dimethyl-aminopropyl)-carbodiimide (EDC). These esters then react spontaneously with amines and other nucleophilic groups on the ligand to form covalent links (236) (Figure 2.12). The coupling reaction requires that the amino groups on the ligand are uncharged. Amine coupling may cause surface heterogeneity, since most macromolecules have a diversity of potential attachment points.

Most macromolecules contain many groups which can participate in the amine coupling reaction and immobilization is usually easy. Other coupling techniques may however be preferable when a homogeneous ligand population is important. The

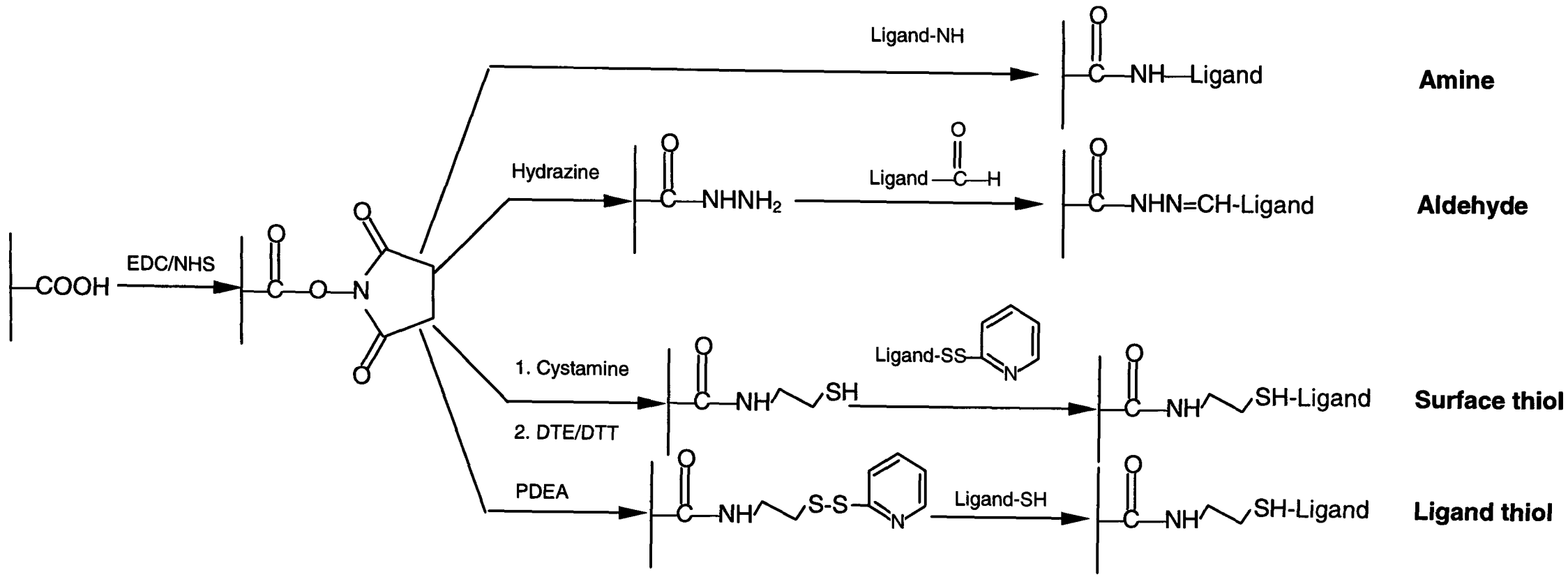

Figure 2.12: BIA coupling chemistries (222).
NHS, *N*-hydroxysuccinimide; EDC, *N*-ethyl-*N'*-(dimethylaminopropyl)-carbodiimide; DTE, dithioerythritol
PDEA, 2-(2-pyridinyldithio)-ethaneamine; DTT, dithiothreitol

capturing technique can help to create a homogeneous surface with the ligand attached in the same orientation. It may be necessary to avoid amine coupling when the ligand contains reactive amines or other nucleophilic groups at the analyte binding site. Amine coupling also has a difficulty with acidic ligands (pI < 3.5), because the ligand needs to be positively charged. The low pH requirement for charging the ligand may protonate the primary amino groups and reduce the coupling efficiency. Some of the frequently used coupling chemistries are showed in Figure 2.12.

2.4.3.3 Detection of the interaction between analyte and surface immobilized ligand

Real-time BIA registers the association and dissociation of an analyte with surface immobilized ligand by monitoring changes in resonance signal during the course of the interaction (Figure 2.10). In the association phase, the analyte is injected over the surface immobilized ligand at a constant flow rate for a defined contact time. Any mass increase on the surface, including mass of bound analyte and mass due to non-specific binding, is detected as an increase in response. When the entire surface binding site has been saturated, a steady state is obtained, which is treated here as equilibrium. At equilibrium no further increase in signal is detected as a function of time and the response level is determined by the concentration of analyte in solution. The equilibrium phase provides valuable information about affinity constants of the binding event. To obtain accurate kinetic information, a wide range of analyte concentration, within the signal to noise limitations, should be used in each experiment. The contact time and flow rate should also be adjusted to minimize overall experimental time and the effect of mass transport limitation depending on the interaction of interest.

After the injection is completed, only the running buffer will be applied to the chip surface. More and more bound analyte will be detached from the chip surface and the sensorgram shows a decrease in response. This is the dissociation phase in Figure 2.10. Ideally all the non-covalently bound material will be removed from the chip surface, allowing the baseline to return to the initial value. Due to the increase of free binding sites during the course of dissociation, some analytes may rebind to the surface. This can cause a residual signal and make the apparent dissociation rate slower than the true dissociation rate. A reduction in surface density of ligand and faster flow rates should be used to reduce this artifact (228). If the signal does not return to the baseline after reasonable buffer washing, the surface should be regenerated.

To ensure the reliability of BIA data, binding experiments should be repeated in various conditions. The maximum binding capacity of the surface should be tested in order to design a suitable analyte concentration range. Negative and positive controls are valuable additions for binding data validation. A reference surface is critical to minimize artifacts. Periodic repeated injections of analyte during the course of a series of injections can be used to monitor the integrity of the sensor surface.

2.4.3.4 Surface regeneration

Surface regeneration is intended to remove all analyte and other non-specific bound material from the chip surface. Ideally it provides the opportunity to work with identical surfaces on a series of experiments. Since regeneration conditions may damage the chip surface, the mildest possible regeneration conditions should be used.

A selection of regeneration buffers can be found in the BIAcore2000 Instrument Handbook (233).

2.4.4 Interpreting experimental data

2.4.4.1 Basic kinetic measurements

Kinetic data are interpreted in terms of a chosen interaction model, and kinetic rate constants obtained from the analysis of apparent rate constants in the context of that model. Biochemical and biophysical background knowledge of the interaction provides guidance for the choice of model. The arbitrary application of models to binding data in the calculation is strongly discouraged (237,238). Complex models should only be chosen when simple models have failed. Different experiments should be designed to test the applied model. Whenever possible, different biophysical techniques should be used to aid in the selection and validation of a model.

A homogeneous interaction with a stoichiometry of 1:1 between analyte A and an immobilized ligand B may be described by the equation:

$$A + B \underset{k_{off}}{\overset{k_{on}}{\rightleftharpoons}} AB \qquad \textbf{(29)}$$

Here, k_{on} is the association rate constant and k_{off} is the dissociation rate constant. The rate of complex formation during sample injection is given by:

$$\frac{d[AB]}{dt} = k_{on}[A][B] - k_{off}[AB] \qquad \textbf{(30)}$$

In real-time BIA, B is the immobilized ligand on the chip surface. The concentration of B, [*B*], the baseline signal and the concentration of the complex, [*AB*], are measured as the response, *R*, at time *t*. Consequently equation (30) may be expressed in terms of a SPR signal as:

$$\frac{dR}{dt} = k_{on}[A]R_{\max} - (k_{on}[A] + k_{off})R \tag{31}$$

where *dR/dt* is the rate of change of the SPR signal, [*A*] is the concentration of analyte, and R_{max} is the maximum analyte binding capacity in RU. The term (k_{on}[*A*] + k_{off}) is defined as k_s. According to this model, a plot of *dR/dt* against *R* will be a straight line with slope k_s. Plotting the values of the slope obtained at different analyte concentrations will give a line with slope k_{on} and intercept on the ordinate of k_{off}.

In the dissociation phase, the concentration of A, [*A*], is equal to zero. Hence, the equation (31) simplifies to:

$$\frac{dR}{dt} = -k_{off} R \tag{32}$$

the integrated logarithmic form of the above equation is:

$$\ln \frac{R_0}{R_t} = k_{off}(t - t_0) \tag{33}$$

A plot of ln(R_t/R_0) against t-t_0, where R_0 is the response at an arbitrary starting time t_0, will be a straight line with slope of k_{off}.

In practice, the plot of $\ln(R_t/R_0)$ against elapsed time often shows a downward curvature as dissociation progresses indicating faster dissociation at the beginning of the dissociation phase than at the end. This may reflect heterogeneity or cooperativity in the binding, or may be a result of rebinding of analyte to the ligand as the number of available ligand sites increases (223).

This 1:1 binding model, analogous to the Langmuir equation (239), treats the immobilized ligand as a solid phase component, and assumes rapid mixing of the analyte in the bulk phase with the sensor surface layer and a single binding step. One should be aware that a linear plot of that does not necessarily validate the model. Moreover, it is important to realize that agreement between the experimental data and the model equation does not necessarily indicate that the model represents the physical system. Conclusions drawn from analysis of the experimental data should always be stated within the framework of the analysis model and its limitations. Whenever possible, different biophysical techniques should be applied to evaluate the results.

2.4.4.2 Equilibrium measurements

Equilibrium constants can be measured directly by BIA as long as the interaction can reach equilibrium, which is actually a steady state, in a reasonable time. The phrase "equilibrium measurement" will still be used in this thesis to following the convention. The primary requirement for this condition to be met is that dissociation is fast.

Equilibrium constants are determined by measuring the concentrations of the free and the bound form of the components at equilibrium:

$$K_D = \frac{[A][B]}{[AB]} \tag{34}$$

$$K_A = \frac{[AB]}{[A][B]} \tag{35}$$

In equilibrium, the concentration of complex can be measured directly as the steady state response. The concentration of free analyte is equal to the concentration of the analyte injected. The concentration of free ligand on the surface can be derived from the concentration of complex, if the surface binding capacity is known. When the parameters are expressed in RU, no conversion from response to absolute surface concentration is required:

$$K_A = \frac{R_{eq}}{C(R_{\max} - R_{eq})} \tag{36}$$

where C is the analyte concentration, R_{max} is the total surface binding capacity in RU and R_{eq} is the steady state binding level in RU. Rearranging equation (36) yields:

$$\frac{R_{eq}}{C} = K_A R_{\max} - K_A R_{eq} \tag{37}$$

A plot of R_{eq}/C against R_{eq} at different analyte concentrations thus gives a straight line from which R_{max} and K_A can be calculated. This plot is analogous to a standard Scatchard plot (240).

The steady state binding response should be the absolute value of the response arising from the complexes formed. Corrections for any contribution to the response from the bulk solution have to be made. The contribution of the injected analyte to

the bulk refractive index can be determined from a sensorgram of a reference cell without immobilized ligand.

2.4.4.3 Competitive kinetics

According to which component is competed, competitive studies can be divided into surface competition (i.e. analytes compete for same ligand) and solution competition (i.e. analyte and ligand compete for a third molecule in bulk solution) (222). The situations are illustrated in Figure 2.13. Although competitive binding can be found in heterogeneous analyte kinetics, it is the deliberate use of these situations that holds more interest. Competitive analysis opens the opportunity to study interactions involving low molecular weight analytes and to determine the affinity of the interaction in solution (222,223)(Chapter 3).

In surface competition, the analyte of interest (usually with a low molecular weight) is mixed with a high molecular weight species, which competes with the analyte for binding to the ligand. Since the signal generated by the analyte is very weak, the observed sensorgram reflects almost exclusively the binding of the high molecular weight component. The influence of the analyte can be evaluated indirectly and rate constants can be derived from the data. The approach is most suitable for comparative studies, and allows rapid affinity ranking of different low molecular weight analytes that bind to the same ligand (222).

In solution competition measurements, the analyte is mixed with ligand in solution and allowed to reach equilibrium. The sample is then injected over immobilized ligand. The sensorgram can be used to estimate the concentration of free ligand in the sample, from which the affinity of the interaction in solution can be

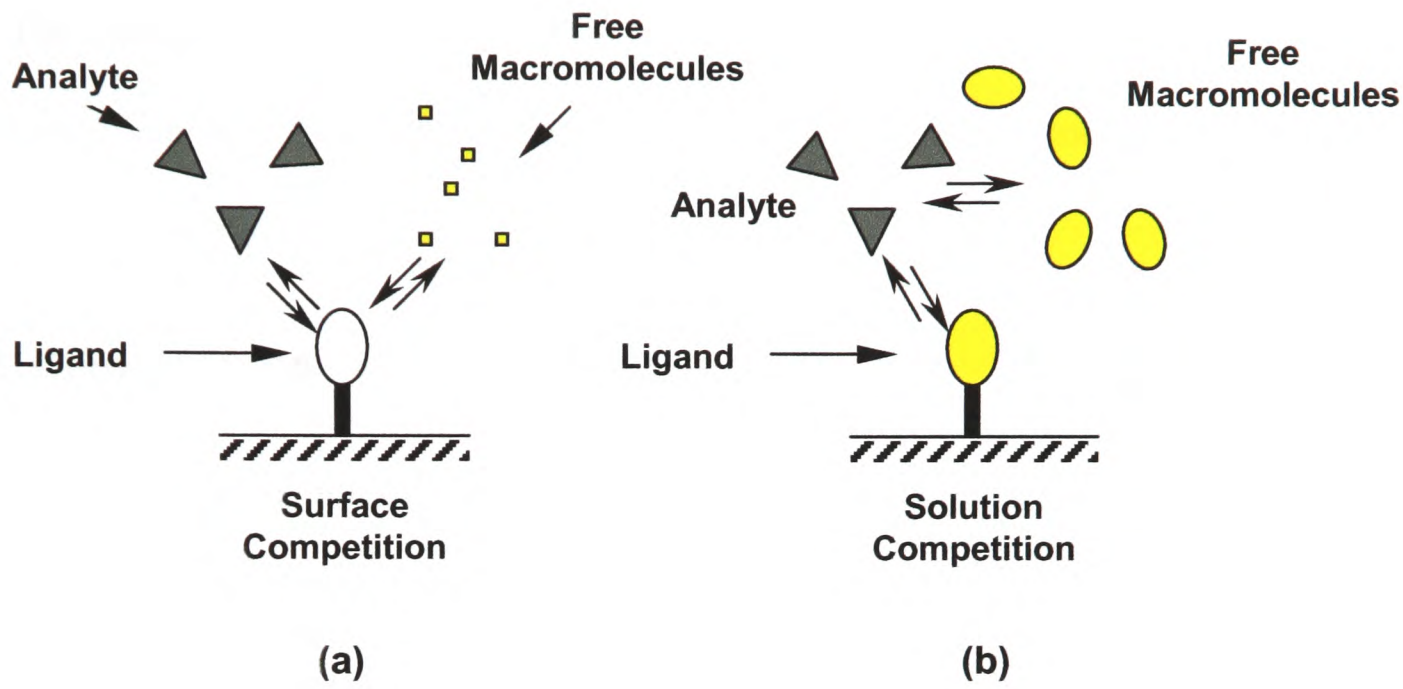

Figure 2.13: Illustrating of competitive studies. (a) Surface competition occurs when macromolecules in the bulk solution are competing with the analyte for immobilized ligand. (b) In solution competition, the macromolecules in solution can bind to the same binding site of the analyte as the immobilized ligand does.

determined (240). In order to determine the solution affinity accurately, samples with the same analyte concentration and a range of ligand concentrations are required.

The competitive studies are valid only when both competitors compete for the same binding site on the ligand and the binding of one competitor does not interfere with the binding of the other.

2.4.4.4 Complex models and artifacts

Sensorgrams that do not fit a homogeneous interaction with 1:1 stoichiometry may indicate a more complex mode of interaction or maybe due to artifacts of the measurement (232). Several frequently observed causes of deviation are discussed below:

2.4.4.4.1 Mass transport limitations

The kinetic model in equation (29) measurements assumes that the observed rate of binding reflects the interaction kinetics between analyte and ligand. In practice, mass transport of analyte to the sensor chip surface can be a limiting factor (223). To take account of this factor, the reaction should be described as:

$$A_{bulk} \underset{k_m}{\overset{k_m}{\rightleftharpoons}} A_{surface} + B \underset{k_{off}}{\overset{k_{on}}{\rightleftharpoons}} AB \qquad (38)$$

where k_m is the rate constant for mass transport to and from the surface assuming that the rate constant for mass transport is the same in both directions.

During the association phase, if the mass transport is much faster than association of analyte with ligand, the observed binding will be governed by the

kinetics between analyte and ligand. On the contrary, if mass transport is slower than association, the mass transport process will limit the binding and the apparent on rate will be slower than the true on rate k_{on} (226,239).

During the dissociation phase, analyte molecules removed from the surface by dissociation can either be transported to the bulk solution or rebind to free ligand sites on the surface. The observed dissociation rate is the result of competition between these two processes, and will reflect the dissociation rate constant only when mass transport is fast compared to rebinding. Including free ligand in the buffer used during the dissociation phase can reduce the mass transport limitations during dissociation (223). Free ligand in the buffer competes with immobilized ligand and creates an apparent reduction in surface binding site concentration.

For a given analyte and given flow cell dimensions, two factors can have significant effects on mass transport limitations: the flow rate and the concentration of surface binding sites (232). Since the rate constant for mass transport, k_m, is proportional to the cube root of the flow rate, the surface binding site concentration shows a greater effect on k_m. The same factors, which control mass transport limitations during association, also apply during dissociation. The limitation is most pronounced when the concentration of free ligand sites is highest, at the beginning of association and at the end of dissociation. The mass transport rate is also influenced by the diffusion coefficient of the analyte, which in turn depends on the molecular weight. A large analyte has a low diffusion coefficient, and the experiments will be more susceptible to mass transport limitations.

When mass transport is limiting, the plots of *dR/dt* versus *R* or ln (R_1-R_t) against t-t_1 curve downwards instead of being linear. It is important to be aware, however, that downward curvature in the plots can also be caused by heterogeneity in either ligand or analyte (222,223). Experiments running under different flow rates and surface immobilization levels can be used to study mass transport limitations. A method that detects solution interaction can also eliminate the problems from mass transport limitation, which is arisen with surface binding studies. Ligand heterogeneity will be discussed in following section.

2.4.4.4.2 Heterogeneous ligands

If ligands with more than one binding constant are present on the same surface, the observed sensorgram is, in principle, the sum of two or more independent sensorgrams, one for each ligand species. For the association phase, the plot of *dR/dt* over *R* is usually non-linear, although linear regions may be apparent where one of the kinetic components is dominant. In dissociation phase, the dissociation plot curves downward indicating non-identical dissociation rates. The possibility of parallel, non-equal interactions can be tested by varying the analyte concentrations. At low concentrations, the binding will be dominated by the high affinity sites, whereas at high concentrations, the low affinity process will become more evident.

Ligand heterogeneity may be caused by either the heterogeneity of the starting material or may be created during the immobilization process. For the latter, the heterogeneity may be avoided by using selective immobilization chemistry or employing a specific capturing method (222,223).

2.4.4.4.3 Linked interactions

Linked interactions arise from the association of additional analyte after the initial complex is formed or from a change of affinity arising from a conformational change induced by the initial binding (232). Since the equilibrium between bound and free analyte changes with time, a bivalent model (224) will not be appropriate. Linear transformations of *dR/dt* (see section 2.4.4.1) may deviate from straight lines. In these circumstances, a sensorgram should be interpreted by using appropriate models (237,241).

2.4.4.4.4 Avidity effects with multivalent analytes

Multivalent analytes such as antibodies will bind with different affinities depending on the number of sites that participate in ligand binding. If the ligand, antigen in this case, is monomeric, the complexity can be overcome by immobilizing the antibody to the chip surface (242).

2.4.5 BIA application areas

The BIA techniques have been applied to different areas, such as the studies of protein/protein interactions and protein/DNA binding. The following section will use examples to demonstrate how BIA could be applied in cytokine receptor interaction studies. A detailed description of a range of applications of BIA can be found in recent reviews (232,235).

Generally, the BIAcore instrument is a versatile tool to address a variety of questions:

- The instrument provides a convenient way of screening binding activities from samples without the need for labeling and with minimum pre-purification.

- The on and off rate of binding can be determined from the association and dissociation phases of a sensorgram. Equilibrium constants can be calculated from rate constants or equilibrium measurements.

- Binding of an analyte to a ligand can be monitored in the presence of a preexisting complex or between a preexisting analyte complex and an immobilized ligand.

- The relative binding affinities and rate constants of a series of analytes can be evaluated.

- Binding sites can be mapped in structural terms by testing the ability of analogues or fragments of one interactant to inhibit the binding of another.

Although qualitative analysis of binding data may suffice to determine whether a specific interaction has occurred, quantitative answers usually demand multiple data sets from different experimental designs and comprehensive data analysis based on various interaction models.

Some recent examples of BIA with cytokine receptor systems are given below. In the study of the interaction of human IFNαR2 with IFNα2 (243), BIA was used to screen the binding activity, measure binding kinetics and map binding sites by mutational analysis. BIA, as a means to measure binding kinetics, has also been used successfully in cytokine targetting of tumors (244), evaluating binding characteristics of the human IFNγ receptor (245) and the binding characteristics of IL-13 with its

receptor (246). Other examples of binding site mapping can be found in studies of: production and characterization of anti-human IFNγ receptor antibody fragments (247), mapping of monoclonal antibody- and receptor-binding domains on human GM-CSF (248), functional epitope mapping of human IL-1 beta (249) and characterization of a humanized mAb for human IL-5 (250). BIA provides a rapid and accurate binding activity screen. In this case the sample does not have to be pre-purified. For example, whole-cell lysates have been used for studying the interaction of IFNγ induced signaling events (251).

Due to the complexity of the cytokine receptor complexes, cell-based assays provide only limited quantitative information on their binding characteristics. BIA promises to be a powerful technique for the quantitative analysis of complex receptor systems, since individual stages of the complex formation can be monitored in terms of both kinetics and affinity. The study on the IL-2 receptor complex provides a good example of using BIA for functional studies involving a multi-molecular complex (252,253).

2.5 Nuclear Magnetic Resonance (NMR)

Nuclear magnetic resonance (NMR) spectroscopy is a powerful analytical technique with many applications. A detailed description of the theory is outside the scope of this thesis. This section intends to introduce only the concepts important for this study in particular the chemical shift. More thorough and fundamental introductions to the field can be found in many excellent textbooks (254-257).

Descriptions of modern experiments and their analysis can also be found in numerous publications (257-260).

2.5.1 The principle of NMR

Like electrical charge and mass, spin is a fundamental physical property of particles. A nucleus with spin I can assume 2I+1 spin-states. Since a magnetic moment is associated with spin, the different spin-states develop different energies, when placed in a magnetic field. Transitions between spin-states are caused by energy changes of the particle. If exposed to a radio-frequency electromagnetic field, the spin of particle can perform a transition from a lower energy state to a higher one by absorbing a photon, provided it has an energy that matches the energy difference between the two states. In NMR, the frequency of the photon absorbed is called the resonance frequency for that transition. Since the exact frequency of the photon absorbed depends on the electronic environment of the nucleus, the NMR spectrum of a compound can give information about the local environment of the nucleus.

Most elements found in bio-molecules have at least one isotope with spin (e.g. ^{1}H, ^{15}N, ^{13}C). Since the natural abundance of ^{15}N and ^{13}C are very low, bio-molecules are usually artificially enriched (labelled) with those isotopes before subjecting them to NMR studies involving nitrogen or carbon nuclei. Some NMR experiments take advantage of isotope labelling to reduce the complexity of the resulting spectrum.

2.5.1.1 Chemical shift

The local electron density influences the strength of the effective magnetic field at the nucleus and as a consequence modifies the resonant frequency. This

change in resonance frequency is termed the chemical shift. The observed shift is directly proportional to the applied field strength. Since the chemical shift correlates to the chemical environment of a nucleus, it can provide valuable structural information.

2.5.1.2 Scalar coupling

Electrons that are shared between nuclei also effect on the spin-states of the nuclei. The overlapping electron orbitals in chemical bonds of adjacent nuclei couple the nuclei and allow the transfers of magnetization through bonds. This is the so-called scalar coupling. The magnitude of the scalar coupling decreases as the number of connecting bonds increases. In macromolecules, scalar coupling over more than three bonds are usually too small to be observable.

Scalar coupling causes splitting of resonance lines. The difference in resonance frequency between the lines is called the coupling constant (^nJ, where n is the number of bonds between the coupled nuclei) and usually given in Hertz (Hz). The coupling constant is independent of the strength of the magnetic field.

Scalar coupling provides information of through-bond connectivity of nuclei in a bio-molecule. In many NMR experiments, magnetization initially generated on one nucleus is transferred via chemical bonds to other nuclei by means of scalar couplings. The dependence of the $3J$ couplings on the dihedral angle defined the 3 bonds is used to obtain structural information.

2.5.1.3 Dipolar coupling and nuclear Overhauser effect (NOE)

The magnetic moments associated with nuclear spins interact with each other through space. This through-space interaction of spins is called dipolar coupling. Rapid random fluctuation of a spin pair with a dipolar interaction caused by molecular motion gives rise to the nuclear Overhauser effect (NOE). Because of the strong distance dependency of the NOE, only spin pairs that are close in space (~ 5 Å) can be observed. The NOE provides information about through-space connectivity, which is the main source of information for the determination of a three dimensional structure of a macromolecule by solution NMR.

2.5.2 NMR of protein

Because of its high gyromagnetic ratio and natural abundance, the ^{1}H-nucleus is the nucleus of choice for solution NMR of proteins. Other nuclei (e.g. ^{2}H, ^{15}N and ^{13}C) are often used to edit proton spectra to give more information and better resolution. Since the resonance frequency of a nucleus in a molecule depends on its local electronic environment, similar environment e.g. those for amide protons, aliphatic or aromatic side-chains produce resonances with similar chemical shift.

In addition a protein contains a large number of ^{1}H-nuclei and this causes severe overlap of signals in one-dimensional ^{1}H-NMR spectra. Each peak in the spectrum could arise from a large number of ^{1}H-nuclei. With the increasing size of a protein, the number of resonances in the limited chemical shift range increases and it becomes increasingly difficult to assign the individual signals unambiguously.

The problem of overlap can be reduced by introducing higher dimensional spectra (two, three and four dimensions). While the number of nuclei remains the same, the experiments are designed to only show correlation between nuclei (259). E.g. in an NOE experiment only nuclei close in space produce a cross peak while in a through bond correlation spectrum only nuclei connected by certain number of bonds are observed.

Two-dimensional (2D) NMR was emerged from an idea of the Belgian physicist Jeener (261). Two-dimensional NMR spectra reveal the connectivity between nuclei. They are displayed as two frequency axes and absorbance peaks occur at the intersection of the frequencies of the nuclei that are linked by the connectivity. A 2D NMR experiment can be divided into four periods: preparation, evolution (t_1), mixing time and detection (t_2). In the preparation period the initial state (typically equilibrium magnetization) is generated. During the evolution period the modulation of signal amplitude and phase is recorded. Mixing is arranged such that the magnetization which evolved with some frequency during t_1 (frequency labelling) evolves with a different frequency during t_2. The resulting magnetization is recorded during the detection period (t_2). For a heteronuclear 2D NMR experiment, e.g. heteronuclear single-quantum correlation (HSQC), the proton resonances are spread out according to the shifts of the heteronuclei to which they are coupled. For example, an HSQC experiment on a ^{15}N labelled protein sample resolves the NH resonances along the ^{15}N dimension.

2.5.3 NMR spectroscopy of ligand receptor binding site mapping in solution

When a ligand and its receptor form a complex, the local chemical environment of the nucleus in the binding site will change (Figure 2.14). Thus, the binding site can be mapped by comparing the chemical shifts of the free and bound state. This is the rationale behind our study of the binding site of the interaction between OSM and gp130-CHR using NMR.

The ^{1}H spectrum of the complex with all isotopes at natural abundance contains resonances arising from both ligand and receptor. With a 47 kDa complex (e.g. OSM187/gp130-CHR), it is impossible to distinguish the signals arising from the ligand from those originating from the receptor. The spectra can be simplified by isotope editing techniques using labelled ligand or receptor. In our case the OSM187 was uniformly labelled with ^{15}N. By applying a ^{15}N edited pulse sequence, resonances from labelled OSM187 can be selectively recorded. The resonances from unlabelled gp130-CHR are not detected. Hence the resulting spectra are vastly simplified.

NMR structural studies rely on the ability to acquire high-quality NMR spectra with good sensitivity and spectral resolution. With the increase in molecular weight, these basic requirements are harder to satisfy. Conventional NMR techniques are rarely capable of structural characterization of proteins bigger than 35 kDa (262). A ligand receptor complex usually exceeds this size limitation of NMR. The recent development of TROSY (transverse relaxation-optimized spectroscopy) (263) techniques greatly increases the size of molecule that can be studied by NMR.

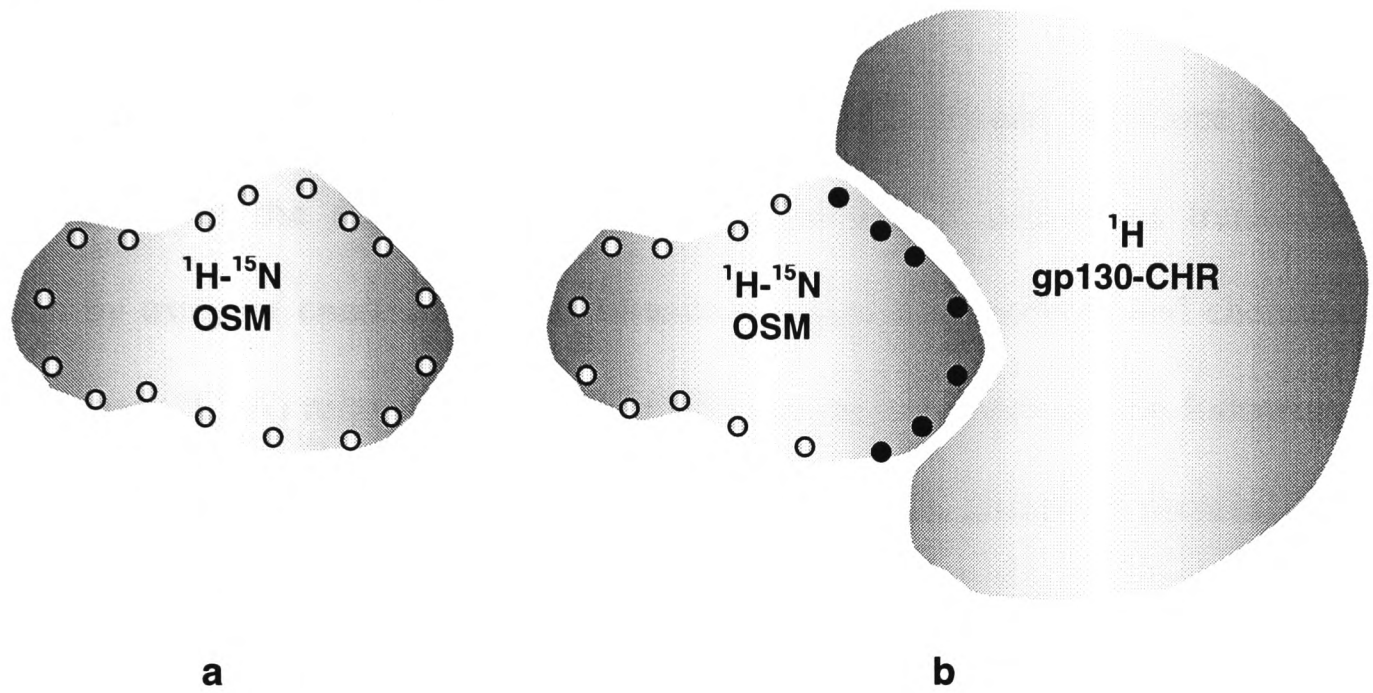

Figure 2.14: Chemical shifts in binding site mapping. (a) Shows ^{15}N labelled OSM in the free state. The open circles are ^{15}N labelled NHs. (b) ^{15}N labelled OSM binds with gp130-CHR. On binding, the NHs at binding site (solid circles) will experience changes of the local environment. The changes are recorded as a new set of chemical shifts. Compared with data from the free state, the residues involving complex formation can be pin-pointed. ^{15}N allows selective detection of the signals from OSM only.

TROSY techniques have been shown to enable complete chemical shift mapping in complexes with molecular weights above 50 kDa (264).

A detailed explanation of the TROSY technique is beyond the scope of this thesis. However the main feature of TROSY is that it suppresses transverse relaxation by using of constructive interference between dipole-dipole and chemical shift anisotropy (CSA) relaxation. The TROSY approach is based on the following: in heteronuclear two-spin systems, such as ^{15}N-^{1}H in amide groups of proteins, the NMR signal of each nucleus is split into two components by scalar spin-spin coupling. In 2D correlation experiments, one therefore observes a four-line fine structure. In conventional multidimensional NMR, this four-line pattern will be transformed into a single, centrally located line by broad-band decoupling techniques (265,266). Since the individual multiplet components have different transverse relaxation times and, hence, different line widths, the signal averaging in large molecules will cause signal deterioration. Using the TROSY technique, the multiplet structure is not decoupled and only the narrowest, most slowly relaxing line of each multiplet is retained. In TROSY-type experiments, transverse relaxation is optimized by minimizing the interaction energy that might induce relaxation. Since the minimization is field strength dependent, the theory implies the presence of a "magic field". For a ^{1}H-^{15}N spin pair, under ideal conditions, this magic field is expected in the ^{1}H frequency range about 950 to 1050 MHz.

In our studies of the interaction between OSM187 and gp130-CHR, TROSY techniques were applied to acquire spectra of the isolated ^{15}N labelled OSM187 and

of ^{15}N labelled OSM187 in an equal-molar mixture with unlabelled gp130-CHR at the highest available field (equivalent to 750 MHz).

3 Methods

3.1 Cloning of OSM

E.coli strain JM109 was chosen to clone the OSM constructs. The cloning sites of a GST fusion vector pGEX-6P-2 from Pharmacia are illustrated in Figure 3.1.

3.1.1 Ethanol precipitation

A one-tenth volume of 3M sodium acetate and three volumes of absolute ethanol were added to the DNA solution which was then chilled to -20 °C for two hours. The resulting DNA precipitate was pelleted by centrifugation (11,000 g for 15 minutes at 4 °C) and the supernatant discarded. The pellet was washed with 70% ethanol to remove residual salt, centrifuged again at 11,000 g for 10min at 4°C and dried in a DNA Speedvac (Savant) at medium heat for 10 minutes.

3.1.2 Phenol-chloroform extraction

Protein was removed from DNA samples by vortex mixing with an equal volume of phenol-chloroform (a 25:24:1 phenol/chloroform/isoamyl alcohol mixture from Sigma). Following brief centrifugation, the upper aqueous layer was transferred to a clean tube, vortexed with an equal volume of chloroform to remove any traces of phenol, re-spun and again decanted to a clean tube.

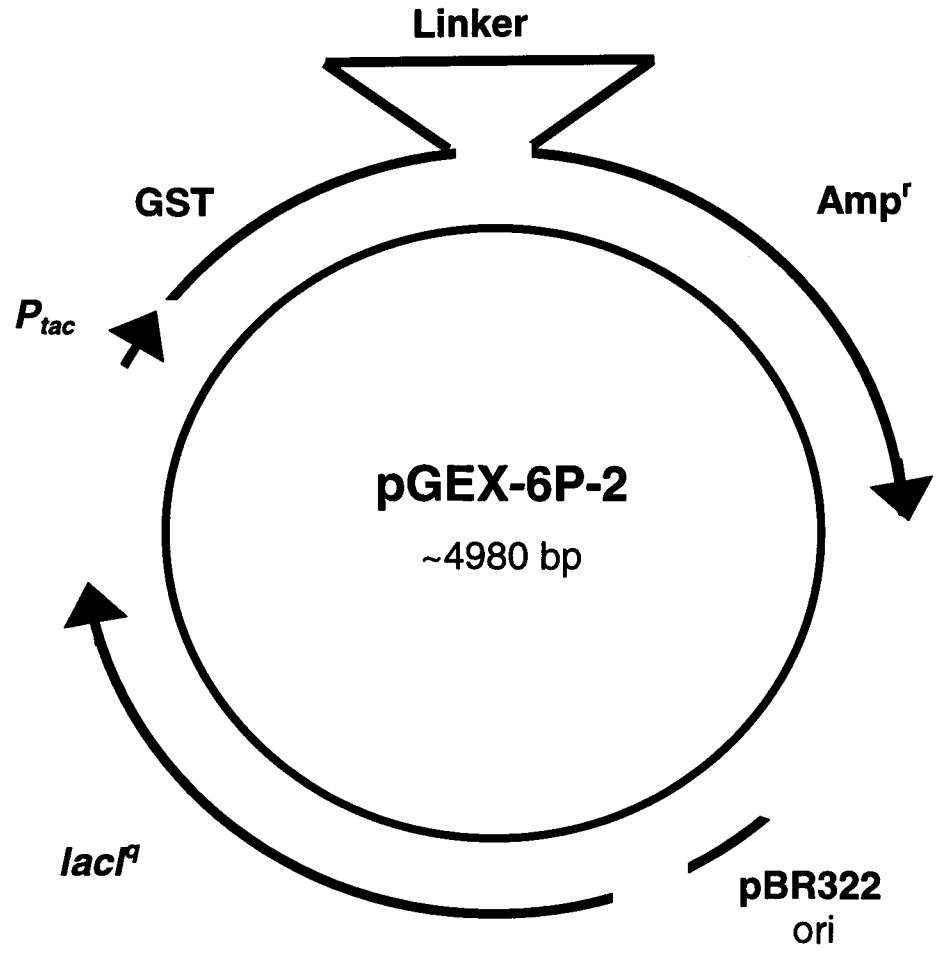

Linker

BamH I *Sma I*

L E V L F Q G P L

GST... CTG GAA GTT CTG TTC CAG GGG CCC CTG GGA TCC CCA GGA ATT CCC GGG TCG ACT CGA GCG GCC GCA TCG TCG TGA CTG ACT GAC

3C protease cleavage site

Key

lacI^q : Lac repressor gene, which turns off transcription from Ptac until IPTG is added
P_{tac} : Promoter for GST gene
GST : Glutathione S transferase

Figure 3.1: The expression vector pGEX-6P-2. The vector map is modified according to Amersham Pharmacia Biotech catalogue. The vector is used to express GST fusion protein in the cytoplasm. The OSM gene was inserted into the vector between *BamH I* and *Sma I* sites. There is a 3C protease cleavage site preceding the recombinant site to facilitate the separation between GST and the protein of interest.

3.1.3 Agarose gel electrophoresis

DNA samples were analyzed by electrophoresis on 1% (w/v) agarose gels, produced by dissolving agarose (Sigma) in 0.5x TBE buffer and adding ethidium bromide to 0.5 μg/ml. After addition of loading buffer, the DNA samples were electrophoresed against 1 Kb DNA ladder (GibcoBRL) in 0.5x TBE buffer at 100 V for 30-45minutes. Under UV light wavelength, the size and yield of the ethidium bromide-stained DNA fragments was estimated by comparison with the 1 Kb ladder.

- 5x TBE buffer: 54 g Tris, 27.5 g boric acid, 20 ml 0.5 M EDTA (pH8.0), distilled water to 1L.
- 6x DNA loading buffer: 0.25 % bromophenol blue, 0.25 % xylenecyanol FF, 15 % Ficoll (Type 400, Pharmacia) in distilled water.

3.1.4 Oligonucleotides

The native OSM has 196 amino acid residues (OSM196). The protein sequence for human OSM can be found in EMBL (code M27288) and the OSM196 is from amino acid residue 26 to 221 (AAIGS...NRSRR). Two C-terminal truncated forms of OSM were designed with 185 (AAIGS...GRVFS) and 187 (AAIGS...VFSKW) amino acid residues (see appendix I). Oligonucleotides for PCR amplification (PE-Applied Biosystems UK) and sequencing (Amersham Pharmacia Biotech) are listed in table 3.1.

3.1.5 PCR amplification

The gene fragment of interest was amplified from cDNA using the thermostable polymerase *Tli* (Promega). Unlike *Taq*, *Tli* has 3'-5' proofreading activity for greater fidelity of nucleotide incorporation. The reaction conditions were 0.2 mM dNTP, 1.5 mM $MgCl_2$, 0.5 mM of each primer and 1 μl *Tli* in the supplied

Purpose	Sequence Name	Sequence of oligonucleotide (5'-3')	Melting temperature
PCR upstream	OSMGST-F2	CGC GGA TCC GCG GCT ATA GGC AGC TGC	60 °C
PCR downstream	OSMGST187-R	TTA CCA CTT GCT GAA GAC CCG C	62 °C
	OSMGST185-R	TTA GCT GAA GAC CCG CCC CAC	62 °C
DNA sequencing	pGEX 5' Sequencing Primer	GGG CTG GCA AGC CAC GTT TGG TG	N/A
	pGEX 3' Sequencing Primer	CCG GGA GCT GCA TGT GTC AGA GG	N/A

Table 3.1: Oligonucleotides for PCR and DNA sequencing of the OSM constructs. PCR primers OSMGST187-R and OSMGST185-R were used for constructs OSM187 and OSM185 respectively. Coding regions are underlined. There is a restriction cleavage enzyme (*BamH I*) site (GGA TTC) in the 5' end of the forward primer (OSMGST-F2). The sequence CGC in front of the *BamH I* site is a spacer for the restriction enzyme. Transcription terminal code TTA was applied in the downstream PCR primers.

reaction buffer. Melting of duplex DNA (94°C for 30 s), annealing of templates (according to the calculation of different primer) and extension of amplification product were performed for 30 cycles in each amplification reaction. The PCR product was analyzed by agarose gel electrophoresis and purified by Wizard PCR Preps DNA purification system from Promega.

- Calculation of annealing temperature : based on the primer's sequence, add 4 °C per GC pair and 2 °C per AT pair

3.1.6 Restriction enzyme digestion

DNA samples were digested with restriction enzymes (NEB, approximately 20 units per μg DNA) in the recommended buffer. Samples were incubated at recommended temperature for the minimum time required for near-complete digestion whilst avoiding non-specific "star-activity" (typically 3-4h). Where appropriate, the products were analyzed by agarose gel electrophoresis.

3.1.7 5'-dephosphorylation of double-stranded DNA

Terminal 5'-phosphates were removed using the enzyme shrimp alkaline phosphatase (SAP, USB). 1 Unit of SAP was used per pmol of DNA termini during restriction enzyme digest. After dephosphorylation, heating at 70 °C for 15 minutes inactivated the enzyme.

3.1.8 Ligations

T4 DNA ligase (NEB) was used to ligate the insert to plasmid. DNA fragments were incubated with T4 ligase (1 U/pmol DNA termini) in the recommended buffer at 17 °C overnight.

3.1.9 Preparation of $CaCl_2$-competent JM109

E.coli strain JM109 was streaked out on a LB plate and grown at 37 °C overnight. A single colony was inoculated into 50 ml LB media and grown overnight at 37 °C with moderate shaking (200 rpm). 1 ml of this culture was transferred into 100 ml LB media and grown as before, to an OD_{600} of 0.3. The culture was divided into two 50ml pre-chilled, sterile polypropylene tubes and left on ice for 10 minutes. The cells were pelleted by centrifugation (3000 g for 5 minutes at 4 °C), the supernatants removed, and each pellet gently re-suspended in 25 ml of ice-cold 50 mM $CaCl_2$. The cells were kept on ice for 30 minutes, and then centrifuged on 1000g for 2 minutes at 4 °C. After removing the supernatant, pellets were gently re-suspended in 5 ml of ice-cold 50 mM $CaCl_2$/15 % glycerol. The $CaCl_2$-competent cells were then dispensed, in 200 µl aliquots, into pre-chilled, sterile polypropylene tubes, frozen in liquid nitrogen, and stored at –70 °C.

- LB medium: 10 g tryptone, 5 g yeast extract, 10 g NaCl, distilled water to 1 litre (for plates add 15 g bacto-agar).

3.1.10 Transformation

100 µl of competent *E.coli* cells were incubated with no more than 10 µl DNA solution (containing 0.01-0.1 µg of DNA) on ice for 10 minutes. After a heat shock of 1 minute at 42 °C, the cells were incubated on ice for 1 minutes. Then 1 ml LB was added to the transformation reaction and the cells were incubated at 37 °C for 30 minutes (to allow expression of plasmid-encoded antibiotic resistance proteins). 100µl of cells were plated out on a LB-amp-glucose plate, and incubated overnight at 37°C.

- LB-amp-glucose: Add ampicillin (100 mg/l) and 0.3 % (w/v) glucose to LB. The ampicillin may be substituted by Carbenicillin for better antibiotic suppression.

3.1.11 Miniprep and Maxprep of plasmid DNA

Hybaid Miniprep and Qiagen Maxiprep kits were used on plasmid DNA preparations. In brief, cell lysates were prepared from overnight cultures of transformed *E.coli* cells, and the DNA extracted by specific methods provided by those kits. After extensive washing, the plasmid DNA was separated from other components of the cells. The purified miniprep plasmid DNA was used directly for restriction digestion or sequencing without further manipulation. The DNA samples from Maxiprep required ethanol precipitation before further usage.

3.1.12 Sequencing the constructs

Dye terminator sequencing was performed using an ABI machine by the Automatic Sequencing Facility in Biochemistry Department and Sir William Dunne School of Pathology.

3.2 Expression of OSM and gp130-CHR

3.2.1 Host strains and expression media

The *E.coli* strains used for OSM and gp130-CHR expression are summarized in table 3.2. Expression media are listed in table 3.3. All the media in later sections are supplied with carbenicillin (Melford Laboratories Ltd. UK Tel. 01449741178) unless otherwise mentioned.

Protein	*E.coli* strain	Purpose	Supplier
OSM	JM109	Cloning, plasmid extraction	Promega
	BL21	Expression	Promega
gp130-CHR	JM109	Cloning, plasmid extraction	Promega
	WH110	Expression	A gift from British Biotech

Table 3.2: *E.coli* strains used for OSM and gp130-CHR expression.

	LB	2xTY	M9
Ingredients (per litre)			
Tryptone	10.00 g	16.00 g	
Yeast extract	5.00 g	10.00 g	
NaCl	10.00 g	5.00 g	
Na_2HPO_4			0.50 g
KH_2PO_4			6.78 g
NH_4Cl			3.00 g
			1.35 g
Trace elements (final conc.)			
$CaCl_2$			0.10 mM
$MgSO_4 \cdot 7H_2O$			2.00 mM
Thiamine			0.02 ‰
Glucose (W/V)			0.40 %
YNB* (W/V)			0.17 %

* YNB is the yeast nutrition base (without amino acids)

Table 3.3: Growth media for OSM and gp130-CHR expression. The tryptone, yeast extract and YNB are from *Becton Dickinson*. Thiamine is from Sigma and other chemicals are supplied by *BDH*. For stable isotope labelling, NH_4Cl was purchased from *CK Gas*. Carbenicillin with final concentration of 50 mg/L was added to selectively suppress the growth of *E.coli* without appropriate plasmid.

3.2.2 Small scale protein expression

3.2.2.1 Small scale expression of OSM

A starter culture was prepared by inoculating 10 ml M9 medium with a single clone of freshly transformed BL21, and incubating in a rotary shaking incubator at 37°C overnight. A portion of this culture was used to seed 100 ml M9 medium in 200ml baffled flask with a starting OD_{600} of about 0.1. The culture was then incubated at 37 °C until the OD_{600} reached 1.0. The cells were then induced by 0.1 mM IPTG for 3 hours. The cells were then pelleted (5000 rpm 10 minutes at 4 °C) and processed.

3.2.2.2 Small scale expression of gp130-CHR

A starter culture was prepared by inoculating 10 ml LB medium with a single clone of freshly transformed WH110, and incubating in a rotary shaking incubator (200rpm overnight at 37 °C). A corresponding amount of this culture was used to seed 500 ml 2TY medium (in a 2L baffled flask with a starting OD_{600} of about 0.5), which was then incubated (200rpm at 37 °C) until the OD_{600} reached 3.0. The cells were then transferred to a 27°C rotary incubator. After a further 30 minutes incubation, protein expression was induced with 0.1 mM IPTG for 3 hours. The cells were then pelleted (5000 rpm for 10 minutes at 4°C) and used for periplasmic preparation.

3.2.3 Fermentation

3.2.3.1 Large scale expression of OSM

A starter culture was prepared by inoculating 10 ml M9 medium with a single clone of freshly transformed BL21, and incubating in a rotary shaking incubator at 37°C overnight. A portion of this culture was used to seed 100 ml M9 medium in 200ml baffled flask with a starting OD_{600} of about 0.1. The culture was then incubated at 37 °C until the OD_{600} reached 2.0. The cells were then pelleted and re-suspended in fresh M9 medium. The re-suspended cells were transferred to a New Brunswick Bioflo 5L fermenter. The culture was grown in M9 medium, supplied with 0.02 % (v/v) polypropylene glycerol, at 37 °C. When the culture reached midlog phase (OD_{600} = 0.4 – 0.7), the temperature was dropped to 27 °C. After another 30 minutes, IPTG was added to the culture to a final concentration of 0.1 mM. The culture was then incubated for additional 15 hr.

3.2.3.2 Large scale expression of gp130-CHR

A starter culture was prepared by inoculating 500 ml LB medium with a single clone of freshly transformed WH110, and incubating in a rotary shaking incubator at 27 °C overnight. A portion of this culture was used to seed 10L 2TY medium in a 10L New Brunswick Microferm fermentor. The culture was supplied with 0.02 % (v/v) polypropylene glycerol and inoculated at 37 °C. When the culture reached midlog phase (OD_{600} = 0.8 – 1.0), the temperature was dropped to 27 °C. After another 30 minutes, IPTG was added to the culture to a final concentration of 0.1 mM. The culture was then incubated for additional 3 hours.

For 30L fermentation, the growth conditions are essentially the same. The fermentor was also supplied by New Brunswick (Mobile Pilot Plant Fermentor).

3.2.4 Isotope labelling of OSM187

Labelling procedures are the same as ordinary fermentation, but with $^{15}NH_4Cl$ as nitrogen source. It is safer to filter sterilise the stable isotope instead of the usual autoclave, which might spill the expensive chemical.

3.3 Purification of OSM and gp130-CHR

3.3.1 Periplasmic purification of MBP-gp130-CHR

Pellets from the expression culture were re-suspended in 30 mM Tris pH 8.0 containing 20% sucrose. EDTA was added to a final concentration of 1 mM and mixed gently at room temperature. After 5 minutes the cells were again pelleted (10,000 rpm for 5 minutes at 4 °C) and re-suspended in 1L of 5 mM $MgSO_4$. The cells were left on ice and occasionally re-suspended gently. After a further 10 minutes, the cells were spun down (10,000 rpm for 10 minutes at 4 °C) and the protein containing supernatant was removed to a clean flask. The supernatant should be subjected to anion exchange purification immediately in order to preserve sample activity.

3.3.2 Purification of the GST-OSM fusion protein

Intracellular GST-OSM fusion protein was recovered from cell extracts by affinity purification as described for human LIF (267). The Glutathione 4B affinity

resin was purchased from Amersham Pharmacia Biotech. The purification procedures were the same as provided by manufacture apart from the Glutathione concentration in elution buffer. Here, a 5 mM solution (1.8 ml per gram of cell) of reduced Glutathione was used instead of 10 mM.

3.3.3 Cleavage of the fusion proteins

Both OSM and gp130-CHR were expressed as fusion proteins and the same cleavage site was introduced in both systems. The MBP-gp130-CHR fusion protein was cleaved by incubation in the presence of 3C protease (encoded by the genome of a human rhinovirus) (268), 10 mM EDTA and 1 mM DTT at 4 °C overnight. For GST-OSM fusion, the cleavage time was 3 hours and no DTT was added, since the elution buffer for affinity purification contained 5 mM reduced form Glutathione. The 3C protease is a "home-made" GST fusion protein. A time course study of the cleavage was performed to determine the minimum time and amount needed for complete cleavage.

3.3.4 Ion-exchange chromatography

Ion-exchange columns and the Fastflow Q matrix were all from Amersham Pharmacia Biotech.

3.3.4.1 Ion-exchange purification of OSM

A Mono S column was used for high-resolution cationic exchange purification. The purpose for this step is to purify OSM from the cleavage mixture.

Elution was carried out with a linear gradient of 0 to 1 M NaCl in 20 mM MES (pH 6.0). The fractions were analyzed by SDS-PAGE analysis.

3.3.4.2 Ion-exchange purification of gp130-CHR

There are two anion exchange steps in gp130-CHR purification procedure: a preliminary purification by Fastflow Q column (50 ml) and a high-resolution purification by Resource Q (6 ml).

The preliminary purification was used to extract MBP-gp130-CHR fusion protein from the supernatant created by periplasmic purification. Elution was carried out with a linear gradient of 0 to 1 M NaCl in 20 mM Tris buffer (pH 8.0). The active fractions were subjected to 3C protease cleavage.

High-resolution purification was used to purify gp130-CHR from the cleavage mixture. A step gradient method was applied in sample elution with a step gradient of 0%-35%-100% to optimize the separation between gp130-CHR and the MBP. The elution buffers are the same as those in the Fastflow purification step.

3.3.5 Gel-filtration chromatography

Gel-filtration was performed on a Pharmacia Gradifrac system with a 100 ml Sephacryl-S100 column. A set of molecular weight markers (Pharmacia MW-GF-70 Range 6,500-66,000) was used to calibrate the column. Protein samples of approximately 0.4 ml were loaded at a flow rate of 2 ml/min.

3.3.5.1 Purification of OSM

Fractions corresponding to the expected molecular weight by SDS-PAGE from the Mono S column elution were affinity purified again with Glutathione 4B resin in order to remove any remaining GST protein. The sample was then concentrated and loaded on the gel-filtration column. Elution was carried out with a 50 mM potassium phosphate buffer (pH 5.2) containing 150 mM NaCl. Fractions correlated to correct molecular weight were collected and buffer exchanged into appropriate buffers.

3.3.5.2 Purification of gp130-CHR

Fractions from Resource Q column purification were concentrated and loaded on the Gel-filtration column. A 50 mM potassium phosphate buffer (pH 7.4) with 150 mM NaCl was used for elution. Active fractions were collected and buffer exchanged.

3.4 Determination of sample quality

3.4.1 Analysis of protein by SDS-PAGE

Samples for SDS-PAGE analysis were heated to 95°C for 5 minutes with 4x sample buffer (Novex) prior to loading onto the 10 % NuPAGE Bis-Tris Pre-Cast Gels from Novex. The proteins in each sample were separated by electrophoresis at 200V for 40 minutes in the running buffer supplied with the gels. A Mark12™ wide-range protein standard was also purchased from Novex. After electrophoresis, the gels were stained by Coomassie Brilliant Blue dye for 5 minutes and destained for

observation. The destained gels need to be treated with gel-drying buffer before being dried for storage. For reducing sample buffer, 10 % β-mercaptoethanol was added to the Novex sample buffer.

- Coomassie Brilliant Blue dye (1 L) contains Coomassie blue (Sigma) 2.5 g, methanol 450 ml, acetic acid 100 ml and 450 ml water.
- Destaining buffer contains 10 % acetic acid and 7.5 % methanol.
- Gel-drying buffer contains 5 % glycerol and 30 % methanol.

3.4.2 Electrospray mass spectrometry

The molecular weights of recombinant proteins were determined by a Micromass BIOQII-ZS electrospray mass spectroscope machine (Manchester UK). The experiments were carried out by Dr. Robin Aplin in Dyson Perrins Laboratory, Oxford University.

3.4.3 N-terminal sequencing and amino acid analysis

Recombinant proteins were N-terminal sequenced to check the cleavage accuracy. The N-terminal sequences were carried out by Dr. Tony Willis using an Applied Biosystem 494A 'Procise' Sequencer. Amino acid analysis was also used to calibrate the UV absorption for accurate protein concentration estimation.

3.4.4 Sample screening by activity

Sample activity screening by a BIAcore machine was mainly used to identify gp130-CHR containing fractions. The OSM was immobilized on chip surface by amine coupling. Fractions from gp130-CHR purification were injected over OSM. Standard BIAcore experimental protocols were applied.

3.4.5 Sample folding status

Sample folding status was checked by 1D NMR studies. Generally speaking, properly folding protein showed a well-dispersed NH region and methyl groups with high field shifts.

3.5 Characterization of binding

3.5.1 Analytical ultracentrifugation

The binding characterization and the NMR studies need information about sample stability and stoichiometry of binding. Buffers of different pHs were tested to optimize experimental conditions for these studies.

The solution behaviour of OSM187, gp130-CHR and the stoichiometry of their complex were studied by sedimentation equilibrium in a Beckman Optima XL-A analytical ultracentrifuge. Samples were dialyzed extensively against 50mM phosphate buffer, 150mM NaCl. The buffer pHs were 5.2 and 7.4 for different experiments. The A_{280} of samples was adjusted by dilution with dialysis buffer. Samples of the proteins and their corresponding dialysis buffer were introduced into the sectors of the centerpieces, at a rotor temperature of 25 °C. The rotor speed was between 8,000 and 26,000 depending upon the molar mass of the protein being studied.

For OSM187, five speeds (8,000, 12,000, 16,000, 20,000 and 26,000 rpm) were used to observe the correlation between apparent molecular weight (MW_{appr}) and rotor speed. The protein distribution was analyzed by continuous radial scanning of

the A_{280} in each cell. Radial increments of 0.001 cm were used, without delay time between scans in order to maximize the frequency of scans. Scans were carried out 6, 12, 18, 21, 24 and 26 hours after the desired rotor speed were reached. The data were fitted to an 'Ideal I' model using the program supplied by Beckman. The MW_{appr} were determined according to the Equation (10).

The partial specific volume of the OSM187 and gp130-CHR at 25 °C are 0.7338 and 0.7296, calculated based on the method of Cohn and Edsall (269):

$$v_c = \frac{\sum_i N_i M_i v_i}{\sum_i N_i M_i} \qquad \textbf{(39)}$$

Where, v_c is the calculated partial specific volume, N_i is the number of residues, M_i is the molecular weight of the corresponding component and v_i is the partial specific volume of the component.

For gp130-CHR and the gp130/OSM187 complex (1:1 complex and 2:1 complex), three speeds (10,000, 15,000 and 20,000 rpm) were applied and the data were acquired and analyzed using the same ways as above.

3.5.2 Isothermal titration calorimetry

The enthalpy of binding was determined by titrating a 1.3 ml, 12.3 μM solution of OSM187 with 125 μM gp130-CHR in 50 mM phosphate buffer (pH 7.4), 50 mM NaCl using an VP-ITC instrument from MicroCal. The reciprocal experiment with gp130 (13 μM) in sample cell and OSM187 (133 μM) in the syringe, was also performed. The sample cell was thermostatted to 30 °C using a circulating bath. The

samples were dialysised beforehand and degassed prior to use. Sample concentrations were determined by A_{280} readings, which were calibrated by amino acid analysis. The enthalpy of binding between OSM187 and gp130-CHR was determined from heats of multiple single injections of 5 µl, and an equilibration time of 8 min was allowed between injections. The heat of dilution of each injection was determined and used to calculate the heat generated by binding.

The equilibrium association constant, K_A, and the number of binding sites, n, were obtained from the calorimetric data, employing the Origin data-analysis supplied with the Omega titration calorimeter, fitting with 1:1 model. The data analysis routines were based on Wiseman's studies as discussed in Chapter two.

3.5.3 Surface plasmon resonance

Surface plasmon resonance (SPR) experiments were performed on a Pharmacia BIAcore 2000 machine. Proteins were covalently bound to the dextran matrix of a CM5 sensorchip using amine coupling method as described in chapter two. Immobilization was carried out in 10 mM sodium acetate buffer (pH 4.5). The amount of protein bound to the sensorchip was monitored by the change in resonance units. In order to avoid mass transport limitation, the immobilization was controlled to the lowest possible level. Binding experiments were carried out at 25 °C in HBS running buffer (20 mM Hepes, pH 7.4, 150 mM NaCl, 0.005 % (v/v) Tween 20) with appropriate flow rate. Due to the fast on /fast off nature of binding, no regeneration step was needed after each injection. This allows the same sensor chip surfaces to be

used in the entire set of experiments. The data were analyzed using global fitting procedures in the BIAevaluation 3.0 program.

During the kinetic and equilibrium analysis, gp130-CHR was injected over the flow cells at a flow rate of 50µl/min and 1µl/min respectively. For kinetic experiments, triplicates of 5 serial dilutions (50-200 µM) of gp130-CHR were injected over the immobilized OSM187 and OSM196. For equilibrium measurements, a set of gp130 samples (20-400 µM) were used.

For antibody capture immobilization of OSM-GST fusion, the anti-GST antibody (Pharmacia Biosensor) was immobilized using amine coupling as described by the manufacturer. OSM-GST was then passed over the chip surface and captured by the antibody. Interaction studies were then performed on this surface as previously described.

3.6 Nuclear Magnetic Resonance (NMR) studies on the interaction

3.6.1 Sample preparation

A 50 mM potassium phosphate buffer containing 0.5 mM NaN_3 and 10 % D_2O was used for all NMR samples. For free form samples the buffer pH values were 5.2 and 7.4. In order to form the complex, free form samples were diluted to about 40 µM in the same buffer above but with a of pH 6.8. Appropriate volumes of each were mixed together to a ratio of 1:1. The mixture was then concentrated to 0.8 mM, which is a 0.4 mM complex, by Millipore Ultrafree Filter units.

3.6.2 Experiments

3.6.2.1 One dimensional NMR spectroscopy

One-dimensional proton experiments were acquired on a home built three-channel 600 MHz (^{1}H) spectrometer equipped with tri-axial gradients and a triple resonance probe. The sample temperature was 25°C. Water suppression was achieved by a Watergate sequence (270).

3.6.2.2 2D spectra (HSQC, 2D-NOESY, TROSY)

Transverse relaxation optimized ^{1}H-^{15}N spectra (TROSY) were recorded on a home built three channel 750 MHz (^{1}H) spectrometer equipped with tri-axial gradients and a triple resonance probe with acquisition times of 81.9 ms in t_2 (^{1}H) and 69.6 ms in t_1 (^{15}N) (263,271). Spectra were recorded at 35°C on a 0.3 mM ^{15}N labeled OSM187 sample and on a 0.4mM sample of the 1:1 complex of ^{15}N-labelled OSM187 with unlabeled gp130-CHR.

3.6.3 Data processing

The NMR spectra were processed using Felix 2.3 (Biosym, Inc. San Diego, CA USA) employing water deconvolution, mild resolution enhancement and polynomial baseline corrections.

4 Expression and purification of OSM and gp130-CHR

4.1 DNA sequencing of the constructs

The DNA sequences for OSM185 and OSM187 were PCR amplified (Figure 4.1) and cloned into *E.coli* strain JM109. The DNA sequencing data of cloned OSM constructs (OSM185, OSM187) were compared with the published sequence (see Appendix I) and proved to be correct.

4.2 Expression and purification of OSM

OSM185 and OSM187 genes were inserted into expression vector pGEX-6p-2 as designed. Although both constructs have the correct DNA sequence, the OSM185 construct cannot produce detectable OSM185. OSM187 was ^{15}N or $^{15}N/^{13}C$ labelled and expressed as a GST fusion protein and the final yield of purified OSM187 was 1.5 mg/L and 1.1 mg/L respectively. The OSM196 construct was obtained from Dr. Staunton and references can be found in his recent paper (72). The production of

Figure 4.1: PCR products for OSM185 and OSM187 constructs. The lengths of the PCR products of OSM185 (1) and OSM187 (2) constructs are 561 bp and 567 bp respectively, including 6 bp from *BamH I* site on 5' end. Sample 1 and 2 are shown as bands running slower than the 500 bp band of the 1Kb ladder (M) as expected.

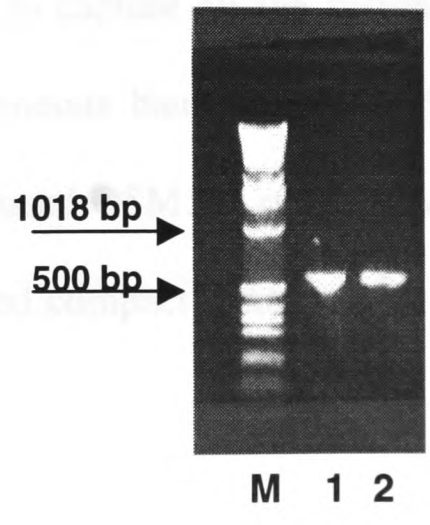

OSM is summarized in Figure 4.2.

4.2.1 Analysis the OSM proteins by SDS-PAGE

The expression of OSM187 was monitored following induction (Figure 4.3A). Comparing *Lane 1-3*, it is clear that the expression of fusion GST-OSM187 was detectable after 2 hours of induction and that the yield was higher at a longer induction time (3.5 hours). The affinity purification produced an 85 % percent pure GST fusion protein running as a 50 kDa band (Figure 4.3A, *Lane 5*). The 3C protease can cleave the fusion protein and produce two bands at molecular weight around 26 kDa and 21 kDa (Figure 4.3A *Lane 6*), which correspond to the size of GST and OSM187. Cells cloned with OSM185 were tested in the same manner but affinity purified GST-OSM185 sample contained multiple bands with molecular weights higher than GST but lower than the expected fusion protein, GST-OSM185 (Gel not shown). After 3C protease cleavage, only the GST protein is detectable (Figure 4.3A *Lane 7*). The result indicated the presence of a proteolytic event. The expression and purification of OSM187 were monitored by SDS-PAGE (Figure 4.3B). The loading flow-through from the affinity column was loaded on a freshly prepared affinity column, but no GST fusion protein could be extracted from it. The result indicated that the first affinity column has sufficient capacity to capture all the fusion GST-OSM187. Purified OSM187 appeared as a homogeneous band around 21.5 kDa, which was the expected size for the protein. The reduced OSM187 runs slower than its un-reduced form. This may be due to the preserved compact conformation of the un-reduced OSM187.

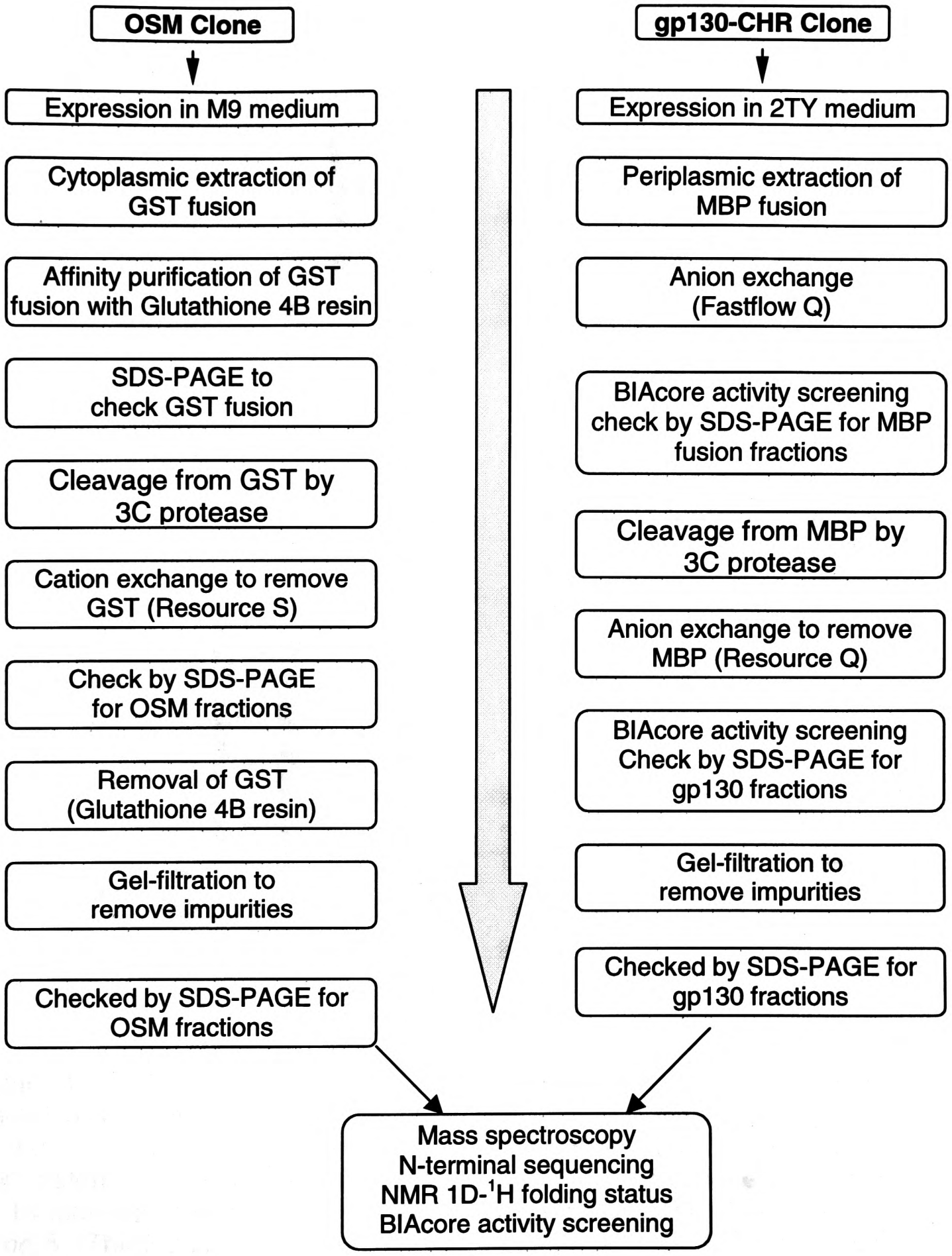

Figure 4.2: Production of OSM and gp130-CHR. The OSM and gp130-CHR were expressed as fusion proteins by cytoplasmic and periplasmic expression systems respectively. The diagram highlights basic procedures used in the expression and purification of OSM and gp130-CHR.

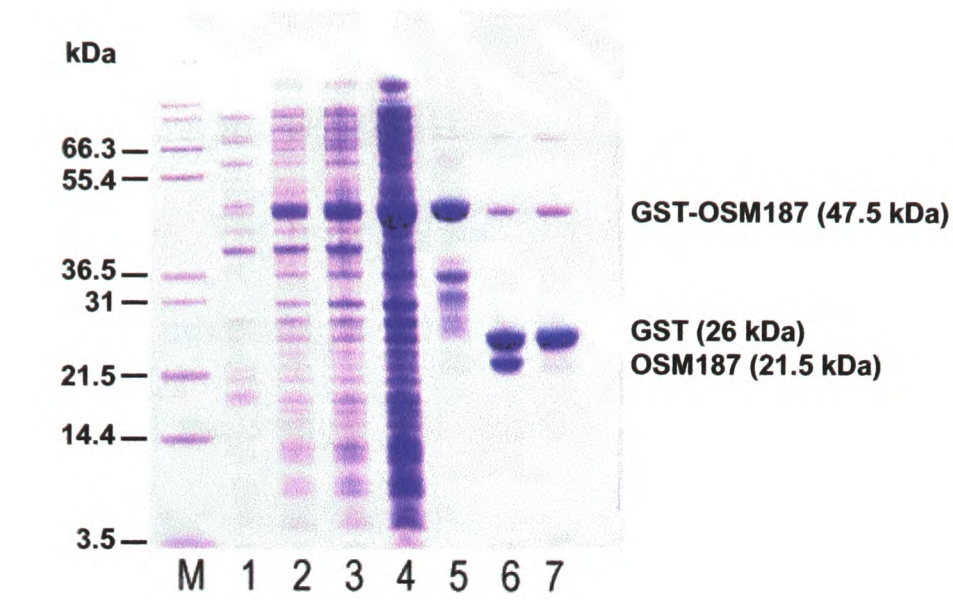

A

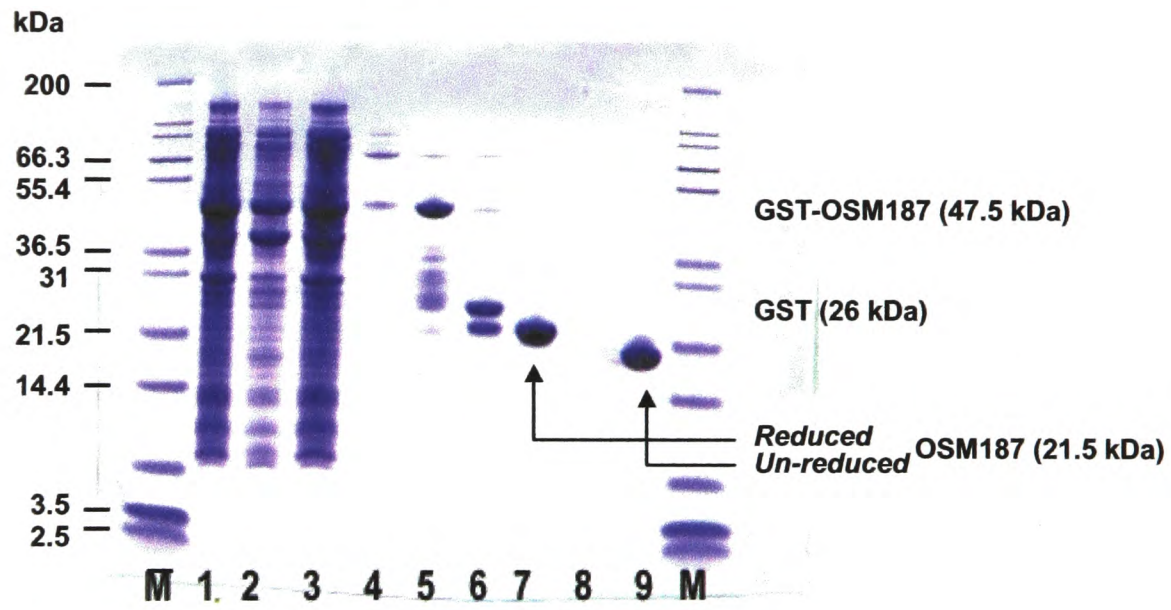

B

Figure 4.3: SDS-PAGE analysis of expressed recombinant OSM proteins. Samples were reduced prior to loading unless marked differently. A) The expression of OSM187 was monitored following induction. The cell lysates from before induction, 2 hours and 3.5 hours of induction were in *Lane 1-3*. Lysate supernatant is in *Lane 4*. Affinity purified GST-OSM187 was in *Lane 5*. The 3C protease cleaved GST-OSM187 and GST-OSM185 was in *Lane 6* and *Lane 7*. B) Purification of OSM187. The cell lysate supernatant, cell lysate precipitant, loading flow-through and the washing flow-through of the affinity column were in *Lane 1-4*. The eluted fusion protein and 3C protease cleaved sample were in *Lane 5* and *Lane 6*. The reduced and unreduced forms of purified OSM187 were in *Lane 7* and *Lane 9* respectively. The *Lane 8* was a blank.

4.2.2 Electrospray mass spectrometry

The molecular weight of OSM187 was measured by electrospray mass spectrometry (Figure 4.4). The resulting molecular weight was 21517.8 ± 0.4, which is close to the calculated molecular weight 21522.5. Since the OSM187 had two pairs of cysteine residues and the sample was running under un-reduced conditions, the measured molecular weight should be 4 Da lower than the calculated one. This may be accounted for by the 4.6 Da difference between the two values for the molecular weight of OSM187.

4.2.3 N-terminal sequencing and amino acid analysis.

The purified OSM187 was N-terminal sequenced and gave an N-terminal of GPLGSAAIGS, which is in agreement with the expected OSM187 sequence (see appendix I). Since the accuracy of the sample concentration is critical for biophysical studies, amino acid analysis was performed to obtain an accurate sample concentration and to provide calibration for the A_{280} measurements.

4.2.4 Sample activity and folding status

The OSM187 samples were checked by the BIAcore machine and proved to be active. The binding properties of the protein will be described in detail on chapter 5. One-dimensional NMR was used to assess sample folding status (Figure 4.5). At 600 MHz, pH 5.2 and 35 °C, the 0.1 mM OSM187 presented features for a properly folded protein, i.e. well dispersed NH region and methyl groups with high field shifts.

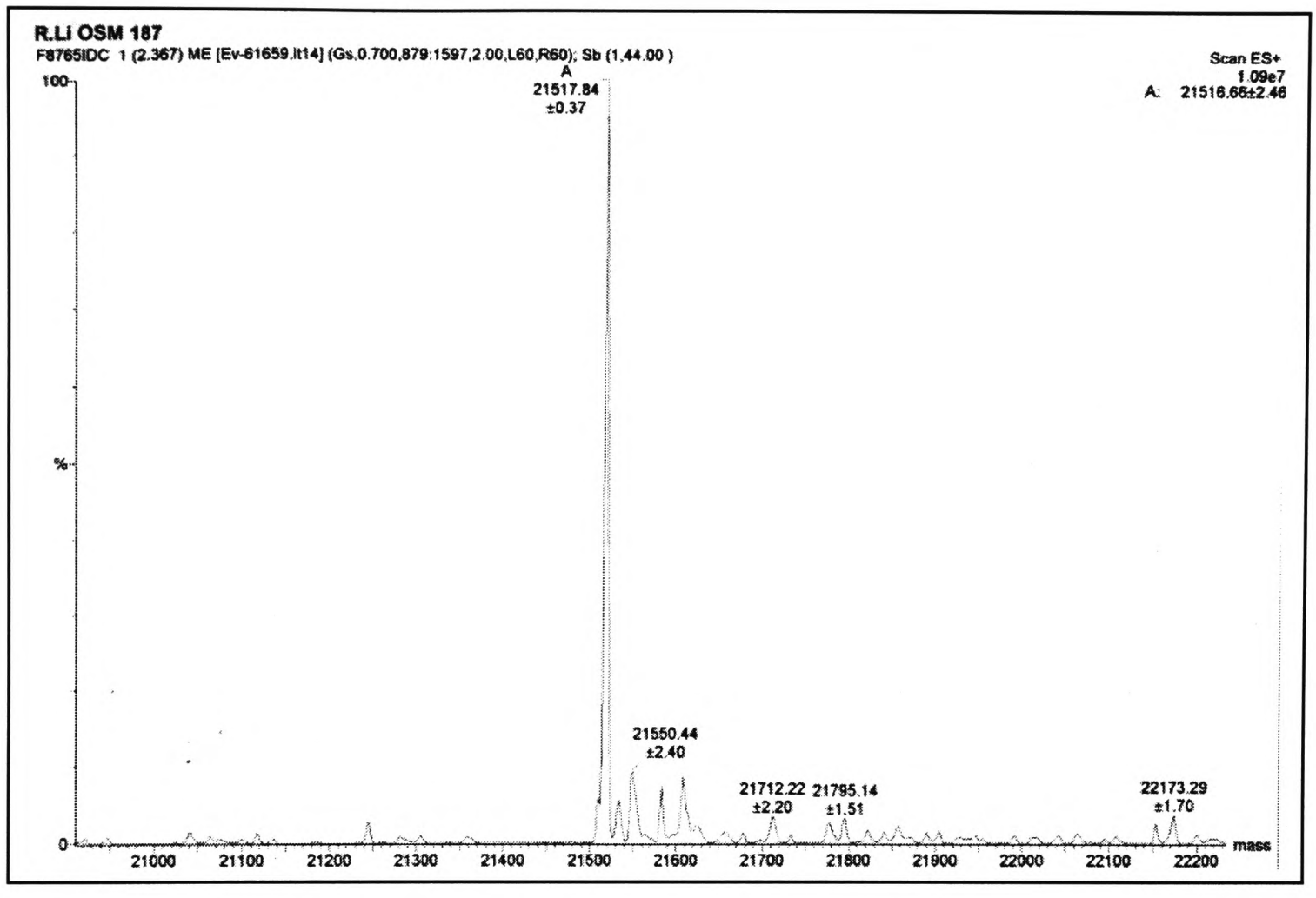

Figure 4.4: Mass spectra of OSM187. The measured and the calculated molecular weight were 21517.8 ± 0.4 and 21522.5 respectively.

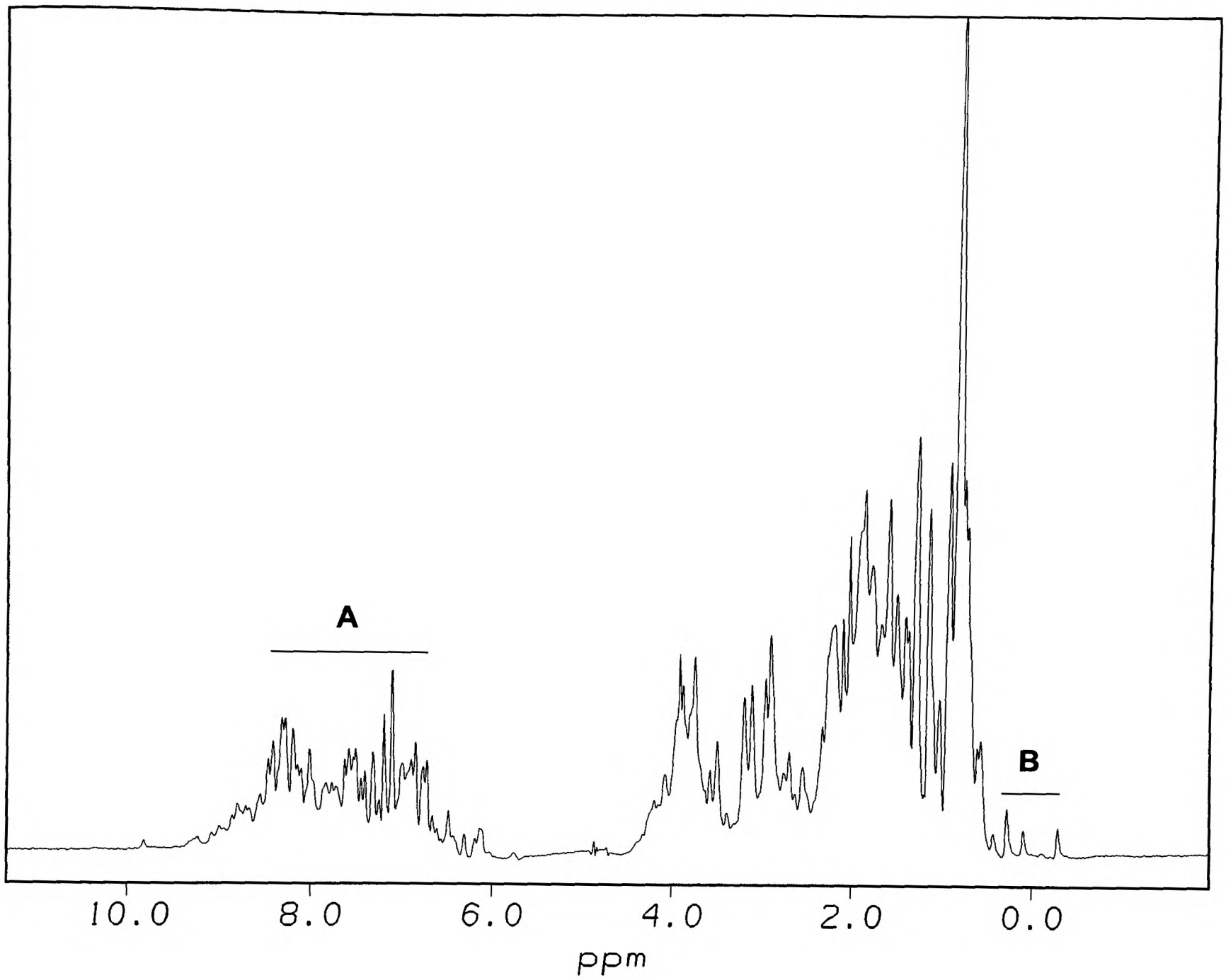

Figure 4.5: 1D-^{1}H spectrum of OSM187. The spectrum was recorded at 600 MHz, pH 5.2 and 35 °C on a 0.1 mM sample. Features of a folded protein are highlighted, i.e. a well dispersed NH region (A) and methyl groups with high field shifts (B).

4.3 Expression and purification of gp130-CHR

The gp130-CHR construct was obtained from Dr. Staunton and references can be found in his recent paper (72). The yield of purified gp130-CHR was 0.5 mg/L. An outline of gp130-CHR expression can be found in Figure 4.2.

4.3.1 Analysis gp130-CHR by SDS-PAGE

The fusion MBP-gp130-CHR and purified gp130-CHR were analyzed by SDS-PAGE (Figure 4.6). The fusion protein was extracted by a periplasmic purification step using anion exchange chromatography and appeared as a band around 66 kDa (Figure 4.6A). This is close to the calculated molecular weight of the fusion (70.2 kDa). Cleaved by 3C protease, the gp130-CHR was separated from the MBP. On the gel, this showed as two bands around 45 kDa and 25 kDa respectively (Figure 4.6A). Purified by gel-filtration chromatography, the gp130-CHR showed as homogeneous band at around 25 kDa (Figure 4.6B). Both un-reduced and reduced samples were tested and appeared identical on SDS-PAGE (Figure 4.6B).

4.3.2 Electrospray mass spectrometry

The molecular weight of gp130-CHR was measured by electrospray mass spectrometry (Figure 4.7). The resulting molecular weight was 25208.1 $\pm$ 0.2, which is close to the calculated molecular weight 25210.2. Since the gp130-CHR was prepared in potassium phosphate buffer, potassium ions may attach to the protein. The peak B, had a molecular weight 36 Da higher than gp130-CHR, may be the result of the attachment of one potassium ion.

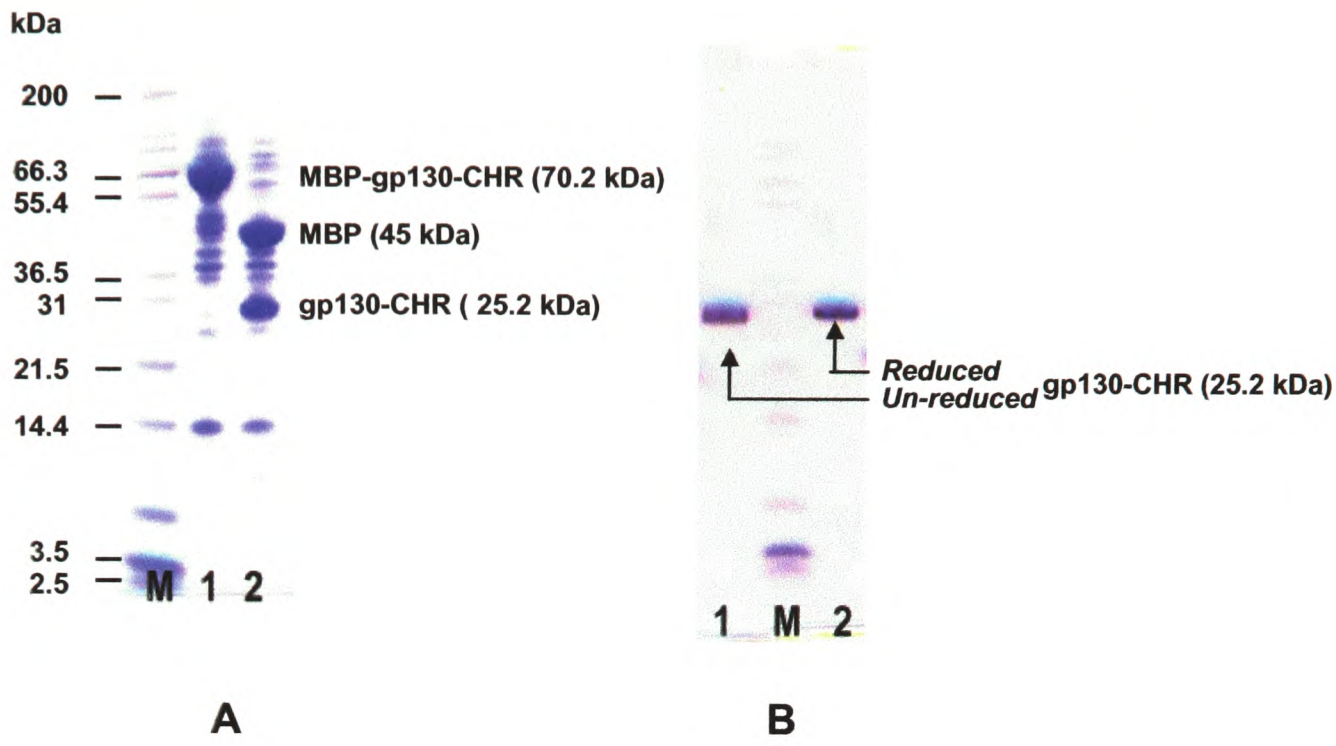

Figure 4.6: SDS-PAGE analysis of gp130-CHR. A) The fusion MBP-gp130-CHR showed as a high-density band around 66.3 kDa. After cleavage, the band at 70 kDa disappeared and two bands appeared at molecular weight about 45 kDa and 25 kDa. B) The purified gp130-CHR runs as homogeneous bands under both un-reduced and reduced conditions.

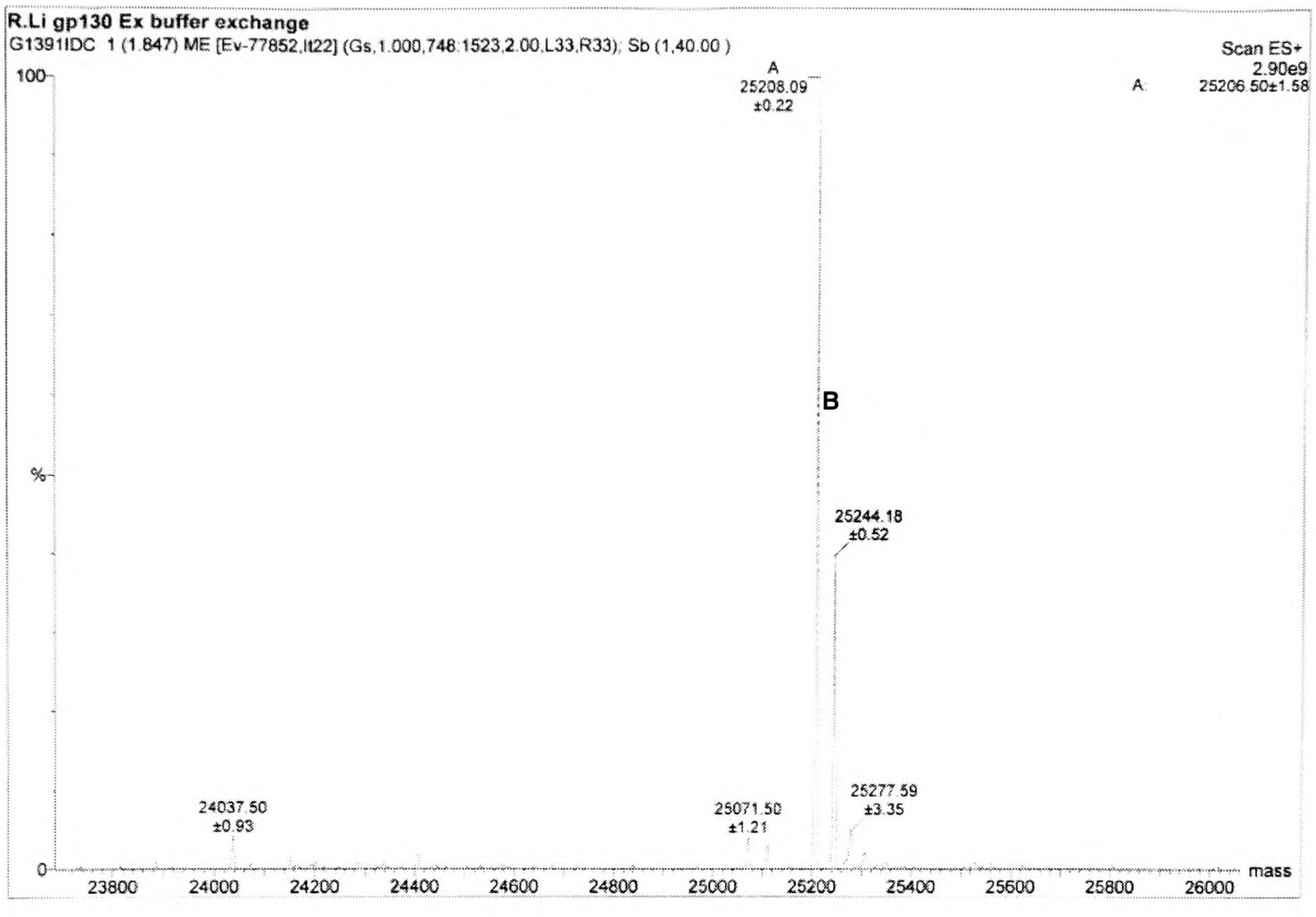

Figure 4.7: Mass spectra of gp130-CHR. The measured and the calculated molecular weight were 25208.1 $\pm$ 0.2 and 25210.2 respectively. The peak B corresponds to a protein with molecular weight of 25244.2 $\pm$ 0.5, which is 36 Da higher than expected. Since the sample was in potassium phosphate buffer previously, the extra weight may be due to the attachment of one potassium ion.

4.3.3 N-terminal sequencing and amino acid analysis

The purified gp130-CHR was N-terminal sequenced and gave an N-terminal of GPGSSPLPPE, which is in agreement with the designed gp130-CHR sequence (see appendix II). Since the accuracy of the sample concentration is critical for biophysical studies, amino acid analysis was performed to obtain accurate sample concentration and to provide calibration for the A_{280} measurements.

4.3.4 Sample activity and folding status

The fractions from anion exchange purification were screened for activity by BIAcore (Figure 4.8A and 4.8B) and active fractions were collected for further purification. From study of the BIAcore response level data (Figure 4.8C), it is quite clear that the response from fraction 9 and 10 were higher than other fractions. This is consistent with the result from SDS-PAGE, which indicated that fraction 9 and 10 (*Lane 4-5*) contained higher concentration of the fusion protein. At 750 MHz, pH 7.1 and 25 °C, the 0.1 mM gp130-CHR appears to be a properly folded protein (Figure 4.9).

4.4 1D-^{1}H NMR study on the 1:1 complex

The 1D-^{1}H NMR experiment was used to analyze a 1:1 complex of OSM187 and gp130-CHR (Figure 4.10). The experiment was run at 600 MHz, pH 6.5 and 25°C on a 0.7 mM sample. The free state spectra of OSM187 and gp130-CHR were tested under the same conditions. All three spectra showed features of a properly folded protein. Comparing the high field shifts (Figure 4.10, right panel), it is obvious

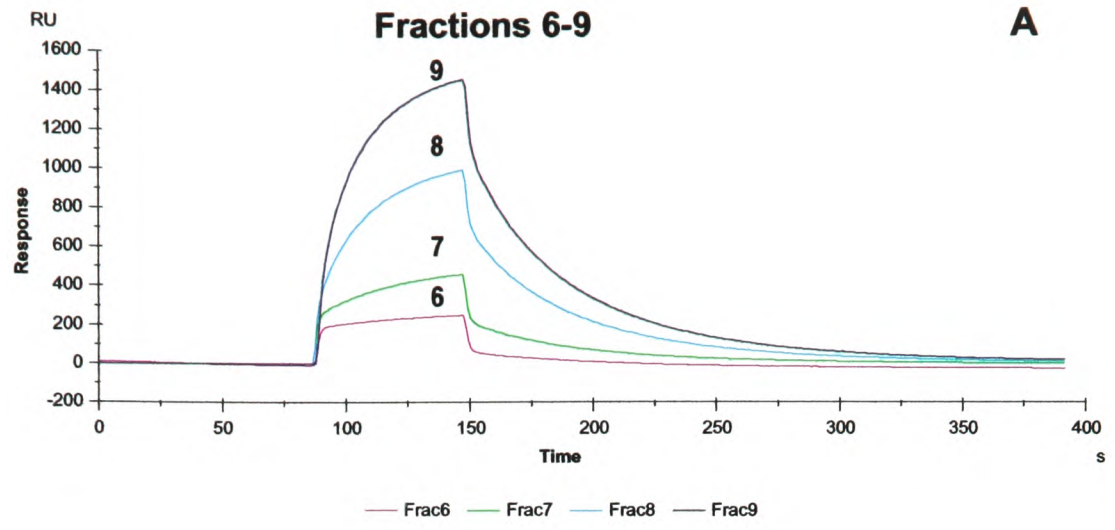

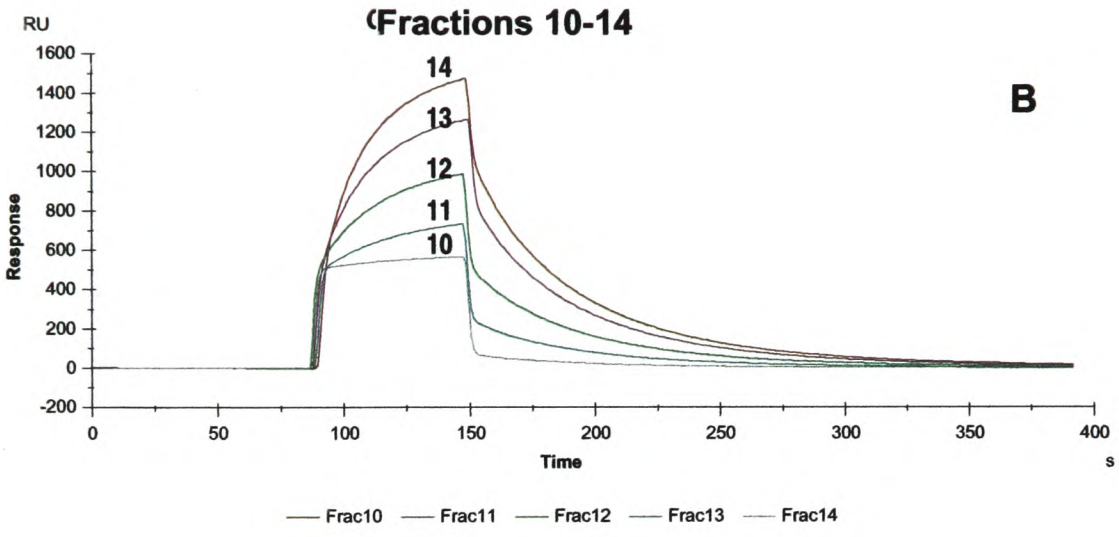

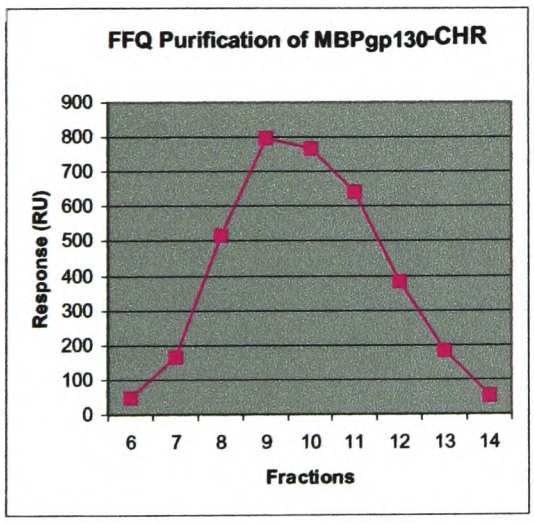

C

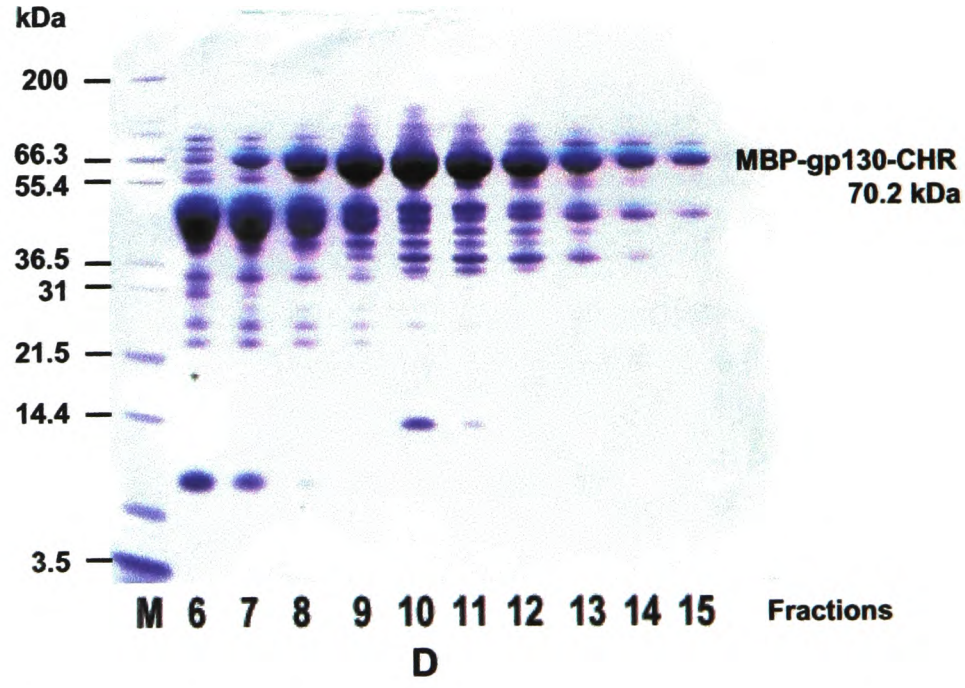

D

Figure 4.8: BIAcore activity screening for fusion MPB-gp130-CHR fractions. The fractions from anion exchange purification (Fastflow Q column) were injected over immobilized OSM187. Sensorgrams, in A and B, of these fractions indicated the presence of binding activity. C) For same volume of sample, the responses increased from fractions 6-9 and then came back down from fractions 10-14. D) SDS-PAGE profile of fractions 6-15. The bands around 66.3 kDa were those from the fusion protein. Comparing the density of the bands, fraction 6 had the lowest and fractions 9-10 had the highest. This is consistent with the response level tested by BIAcore.

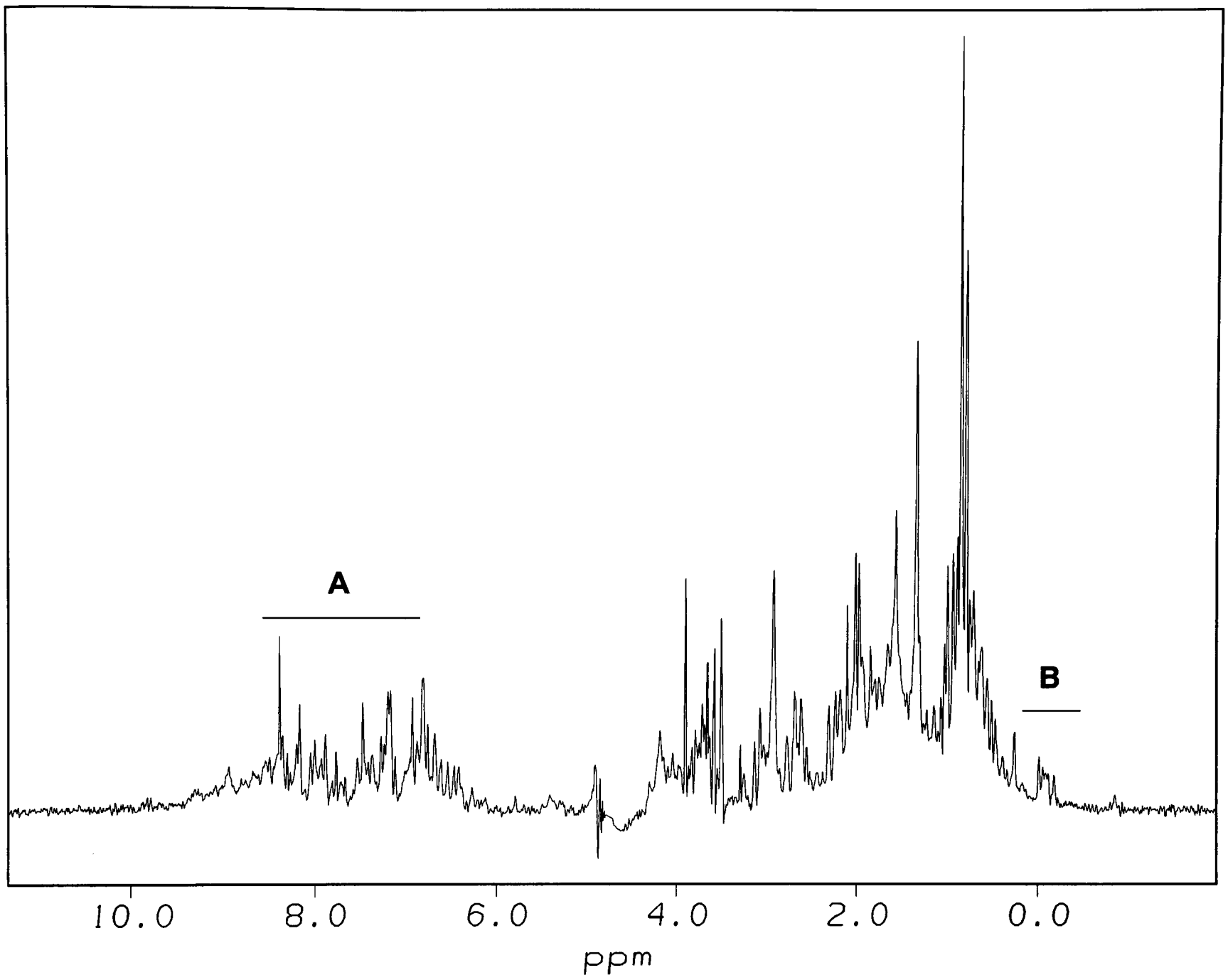

Figure 4.9: 1D-^{1}H spectrum of gp130-CHR. The spectrum was recorded at 750 MHz, pH 7.1 and 25 °C on a 0.1 mM sample. Features of a folded protein are highlighted: A) a well dispersed NH region and B) methyl groups with high field shifts.

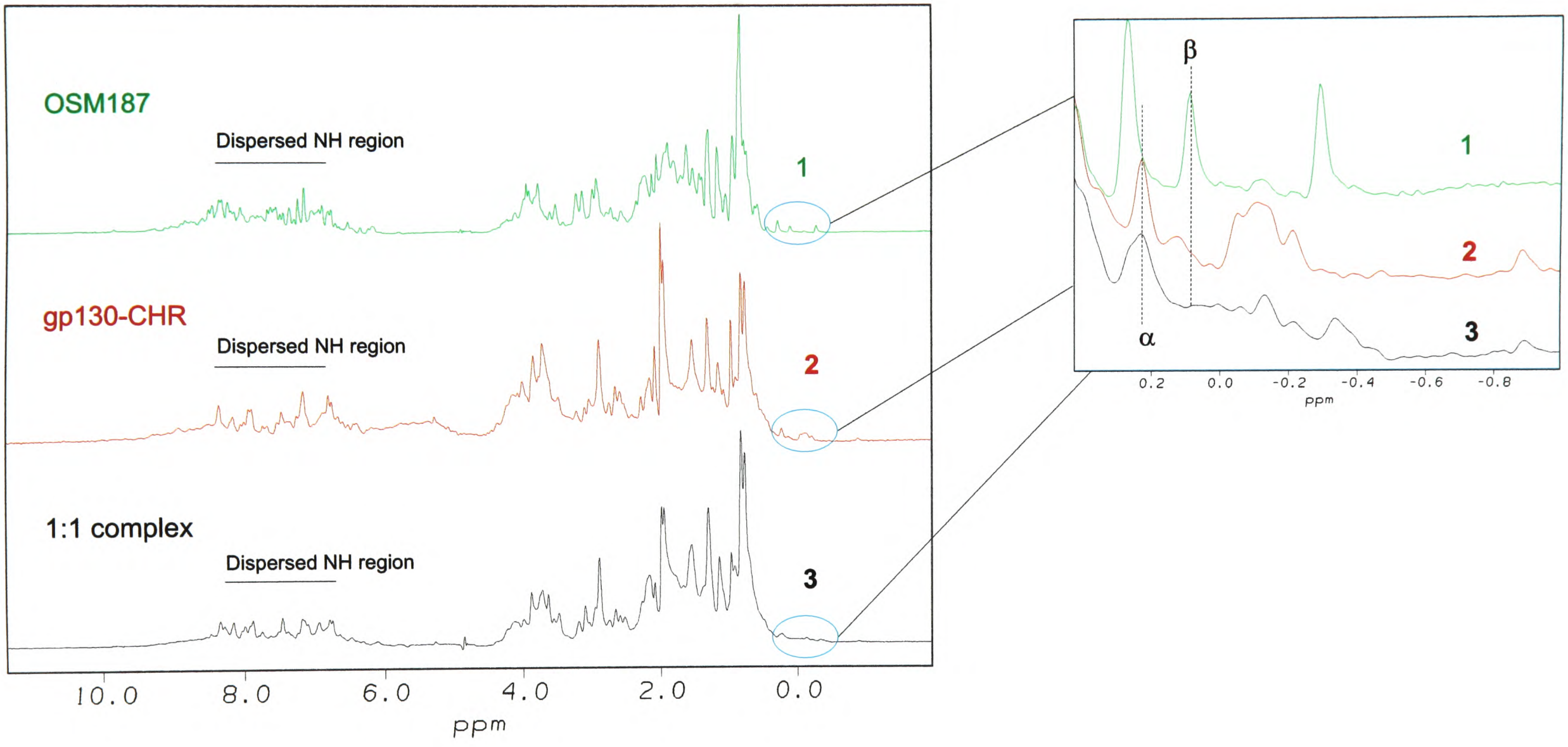

Figure 4.10: Comparison of 1D-^{1}H spectra for free OSM187, gp130-CHR and their 1:1 complex. The data were collected at 600 MHz, pH 6.5 and 25 ^{0}C on a 0.7 mM samples. The spectra on the left panel show features of folded protein. The high field shifts of methyl groups (1,2,3) are zoomed in the right panel. Comparing the spectra in the right panel, it is clear that peak α of the complex is at the same position as the one in gp130-CHR and peak β from OSM187 cannot be detected in the complex. The results indicate the presence of a complex and that some residues are involved in binding and other are not.

that peak α in the complex was at the same position as the peak in gp130-CHR and peak β from OSM187 cannot be detected in the complex. The results indicate the presence of binding and the involvement of some residues in complex formation, while others are not.

5 Interactions between the OSM and gp130-CHR

Biophysical properties of the interactions between the OSM (OSM187) and gp130-CHR were studied by AUC, ITC and SPR techniques. The two proteins form a 1:1 complex with a K_D around 100 nM. The free energy of binding is about 9 Kcal/mole. Detailed analysis can be found in following sections.

5.1 Analytical ultracentrifugation

5.1.1 Solution behaviour of OSM187

OSM187 samples under different concentration and buffer pHs were tested by AUC at 25 °C. A typical AUC profile can be found in Figure 5.1A. The first sample had a concentration of 10 μM at pH 7.4. The second sample had a concentration of 40 μM at pH 5.2. A series of speeds were used on the two samples and a plot was made to analyze the changes of sample's apparent molecular weight (M_{app}) under different rotor speed (Figure 5.1B). Speeds of 10,000, 15,000 and 20,000 rpm were applied to the first sample. For the other sample, rotor speeds of 12,000, 16,000, 20,000 and 26,000 were used. The M_{app} obtained for both samples were close to the calculated molecular weight (M_{calc}). For the first sample, the deviations between M_{app} and M_{calc} were from 9.9 % (at 10,000 rpm) to 5 % (15,000 and 20,000 rpm). Data from the second sample showed a deviation of around 3 %. Thus the M_{app} of OSM187 did not show large changes (>10 %) following the increase of rotor speed, which is the expected feature for a homogeneous solute. It is clear that although

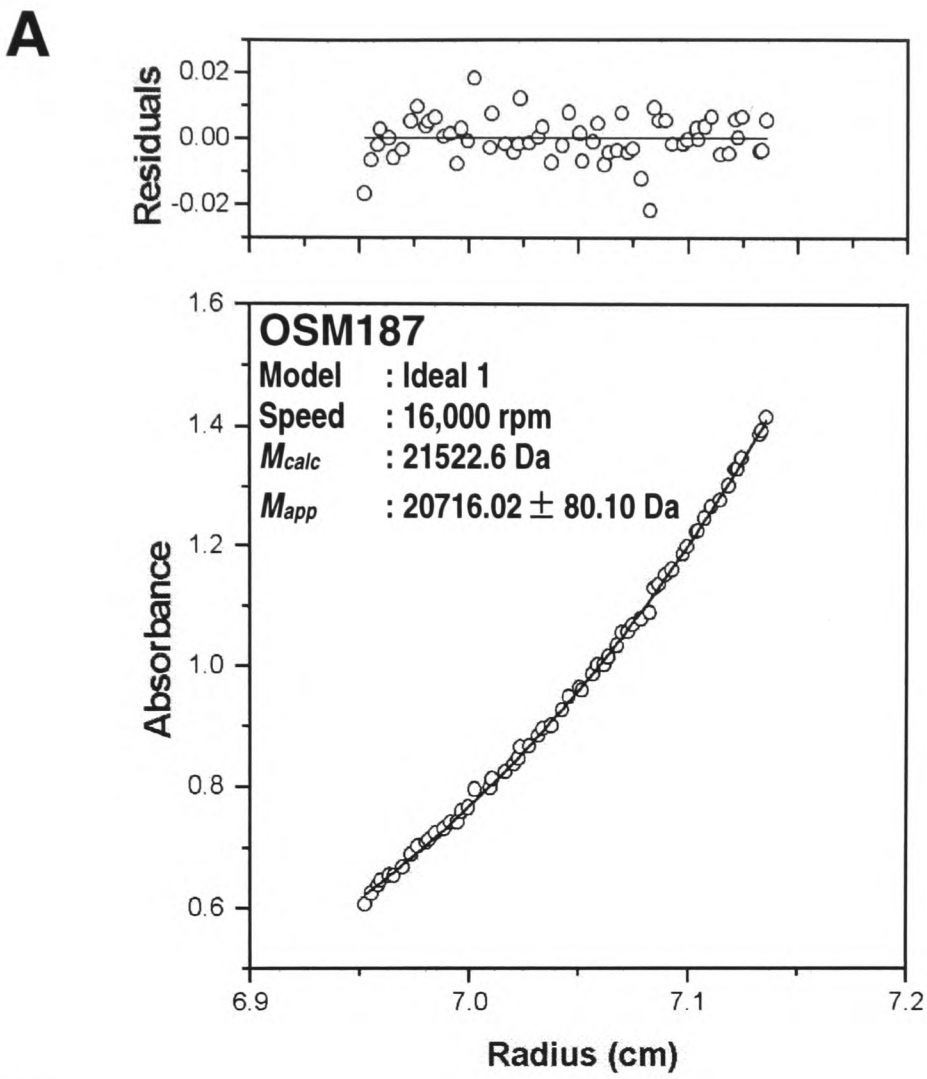

Figure 5.1: The OSM187 forms a homogeneous solute. A) Sedimentation equilibriu profile for OSM187 shown as a distribution of A_{280} at equilibrium. Data were collected 25 °C. The cells were scanned in increments of 0.001 cm at 280 nm. The results w analyzed by an ideal 1 model, shown as a line through the experimental poi Corresponding distributions of the residuals are shown in the upper panel of (A). B) correlation between apparent molecular weight (M_{app}), rotor speed and buffer pH are presented. The M_{app} of OSM187 remains close to the calculated molecular weight (M under different rotor speed and buffer pHs. This indicates that the OSM187 sample homogeneous solute.

OSM187 is monomeric at both pH 7.4 and pH 5.2, the sample behaved better at pH 5.2 even with a higher concentration.

5.1.2 Solution behaviour of gp130-CHR

The solution behaviour of gp130-CHR was tested by AUC under different sample concentration and buffer pHs. For pH 7.4, three concentrations (6, 10 and 20 μM) were studied. At pH 5.2, a 10 μM sample was tested, in order to compare with the pH 7.4 sample. A typical AUC profile can be found in Figure 5.2A. The ideal 1 model was used and the resulting distributions of the residuals were within 0.02. The change of M_{app} at different rotor speed was analyzed in Figure 5.2B. The overall deviation between M_{app} and M_{calc} was larger than that of OSM187. At pH 7.4, it is clear that the higher the concentration the bigger the deviation will be. For the 10 μM sample, at pH 5.2 the slope is shallower than that of the pH 7.4 sample. The results indicate the presence of heterogeneity for the gp130-CHR sample. Based on this result, pH 5.2 was chosen for the binding stoichiometry study.

5.1.3 The stoichiometry of binding

The binding stoichiometry was studied with a 1:1 and 1:2 ratio ~~complex~~ of OSM187/gp130-CHR. The experiments were run at 16,000 rpm with buffer pH 5.2 on samples that contained 4.5 μM OSM187. The AUC profiles, fitting with ideal 1 model, are shown in Figure 5.3A and 5.3B. The obtained M_{app} were 41218 Da and 32943 Da for the 1:1 and 1:2 complex respectively. The M_{app} from the 1:1 complex is close to that of the M_{calc} (46733 Da). If the OSM187 and gp130-CHR can form a 1:2 complex, the data from the 1:2 complex should give a M_{app} close to 71943 Da. On the

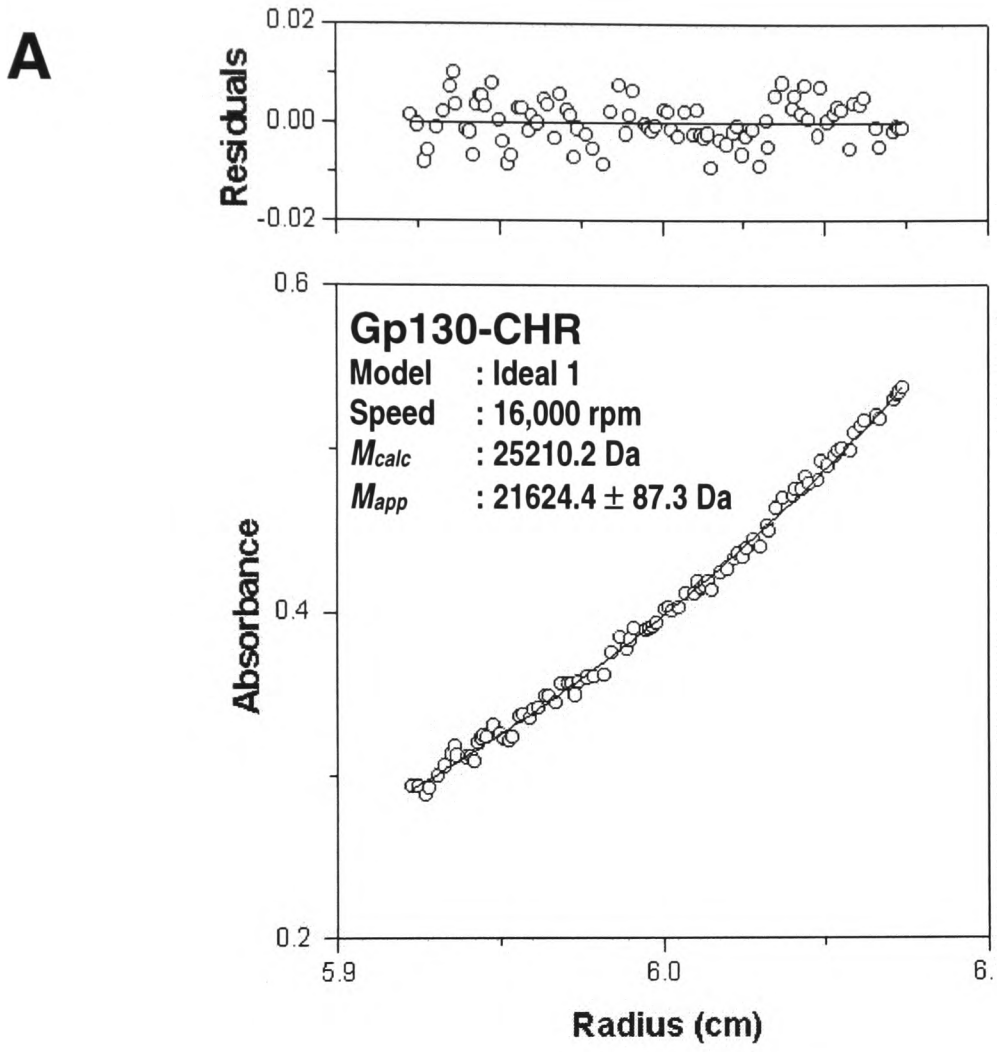

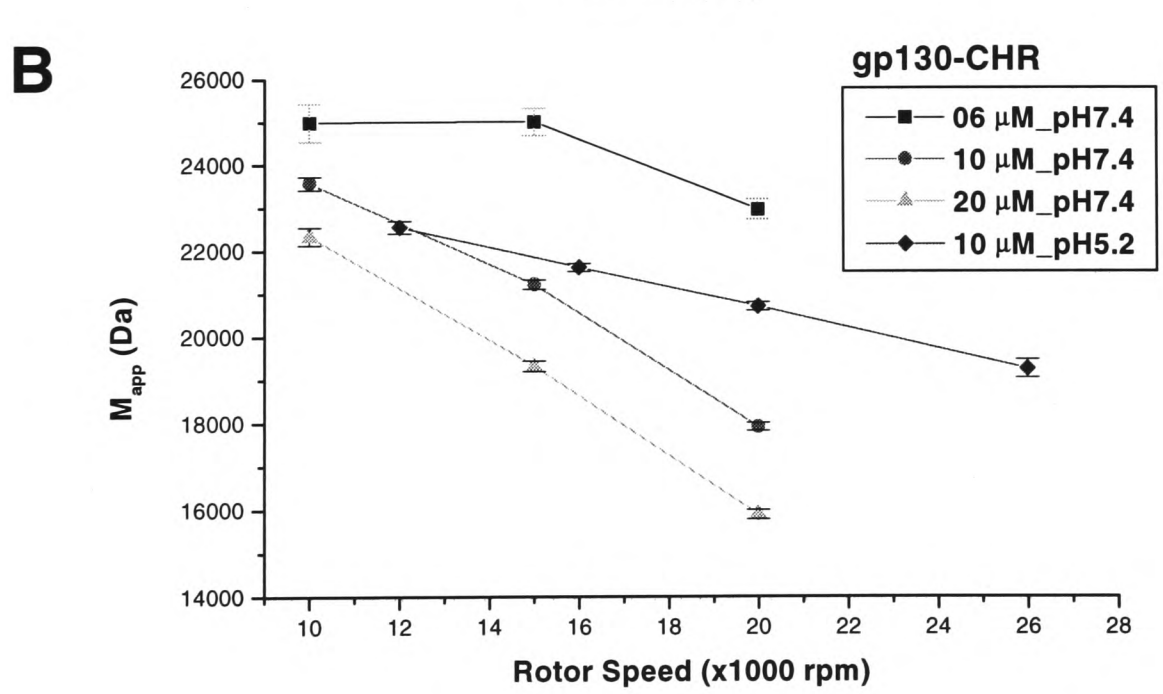

Figure 5.2: Solution behaviour of gp130-CHR. A) Sedimentation equilibrium profile for gp130-CHR is shown as a distribution of A_{280} at equilibrium. Data were collected at 25 °C. The cells were scanned in increments of 0.001 cm at 280 nm. The results were analyzed by an ideal 1 model, shown as a line through the experimental points. Corresponding distributions of the residuals are shown above each plot. B) The correlation between apparent molecular weight (M_{app}), rotor speed and buffer pH are presented. The M_{app} of gp130-CHR decreases as rotor speed or starting concentration increases. This indicates the present of heterogeneity for the gp130-CHR sample. For the 10 μM sample, at pH 5.2 the slope is shallower than pH 7.4 suggesting the sample behaves more like a homogenous solute than at pH 7.4.

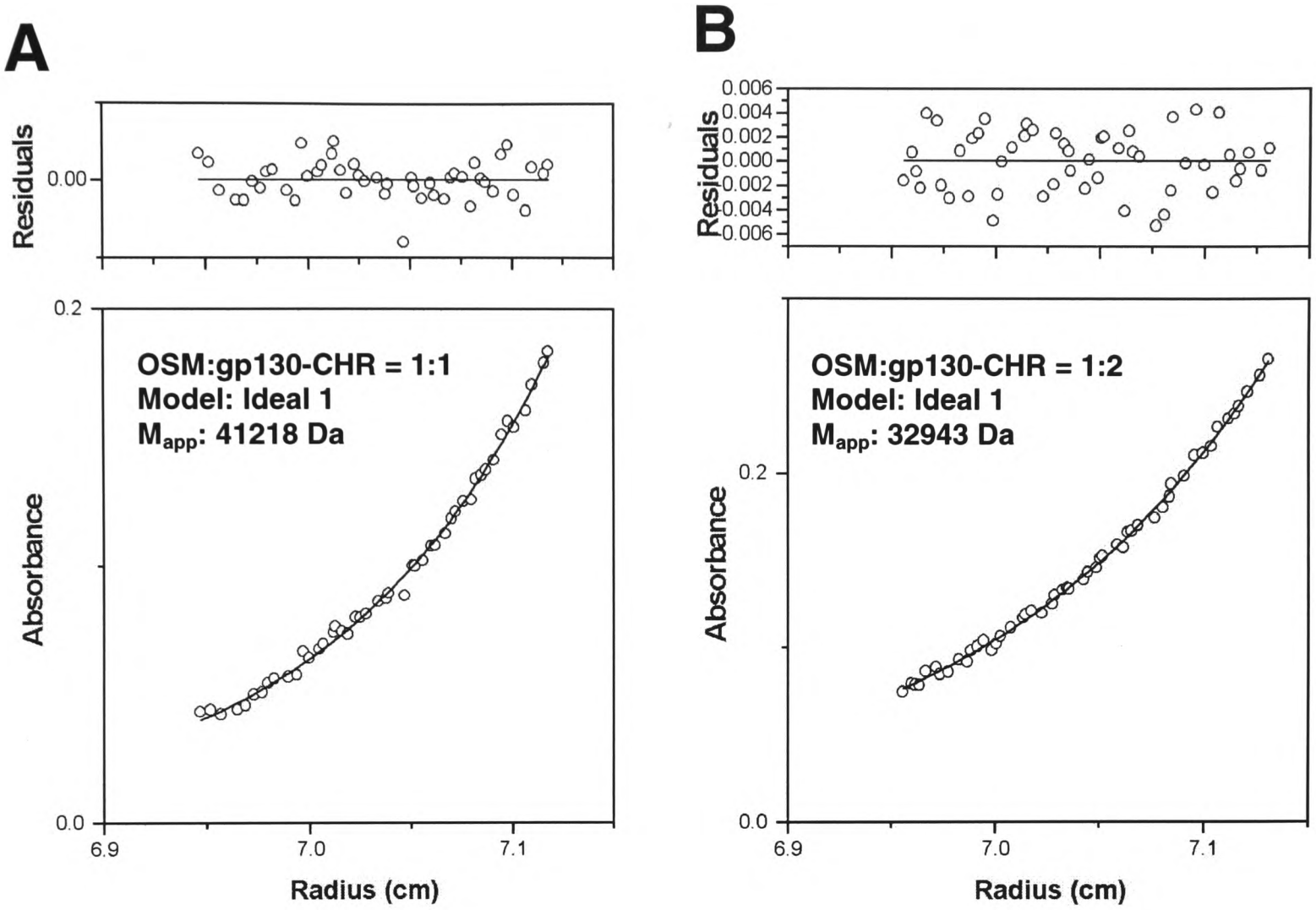

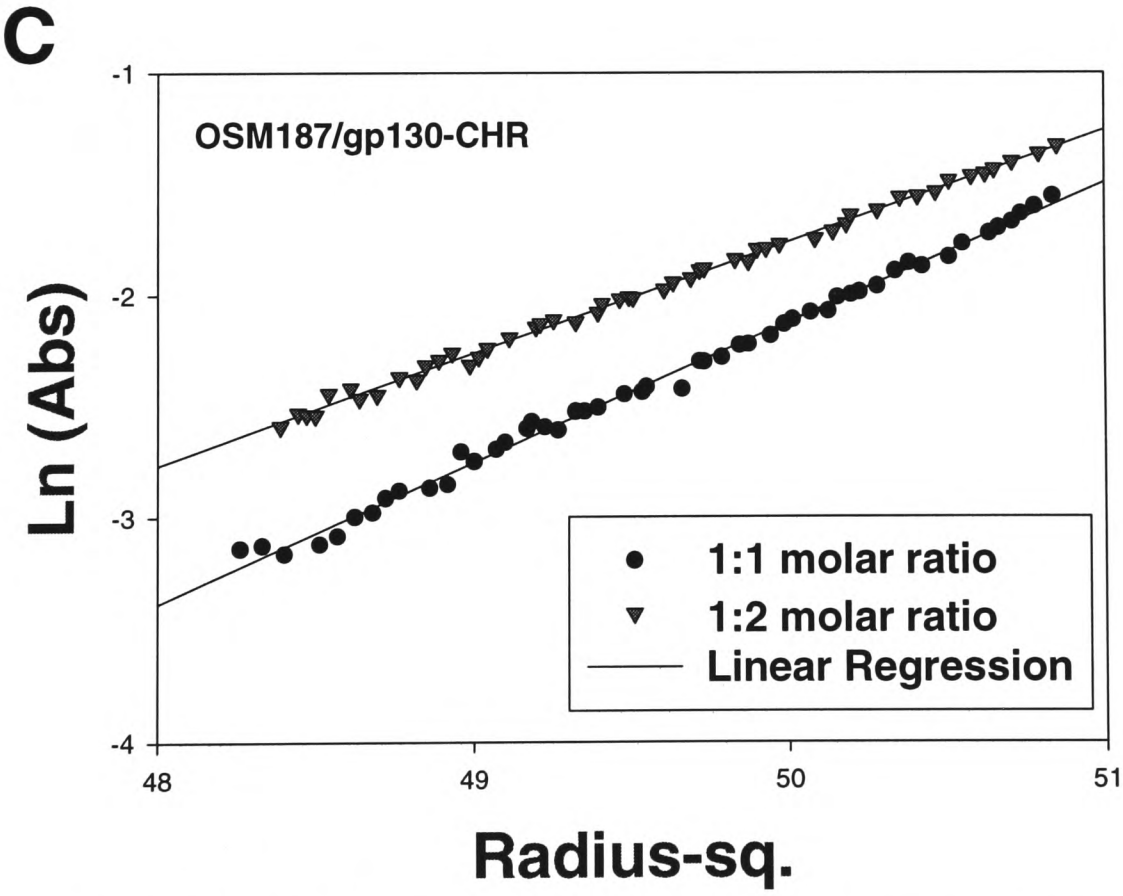

Figure 5.3: AUC studies indicate a 1:1 binding stoichiometry. A) and B) shows the sedimentation equilibrium profiles of OSM187/gp130-CHR 1:1 and 1:2 molar ratio mixtures respectively. The calculated molecular weight for a 1:1 complex is 46733 Da, while the M_{app} were 41218 and 32943 for the 1:1 and the 1:2 molar ratio mixtures respectively. C) The sedimentation equilibrium distribution for the 1:1 (circles) and 1:2 (triangles) molar ratio mixture (4.5 μM). The slope represents the apparent molecular weight. Both samples were in potassium phosphate buffer pH 5.2, temperature 25 °C, speed 16,000 rpm. The cells were scanned in increments of 0.001 cm at 280 nm.

contrary, the 1:2 complex gave M_{app} even smaller than that of the 1:1 complex. This is because the data was treated as a single component solute. Since the fitted M_{app} actually originated from both the complex and the free gp130, the average molecular weight should be smaller than that of the 1:1 complex. The results indicate that OSM187 and gp130-CHR bind with a 1:1 stoichiometry.

5.2 Isothermal titration calorimetry

Calorimetric titration of OSM187 by gp130-CHR and its reciprocal gave the isotherms shown in Figure 5.4. The thermodynamic parameters n, K_A, ΔH_b^0, ΔS_b^0, and ΔG_b^0 extracted from the calorimetric data are listed in Table 5.1. The results indicate that the entropy factor is a relatively large contributor for the free energy of OSM187 and gp130-CHR binding, which is comparable with the GH/GHR interaction (ΔH_b^0=-9.4 ± 0.3 kcal/mole; ΔS_b^0=7.7 ± 1.2 cal/moleK) (272). Although the entropy factor in OSM/gp130-CHR binding is not as dominant as the ones in entropy-driven systems like: Shc phosphotyrosine binding (PTB) domains insulin receptor substrate (IRS-1) (216) and IRS-1 PTB domain-IL-4R peptide (273), the relatively high entropy suggests that the binding may involve the burial of

	OSM187 in sample cell	Gp130-CHR in sample cell
n	1.08 ± 0.01	1.11 ± 0.01
K_A (M^{-1}) x 10^7	1.71 ± 0.54	1.62 ± 0.44
ΔH_b^0 (kcal/mole)	-7.96 ± 0.15	-5.81 ± 0.09
ΔS_b^0 (cal/moleK)	6.39	13.52
ΔG_b^0 (kcal/mole)	- 9.90 *	- 9.90*

* $\Delta G_b^0 = \Delta H_b^0 - T\Delta S_b^0$

Table 5.1: ITC studies of OSM187 and gp130-CHR.

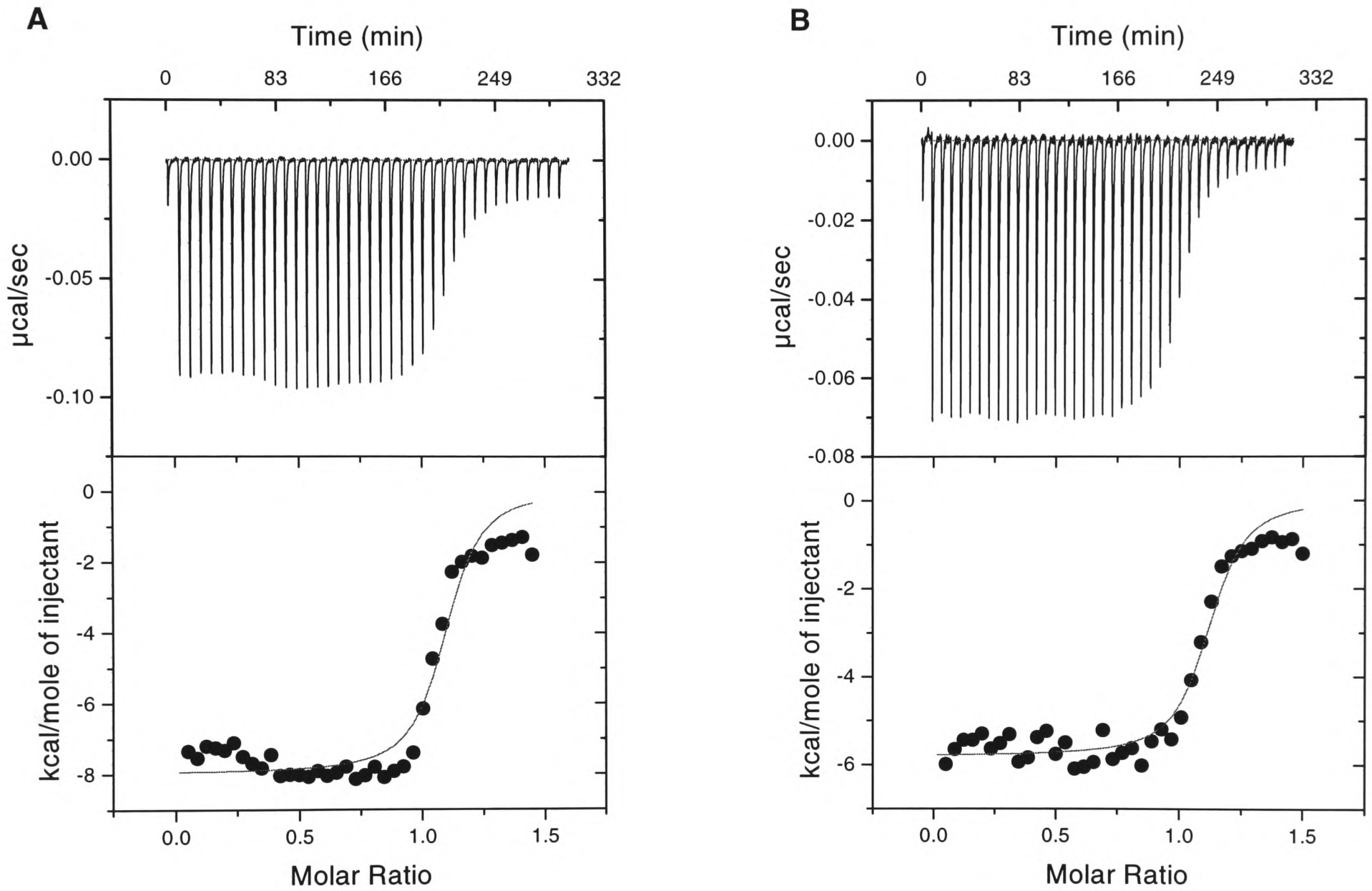

Figure 5.4: ITC studies of the binding between OSM187 and gp130-CHR. ITC titration profiles: A) Calorimetric titration of OSM187 (12.3 µM) with gp130 (125 µM) and B) Calorimetric titration of gp130 (13 µM) with OSM187 (133 µM) at 30 °C. Samples were dialysed against 50 mM potassium phosphate buffer, pH 7.4, 150 mM NaCl. The upper panels showed heat released per addition of 5 µl sample from the syringe. The integration of the peaks in the upper panels yielded a ΔH_b^0 per injection (lower panels). Thirty-eight and thirty-nine consecutive injections (8 minutes interval) were used for (A) and (B) respectively. The rest of the sample in the syringe was used to obtain heat of dilution data, which were subtracted from the results. The solid lines showed the best fit obtained by least-squares regression using a one-site model. Measured thermodynamic parameters are listed in table 5.1.

hydrophobic surface and/or an increase in the conformational freedom upon complex formation. NMR binding studies can be used to gain more insight on the matter.

The entropy value obtained when gp130-CHR was in sample cell (13.52 cal/moleK) was much bigger than that when OSM187 was in sample cell (6.39 cal/moleK). A positive entropy of binding is a strong indication of the hydration change at the complex interface. The difference of the two entropy values perhaps indicates the presence of different hydration changes. The AUC studies revealed that gp130-CHR does not behave well at high concentrations, higher than 10 μM (see section 5.1.2). Although both ITC experiments used gp130-CHR in high concentrations, the gp130-CHR sample in the syringe (125 μM) had much higher concentration than the gp130-CHR sample in the sample cell (13 μM). A probable consequence is that the gp130-CHR molecules may not be completely covered by water molecules. On complex formation, water molecules will be expelled from the complex interface. The differences in solvation status could be a source for the different entropy values.

Due to the large entropy component of the free energy of binding, the heat changes in each injection are relatively small. This leads to low signal to noise ratio of the data acquired. It may seem obvious that a higher starting concentration should be used, but the starting concentration was limited by the *experimental K window* (see section 2.3). For ideal conditions, the *experimental K window* (c value) should be around 10 to 100. The c value is determined by $K_A M_{tot}$. Since the equilibrium association constant, K_A, of OSM/gp130-CHR interaction is about 10^7 M. The M_{tot} should be around 10^{-6} to 10^{-5}. The starting concentrations used here were 12.3 μM

(OSM187) and 13 μM (gp130-CHR), which corresponds to *c* values of 123 and 130, larger than 100, the optimum *c* value. This compromise was made in order to obtain better signal to noise within a reasonable *experimental K window*.

Based on previous study (19,72), the OSM binds to gp130-CHR with a single binding site. Here, the idea was tested by the reciprocal titration experiment mentioned previously, assuming that gp130-CHR has two fairly strong sites with differing affinity for OSM187. When we put gp130-CHR in the reaction cell and the OSM187 in the syringe, then the tightest of the two sites, with heat change H1, will titrate in the early injections and the weakest of the two, with heat change H2, will titrate in subsequent injections until both sites are saturated, whereupon the heat change goes to zero. However, if the OSM187 is in the reaction cell, then the heat change will be a different route. Because the OSM187 will be in excess in the early injections, both sites will titrate with heat exchange H1 + H2. When sufficient gp130-CHR has been introduced to the reaction cell (i.e. molar ratio of OSM/gp130-CHR of 0.5) to form a 2:1 complex with OSM187, further addition of gp130-CHR will result in some of the OSM187 being removed from the weaker site in the 2:1 complex so that it can bind to the stronger site on the newly injected gp130-CHR. The heat change for this second phase of titration will then be H1-H2, as long as site 1 is sufficiently stronger than site 2. A comparison of the two sets of data obtained could easily rule out the two-sites hypothesis. Fitted with one-site model, both data gave a transition point at molar ratio 1.0 (Figure 5.4). These results indicated a 1:1 stoichiometry of the OSM187/gp130 complex, which is consistent with the result from AUC.

5.3 Surface plasmon resonance

5.3.1 The kinetic rate constants

Kinetic rate constants of the binding between OSM187 and gp130-CHR were measured by injecting a series of concentrations of gp130-CHR over immobilized OSM187 (Figure 5.5). The k_{on} and k_{off} were evaluated by analyzing appropriate components of the sensorgram curve using the global fitting from BIAevaluation 3.0 software. For data analysis, the 1:1 Langmuir binding with or without mass transport correction term and the heterogeneous ligand-Parallel reaction models were compared. There is no significant difference in fits of 1:1 binding with or without the mass transport factor. This is what is expected, since the immobilization level was kept low (400 RU) and the flow rate is quite high (50 µl/min), the mass transport effect has been minimized (228). The heterogeneous ligand-Parallel reaction model was applied to the data, due to surface heterogeneity. The model indicated two surface ligand species, which occupied 53.8 % and 46.2 % surface respectively. The measured R_{max}, k_{on} and k_{off} are listed in table 5.2. The dissociation constant was calculated from k_{off} / k_{on}.

	Species I	Species II
k_{on} ($M^{-1}s^{-1}$) x 10^5	3.10 ± 0.07	2.62 ± 0.03
k_{off} (s^{-1}) x 10^{-2}	4.54 ± 0.13	2.06 ± 0.03
R_{max} (RU) x 10^2	1.20 ± 0.05	1.03 ± 0.05
K_A (M^{-1}) x 10^7	0.68	1.27
K_D (nM)	145 ± 6	77 ± 1

Table 5.2: SPR kinetic studies of OSM187 and gp130-CHR. Data from kinetic measurement were analysed by heterogeneous ligand-Parallel reaction model. The resulting two surface ligand species gave binding parameters as listed in the table. Based on the R_{max} values, species I and II occupied 53.8 % and 46.2 % chip surface respectively.

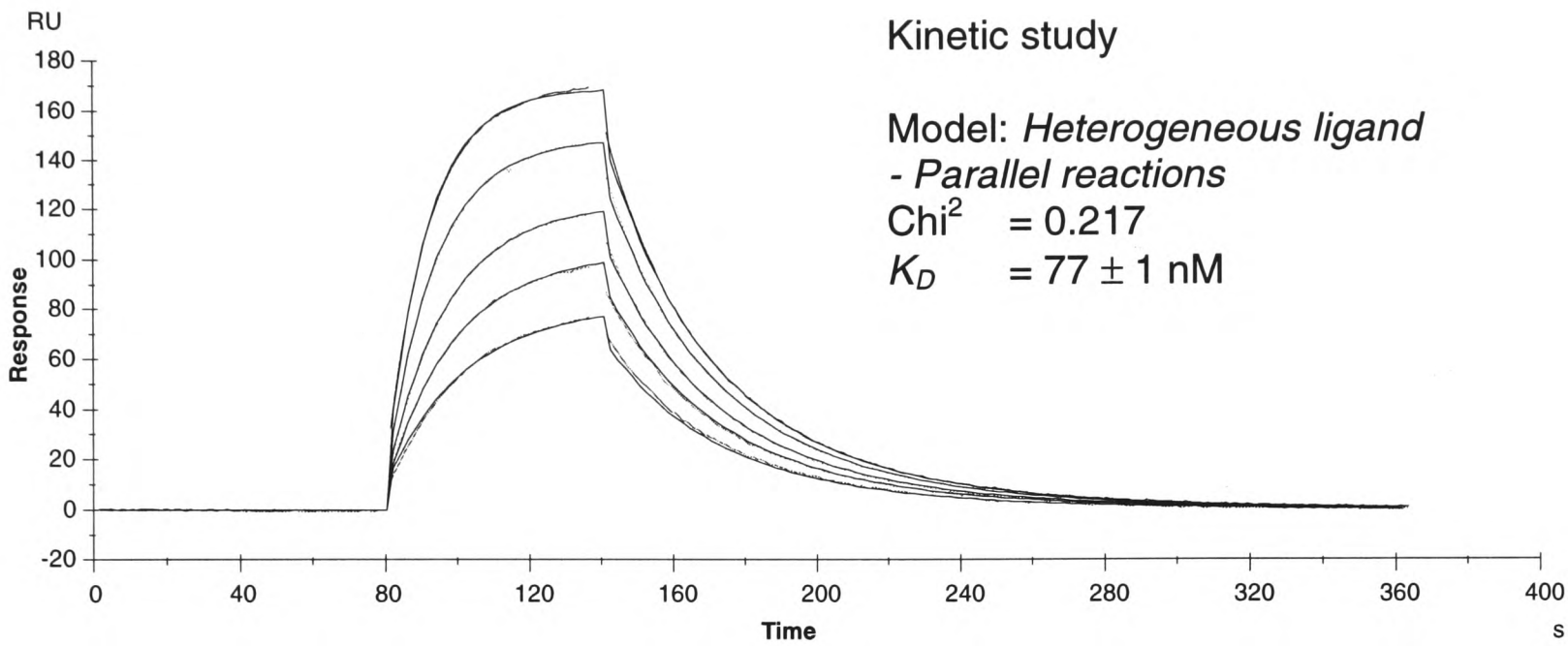

Figure 5.5 Kinetic studies of gp130 with immobilized OSM187. A series of concentrations of gp130 (50, 75, 100, 150, 200 nM) were injected over immobilized OSM187. Flow speed was 50 µl/min. The k_{on} and k_{off} were derived from the appropriate components of the sensorgram curve by the BIAevaluation 3.0 software using global fitting. The fitted curves are overlaid on the sensorgram traces. Samples were in HBS buffer pH 7.4 and 25 °C. The K_D was calculated from k_{off}/k_{on}.

Because SPR studies detect binding between immobilized ligand and solution analyte, many artifacts can be introduced to the system. The mass transport effect and heterogeneous surface ligand are two of the most obvious (see section 2.4.4.4). Surface heterogeneity can be overcome by using specific coupling techniques. In our study, antibody capturing was used and compared with amine coupling. Typical sensorgram fits are compared in Figure 5.6 to emphasise the effect surface heterogeneity has on data fitting. Although antibody-capturing produces well oriented immobilization, it is not suitable for the study here. First, the technique cannot provide an identical surface for a series of experiments. Since the GST-OSM was not immobilized covalently, it could be easily washed off the surface. Second, the anti-GST antibody cannot distinguish GST and GST-OSM. The linker between GST and OSM in the fusion protein is not very stable. During experiments the fusion protein can be cleaved to GST and OSM. This produces GST that can bind to the anti-GST antibody, which adds background noise to the resulting sensorgram.

5.3.2 The equilibrium binding constants

Equilibrium binding constants were measured for the binding of OSM187/gp130-CHR and OSM196/gp130-CHR. A series of concentrations of gp130-CHR (20-400 nM) was injected over immobilized OSM187 and OSM196 until equilibrium was reached (Figure 5.7A). The flow speed was 5 µl/min. Responses at equilibrium, corrected for background from control flow cells, were recorded as R_{eq} for individual injections. Scatchard analysis was used to evaluate the binding constants from triplicate data sets. A straight line was fitting using a linear regression model in Origin 5.0 software, which gives $-1/K_D$ as slope and R_{max} as intercept on the

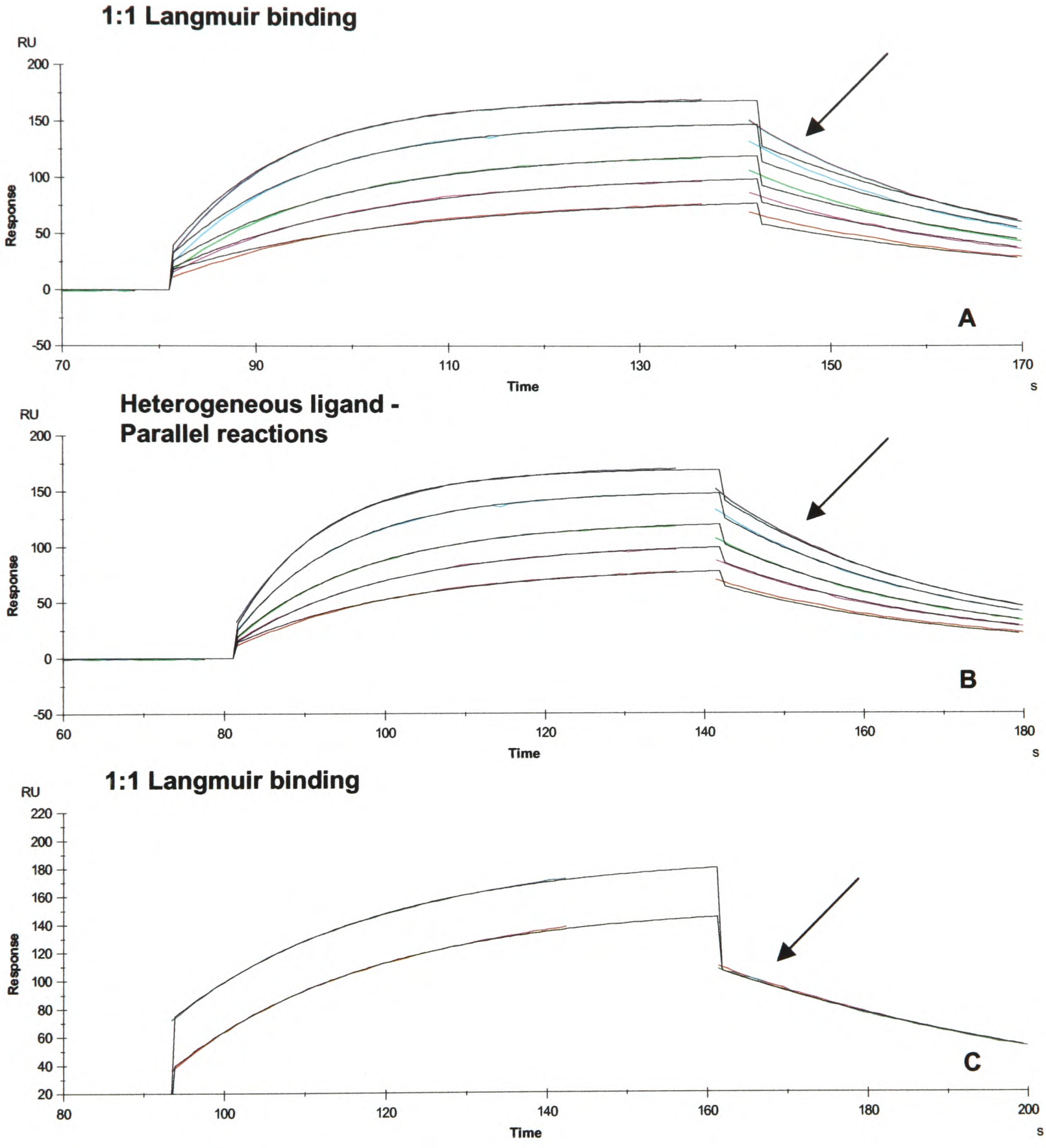

Figure 5.6: The heterogeneous chip surface caused by amine coupling. The figure showed sensorgrams obtained by injecting gp130-CHR over immobilized OSM. The fitted curves were overlaid on top of the original data. Dissociation phases are emphasised by arrows. In (A) and (B) OSM187 was immobilized by amine coupling. Comparing the dissociation phases, the fit for (B) was tighter than that for (A). This is because (B) was fitted with a heterogeneous ligand model, while the model in (A) assumes the surface was homogeneous. C) Anti-GST antibody was immobilized on the chip surface first and used to capture the GST-OSM fusion. The method gives a well-oriented surface ligand. Fitted with same model as in (A), the fit agreed with experimental data very well. This is because the assumption of a homogeneous surface was satisfied.

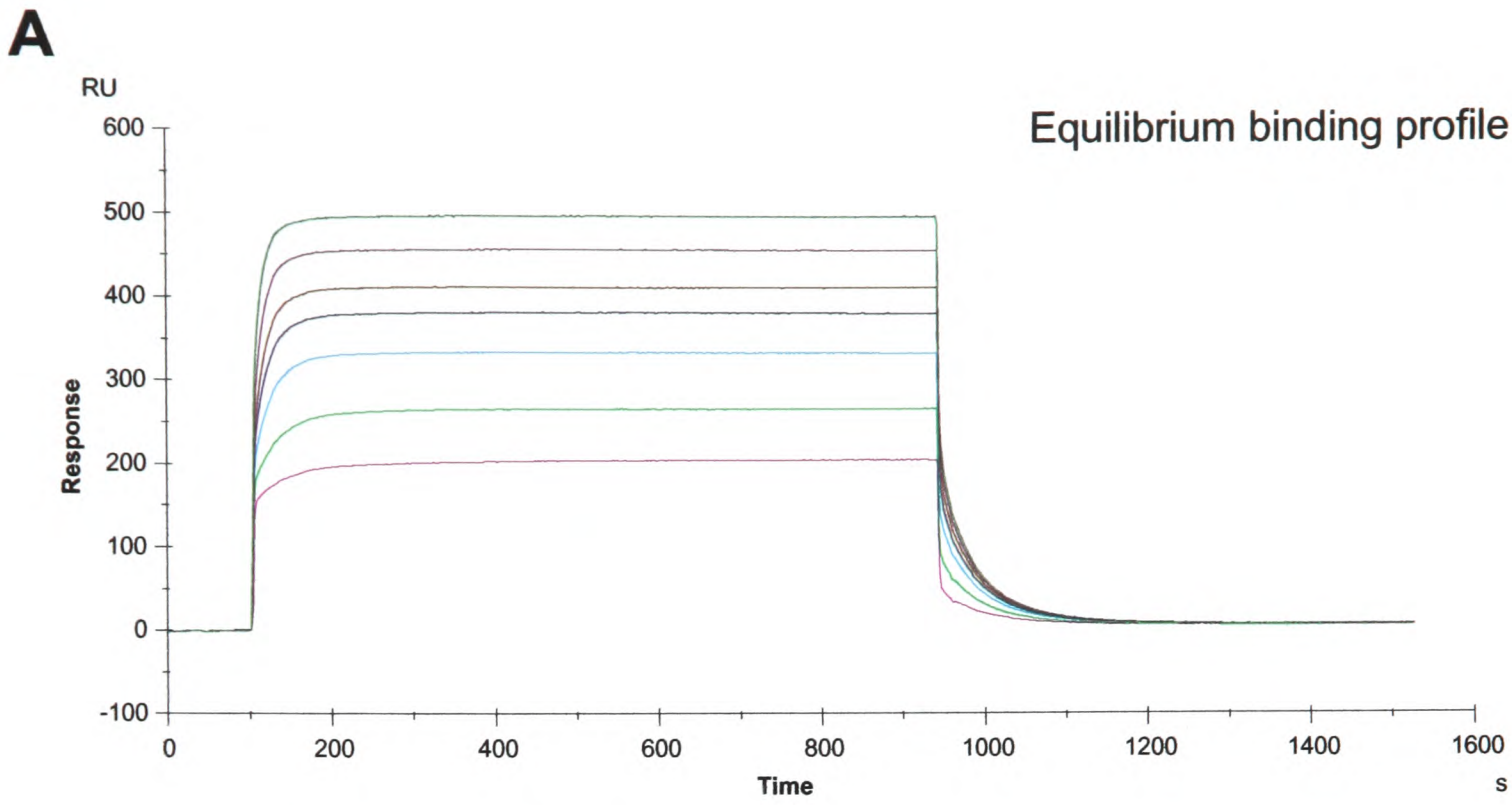

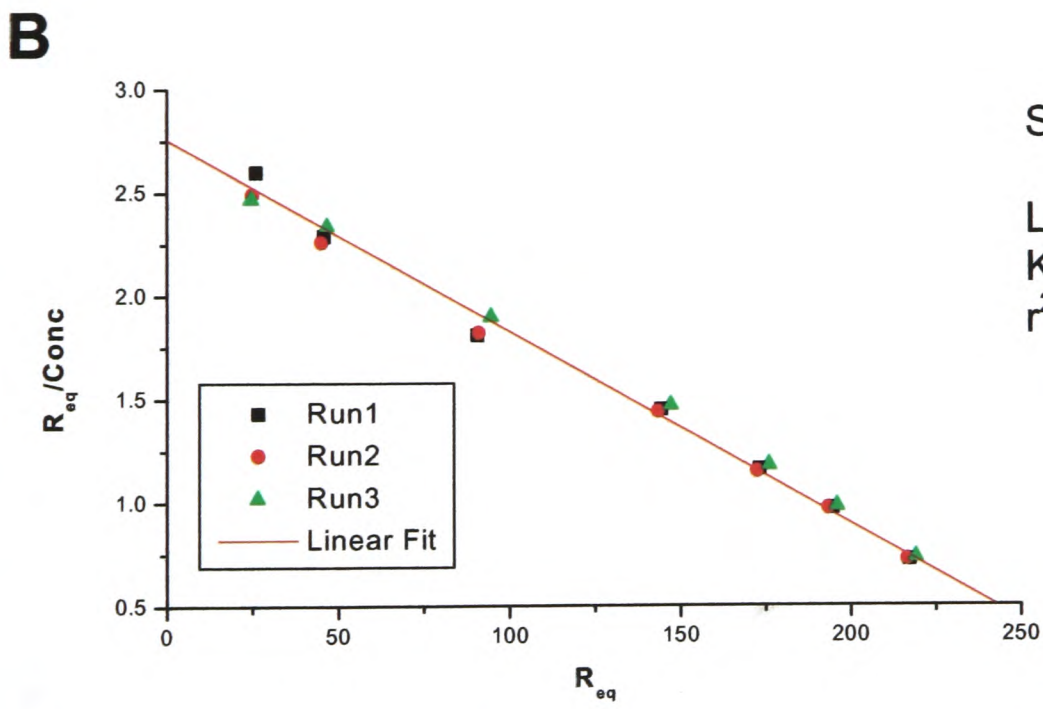

Figure 5.7: BIAcore equilibrium studies of OSM187. A) A series of concentrations of gp130 samples (20, 50, 100, 150, 200, 300 and 400 nM) were injected over immobilized OSM187. Flow speed was 5 µl/min. Response at equilibrium, corrected for background from control flow cell, was recorded as R_{eq}. Samples were in HBS buffer pH 7.4 and 25 °C. B) A Scatchard plot (triplicate data sets) was used to evaluate the binding constants. Data from triplicate runs were showed as squares (Run1), dots (Run2) and triangles (Run3). A straight line was fitted using linear regression model in Origin 5.0, which gave the $-1/K_D$ as slope and maximum binding capacity (R_{max}) as intercept on X-axis.

X-axis (Figure 5.7B). The calculated K_D values for OSM187 and OSM196 (Figure 5.8) were 108 nM and 116 nM respectively. The R_{max} values for OSM187 and OSM196 were about 270 RU and 1720 RU, which were much smaller than their immobilization level (400 RU for OSM187 and 4000 RU for OSM196). Since the size of OSM is very close to that of gp130-CHR, if all the immobilized OSM were active, the R_{max} values should be around the immobilization values. The low R_{max} values, as measured, indicated that not all the immobilized molecule could bind with gp130-CHR.

5.3.3 The OSM187 and OSM196 bind gp130-CHR in similar manners

The truncated OSM (OSM187) was compared with its native form (OSM196) for binding properties. The dissociation constants, obtained from equilibrium binding studies above, were 108 nM and 116 nM for OSM187 and OSM196 respectively. A solution competition experiment was designed to test if both OSM187 and OSM196 bind to gp130-CHR at the same binding site. Samples were made with 100 nM gp130-CHR and different concentrations of OSM187 (0, 5, 10, 20, 50, 75, 100, 150, 200, 300 and 400 nM). The mixtures were injected over immobilized OSM187 and OSM196 at 50 µl/min. Triplicate data points were obtained. The higher the OSM187 concentration in solution the lower the BIAcore response level was. This indicated that OSM187 competed with OSM196 for gp130-CHR binding sites in solution. Plots were made to correlate the percentage response of an individual sample with the Log of the concentration of the OSM187 added (Figure 5.9a). Comparing the

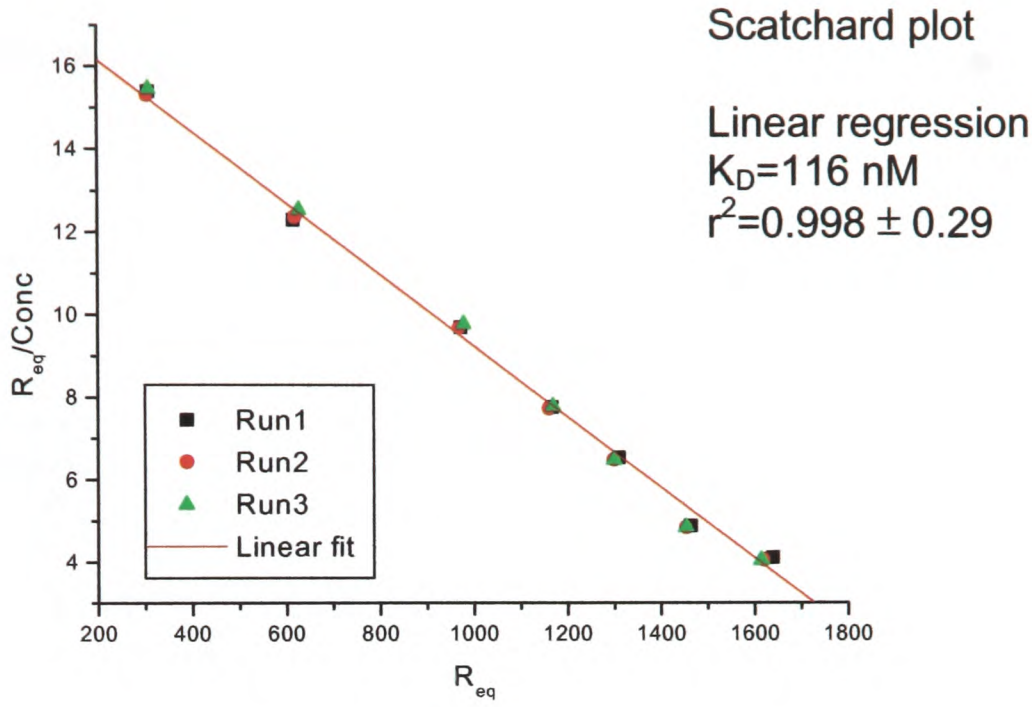

Figure 5.8: BIAcore equilibrium studies of OSM196. A series of concentrations of gp130 samples (20, 50, 100, 150, 200, 300 and 400 nM) were injected over immobilized OSM196. Flow speed was 5 µl/min. Response at equilibrium, corrected for background from control flow cell, was recorded as R_{eq}. Samples were in HBS buffer pH 7.4 and 25 °C. A Scatchard plot (triplicate data sets) was used to evaluate the binding constants. Data from triplicate runs are shown as squares (Run1), dots (Run2) and triangles (Run3).

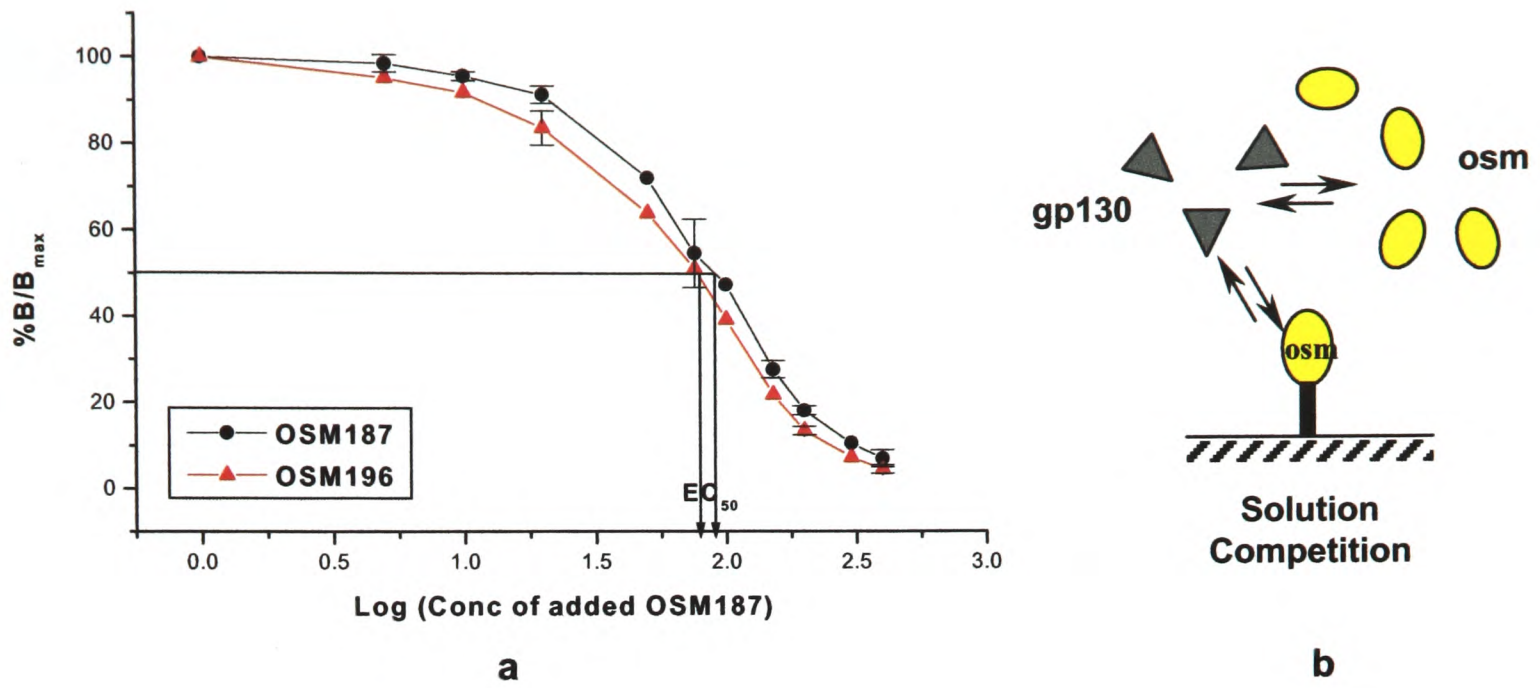

Figure 5.9: BIAcore competitive binding studies. Surface competition (b) was used to compare the binding properties of the OSM187 with the native OSM (OSM196). a) To a constant concentration of gp130-CHR (100 nM), a series of OSM187 concentrations (0-400 nM) were applied. The mixture was then injected (50 ml/min, triplicate) over immobilized OSM187 and OSM196. The percentage response of individual sample was plotted against Log (concentration of added OSM187), where B is the response measured from each injection of the mixture and B_{max} is the response when no OSM187 was added. EC_{50} was used to indicate the concentration of competitor, which effectively competes for 50% of specific binding. Error bars were calculated as the difference between the maximum and the minimum. Samples were in HBS buffer pH7.4 and 25 °C.

competition binding profiles reveal that both OSM187 and OSM196 have similar competition traces and EC_{50} values (about 100 nM).

5.4 Preliminary NMR studies on a 1:1 complex of ^{15}N OSM187 and gp130-CHR

Due to the size of the 1:1 complex (46.7 kDa), the TROSY technique was used to acquire the ^{1}H-^{15}N data for ^{15}N labelled OSM187 at free and bound state (Figure 5.10). Both spectra had around 200 peaks, which was the expected number from OSM187 (193 amino acids). Comparing the peaks from both free and bound states, it is clear that most peaks remain at the same position. There are some new peaks that appear in the spectrum of the 1:1 complex, which are not in the free state spectrum. The result indicates the presence of binding and that only a few residues are involved in complex formation. There are also peaks that have a shoulder in the spectrum of 1:1 complex but have no shoulder in the free state spectrum. The binding studies above indicate that the binding between OSM187 and gp130-CHR is in the slow exchange mode with a 1:1 stoichiometry. This means that the chemical shift changes of the residues involved in complex formation will not show a titration effect. They will totally disappear from one position and show up in another. Thus, the shoulder in the rectangular shape frames in Figure 5.10 suggests that not all the OSM187 participate in binding with gp130-CHR. A portion of OSM187 was free, which gave a signal for a peak at same position as the one in free state spectrum. While, the bound OSM187 gave a signal for the shoulder. Since the concentrations of OSM187 and gp130-CHR were carefully calibrated, a portion of gp130-CHR may not be active.

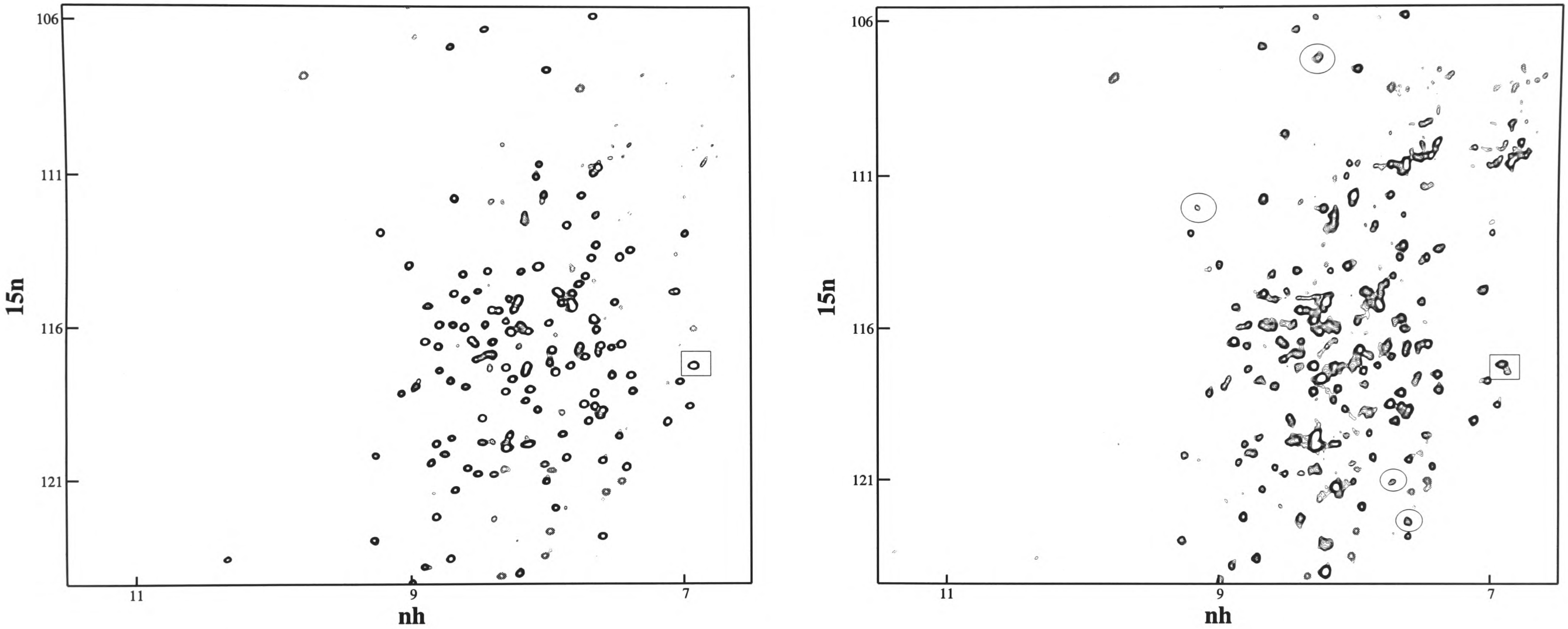

Figure 5.10: Comparison of ^{1}H-^{15}N spectra of free OSM187 and the 1:1 OSM187/gp130-CHR complex. TROSY experiments were used to acquire ^{1}H-^{15}N data of free OSM187 (Left panel) and the 1:1 complex (Right panel). Both spectra had approximate number of expected peaks. Comparing peaks from the 1:1 complex with those from free state OSM187, it is clear that most of the peaks remain unchanged. However, peaks circled in the spectrum of 1:1 complex were not in the free state spectrum. There are also peaks that had a shoulder peak in the 1:1 complex, such as the one framed in rectangular marker. The experiments were run at 750 MHz, pH 6.8 and 35 ^{0}C. A 0.3 mM sample was used to acquire free state OSM187 data. The data for the 1:1 complex were recorded on a 0.4 mM sample.

6 Interactions between the IL-2 and IL-2 receptor beta chain

6.1 Introduction

Interleukin-2 (IL-2) is a cytokine, initially detected as a T cell growth factor (274). Produced by T helper 1 (Th1) cells, IL-2 is involved in multiple biological responses of various types of cells, such as growth and differentiation of T cells, B cells, natural killer (NK) cells and glioma cells (275-277), as well as activation of immunoglobulin (Ig) production by B cells (278), and cytotoxicities of natural killer (NK) cells (279,280), and monocytes/macrophages (281,282). All these biological responses are important for the development of cell-mediated immunity.

The effects of IL-2 are mediated through specific cell-surface receptors (IL-2R). Receptor binding studies have classified three types of IL-2R (the high, intermediate and low affinity receptors) according to their affinity for IL-2. There are at least three subunits (α, β and γ), encoded by different genes, constituting these receptors (283). The first subunit, identified by a monoclonal antibody recognizing the Tac antigen (284), IL-2Rα, is a 55 kDa cell surface molecule (p55) that binds IL-2 with a K_D of about 10 nM (low affinity receptor). Cloning of the IL-2Rα gene (285,286) revealed that IL-2Rα has no ability to transduce intracellular signals. In addition, IL-2Rα has no significant homology to known cytokine receptors. The second subunit, IL-2Rβ, was initially identified by affinity cross-linking experiments with radio-labelled IL-2 (287-291) and subsequently by a monoclonal antibody (mAb)

specific for the human IL-2Rβ; it was shown to be a 75 kDa cell surface glycoprotein (p75) (292,293). The third subunit, IL-2Rγ, was purified by immuno-affinity chromatography with another mAb (283). The 64 kDa (p64) γ-chain and the β-chain both belong to the haematopoietin receptor family. Two types of IL-2R that are able to transmit signals are expressed in humans: IL-2Rα plus IL-2Rβ, which form an intermediate affinity IL-2R with a K_D of around 1 nM when all three chains are involved a high affinity IL-2R (K_D > 10 pM) is formed.

Hetero-trimerization of the IL-2R subunits triggers downstream signalling events that involve tyrosine phosphorylation of a large array of cellular proteins. The IL-2R complex does not exhibit protein tyrosine kinase (PTK) activity but is coupled to soluble non-receptor PTKs. These various kinases (p56Lck, Syk or JAK) phosphorylate specific substrates, triggering a cascade of events organized in three major pathways:

1. Shc activation and induction of the Ras pathway.
2. The JAK-STAT (signal transducers and activators of transcription) pathway.
3. The phosphoinositide-3-kinase (PI 3-K) pathway.

The study of all the above signalling pathways indicated that IL-2Rβ plays a vital role in IL-2R complex signal transduction. Both the acidic and serine-rich regions (Figure 6.1) of the IL-2Rβ chain cooperate to trigger the activation of Ras (294) as well as the PI 3-K pathway (295-297). The box1/box2 motif of the

intracellular part of IL-2Rβ is used by Janus kinase 1 (JAK1) which is required for the phosphorylation and activation of the DNA-binding STATs.

All the three subunits are important in the formation of the intact IL-2R complex. Gene-knockout mice demonstrated inflammatory bowel disease (IL-2Rα deficient) and myeloproliferative disorder (IL-2Rβ deficient) (298). IL-2Rγ deficiency in humans leads to X-linked severe combined immunodeficiency (XSCID) (35,299).

The mature form of IL-2Rβ consists of 525 amino acid residues. Being the same family member (class I cytokine receptor family) as the gp130, IL-2Rβ has the common features of the family: two pairs of conserved cysteine residues near the amino-terminal and the WSXWS motif in the extra-cellular domain (17,300). The cytoplasmic, serine-rich, region is necessary for signal transduction and the membrane proximal WSXWS motif is essential for IL-2 binding (301,302). The extra-cellular region of IL-2Rβ, consisting of 214 amino acid residues, has two domains: a cytokine receptor (CK) domain and a fibronectin type III (F3) domain (Figure 6.1) (303).

The aim of this project is to use recombinant expression to produce the IL-2Rβ extra-cellular region for structural and functional analysis.

6.2 Methods

6.2.1 Cloning IL-2Rβ

Two *E.coli* strains (JM109 and HW110) were chosen to clone and express the MBP fusion IL-2Rβ. The cloning sites of pMalp2-3C are marked in Figure 6.2. For

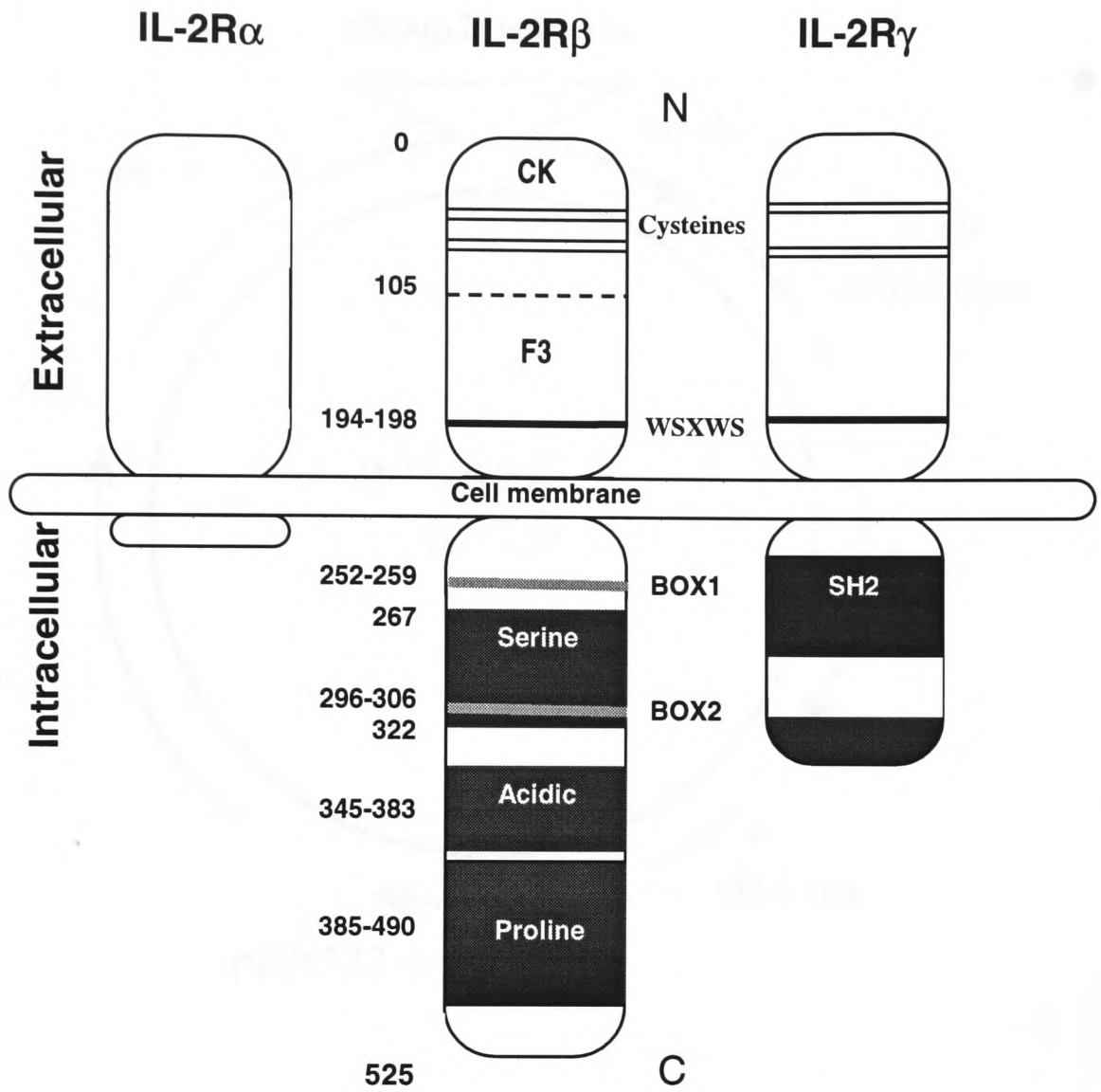

Figure 6.1: The IL-2 receptor complex. IL-2 receptors are transmembrane proteins with extracellular N-termini (marked as N). Three chains (α, β and γ) form the high affinity IL-2R complex. The whole IL-2Rβ chain has 525 amino acids. Functional regions on IL-2Rβ are marked according to their locations on the protein. The IL-2Rβ belongs to the class I cytokine receptor family. The extracellular region of IL-2Rβ contains two domains, the cytokine receptor domain (CK) and the fibronectin type III domain (F3). The two pairs of thin lines within the CK represent conserved cysteines and the thicker line in F3 is the WSXWS motif. These features are also represented in IL-2Rγ. The intracellular region of IL-2Rβ contains the box1/box2 motifs (indicated by the grey lines). The serine-rich, acidic and proline-rich domains are represented by black boxes. There is an SH2-like domain in IL-2Rγ's intracellular region, also marked as a black box.

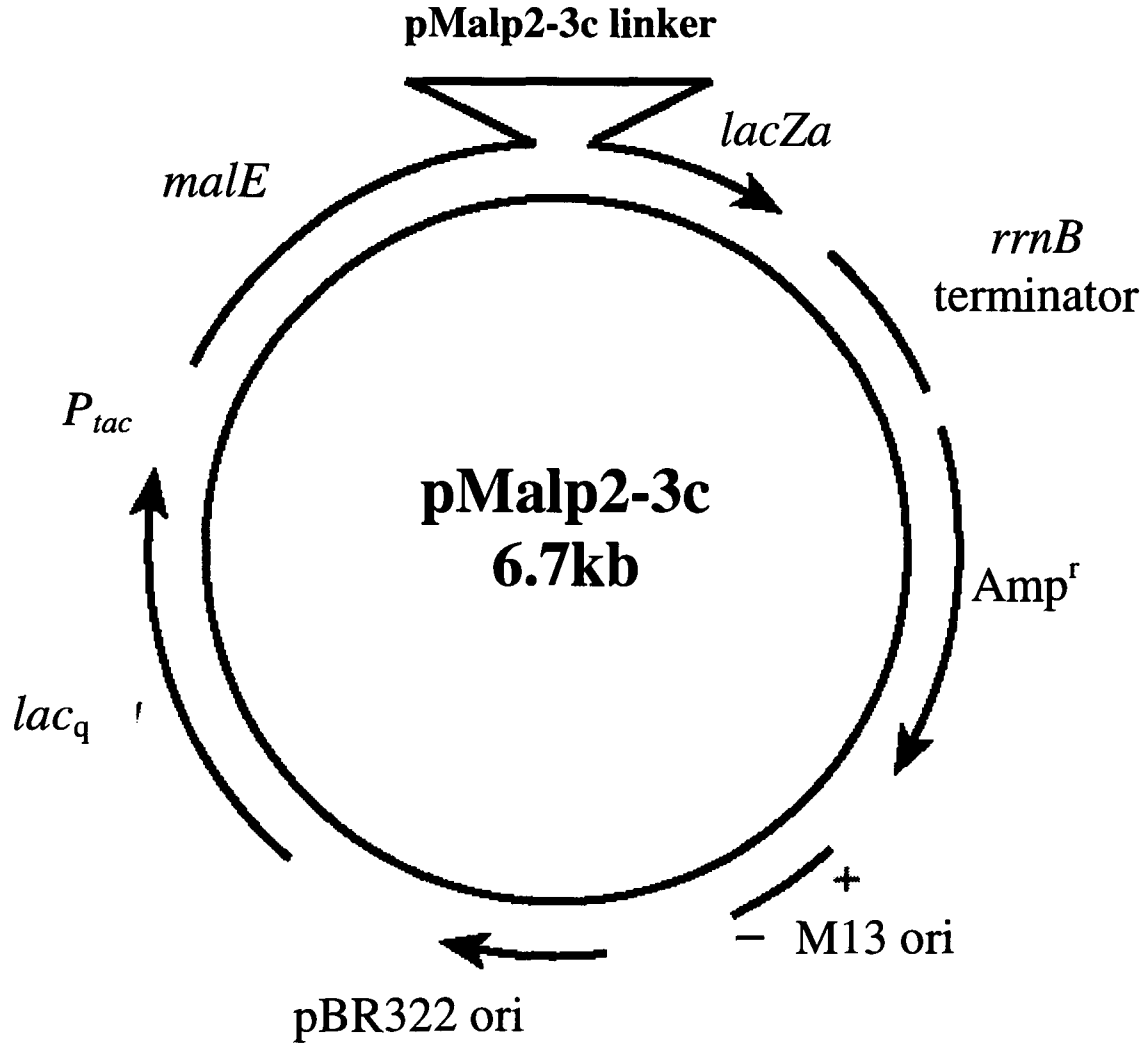

pMalp2-3c linker

Ecl136II
Sac I

malE ... TCG AGC TCG AAC AAC AAC AAC AAT AAC AAT AAC AAC AAC CTC GGG

SmaI ***XbaI***

E V L F Q G P G

ATC GAG GGA AGG GAG GTG CTA TTC CAG GGA CCC GGG AAT TCT AGA ... *lacZα*

Factor Xa cleavage site

Protease 3C cleavage site

Key

- ***lacI*** ^{q} : *Lac* repressor gene, which turns off transcription from P_{tac} until IPTG is added
- ***P*** $_{tac}$: Promoter for *malE-lacZα* gene fusion
- ***malE*** : Encoding the maltose binding protein.
- The IL-2Rβ gene was inserted into the vector between *Sam*I and *Xba*I sites

Figure 6.2: The expression vector ***pMalp2-3C***

GST fusion IL-2Rβ, pGEX-6p-2 was used. The oligonucleotides for PCR and DNA sequencing are summarized in table 6.1. Both of the constructs contained a cmyc tag at the C-terminal of the IL-2Rβ gene.

Gene cloning procedures were essentially the same as those described in chapter 3.

6.2.2 Expression and purification

The expression and purification of MBP-IL-2Rβ and GST-IL-2Rβ followed the methods for MBP-gp130-CHR and GST-OSM respectively.

6.2.2.1 Western blotting

The Western blot technique was used to detect the expression of the IL-2Rβ proteins. The Promega ProtoBlot II AP System was used for the Western Blotting. Protein samples were run duplicated on two NuPAGE pre-cast gels. The Novex Mark12 marker was applied to one gel, while the other used the MultiMark Multi-Colored marker from the same company. Following the instructions accompanying the ProtoBlot II system, proteins on the second gel were transferred (maximum power of 8 W for 2 hours) to a PVDF membrane. The membrane was then blocked by BSA to saturate nonspecific protein binding sites. The BSA blocked membrane was then incubated with primary antibody (anti-cmyc antibody from Invitrogen) and secondary antibody (anti-rabbit IgG AP conjugate from Promega). After incubation and washing, a colour reaction was induced by incubating the membrane in the substrate for alkaline phosphatase.

Purpose	Sequence Name	Sequence of oligonucleotide (5'-3')	Melting temperature
PCR upstream	IL-2RβCK_F3C	GGC TCT GCG GTG AAT GGC ACT TCC C	62 °C
	IL-2RβGST_F	CG GGA TCC GCG GTG AAT GGC ACT TCC	58 °C
PCR downstream	IL-2RCmycR	G CAG GTC GAC TCT AGA TTA ATT CAG ATC CTC TTC TGA GAT GAG TTT TTG TTC CGT GGC CGC GGT GTC CTT CCC AAG GGC	60 °C
	IL-2RbGST_RSMA	TTA ATT CAG ATC CTC TTC TGA GAT GAG TTT TTG TTC CCC GGG GGT GTC CTT CCC AAG GGC	60 °C
DNA sequencing	malE primer	GGT CGT CAG ACT GTC GAT GAA GCC	N/A
	M13/pUC Sequencing Primer	CGC CAG GGT TTT CCC AGT CAC GAC	N/A
	pGEX 5' Sequencing Primer	GGG CTG GCA AGC CAC GTT TGG TG	N/A
	pGEX 3' Sequencing Primer	CCG GGA GCT GCA TGT GTC AGA GG	N/A

Table 6.1: Oligonucleotides for PCR and DNA sequencing of the IL-2Rβ constructs. PCR primers IL-2RβCK_F3C and IL-2RCmycR were used for the MBP fusion. Inserts for the GST fusion were amplified by IL-2RβGST_F and IL-2RbGST_RSMA. Coding regions are underlined. There is a restriction cleavage enzyme (*Xba I*) site (TCT AGA) right before the terminal code at the 5' end of the reverse primer (IL-2RCmycR). The sequence in front of the *Xba I* site is a spacer for the restriction enzyme. The forward primer for GST fusion has a *BamH I* site (GGA TCC) attached. Transcription terminal code TTA was applied in the downstream PCR primers.

- Titer for the anti-cmyc antibody and the anti-rabbit IgG AP conjugate were 1:5000 and 1:7500 respectively.
- Alkaline phosphatase substrate contains NBT (nitro blue tetrazolium) BCIP (5-bromo-4-chloro-3indolyl-phosphate) in a proprietary buffer.

6.2.2.2 Purification of IL-2Rβ with anion exchange chromatography

There are two anion exchange steps in the IL-2Rβ purification procedure: a preliminary purification by Fastflow Q column (50 ml) and a high-resolution purification by Resource Q (1 ml).

The preliminary purification was used to extract MBP-IL-2Rβ fusion protein from the supernatant of periplasmic purification. Elution was carried out with a linear gradient of 0 to 1 M NaCl in 20 mM Tris buffer (pH 8.0). Fractions that contained the fusion protein were subjected to 3C protease cleavage.

High-resolution purification was used to purify IL-2Rβ from the cleavage mixture. The step gradient method was applied in sample elution. A step gradient of 0%-20%-20%- 40%-100% was used to optimize the separation between IL-2Rβ and the MBP. The elution volumes that were used to achieve the gradient were 0-15-20-24-60 ml. The elution buffers were the same as those in the Fastflow purification step.

6.2.2.3 Affinity chromatography

Amylose affinity resin from NEB was used to perform affinity purification. Columns were first equilibrated with 5 column volumes of 20mM Tris-HCl pH7.6, 0.2M NaCl. Active fractions were loaded onto the column at a flow rate of 1.25 ml/min, followed by a 10 column volume washing step. Elution buffer was then applied and fractions of 1ml each were collected for further investigation.

- Elution Buffer: 20mM Tris pH 7.6 / 0.2M NaCl with 1 mM maltose

6.2.3 One dimensional NMR spectroscopy

One-dimensional proton experiments were acquired on a home built three-channel 600 MHz (^{1}H) spectrometer equipped with tri-axial gradients and a triple resonance probe. The sample temperature was 25°C. Water suppression was achieved by a Watergate sequence (270).

6.3 Results

6.3.1 PCR screening for positive clones

Clones from an IL-2Rβ transformed plate were randomly picked and used as a PCR template. A positive clone, which contains the IL-2Rβ DNA, will produce a band with a size of about 600 bp on agarose gel (Figure 6.3). Among the 15 clones, clone number 2 and 9 contained the IL-2Rβ DNA. From which, clone number 2 was chosen for further studies. There were trace amounts of the IL-2Rβ PCR product in clone numbers 7 and 8. The PCR product in clone numbers 7 and 8 are more likely to

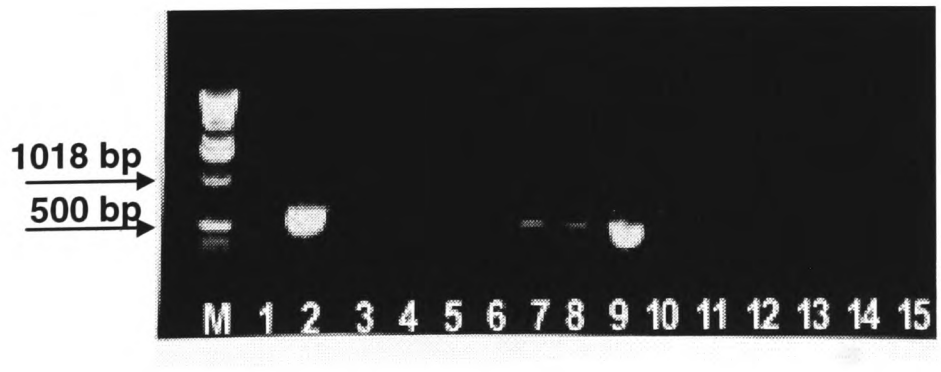

Figure 6.3: PCR screening for IL-2Rβ clones (MBP fusion). The IL-2Rβ gene was cloned into *E.coli* strain JM109. Fifteen randomly picked clones were screened for the recombinant DNA using the PCR primers. From left to right shows: 1Kb ladder, IL-2Rβ clones number 1-15. The IL-2Rβ is 685 bp long. PCR products from clones 2 and 9 contained DNA with expected size, from which clone number 2 was chosen for DNA sequencing and further studies.

have originated from the DNA left on the surface of the agar plate, since the PCR was performed on clones taken from the plate directly.

6.3.2 DNA sequencing of the IL-2Rβ constructs

The DNA sequence for IL-2Rβ was PCR amplified and gel-purified using Genomed Jetsorb Gel Extraction kit. The DNA sequencing data of cloned IL-2Rβ construct (MBP- IL-2Rβ) were compared with the published sequence (see Appendix III) and proved to be correct.

6.3.3 Expression and purification of IL-2Rβ from MBP fusion system

6.3.3.1 Analysis the IL-2Rβ proteins by SDS-PAGE

The MBP-IL-2Rβ was expressed and purified following procedures similar to those for MBP-gp130-CHR, summarized in Figure 4.2. The fusion MBP-IL-2Rβ was cleaved with 3C protease. Complete cleavage was achieved after 4 hours in 4 °C (Figure 6.4B). The IL-2Rβ was purified from MBP by anion exchange chromatography with a Resource Q column (Figure 6.4A). Fractions from the peak 2 were tested by PhastGel (Pharmacia). The IL-2Rβ was eluted at fractions 13-15 (Figure 6.4C *Lane 5-7*).

6.3.3.2 Electrospray mass spectrometry

Resource Q purified IL-2Rβ sample was measured with electrospray mass spectrometry (Figure 6.5). The profile indicated that the sample purity is poor. The

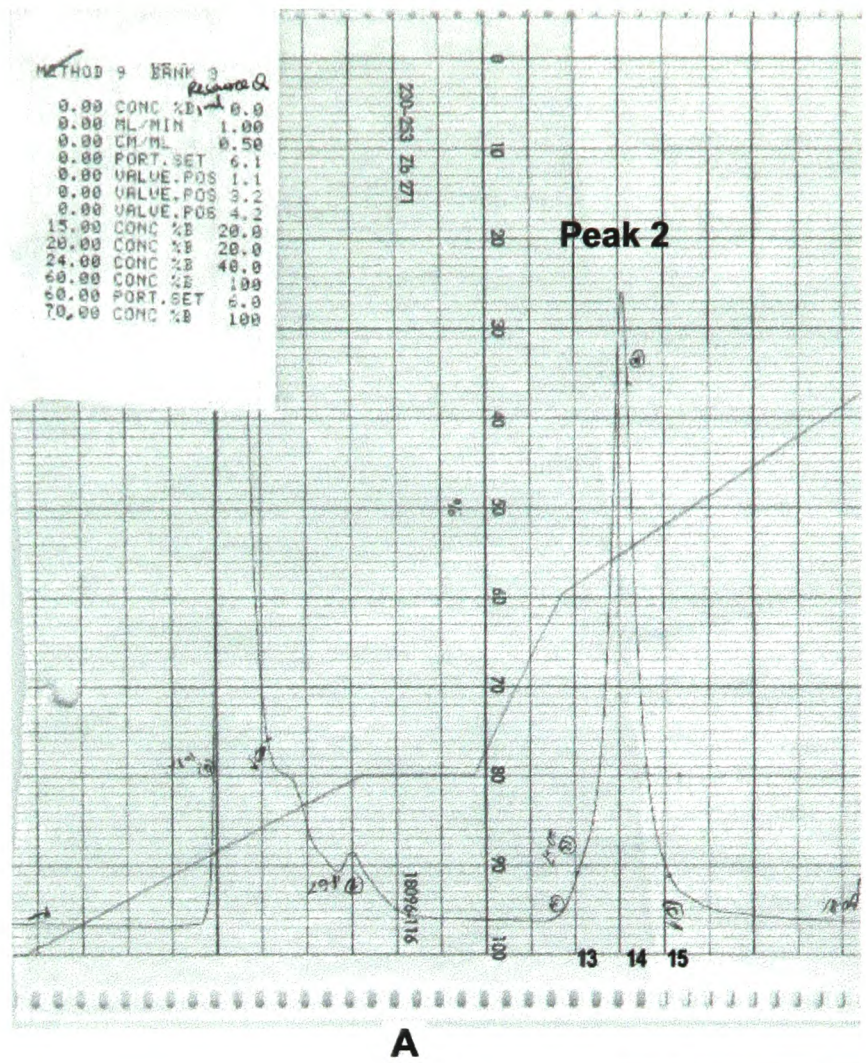

A

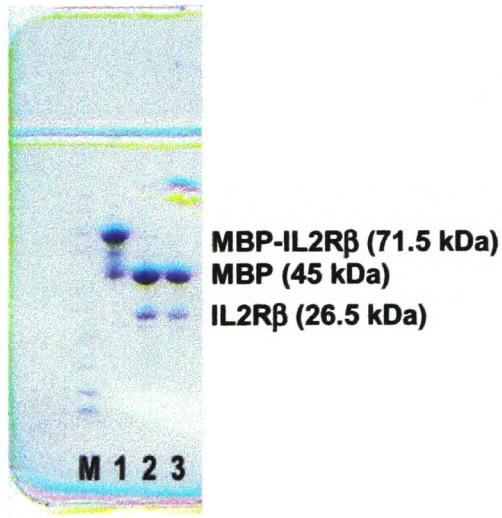

B

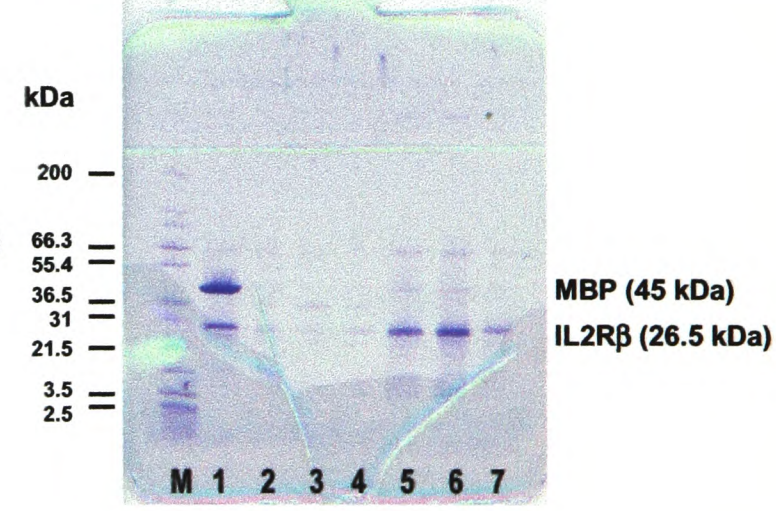

C

profile. Fraction numbers for the second major peak were 13-15. B) The fusion MBP-IL-2Rβ (*Lane 1*) was treated with 3C protease. After 4 hours (*Lane 2*) the band represent the fusion protein disappeared and two bands appeared with the sizes correspondent to MBP and IL-2Rβ. Overnight cleavage with 3C protease produces same effect as the 4 hours treatment (*Lane 3*). C) Purify the IL-2Rβ from MBP. After cleavage, the sample (*Lane 1*) was loaded to a Resource Q column. The elution fractions 10-15 (*Lane 2-7*) were analysed by PhastGel. Fractions 13-15 (*Lane 5-7*) contains a band with the size of a 26 kDa protein, which is the expected size for IL-2Rβ.

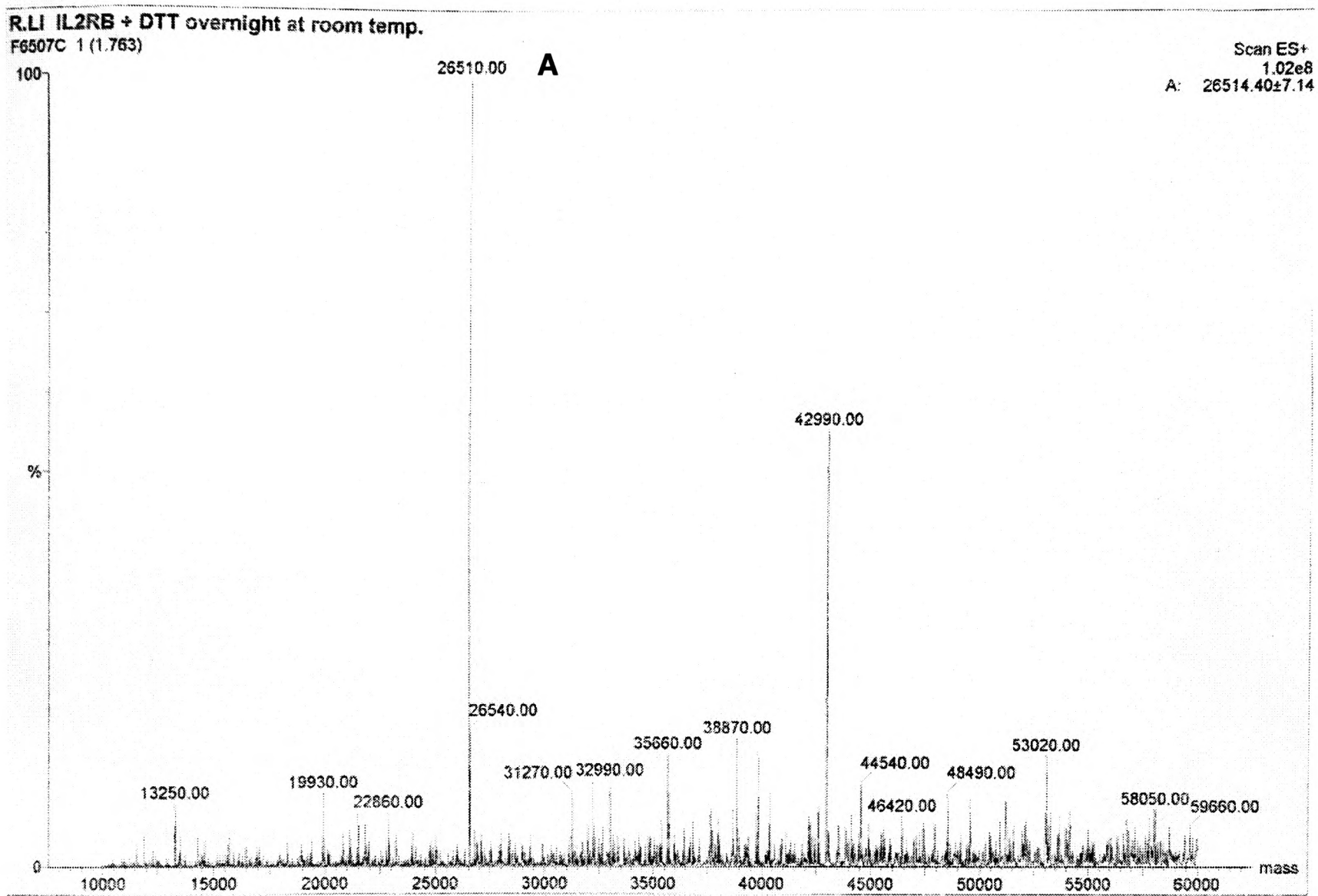

Figure 6.5: Mass spectra of IL-2Rβ. Mass spectra analysis profile for Resource Q column purified IL-2Rβ. The major species (Peak A) has a molecular weight of 26514.4 ±7 Da, which is close to the calculated molecular weight of IL-2Rβ (26502.2 Da).

major species in the sample gave a molecular weight of 26514.4 ± 7 Da, which is close to the calculated molecular weight (26502.2 Da).

6.3.3.3 N-terminal sequencing

The purified IL-2Rβ was N-terminal sequenced and gave an N-terminal of GPGSAVNG, which is in agreement with the designed IL-2Rβ sequence (see appendix III).

6.3.3.4 Sample folding status

One-dimensional NMR was used to assess sample folding status (Figure 6.6). At 750 MHz, pH 6.5 and 10 °C, the 0.3 mM IL-2Rβ did not show obvious features for a folded protein.

6.3.4 Expression IL-2Rβ in other expression systems

6.3.4.1 Express IL-2Rβ in GST fusion systems

The IL-2Rβ was cloned into a GST fusion expression system. PCR screening was used to detect the presence of the IL-2Rβ gene in transformed clones (Figure 6.7). Apart from one clone, all the others contained IL-2Rβ DNA and clone number 4

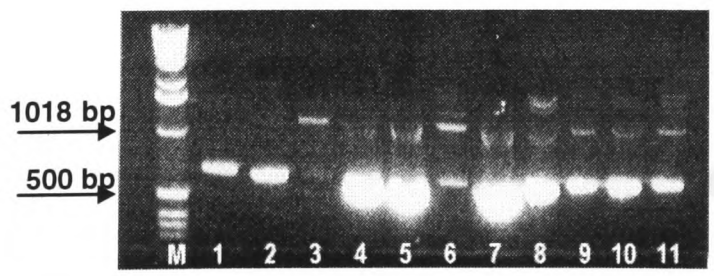

Figure 6.7: PCR screening for IL-2Rβ clones (GST fusiion). The IL-2Rβ gene was cloned in to *E.coli* strain JM109. Ten randomly picked clones were screened for the recombinant DNA using the PCR primers. From left to right shows: 1Kb ladder, positive control (original IL-2Rβ inserts), IL-2Rβ clones number 1-10. The IL-2Rβ is 685 bp long. Apart from Lane 3 (clone 2), PCR products from all other clones contain DNA that can be amplified by the PCR primers. Of these, Lane 5 and 7 (clone 4 and 6) had the highest yield.

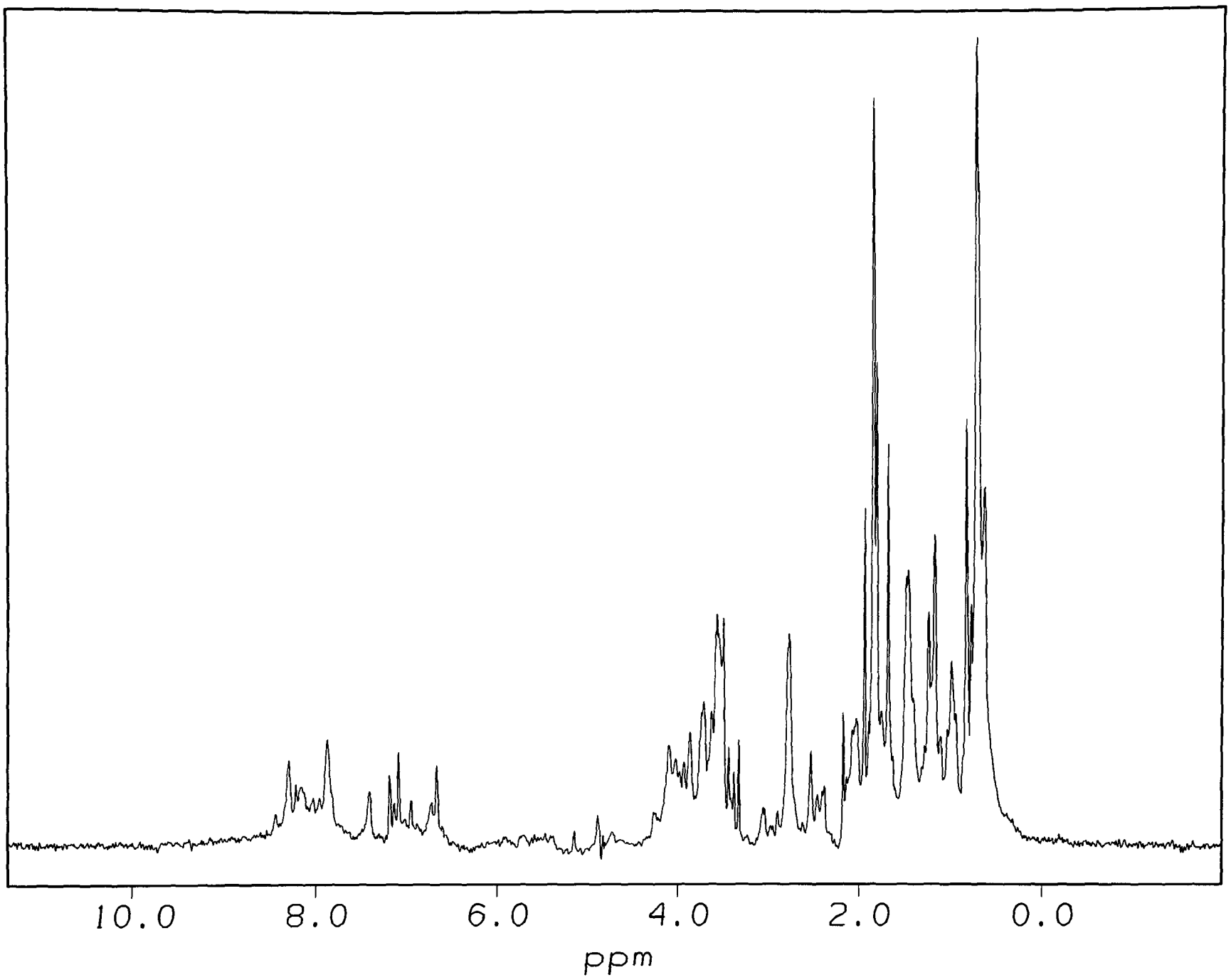

Figure 6.6: ^{1}H spectrum of IL-2Rβ in D_2O indicated an unfolded protein. The spectrum was recorded at 750 MHz, pH6.5 and 10 °C on a 0.3 mM sample. It is clear that the spectrum does not have well dispersed NH region and the high field methyl shifts, which are the characteristic features of a folded protein.

and 6 had the highest yield. Although clone number 5 showed as positive on PCR screening. The IL-2Rβ gene was more likely from the original inserts left on the plate surface. Clone 6 was picked for expression trails.

Western blotting was used to screen for IL-2Rβ expression (Figure 6.8). The affinity purified GST-IL-2Rβ and its cleaved form were included (*Lane 1-2*) as positive controls. Negative controls were from un-induced cells of clone number 2 and 6 (*Lane 3-4*). Cell lysates of induced cells from clone number 1, 2, 3, 5, 6, 7 and 8 (*Lane 5-11*) were checked. The anti-cmyc antibody was used to detect the presence of IL-2Rβ. The expression of IL-2Rβ were detected at *Lane 1-2* (positive controls) and Lane 9 (clone 6). Since the positive controls were purified from cells of clone 6, the detection of IL-2Rβ expression directly from cell lysates of clone 6 validated the above experimental setup.

6.3.4.2 Expression of IL-2Rβ in yeast *Pichia pastoris*

Dr. Jeremy Bright helped to clone the IL-2Rβ gene into the yeast Pichia pastoris. Two yeast clones (clone number 1 and 4) were sequenced and proved to be correct. Both of the constructs were used for minimal media expression trails. The expression temperature and media pH were varied to optimize the yield. At 30 °C and 37 °C both clones were tested for growth media pH of 6 and 7 (Figure 6.9). After induction, yeast cells were spun down and the supernatants were sampled. The expression level of clone 1 was also tested in complex media at 30 °C, pH 6. The expression of IL-2Rβ was difficult to judge from SDS-PAGE. The Western Blot detected the presence of the cmyc tag, which was engineered to the C-terminal of

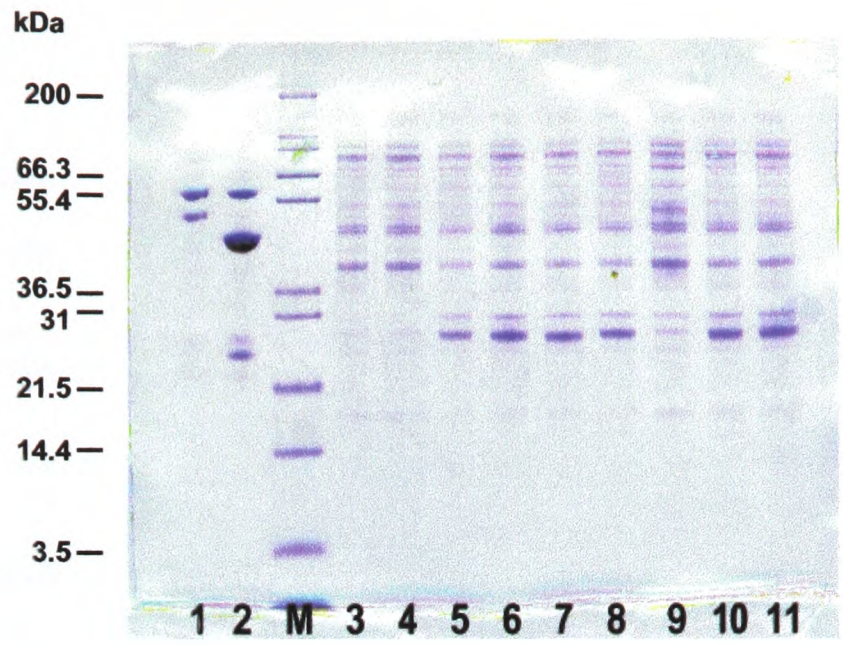

A

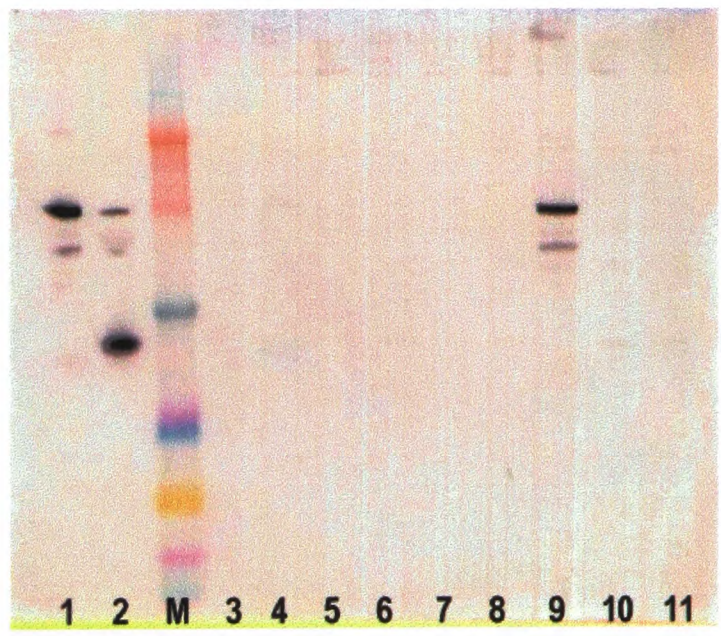

B

Figure 6.8: IL-2Rβ expressed as a GST fusion protein. SDS-PAGE (A) and Western blotting (B) were applied to analyse the expression of IL-2Rβ as a GST fusion protein. The sample layout in both A and B are identical. A) SDS-PAGE analysis. *Lane 1* and *2* are affinity purified fusion GST- IL-2Rβ and the same sample with 3C protease cleavage. Comparing the two, it is clear that the cleavage was not complete. But *Lane 2* did have an extra band at around 26 kDa, which is about the size of the IL-2Rβ. The thick band in Lane 2, with a size about 45 kDa, originated from the added 3C protease. Samples in Lane 3-11 were cell lysates from different GST-IL-2Rβ clones (see figure 6.7). Clone numbers were as follow: 2, 6, 1, 2, 3, 5, 6, 7 and 8. Negative controls were placed at *Lane 3-4*, which were from un-induced cells of clone number 2 and 6. The samples in *Lane 5-11* were from induced cells. B) Western blotting. Anti-cmyc antibody was used to detect expression of the IL-2Rβ. Presence of IL-2Rβ was detected at *Lane 1-2*, which were the positive controls, and *Lane 9*. As expected, no bands developed in *Lane 3-4*, which were the negative controls.

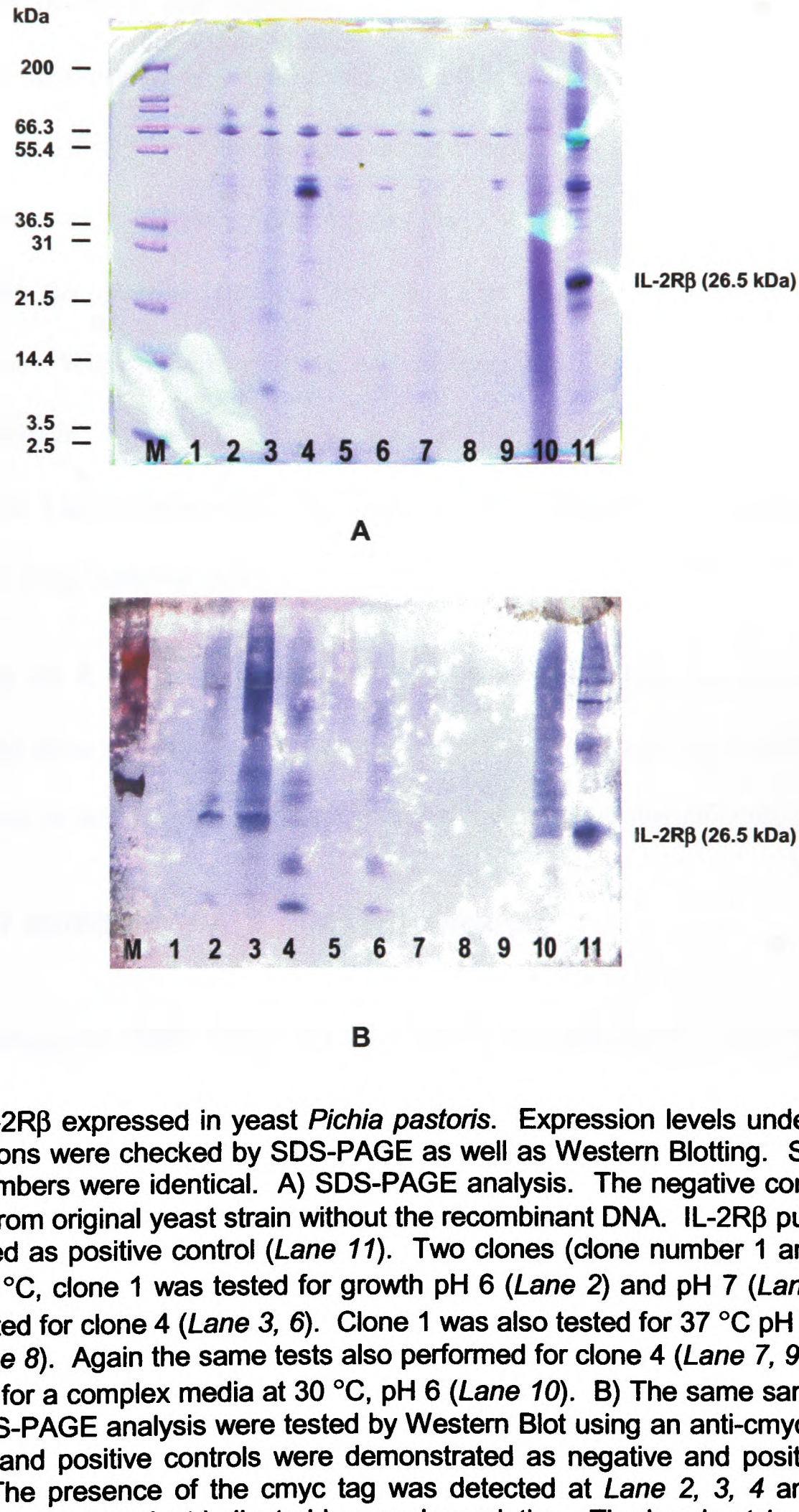

Figure 6.9: IL-2Rβ expressed in yeast *Pichia pastoris*. Expression levels under different growth conditions were checked by SDS-PAGE as well as Western Blotting. Samples at same lane numbers were identical. A) SDS-PAGE analysis. The negative control (*Lane 1*) was taken from original yeast strain without the recombinant DNA. IL-2Rβ purified from *E.coli* was used as positive control (*Lane 11*). Two clones (clone number 1 and 4) were tested. At 30 °C, clone 1 was tested for growth pH 6 (*Lane 2*) and pH 7 (*Lane 4*). The same was tested for clone 4 (*Lane 3, 6*). Clone 1 was also tested for 37 °C pH 6 (*Lane 5*) and pH 7 (*Lane 8*). Again the same tests also performed for clone 4 (*Lane 7, 9*). Clone 1 was also tried for a complex media at 30 °C, pH 6 (*Lane 10*). B) The same samples from the above SDS-PAGE analysis were tested by Western Blot using an anti-cmyc antibody. The negative and positive controls were demonstrated as negative and positive on the membrane. The presence of the cmyc tag was detected at *Lane 2, 3, 4* and *6*. The smearing of the yeast product indicated heavy glycosylation. The bands at *Lane 4* and *6* run at much lower molecular weight than the IL-2Rβ in *Lane 11* (positive control). This might be an indication of the presence of proteolytic event during expression.

yeast IL-2Rβ construct. At 30 °C and pH 6, both clones produced bands that ran at similar positions to the *E. coli* originated IL-2Rβ. The smearing of the samples indicated heavy glycosylation. Comparing the results for different expression conditions, it is clear that both clone 1 and 4 can express IL-2Rβ at 30 °C, pH 6 (*Lane 2 and 3*). At the same temperature (30 °C) and pH 7, the expressed IL-2Rβ breaks down to smaller size proteins (*Lane 4 and 6*). This implies the presence of a proteolytic event. When the temperature was increased to 37 °C, the expression became un-detectable. Comparing the expression of clone 1 and 4 (*Lane 2* and *3*), it is clear that clone 4 has a better yield. For clone 1 at 30 °C and pH 6, the expression was better when using complex media.

Although the IL-2Rβ can be expressed in the yeast *Pichia pastoris* expression system, the yield does not show a dramatic improvement over the *E.coli* expression system. This may be improved through optimizing growth and expression conditions.

6.4 A short summary for IL-2Rβ expression

Both prokaryotic (MBP fusion and GST fusion) and eukaryotic (yeast *Pichia pastoris*) expression systems were tested for IL-2Rβ expression (Figure 6.10). Among the three systems used, the MBP fusion system gave the best yield, but most of the purified IL-2Rβ was unfolded.

Since the gp130-CHR, a member of the same family as IL-2Rβ, was successfully expressed in MBP fusion system, it is not too surprising that IL-2Rβ can be expressed in the MBP fusion system. The MBP fusion system applied here is a

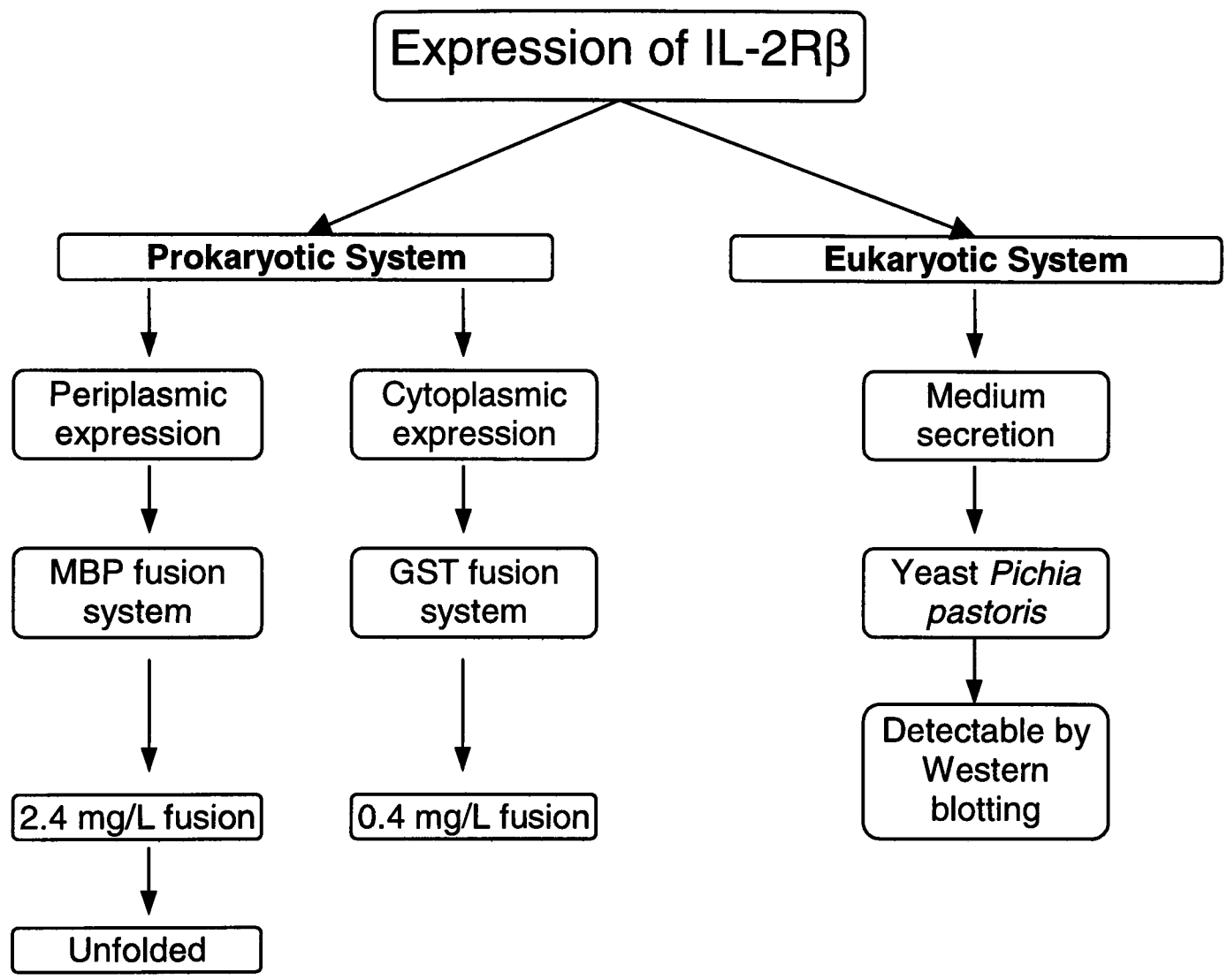

Figure 6.10: IL-2Rβ production in different expression systems. Different expression systems were evaluated for IL-2Rβ expression. Among the three systems tested, the MBP fusion system gave better yields, but the purified protein was unfolded.

periplasmic expression system, the fusion protein will be secreted to the periplasmic environment. One of the advantages of this system over the cytoplasmic system is that the disulfide bonds can be formed in the periplasm, which is essential for maintaining the three-dimensional structure of protein. There are 4 pairs of cysteine residues in the IL-2Rβ, which could cause difficulties in the proper folding of the recombinant protein. Through secretion to the periplasm, the fusion protein is separated from other host expressed proteins. This brings convenience to the purification procedures later on.

The yeast *Pichia pastoris* expression system, as an eukaryotic expression system, has advanced machinery for post expression modification. This is sometimes critical for the expression of human genes. The system is also very good for stable isotope labelling, which is of high demand for NMR structure assignments. People in our group have successfully used this system to produce a variety of labelled human fibronectin modules for NMR studies. The yield of IL-2Rβ in the *Pichia pastoris* was very low. The expressed IL-2Rβ protein can only be detected through Western blotting.

So far, the successful stories about IL-2Rβ express have been limited to CHO cells (304) and insect cells using baculovirus expression vector (252,305). Our goal for the IL-2Rβ expression is to produce large amount of labelled protein for NMR studies. Stable isotope labelling in the above system is difficult and the expense is prohibitory.

The expression level of IL-2Rβ in MBP system is low (2.4 mg/L fusion protein). Expressed IL-2Rβ easily forms aggregates. To achieve the above goal, mutant forms of IL-2Rβ may be needed. The refolding procedures are also worth exploring further. Although the IL-2Rβ contains a cytokine receptor domain and a fibronectin type III domain, individual expression of these two domains are not advisable for structure-function studies. Studies on the structure of the gp130-CHR revealed that its binding site was formed between the two fibronectin type III domains. If this is the case for IL-2Rβ, individually expressed domains will not contain the functional binding site for the IL-2.

7 Conclusions

The thesis presents a detailed biophysical analysis of the OSM/gp130-CHR interaction. The obtained biophysical parameters of this system are listed in table 7.1. Three OSM constructs (OSM185, OSM187 and OSM196), different in length, were compared to optimize OSM expression and the labelling conditions. OSM187 was chosen, based on its yield and stability, for binding studies and stable isotope labelling, which is essential for the NMR binding site mapping. SPR competitive studies confirmed that OSM187 and OSM196 have very similar binding properties. The studies on OSM187 are relevant to OSM196, which is the native form of OSM.

7.1 Comparison of the results obtained from different techniques.

Analysis of OSM/gp130-CHR complex by SPR gave a K_D for the interaction larger than that obtained from ITC (table 5.1). This is perhaps to be expected, since the amine coupling immobilization of OSM could have impaired its ability to bind gp130-CHR; a weaker binding in such SPR experiments, compared with solution techniques, is often observed (306,307). It may also indicate, as a result of the immobilization procedure, the presence of heterogeneous ligand on the chip surface, each with a different ability to bind gp130-CHR. The K_D obtained under this condition is actually a weighted average of the values arising from different species.

The kinetic studies revealed two surface ligand species with a total R_{max} of 223 RU, which is in agreement with the R_{max} determined by SPR equilibrium studies

	AUC	ITC	SPR
K_{on} ($M^{-1}s^{-1}$) x 10^5			2.62 ± 0.03
K_{off} (s^{-1}) x 10^{-2}			2.06 ± 0.03
K_D (nM)		62	108 (77*)
K_A (M^{-1}) x 10^7		1.62 ± 0.44	0.93
ΔH_b^0 (Kcal/mole)		-5.81 ± 0.09	
ΔS_b^0 (cal/mole.K)		13.52	
ΔG_b^0 (Kcal/mole)		- 9.96**	-9.76***
Stoichiometry	1:1	1:1	
Solution behavior (OSM187)	Homogeneous solute		
Solution behavior (gp130-CHR)	Homogeneous solute (low concentration)		

*K_D calculated from K_{off}/K_{on}
**$\Delta G_b^0 = \Delta H_b^0 - T\Delta S_b^0$
***$\Delta G_b^0 = -R\ T\ \ln K_A$

Table 7.1: Biophysical properties of OSM187, gp130-CHR and their complex. The AUC, ITC and SPR confirmed that the binding between OSM187/gp130-CHR has a K_D around 100 nM with a 1:1 stoichiometry. The free energy of binding was –9591.16 cal/mole as determined by ITC, which is in agreement with the calculated value, based on K_A from SPR studies. Since the SPR data were analyzed by heterogeneous ligand-Parallel reaction model, two sets of data were acquired (see table 5.2). Here, only one of the two was listed.

(around 240 RU). The calculated K_D values from these two species are 146 nM and 77 nM respectively. SPR equilibrium studies gave a K_D of 108 nM, which should be a weighted value from those two species. The K_D from the second species (77 nM) is close to the K_D obtained from ITC (around 60 nM). Since the ITC measures solution interaction, the measured interaction is more close to the real event. From this point of view, the binding property of the second ligand species on the chip surface is more or less intact, while the species with weak binding affinity may be the product of non-specific amine coupling or because it is not fully accessible by gp130-CHR. The same effects of amine coupling have also been observed for other protein ligands (227,306,308).

Both ITC and AUC gave a binding stoichiometry of 1:1. For this purpose, ITC is reliable and much quicker than AUC techniques. Accurate sample concentration is a prerequisite for reliable data, but this cannot take account of the possible effects of inactive proteins. An activity calibrated sample concentration is more desirable. The "incompetent species" can be detected by gel filtration experiments, as long as the complex does not break up under gel filtration conditions (210). For a 1:1 binding system, if the concentrations of both reactants are accurately measured, a 1:1 mixture should give a gel filtration profile with one peak of the molecular weight equal to the sum of the two reactants. The NMR studies of OSM187 and the OSM187/gp130 complex indicated that a portion of gp130-CHR was inactive. The result may be caused by the high sample concentration (0.4 mM) under NMR conditions. At lower concentration (4.5 μM), AUC experiments on a 1:1 mixture of OSM187 and gp130-CHR give an homogeneous solute with molecular

weight around the 1:1 complex. This result indicated that both reactants are fully active.

ITC can measure the free energy of binding, ΔG_b^0, accurately even when the heat exchange of binding is not favourable for binding-constant studies. Here, the calculated ΔG_b^0 (-9.76 Kcal/mole) from the equilibrium association constant, K_A, obtain by SPR studies agrees with the one measured by ITC. This is a good indication that the K_A from immobilized conditions is close to the K_A measured in solution conditions.

7.2 Use the right tool for the right task

Here, we used AUC, ITC and SPR to study binding properties and OSM/gp130-CHR interactions. By observation of table 7.1, it is not too difficult to realize that none of these techniques could answer all the questions. Although there are overlapping areas, the answers for a particular question may be a bit different by using different techniques. Also, each of these techniques has its strength and weakness.

The AUC was used to study the solution behaviour of OSM187, gp130-CHR and their complex. Results from these experiments can help in the determination of the best experimental conditions. This is especially important for NMR studies, since NMR needs samples to be as stable as possible at very high protein concentration and rather high temperatures. Studies on the behaviour of the complex also gave insight about the binding stoichiometry; again this information is essential for NMR binding studies. The stoichiometry of binding also guides model selection for data analysis.

Although AUC has been successfully applied for binding constants studies (210,309), it is difficult to do the same for the OSM/gp130-CHR system. Because both OSM187 and gp130-CHR have similar molecular weight, it is not easy to distinguish the two by AUC. The theory behind AUC is simple and robust. With proper experimental conditions, data from AUC is very reliable.

The thermodynamic parameters, such as ΔG_b^0, ΔH_b^0 and ΔS_b^0 were directly measured by ITC. ITC can conveniently measure many biophysical properties in one experiment. Since ITC measures heat exchange during binding, data from ITC can provide information about binding energetics. With structural data, this information can reveal the basic forces governing the interaction. Here, we also used ITC to determine binding stoichiometry and equilibrium constants. The ITC equilibrium constant studies can be limited by the system of interest. The interaction between OSM and gp130-CHR contains a large entropy factor. The low heat exchange of binding leads to a low signal to noise level. Because ITC equilibrium constant studies are limited by the *experiment K window*, the *c* value, one cannot always increase the starting concentration to gain higher signal to noise level. In the study of OSM/gp130-CHR interactions, compromise on the *c* value has to be made to obtain reasonable signal to noise level. Sample purity and accurate sample concentration are critical for successful of ITC experiments.

Since SPR monitors the binding events in real time, it is the only technique of the three that can be used to determine kinetic rate constants of binding. The information can provide insight about the biological nature of binding as well as methodology guidelines. The rate constants of association and dissociation between

OSM187 and gp130-CHR are comparable to that of IL-6/IL-6Rα and IL-15/IL-2Rβ (304,310) and relatively high compared to other cytokine receptor interactions, as for example hGH-receptor (311), IL-4/IL-4α (312) and IL-5/IL-5Rα (313) (table 7.2). The fast interaction dynamics could play an important role in signal transduction, as this means that the complex between OSM and gp130 is short lived, while retaining relatively high affinity. This property gives only a limited time for OSM to associate into the active complex. Considering the role of gp130 as a common signal transducer, the fast transient kinetics could be an important mechanism to maintain signal specificity. A similar situation could be found in the interactions between IL-15 and IL-2Rβ, a common receptor chain for both IL-2 and IL-15. Although the off rate value between IL-2 and IL-2Rβ (252,314) is about two times higher than that of IL-15/IL-2Rβ, it is still within the same order of magnitude. The knowledge of the binding kinetics also has methodological implications, because indirect affinity assays like solid phase detection and binding inhibition can be strongly affected by fast dissociation. Therefore, direct affinity assays like SPR and ITC are much more reliable for an accurate evaluation of affinity.

SPR can also be easily used as an activity-screening tool. In the production of gp130-CHR, SPR has been successfully applied for this purpose. Equipped with automatic sample injection system, the BIAcore machine can handle as many as 192 samples automatically. This is what the AUC (9 samples) and ITC (1 sample) lack. The equilibrium constants of binding can also be determined by the SPR technique. Although it seems to be a criticism of the SPR (225,226), proper experimental design and careful data analysis can help people gain confidence for the results. Here, we

	k_{on} (x 10^5 $M^{-1}s^{-1}$)	k_{off} (x 10^{-2} s^{-1})
hGH/hGHR	4	0.03
IL-2/IL-2Rα	112	3.1
IL-2/IL-2Rβ	12.7	6.6
IL-4/IL-4Rα	130	0.2
IL-5/IL-5Rα	4.9	0.37
IL-6/IL-6Rα	2.6	1
IL-15/IL-2Rβ	1.5	2.9
OSM187/gp130-CHR	2.62	2.06

Table 7.2: Association and dissociation rate constants for various cytokine-receptor systems

used both kinetic and equilibrium studies to obtain binding affinities. The values from both methods agree with each other. As in any other technique, repetitive data acquisition can always help to improve accuracy and filter out non-systematic errors.

Full understanding of a binding event involves knowledge of the molecular basis of the interaction. NMR is a good tool for these studies. An obvious advantage is that NMR studies interactions in solution, which is closer to the biological conditions. Many receptor ligand systems have been studied by NMR techniques. The limitation of NMR application in the field is the size of the system of interest. Using conventional NMR techniques, the complex between OSM187 and gp130-CHR is too big (47.6 kDa) for study. Here we applied the TROSY technique and significant improvement was obtained.

7.3 Outlook

The class I cytokine receptor family functions as a multimeric complex, upon binding of their cognate cytokines. OSM binds directly to gp130 with low affinity and then forms gp130/LIFR or gp130/OSMR heterodimers. The ability of OSM to bind directly to the gp130 with medium binding affinity, which could be easily studied, is one of the main reasons that we chose to study the interaction between OSM and gp130-CHR. Since the gp130 binds to OSM through its cytokine binding homology region (CHR), the studies using gp130-CHR yield relevant information to the binding of OSM and gp130 (see chapter 1). Understanding the interaction between OSM and gp130 provides a starting point for the characterization of the multimeric functional complex.

NMR has proved to be a powerful tool for protein binding analysis (315). With the aid of stable isotope labelling and new NMR techniques, i.e. TROSY, the upper limit of the size of the complex of interest is getting higher and many cytokine receptor complexes are now within range.

The long-term goal of our investigation is to gain a detailed understanding of the molecular basis of the binding between OSM and gp130. The studies presented in this thesis established a solid and promising basis for achieving this goal. First, an efficient procedure for preparation and purification of both OSM187 and gp130-CHR at the amount and quality that can satisfy NMR study was developed. In particular OSM187 has been successfully labelling with ^{15}N or ^{15}N and ^{13}C. This is essential for NMR binding studies. Second, reliable methods have been found for quantitatively assessing the affinity and kinetics of the interaction. The studies here gave a detailed biophysical characterization of the interaction between OSM187 and gp130-CHR and confirmed that the truncated form (OSM187) has similar binding properties to the native form (OSM196). Third, preliminary NMR binding site mapping has begun and the OSM187/gp130-CHR complex has been observed by NMR. This project provides a starting point for the study of higher order receptor ligand complexes.

1. Introduction

Figure 1.1. Class I cytokine receptor family 5
Figure 1.2. Schematic diagram of the signal transducing chain gp130 6
Figure 1.3. Receptor systems sharing gp130 as a common signal transducer 7
Figure 1.4. Structures of IL-6 and LIF 12
Figure 1.5. A ribbon diagram of human gp130-CHR 14
Figure 1.6. Structural organization of Jaks and STATs 16
Figure 1.7. Signalling through gp130/Jak/STAT pathways 16
Figure 1.8. Signalling pathways for class I cytokine receptors 22
Figure 1.9. Negative regulation of the IL-6 family cytokine signal-transduction 23

2. Quantitative techniques in protein/protein interactions

Figure 2.1. Biophysical techniques used in this work 33
Figure 2.2. The forces acting on a solute particle in a centrifugal field 34
Figure 2.3. Schematic diagram of a six-hole centerpiece 41
Figure 2.4. Schematic diagram of the optical system of Optima XL-A analytical ultracentrifuge 42
Figure 2.5. Nomogram for selecting an operating speed for a sedimentation equilibrium experiment 44
Figure 2.6. Simulated binding isotherms for a single-site interaction 47
Figure 2.7. Diagram of the VP-ITC cells, adiabatic shield and injector/stirrer assembly 48
Figure 2.8. Creation of the evanescent wave 56
Figure 2.9. BIA detects changes in the refractive index of the surface layer of a solution in contact with the sensor chip 56
Figure 2.10. A typical sensorgram 60
Figure 2.11. Two methods of immobilization 61
Figure 2.12. BIA coupling chemistries 62
Figure 2.13. Illustrating of competitive studies 69
Figure 2.14. Chemical shifts in binding site mapping 80

3. Methods

Figure 3.1. The expression vector pGEX-6P-2 83

4. Expression and purification of OSM and gp130-CHR

Figure 4.1. PCR products for the OSM185 and OSM187 constructs 100
Figure 4.2. Production of OSM and gp130-CHR 101
Figure 4.3. SDS-PAGE analysis of expressed recombinant OSM proteins 101
Figure 4.4. Mass spectra of OSM187 102
Figure 4.5. 1D-^{1}H spectrum for OSM187 102
Figure 4.6. SDS-PAGE analysis of gp130-CHR 103
Figure 4.7. Mass spectra of gp130-CHR 103
Figure 4.8. BIAcore activity screening for fusion MPB-gp130-CHR fractions 104
Figure 4.9. 1D-^{1}H spectrum for gp130-CHR 104
Figure 4.10. Comparison of 1D-^{1}H spectra for free OSM187, gp130-CHR and their 1:1 complex 104

5. Investigation the interactions between the OSM and gp130-CHR

Figure 5.1. The OSM187 forms a homogeneous solute 106
Figure 5.2. Solution behaviour of gp130-CHR 107
Figure 5.3. AUC studies indicated an 1:1 binding stoichiometry 107
Figure 5.4. ITC studies of the binding between OSM187 and gp130-CHR 108
Figure 5.5. Kinetic studies of gp130 with immobilized OSM187 111
Figure 5.6. The heterogeneous chip surface caused by amine coupling 112
Figure 5.7. BIAcore equilibrium studies of OSM187 112
Figure 5.8. BIAcore equilibrium studies of OSM196 113
Figure 5.9. BIAcore competitive binding studies 113
Figure 5.10. Comparison of 1H-15N spectra of free OSM and the 1:1 OSM/gp130-CHR complex 114

6. Interactions between the IL-2 and IL-2 receptor beta chain (IL-2Rβ)

Figure 6.1. The IL-2 receptor complex 117
Figure 6.2. The expression vector pMalp2-3C 117
Figure 6.3. PCR screening for IL-2Rβ clones (MBP fusion) 120
Figure 6.4. Purification of IL-2Rβ 121
Figure 6.5. Mass spectra of IL-2Rβ 121
Figure 6.6. ^{1}H spectrum of IL-2Rβ in D_2O indicated an unfolded protein 122
Figure 6.7. PCR screening for IL-2Rβ clones (GST fusion) 122
Figure 6.8. IL-2Rβ expressed as a GST fusion protein 123
Figure 6.9. IL-2Rβ expressed in yeast Pichia pastoris 123
Figure 6.10. IL-2Rβ production in different expression systems 124

7. Conclusions

1. Introduction

Table 1.1. Structural classification of cytokines 4
Table 1.2. The three groups of Class I cytokine receptors 6
Table 1.3. Activation of Jaks and STATs by various ligands 7

2. Quantitative techniques in protein/protein interactions

3. Methods

Table 3.1. Oligonucleotides for PCR and DNA sequencing of the OSM constructs 84
Table 3.2. *E.coli* strains used for OSM and gp130-CHR expression 87
Table 3.3. Growth media for OSM and gp130-CHR expression 87

4. Expression and purification of OSM and gp130-CHR

5. Interactions between the OSM and gp130-CHR

Table 5.1. ITC studies of OSM187 and gp130-CHR 108
Table 5.2. SPR kinetic studies of OSM187 and gp130-CHR 111

6. Interactions between the IL-2 and IL-2 receptor beta chain (IL-2Rβ)

Table 6.1. Oligonucleotides for PCR and DNA sequencing of the IL-2Rβ constructs 118

7. Conclusions

Table 7.1. Biophysical properties of OSM187, gp130-CHR and their complex 127
Table 7.2. Association and dissociation rate constants for various cytokine-receptor systems 131

9 References

1. Clark, S. C., and Kamen, R. (1987) *Science* **236**(4806), 1229-1237

2. Nicola, N. A. (1989) *Annual Review of Biochemistry* **58,** 45-77

3. Cohen, S. (1962) *Journal of biological chemistry* **237,** 1555-1562

4. Nicola, N. A. (1994) *Guidebook of Cytokines and their Receptors*, 1st Ed., Oxford University Press New York

5. Taga, T., Hibi, M., Hirata, Y., Yamasaki, K., Yasukawa, K., Matsuda, T., Hirano, T., and Kishimoto, T. (1989) *Cell* **58**(3), 573-581

6. Hanks, S. K., Quinn, A. M., and Hunter, T. (1988) *Science* **241**(4861), 42-52

7. Bazan, J. F. (1989) *Biochemical and Biophysical Research Communications* **164**(2), 788-795

8. Mallett, S., and Barclay, A. N. (1991) *Immunology Today* **12**(7), 220-223

9. Bourne, H. R., Sanders, D. A., and McCormick, F. (1991) *Nature* **349**(6305), 117-127

10. Heldin, C. H. (1995) *Cell* **80**(2), 213-223

11. Rittinger, K., Walker, P. A., Eccleston, J. F., Nurmahomed, K., Owen, D., Laue, E., Gamblin, S. J., and Smerdon, S. J. (1997) *Nature* **388**(6643), 693-697

12. Brown, M. T., and Cooper, J. A. (1996) *Biochimica Et Biophysica Acta-Reviews On Cancer* **1287**(2-3), 121-149

13. Karnitz, L. M., and Abraham, R. T. (1995) *Current Opinion in Immunology* **7**(3), 320-326

14. Ihle, J. N., Witthuhn, B. A., Quelle, F. W., Yamamoto, K., and Silvennoinen, O. (1995) *Annual Review of Immunology* **13,** 369-398

15. Fukunaga, R., Ishizakaikeda, E., and Nagata, S. (1993) *Cell* **74**(6), 1079-1087

16. Murakami, M., Narazaki, M., Hibi, M., Yawata, H., Yasukawa, K., Hamaguchi, M., Taga, T., and Kishimoto, T. (1991) *Proceedings of the National Academy of Sciences of the United States of America* **88**(24), 11349-11353

17. Bazan, J. F. (1990) *Proceedings of the National Academy of Sciences of the United States of America* **87**(18), 6934-6938

18. Patthy, L. (1990) *Cell* **61**(1), 13-14

19. Bravo, J., Staunton, D., Heath, J. K., and Jones, E. Y. (1998) *Embo Journal* **17**(6), 1665-1674

20. Yawata, H., Yasukawa, K., Natsuka, S., Murakami, M., Yamasaki, K., Hibi, M., Taga, T., and Kishimoto, T. (1993) *Embo Journal* **12**(4), 1705-1712

21. Fukunaga, R., Ishizakaikeda, E., Pan, C. X., Seto, Y., and Nagata, S. (1991) *Embo Journal* **10**(10), 2855-2865

22. Baumann, H., Symes, A. J., Comeau, M. R., Morella, K. K., Wang, Y. P., Friend, D., Ziegler, S. F., Fink, J. S., and Gearing, D. P. (1994) *Molecular and Cellular Biology* **14**(1), 138-146

23. Murakami, M., Hibi, M., Nakagawa, N., Nakagawa, T., Yasukawa, K., Yamanishi, K., Taga, T., and Kishimoto, T. (1993) *Science* **260**(5115), 1808-1810

24. Davis, S., Aldrich, T. H., Stahl, N., Pan, L., Taga, T., Kishimoto, T., Ip, N. Y., and Yancopoulos, G. D. (1993) *Science* **260**(5115), 1805-1808

25. Davis, S., Aldrich, T. H., Ip, N. Y., Stahl, N., Scherer, S., Farruggella, T., Distefano, P. S., Curtis, R., Panayotatos, N., Gascan, H., Chevalier, S., and Yancopoulos, G. D. (1993) *Science* **259**(5102), 1736-1739

26. Taga, T., Narazaki, M., Yasukawa, K., Saito, T., Miki, D., Hamaguchi, M., Davis, S., Shoyab, M., Yancopoulos, G. D., and Kishimoto, T. (1992) *Proceedings of the National Academy of Sciences of the United States of America* **89**(22), 10998-11001

27. Yoshida, K., Chambers, I., Nichols, J., Smith, A., Saito, M., Yasukawa, K., Shoyab, M., Taga, T., and Kishimoto, T. (1994) *Mechanisms of Development* **45**(2), 163-171

28. Narazaki, M., Yasukawa, K., Saito, T., Ohsugi, Y., Fukui, H., Koishihara, Y., Yancopoulos, G. D., Taga, T., and Kishimoto, T. (1993) *Blood* **82**(4), 1120-1126

29. Watowich, S. S., Yoshimura, A., Longmore, G. D., Hilton, D. J., Yoshimura, Y., and Lodish, H. F. (1992) *Proceedings of the National Academy of Sciences of the United States of America* **89**(6), 2140-2144

30. Devos, A. M., Ultsch, M., and Kossiakoff, A. A. (1992) *Science* **255**(5042), 306-312

31. Taga, T., and Kishimoto, T. (1997) *Annual Review of Immunology* **15**, 797-819

32. Wells, J. A., and deVos, A. M. (1996) *Annual Review of Biochemistry* **65,** 609-634

33. Ballinger, M. D., and Wells, J. A. (1998) *Nature Structural Biology* **5**(11), 938-940

34. Miyazaki, T., Kawahara, A., Fujii, H., Nakagawa, Y., Minami, Y., Liu, Z. J., Oishi, I., Silvennoinen, O., Witthuhn, B. A., Ihle, J. N., and Taniguchi, T. (1994) *Science* **266**(5187), 1045-1047

35. Russell, S. M., Johnston, J. A., Noguchi, M., Kawamura, M., Bacon, C. M., Friedmann, M., Berg, M., McVicar, D. W., Witthuhn, B. A., Silvennoinen, O., Goldman, A. S., Schmalstieg, F. C., Ihle, J. N., Oshea, J. J., and Leonard, W. J. (1994) *Science* **266**(5187), 1042-1045

36. Tanner, J. W., Chen, W., Young, R. L., Longmore, G. D., and Shaw, A. S. (1995) *Journal of Biological Chemistry* **270**(12), 6523-6530

37. Vanderkuur, J. A., Wang, X. Y., Zhang, L. Y., Campbell, G. S., Allevato, G., Billestrup, N., Norsted, G., and Cartersu, C. (1994) *Journal of Biological Chemistry* **269**(34), 21709-21717

38. Ihle, J. N. (1995) *Advances in Immunology* **60,** 1-35

39. Schindler, C., and Darnell, J. E. (1995) *Annual Review of Biochemistry* **64,** 621-651

40. Ihle, J. N., Thierfelder, W., Teglund, S., Stravapodis, D., Wang, D. M., Feng, J., and Parganas, E. (1998) *Annals of the New York Academy of Sciences* **865,** 1-9

41. Zhou, S. Y., Shoelson, S. E., Chaudhuri, M., Gish, G., Pawson, T., Haser, W. G., King, F., Roberts, T., Ratnofsky, S., Lechleider, R. J., Neel, B. G., Birge, R. B., Fajardo, J. E., Chou, M. M., Hanafusa, H., Schaffhausen, B., and Cantley, L. C. (1993) *Cell* **72**(5), 767-778

42. Avruch, J., Zhang, X. F., and Kyriakis, J. M. (1994) *Trends in Biochemical Sciences* **19**(7), 279-283

43. Schlessinger, J. (1993) *Trends in Biochemical Sciences* **18**(8), 273-275

44. Boyle, W. J., Smeal, T., Defize, L. H. K., Angel, P., Woodgett, J. R., Karin, M., and Hunter, T. (1991) *Cell* **64**(3), 573-584

45. Franklin, C. C., Sanchez, V., Wagner, F., Woodgett, J. R., and Kraft, A. S. (1992) *Proceedings of the National Academy of Sciences of the United States of America* **89**(15), 7247-7251

46. Angel, P., and Karin, M. (1991) *Biochimica Et Biophysica Acta* **1072**(2-3), 129-157

47. Woodgett, J. R. (1990) *Semin. Cancer Biol.* **4,** 389-397

48. Gonzalez, G. A., and Montminy, M. R. (1989) *Cell* **59**(4), 675-680

49. Foulkes, N. S., Borrelli, E., and Sassonecorsi, P. (1991) *Cell* **64**(4), 739-749

50. Dalton, S., and Treisman, R. (1992) *Cell* **68**(3), 597-612

51. Baeuerle, P. A., and Baltimore, D. (1988) *Science* **242**(4878), 540-546

52. Brown, K., Gerstberger, S., Carlson, L., Franzoso, G., and Siebenlist, U. (1995) *Science* **267**(5203), 1485-1488

53. Korzus, E., Nagase, H., Rydell, R., and Travis, J. (1997) *Journal of Biological Chemistry* **272**(2), 1188-1196

54. Zarling, J. M., Shoyab, M., Marquardt, H., Hanson, M. B., Lioubin, M. N., and Todaro, G. J. (1986) *Proceedings of the National Academy of Sciences of the United States of America* **83**(24), 9739-9743

55. Rose, T. M., and Bruce, A. G. (1991) *Proceedings of the National Academy of Sciences of the United States of America* **88**(19), 8641-8645

56. Gearing, D. P., Comeau, M. R., Friend, D. J., Gimpel, S. D., Thut, C. J., McGourty, J., Brasher, K. K., King, J. A., Gillis, S., Mosley, B., Ziegler, S. F., and Cosman, D. (1992) *Science* **255**(5050), 1434-1437

57. Liu, J. W., Modrell, B., Aruffo, A., Marken, J. S., Taga, T., Yasukawa, K., Murakami, M., Kishimoto, T., and Shoyab, M. (1992) *Journal of Biological Chemistry* **267**(24), 16763-16766

58. Thoma, B., Bird, T. A., Friend, D. J., Gearing, D. P., and Dower, S. K. (1994) *Journal of Biological Chemistry* **269**(8), 6215-6222

59. Ichihara, M., Hara, T., Yoshimura, A., and Miyajima, A. (1995) *Experimental Hematology* **23**(8), 847

60. Borba, V. Z. C., Bellido, T., Grigorieva, I., Epstein, J., Stahl, N., Yancopoulos, G., and Manolagas, S. C. (1995) *Journal of Bone and Mineral Research* **10**(S1), S318

61. Modrell, B., Liu, J. W., Miller, H., and Shoyab, M. (1994) *Growth Factors* **11**(2), 81-91

62. Sporeno, E., Paonessa, G., Salvati, A. L., Graziani, R., Delmastro, P., Ciliberto, G., and Toniatti, C. (1994) *Journal of Biological Chemistry* **269**(24), 16984

63. Robinson, R. C., Grey, L. M., Staunton, D., Vankelecom, H., Vernallis, A. B., Moreau, J. F., Stuart, D. I., Heath, J. K., and Jones, E. Y. (1994) *Cell* **77**(7), 1101-1116

64. McDonald, N. Q., Panayotatos, N., and Hendrickson, W. A. (1995) *Embo Journal* **14**(12), 2689-2699

65. Somers, W., Stahl, M., and Seehra, J. S. (1997) *Embo Journal* **16**(5), 989-997

66. Xu, G. Y., Yu, H. A., Hong, J., Stahl, M., McDonagh, T., Kay, L. E., and Cumming, D. A. (1997) *Journal of Molecular Biology* **268**(2), 468-481

67. Hoffman, R. C., Moy, F. J., Price, V., Richardson, J., Kaubisch, D., Frieden, E. A., Krakover, J. D., Castner, B. J., King, J., March, C. J., and Powers, R. (1996) *Journal of Biomolecular Nmr* **7**(4), 273-282

68. Yamasaki, K., Taga, T., Hirata, Y., Yawata, H., Kawanishi, Y., Seed, B., Taniguchi, T., Hirano, T., and Kishimoto, T. (1988) *Proceedings of the Japan Academy Series B-Physical and Biological Sciences* **64**(7), 209-211

69. Hilton, D. J., Hilton, A. A., Raicevic, A., Rakar, S., Harrisonsmith, M., Gough, N. M., Begley, C. G., Metcalf, D., Nicola, N. A., and Willson, T. A. (1994) *Embo Journal* **13**(20), 4765-4775

70. Davis, S., Aldrich, T. H., Valenzuela, D. M., Wong, V., Furth, M. E., Squinto, S. P., and Yancopoulos, G. D. (1991) *Science* **253**(5015), 59-63

71. Hammacher, A., Richardson, R. T., Layton, J. E., Smith, D. K., Angus, L. J. L., Hilton, D. J., Nicola, N. A., Wijdenes, J., and Simpson, R. J. (1998) *Journal of Biological Chemistry* **273**(35), 22701-22707

72. Staunton, D., Hudson, K. R., and Heath, J. K. (1998) *Protein Engineering* **11**(11), 1093-1102

73. Horsten, U., Schmitzvandeleur, H., Mullberg, J., Heinrich, P. C., and Rosejohn, S. (1995) *Febs Letters* **360**(1), 43-46

74. Kalai, M., MonteroJulian, F. A., Grotzinger, J., Fontaine, V., Vandenbussche, P., Deschuyteneer, R., Wollmer, A., Brailly, H., and Content, J. (1997) *Blood* **89**(4), 1319-1333

75. Kalai, M., MonteroJulian, F. A., Grotzinger, J., Wollmer, A., Morelle, D., Brochier, J., RoseJohn, S., Heinrich, P. C., Brailly, H., and Content, J. (1996) *European Journal of Biochemistry* **238**(3), 714-723

76. Grotzinger, J., Kurapkat, G., Wollmer, A., Kalai, M., and RoseJohn, S. (1997) *Proteins-Structure Function and Genetics* **27**(1), 96-109

77. Kurth, I., Horsten, U., Pflanz, S., Dahmen, H., Kuster, A., Grotzinger, J., Heinrich, P. C., and MullerNewen, G. (1999) *Journal of Immunology* **162**(3), 1480-1487

78. Clackson, T., and Wells, J. A. (1995) *Science* **267**(5196), 383-386

79. Simpson, R. J., Hammacher, A., Smith, D. K., Matthews, J. M., and Ward, L. D. (1997) *Protein Science* **6**(5), 929-955

80. Ward, L. D., Howlett, G. J., Discolo, G., Yasukawa, K., Hammacher, A., Moritz, R. L., and Simpson, R. J. (1994) *Journal of Biological Chemistry* **269**(37), 23286-23289

81. Paonessa, G., Graziani, R., Deserio, A., Savino, R., Ciapponi, L., Lahm, A., Salvati, A. L., Toniatti, C., and Ciliberto, G. (1995) *Embo Journal* **14**(9), 1942-1951

82. Deserio, A., Graziani, R., Laufer, R., Ciliberto, G., and Paonessa, G. (1995) *Journal of Molecular Biology* **254**(5), 795-800

83. Stahl, N., Boulton, T. G., Farruggella, T., Ip, N. Y., Davis, S., Witthuhn, B. A., Quelle, F. W., Silvennoinen, O., Barbieri, G., Pellegrini, S., Ihle, J. N., and Yancopoulos, G. D. (1994) *Science* **263**(5143), 92-95

84. Lutticken, C., Wegenka, U. M., Yuan, J. P., Buschmann, J., Schindler, C., Ziemiecki, A., Harpur, A. G., Wilks, A. F., Yasukawa, K., Taga, T., Kishimoto, T., Barbieri, G., Pellegrini, S., Sendtner, M., Heinrich, P. C., and Horn, F. (1994) *Science* **263**(5143), 89-92

85. Yin, T. G., Yasukawa, K., Taga, T., Kishimoto, T., and Yang, Y. C. (1994) *Experimental Hematology* **22**(5), 467-472

86. Darnell, J. E., Kerr, I. M., and Stark, G. R. (1994) *Science* **264**(5164), 1415-1421

87. Stahl, N., Farruggella, T. J., Boulton, T. G., Zhong, Z., Darnell, J. E., and Yancopoulos, G. D. (1995) *Science* **267**(5202), 1349-1353

88. Giordano, V., DeFalco, G., Chiari, R., Quinto, I., Pelicci, P. G., Bartholomew, L., Delmastro, P., Gadina, M., and Scala, G. (1997) *Journal of Immunology* **158**(9), 4097-4103

89. Pellegrini, S., and DusanterFourt, I. (1997) *European Journal of Biochemistry* **248**(3), 615-633

90. Duhe, R. J., and Farrar, W. L. (1998) *Journal of Interferon and Cytokine Research* **18**(1), 1-15

91. Feng, J., Witthuhn, B. A., Matsuda, T., Kohlhuber, F., Kerr, I. M., and Ihle, J. N. (1997) *Molecular and Cellular Biology* **17**(5), 2497-2501

92. Ihle, J. N. (1995) *Nature* **377**(6550), 591-594

93. Quelle, F. W., Sato, N., Witthuhn, B. S., Inhorn, R. C., Eder, M., Miyajima, A., Griffin, J. D., and Ihle, J. N. (1994) *Molecular and Cellular Biology* **14**(7), 4335-4341

94. Duhe, R. J., and Farrar, W. L. (1995) *Journal of Biological Chemistry* **270**(39), 23084-23089

95. Lai, C. F., Ripperger, J., Morella, K. K., Wang, Y. P., Gearing, D. P., Fey, G. H., and Baumann, H. (1995) *Journal of Biological Chemistry* **270**(25), 14847-14850

96. Chen, M., Cheng, A., Chen, Y. Q., Hymel, A., Hanson, E. P., Kimmel, L., Minami, Y., Taniguchi, T., Changelian, P. S., and Oshea, J. J. (1997) *Proceedings of the National Academy of Sciences of the United States of America* **94**(13), 6910-6915

97. Yan, H., Piazza, F., Krishnan, K., Pine, R., and Krolewski, J. J. (1998) *Journal of Biological Chemistry* **273**(7), 4046-4051

98. Gauzzi, M. C., Velazquez, L., McKendry, R., Mogensen, K. E., Fellous, M., and Pellegrini, S. (1996) *Journal of Biological Chemistry* **271**(34), 20494-20500

99. Velazquez, L., Mogensen, K. E., Barbieri, G., Fellous, M., Uze, G., and Pellegrini, S. (1995) *Journal of Biological Chemistry* **270**(7), 3327-3334

100. Gauzzi, M. C., Barbieri, G., Richter, M. F., Uze, G., Ling, L., Fellous, M., and Pellegrini, S. (1997) *Proceedings of the National Academy of Sciences of the United States of America* **94**(22), 11839-11844

101. TakahashiTezuka, M., Hibi, M., Fujitani, Y., Fukada, T., Yamaguchi, T., and Hirano, T. (1997) *Oncogene* **14**(19), 2273-2282

102. Xia, K., Mukhopadhyay, N. K., Inhorn, R. C., Barber, D. L., Rose, P. E., Lee, R. S., Narsimhan, R. P., Dandrea, A. D., Griffin, J. D., and Roberts, T. M. (1996) *Proceedings of the National Academy of Sciences of the United States of America* **93**(21), 11681-11686

103. Yetter, A., Uddin, S., Krolewski, J. J., Jiao, H. Y., Yi, T. L., and Platanias, L. C. (1995) *Journal of Biological Chemistry* **270**(31), 18179-18182

104. Yin, T. G., Shen, R., Feng, G. S., and Yang, Y. C. (1997) *Journal of Biological Chemistry* **272**(2), 1032-1037

105. Takeshita, T., Arita, T., Higuchi, M., Asao, H., Endo, K., Kuroda, H., Tanaka, N., Murata, K., Ishii, N., and Sugamura, K. (1997) *Immunity* **6**(4), 449-457

106. Rui, L. Y., Mathews, L. S., Hotta, K., Gustafson, T. A., and CarterSu, C. (1997) *Molecular and Cellular Biology* **17**(11), 6633-6644

107. Greenlund, A. C., Farrar, M. A., Viviano, B. L., and Schreiber, R. D. (1994) *Embo Journal* **13**(7), 1591-1600

108. Heim, M. H., Kerr, I. M., Stark, G. R., and Darnell, J. E. (1995) *Science* **267**(5202), 1347-1349

109. Shuai, K., Horvath, C. M., Huang, L. H. T., Qureshi, S. A., Cowburn, D., and Darnell, J. E. (1994) *Cell* **76**(5), 821-828

110. Hemmann, U., Gerhartz, C., Heesel, B., Sasse, J., Kurapkat, G., Grotzinger, J., Wollmer, A., Zhong, Z., Darnell, J. E., Graeve, L., Heinrich, P. C., and Horn, F. (1996) *Journal of Biological Chemistry* **271**(22), 12999-13007

111. Zhong, Z., Wen, Z. L., and Darnell, J. E. (1994) *Proceedings of the National Academy of Sciences of the United States of America* **91**(11), 4806-4810

112. Shuai, K., Stark, G. R., Kerr, I. M., and Darnell, J. E. (1993) *Science* **261**(5129), 1744-1746

113. Kaptein, A., Paillard, V., and Saunders, M. (1996) *Journal of Biological Chemistry* **271**(11), 5961-5964

114. Horvath, C. M., Wen, Z. L., and Darnell, J. E. (1995) *Genes & Development* **9**(8), 984-994

115. Schindler, U., Wu, P. G., Rothe, M., Brasseur, M., and McKnight, S. L. (1995) *Immunity* **2**(6), 689-697

116. Seidel, H. M., Milocco, L. H., Lamb, P., Darnell, J. E., Stein, R. B., and Rosen, J. (1995) *Proceedings of the National Academy of Sciences of the United States of America* **92**(7), 3041-3045

117. Wegenka, U. M., Buschmann, J., Lutticken, C., Heinrich, P. C., and Horn, F. (1993) *Molecular and Cellular Biology* **13**(1), 276-288

118. Lutticken, C., Coffer, P., Yuan, J. P., Schwartz, C., Caldenhoven, E., Schindler, C., Kruijer, W., Heinrich, P. C., and Horn, F. (1995) *Febs Letters* **360**(2), 137-143

119. Zhang, X. K., Blenis, J., Li, H. C., Schindler, C., and Chenkiang, S. (1995) *Science* **267**(5206), 1990-1994

120. Wen, Z. L., Zhong, Z., and Darnell, J. E. (1995) *Cell* **82**(2), 241-250

121. Wen, Z. L., and Darnell, J. E. (1997) *Nucleic Acids Research* **25**(11), 2062-2067

122. Chung, J. K., Uchida, E., Grammer, T. C., and Blenis, J. (1997) *Molecular and Cellular Biology* **17**(11), 6508-6516

123. Ng, J., and Cantrell, D. (1997) *Journal of Biological Chemistry* **272**(39), 24542-24549

124. Stancato, L. F., Yu, C. R., Petricoin, E. F., and Larner, A. C. (1998) *Journal of Biological Chemistry* **273**(30), 18701-18704

125. Levy, J. B., Schindler, C., Raz, R., Levy, D. E., Baron, R., and Horowitz, M. C. (1996) *Endocrinology* **137**(4), 1159-1165

126. Auguste, P., Guillet, C., Fourcin, M., Olivier, C., Veziers, J., PouplardBarthelaix, A., and Gascan, H. (1997) *Journal of Biological Chemistry* **272**(25), 15760-15764

127. Chauhan, D., Kharbanda, S. M., Ogata, A., Urashima, M., Frank, D., Malik, N., Kufe, D. W., and Anderson, K. C. (1995) *Journal of Experimental Medicine* **182**(6), 1801-1806

128. Bellido, T., Obrien, C. A., Roberson, P. K., and Manolagas, S. C. (1998) *Journal of Biological Chemistry* **273**(33), 21137-21144

129. Zhang, Y., Willson, T., Metcalf, D., Cary, D., Hilton, D. J., Clark, R., and Nicola, N. A. (1998) *Journal of Biological Chemistry* **273**(51), 34370-34383

130. Narazaki, M., Witthuhn, B. A., Yoshida, K., Silvennoinen, O., Yasukawa, K., Ihle, J. N., Kishimoto, T., and Taga, T. (1994) *Proceedings of the National Academy of Sciences of the United States of America* **91**(6), 2285-2289

131. Lai, C. F., Ripperger, J., Wang, Y. P., Kim, H., Hawley, R. B., and Baumann, H. (1999) *Journal of Biological Chemistry* **274**(12), 7793-7802

132. Kuropatwinski, K. K., DeImus, C., Gearing, D., Baumann, H., and Mosley, B. (1997) *Journal of Biological Chemistry* **272**(24), 15135-15144

133. Gorlich, D., and Mattaj, I. W. (1996) *Science* **271**(5255), 1513-1518

134. Sekimoto, T., Nakajima, K., Tachibana, T., Hirano, T., and Yoneda, Y. (1996) *Journal of Biological Chemistry* **271**(49), 31017-31020

135. Sekimoto, T., Imamoto, N., Nakajima, K., Hirano, T., and Yoneda, Y. (1997) *Embo Journal* **16**(23), 7067-7077

136. Stocklin, E., Wissler, M., Gouilleux, F., and Groner, B. (1996) *Nature* **383**(6602), 726-728

137. Zhang, Z. X., Jones, S., Hagood, J. S., Fuentes, N. L., and Fuller, G. M. (1997) *Journal of Biological Chemistry* **272**(49), 30607-30610

138. Kortylewski, M., Heinrich, P. C., Mackiewicz, A., Schniertshauer, U., Klingmuller, U., Nakajima, K., Hirano, T., Horn, F., and Behrmann, I. (1999) *Oncogene* **18**(25), 3742-3753

139. Kim, H., and Baumann, H. (1999) *Molecular and Cellular Biology* **19**(8), 5326-5338

140. Satoh, T., Nakafuku, M., and Kaziro, Y. (1992) *Journal of Biological Chemistry* **267**(34), 24149-24152

141. Kanakura, Y., Druker, B., Wood, K. W., Mamon, H. J., Okuda, K., Roberts, T. M., and Griffin, J. D. (1991) *Blood* **77**(2), 243-248

142. Nakajima, T., Kinoshita, S., Sasagawa, T., Sasaki, K., Naruto, M., Kishimoto, T., and Akira, S. (1993) *Proceedings of the National Academy of Sciences of the United States of America* **90**(6), 2207-2211

143. Fuhrer, D. K., Feng, G. S., and Yang, Y. C. (1995) *Journal of Biological Chemistry* **270**(42), 24826-24830

144. Feng, G. S., Hui, C. C., and Pawson, T. (1993) *Science* **259**(5101), 1607-1611

145. Tauchi, T., Feng, G. S., Shen, R., Song, H. Y., Donner, D., Pawson, T., and Broxmeyer, H. E. (1994) *Journal of Biological Chemistry* **269**(21), 15381-15387

146. Haspel, R. L., SalditтGeorgieff, M., and Darnell, J. E. (1996) *Embo Journal* **15**(22), 6262-6268

147. Starr, R., and Hilton, D. J. (1999) *Bioessays* **21**(1), 47-52

148. Fukada, T., Yoshida, Y., Nishida, K., Ohtani, T., Shirogane, T., Hibi, M., and Hirano, T. (1999) *Growth Factors* **17**(2), 81-91

149. You, M., Yu, D. H., and Feng, G. S. (1999) *Molecular and Cellular Biology* **19**(3), 2416-2424

150. Bousquet, C., Susini, C., and Melmed, S. (1999) *Journal of Clinical Investigation* **104**(9), 1277-1285

151. Chung, C. D., Liao, J. Y., Liu, B., Rao, X. P., Jay, P., Berta, P., and Shuai, K. (1997) *Science* **278**(5344), 1803-1805

152. Liu, B., Liao, J. Y., Rao, X. P., Kushner, S. A., Chung, C. D., Chang, D. D., and Shuai, K. (1998) *Proceedings of the National Academy of Sciences of the United States of America* **95**(18), 10626-10631

153. Dittrich, E., Haft, C. R., Muys, L., Heinrich, P. C., and Graeve, L. (1996) *Journal of Biological Chemistry* **271**(10), 5487-5494

154. Behrmann, I., Janzen, C., Gerhartz, C., SchmitzVandeLeur, H., Hermanns, H., Heesel, B., Graeve, L., Horn, F., Tavernier, J., and Heinrich, P. C. (1997) *Journal of Biological Chemistry* **272**(8), 5269-5274

155. Thiel, S., Behrmann, I., Dittrich, E., Muys, L., Tavernier, J., Wijdenes, J., Heinrich, P. C., and Graeve, L. (1998) *Biochemical Journal* **330**(Pt1), 47-54

156. Trowbridge, I. S., Collawn, J. F., and Hopkins, C. R. (1993) *Annual Review of Cell Biology* **9**, 129-161

157. Matsumoto, A., Masuhara, M., Mitsui, K., Yokouchi, M., Ohtsubo, M., Misawa, H., Miyajima, A., and Yoshimura, A. (1997) *Blood* **89**(9), 3148-3154

158. Heymann, D., Harb, J., Ringeard, S., Blanchard, F., Lassort, D., Raher, S., and Godard, A. (1995) *Journal of Cellular Biochemistry* **58**(3), 305-314

159. Murakamimori, K., Taga, T., Kishimoto, T., and Nakamura, S. (1995) *Journal of Clinical Investigation* **96**(3), 1319-1327

160. Douglas, A. M., Grant, S. L., Goss, G. A., Clouston, D. R., Sutherland, R. L., and Begley, C. G. (1998) *International Journal of Cancer* **75**(1), 64-73

161. Grant, S. L., and Begley, C. G. (1999) *Molecular Medicine Today* **5**(9), 406-412

162. Li, C., Ahlborn, T. E., Kraemer, F. B., and Liu, J. (1999) *Faseb Journal* **13**(7 SS), A1448

163. Halfter, H., Lotfi, R., Westermann, R., Young, P., Ringelstein, E. B., and Stogbauer, F. T. (1998) *Growth Factors* **15**(2), 135-147

164. Liu, J. W., Spence, M. J., Wallace, P. M., Forcier, K., Hellstrom, I., and Vestal, R. E. (1997) *Cell Growth & Differentiation* **8**(6), 667-676

165. Gibbs, P., Chen, Q., and Robinson, W. A. (1998) *Melanoma Research* **8**(3), 221-226

166. Modur, V., Feldhaus, M. J., Weyrich, A. S., Jicha, D. L., Prescott, S. M., Zimmerman, G. A., and McIntyre, T. M. (1997) *Journal of Clinical Investigation* **100**(1), 158-168

167. Bugno, M., Witek, B., Bereta, J., Bereta, M., Edwards, D. R., and Kordula, T. (1999) *Febs Letters* **448**(1), 9-14

168. Wallace, P. M., MacMaster, J. F., Rouleau, K. A., Brown, T. J., Loy, J. K., Donaldson, K. L., and Wahl, A. F. (1999) *Journal of Immunology* **162**(9), 5547-5555

169. Loy, J. K., Davidson, T. J., Berry, K. K., Macmaster, J. F., Danle, B., and Durham, S. K. (1999) *Toxicologic Pathology* **27**(2), 151-155

170. Jay, P. R., Centrella, M., Lorenzo, J., Bruce, A. G., and Horowitz, M. C. (1996) *Endocrinology* **137**(4), 1151-1158

171. Takashima, S., and Klagsbrun, M. (1996) *Journal of Biological Chemistry* **271**(40), 24901-24906

172. Ensoli, F., Fiorelli, V., DeCristofaro, M., Muratori, D. S., Novi, A., Vannelli, B., Thiele, C. J., Luzi, G., and Aiuti, F. (1999) *Journal of Immunology* **162**(10), 6268-6277

173. Clegg, C. H., Haugen, H. S., Rulffes, J. T., Friend, S. L., and Farr, A. G. (1999) *Experimental Hematology* **27**(4), 712-725

174. Cawston, T. E., Curry, V. A., Summers, C. A., Clark, I. M., Riley, G. P., Life, P. F., Spaull, J. R., Goldring, M. B., Koshy, P. J. T., Rowan, A. D., and Shingleton, W. D. (1998) *Arthritis and Rheumatism* **41**(10), 1760-1771

175. Bernard, C., Merval, R., Lebret, M., Delerive, P., DusanterFourt, I., Lehoux, S., Creminon, C., Staels, B., Maclouf, J., and Tedgui, A. (1999) *Circulation Research* **85**(12), 1124-1131

176. Stahl, N., and Yancopoulos, G. D. (1994) *Journal of Neurobiology* **25**(11), 1454-1466

177. Taguchi, Y., Yamamoto, M., Yamate, T., Lin, S. C., Mocharla, H., DeTogni, P., Nakayama, N., Boyce, B. F., Abe, E., and Manolagas, S. C. (1998) *Proceedings of the Association of American Physicians* **110**(6), 559-574

178. Bellido, T., Stahl, N., Farruggella, T. J., Borba, V., Yancopoulos, G. D., and Manolagas, S. C. (1996) *Journal of Clinical Investigation* **97**(2), 431-437

179. Raz, R., Durbin, J. E., and Levy, D. E. (1994) *Journal of Biological Chemistry* **269**(39), 24391-24395

180. Chida, D., Wakao, H., Yoshimura, A., and Miyajima, A. (1998) *Molecular Endocrinology* **12**(11), 1792-1806

181. Kerr, C., Langdon, C., Graham, F., Gauldie, J., Hara, T., and Richards, C. D. (1999) *Journal of Interferon and Cytokine Research* **19**(10), 1195-1205

182. Lindberg, R. A., Juan, T. S. C., Welcher, A. A., Sun, Y., Cupples, R., Guthrie, B., and Fletcher, F. A. (1998) *Molecular and Cellular Biology* **18**(6), 3357-3367

183. Svedberg, T., and Pedersen, K. O. (1940) *The Ultracentrifuge* (Folwer, R. H., and Kapitza, P., Eds.), Clarendon Press, Oxford

184. Wiseman, T., Williston, S., Brandts, J. F., and Lin, L. N. (1989) *Analytical Biochemistry* **179**(1), 131-137

185. Ralston, G. (1993) *Introduction to analytical ultracentrifugation*, Beckman Instruments, Inc.

186. Fujita, H. (1975) *Fundations of Ultracentrifugal Analysis*, New York, Wiley

187. Harding, S. E., and Rowe, A. J. (1989) *Modelling the gross conformation of assemblies using hydrodynamics: the whole body approach. Dynamic properties of Biomolecular Assemblies*, Cambridge, The Royal Society of Chemistry

188. Schuster, T. M., and Laue, T. M. (1994) *Modern Analytical Ultracentrifugation : Acquisition and Interpretation of Data for Biological and Synthetic Polymer Systems*, Springer Verlag

189. Williams, J. W., and VanHolde, K. E. (1958) *Chemical Review* **58,** 715-806

190. Ogston, A. G., and Winzor, D. J. (1975) *Journal of Physical Chemistry* **79,** 2496-2500

191. Rivas, G., Stafford, W., and Minton, A. P. (1999) *Methods-a Companion to Methods in Enzymology* **19**(2), 194-212

192. Minton, A. P. (1990) *Analytical Biochemistry* **190**(1), 1-6

193. Darawshe, S., and Minton, A. P. (1994) *Analytical Biochemistry* **220**(1), 1-4

194. Tanford, C. (1961) *Physical Chemistry of Macromolecules*, Wiley, New York

195. Braswell, E. H., Knox, J. R., and Frere, J. M. (1986) *Biochemical Journal* **237**(2), 511-517

196. Brian, A. A., Frisch, H. L., and Lerman, L. S. (1981) *Biopolymers* **20**(6), 1305-1328

197. Murthy, N. S., Braswell, E. H., and Knox, J. R. (1988) *Biopolymers* **27**(5), 865-881

198. Arakawa, T., Yphantis, D. A., Lary, J. W., Narhi, L. O., Lu, H. S., Prestrelski, S. J., Clogston, C. L., Zsebo, K. M., Mendiaz, E. A., Wypych, J., and Langley, K. E. (1991) *Journal of Biological Chemistry* **266**(28), 18942-18948

199. Casassa, E. F., and Eisenberg, H. (1964) *Adv. Protein Chemistry* **19,** 287-395

200. Ladbury, J. E., and Chowdhry, B. Z. (1998) *Biocalorimetry: Applications of Calorimetry in the Biological Sciences*, John Wiley & Sons

201. Indyk, L., and Fisher, H. F. (1998) *Methods in Enzymology* **295,** 350-364

202. Philo, J. S., Aoki, K. H., Arakawa, T., Narhi, L. O., and Wen, J. (1996) *Biochemistry* **35**(5), 1681-1691

203. Zolkiewski, M., and Ginsburg, A. (1992) *Biochemistry* **31**(48), 11991-12000

204. Kaspar, S., Perozzo, R., Reinelt, S., Meyer, M., Pfister, K., Scapozza, L., and Bott, M. (1999) *Molecular Microbiology* **33**(4), 858-872

205. Kragelund, B. B., Poulsen, K., Andersen, K. V., Baldursson, T., Kroll, J. B., Neergard, T. B., Jepsen, J., Roepstorff, P., Kristiansen, K., Poulsen, F. M., and Knudsen, J. (1999) *Biochemistry* **38**(8), 2386-2394

206. Chung, E. W., Henriques, D. A., Renzoni, D., Morton, C. J., Mulhern, T. D., Pitkeathly, M. C., Ladbury, J. E., and Robinson, C. V. (1999) *Protein Science* **8**(10), 1962-1970

207. Kozlov, A. G., and Lohman, T. M. (1998) *Journal of Molecular Biology* **278**(5), 999-1014

208. Kvaratskhelia, M., George, S. J., Cooper, A., and White, M. F. (1999) *Biochemistry* **38**(50), 16613-16619

209. Praefcke, G. J. K., Geyer, M., Schwemmle, M., Kalbitzer, H. R., and Herrmann, C. (1999) *Journal of Molecular Biology* **292**(2), 321-332

210. Schiffmann, D. A., White, J. H. M., Cooper, A., Nutley, M. A., Harding, S. E., Jumel, K., Solari, R., Ray, K. P., and Gay, N. J. (1999) *Biochemistry* **38**(36), 11722-11733

211. Samland, A. K., Amrhein, N., and Macheroux, P. (1999) *Biochemistry* **38**(40), 13162-13169

212. Willcox, B. E., Gao, G. F., Wyer, J. R., Ocallaghan, C. A., Boulter, J. M., Jones, E. Y., VanderMerwe, P. A., Bell, J. I., and Jakobsen, B. K. (1999) *Protein Science* **8**(11), 2418-2423

213. Fath, M., VanderNoot, V., Kilpelainen, I., Kinnunen, T., Rauvala, H., and Linhardt, R. J. (1999) *Febs Letters* **454**(1-2), 105-108

214. Fisher, H. F., and Singh, N. (1995) *Methods in Enzymology* **259**, 194-221

215. Pierce, M. M., Raman, C. S., and Nall, B. T. (1999) *Methods-a Companion to Methods in Enzymology* **19**(2), 213-221

216. Farooq, A., Plotnikova, O., Zeng, L., and Zhou, M. M. (1999) *Journal of Biological Chemistry* **274**(10), 6114-6121

217. Lanzilotta, W. N., Parker, V. D., and Seefeldt, L. C. (1999) *Biochimica Et Biophysica Acta-Protein Structure and Molecular Enzymology* **1429**(2), 411-421

218. Ladbury, J. E. (1996) *Chemistry & Biology* **3**(12), 973-980

219. Ladbury, J. E., and Chowdhry, B. Z. (1996) *Chemistry & Biology* **3**(10), 791-801

220. Davies, T. G., Hubbard, R. E., and Tame, J. R. H. (1999) *Protein Science* **8**(7), 1432-1444

221. Murphy, K. P., Baker, B. M., Edgcomb, S. P., and Horn, J. R. (1999) *Pure and Applied Chemistry* **71**(7), 1207-1213

222. Biacore. (1994) *BIAapplications Handbook*, Code No BR-1001-86, Biacore AB

223. Biacore. (1994) *BIAtechnology Handbook*, Code No BR-1001-84, Biacore AB

224. Biacore. (1997) *BIAevaluation 3.0 Software Handbook*, Biacore AB

225. Schuck, P., and Minton, A. P. (1996) *Trends in Biochemical Sciences* **21**(12), 458-460

226. Schuck, P., and Minton, A. P. (1996) *Analytical Biochemistry* **240**(2), 262-272

227. Schuck, P., Millar, D. B., and Kortt, A. A. (1998) *Analytical Biochemistry* **265**(1), 79-91

228. Kortt, A. A., Nice, E., and Gruen, L. C. (1999) *Analytical Biochemistry* **273**(1), 133-141

229. Myszka, D. G., Jonsen, M. D., and Graves, B. J. (1998) *Analytical Biochemistry* **265**(2), 326-330

230. Harrick, N. J. (1967) *Internat. Reflection Spectroscopy*, Interscience, New York

231. Stenberg, E., Persson, B., Roos, H., and Urbaniczky, C. (1991) *Journal of Colloid and Interface Science* **143**(2), 513-526

232. Canziani, G., Zhang, W. T., Cines, D., Rux, A., Willis, S., Cohen, G., Eisenberg, R., and Chaiken, I. (1999) *Methods-a Companion to Methods in Enzymology* **19**(2), 253-269

233. Biacore. (1994) *BIAcore 2000 Instrument Handbook*, Biacore AB

234. Jonsson, U., and Malmqvist, M. (1992) *Adv. Biosensors* **2**, 291-336

235. Morton, T. A., and Myszka, D. G. (1998) *Methods in Enzymology* **295**, 268 (28 pages)

236. Johnsson, B., Lofas, S., and Lindquist, G. (1991) *Analytical Biochemistry* **198**(2), 268-277

237. Karlsson, R., and Falt, A. (1997) *Journal of Immunological Methods* **200**(1-2), 121-133

238. Roden, L. D., and Myszka, D. G. (1996) *Biochemical and Biophysical Research Communications* **225**(3), 1073-1077

239. Fisher, R. J., Fivash, M., CasasFinet, J., Bladen, S., and Mcnitt, K. L. (1994) *Methods Companion Methods Enzymology* **6**, 121-133

240. Limbird, L. E. (1986) *Cell Surface Receptor: A Short Course on Theory and Methods*, Kluwer Academic Publishers, Boston

241. Morton, T. A., Myszka, D. G., and Chaiken, I. M. (1995) *Analytical Biochemistry* **227**(1), 176-185

242. Karlsson, R., Mo, J. A., and Holmdahl, R. (1995) *Journal of Immunological Methods* **188**(1), 63-71

243. Piehler, J., and Schreiber, G. (1999) *Journal of Molecular Biology* **289**(1), 57-67

244. Robert, B., Mach, J. P., Mani, J. C., Yehou, M., Folli, S., Artus, J. C., and Pelegrin, A. (1996) *Cancer Research* **56**(20), 4758-4765

245. Michiels, L., Haelewyn, J., Proost, P., and DeLey, M. (1998) *International Journal of Biochemistry & Cell Biology* **30**(4), 505-516

246. Donaldson, D. D., Whitters, M. J., Fitz, L. J., Neben, T. Y., Finnerty, H., Henderson, S. L., Ohara, R. M., Beier, D. R., Turner, K. J., Wood, C. R., and Collins, M. (1998) *Journal of Immunology* **161**(5), 2317-2324

247. Bridges, A., Stuart, F., Spath, J., Lang, S., Henke, C., Birch, A., and Robinson, J. A. (1996) *Protein Engineering* **9**(4), 365-370

248. LaricchiaRobbio, L., Liedberg, B., PlatouVikinge, T., Rovero, P., Beffy, P., and Revoltella, R. P. (1996) *Hybridoma* **15**(5), 343-350

249. Dettorre, C., DeChiara, G., Casadei, R., Boraschi, D., and Tagliabue, A. (1997) *European Cytokine Network* **8**(2), 161-171

250. Zhang, J., Kuvelkar, R., Murgolo, N. J., Taremi, S. S., Chou, C. C., Wang, P., Billah, M. M., and Egan, R. W. (1999) *International Immunology* **11**(12), 1935-1943

251. Lackmann, M., Harpur, A. G., Oates, A. C., Mann, R. J., Gabriel, A., Meutermans, W., Alewood, P. F., Kerr, I. M., Stark, G. R., and Wilks, A. F. (1998) *Growth Factors* **16**(1), 39-51

252. Baker, D. P., Whitty, A., Zafari, M. R., Olson, D. L., Hession, C. A., Miatkowski, K., Avedissian, L. S., Foley, S. F., McKay, M. L., Benjamin, C. D., and Burkly, L. C. (1998) *Biochemistry* **37**(41), 14337-14349

253. Liparoto, S. F., and Ciardelli, T. L. (1999) *Journal of Molecular Recognition* **12**(5), 316 (7 pages)

254. Derome, A. E. (1987) *Modern NMR Techniques for Chemistry Research*, Pergamon, Oxford

255. Ernst, R. R., Bodenhausen, G., and Wokaun, A. (1987) *Principles of Nuclear Magnetic Resonance in One and Two Dimensions*, Clarendon Press, Oxford

256. Gunther, H. (1995) *NMR Spectroscopy: Basic Principles, Concepts, and Applications in Chemistry*, Wiley, Chichester

257. Cavanagh, J., Fairbrother, W. J., Palmer, A. G., III, and Skelton, N. J. (1996) *Protein NMR Spectroscopy: Principles and Practice*, Academic Press, London, San Diego

258. Roberts, G. C. K. E. (1993) *NMR of macromolecules. A practical Approach*, Oxford University Press, Oxford

259. Kalinowski, H.-O., Braun, S., and Berger, S. (1996) *100 and more basic NMR experiments: a practical course*, VCH, Weinheim, New York, Cambridge

260. Reid, D. G. (1997) *Protein NMR techniques*, Humana Press, Totowa, N.J.

261. Jeener, J. (1971) *Basko Polie, Yugoslavia*

262. Guntert, P. (1998) *Quarterly Reviews of Biophysics* **31**(2), 145-237

263. Pervushin, K., Riek, R., Wider, G., and Wuthrich, K. (1997) *Proceedings of the National Academy of Sciences of the United States of America* **94**(23), 12366-12371

264. Pellecchia, M., Sebbel, P., Hermanns, U., Wuthrich, K., and Glockshuber, R. (1999) *Nature Structural Biology* **6**(4), 336-339

265. Wider, G. (1998) *Progress in Nuclear Magnetic Resonance Spectroscopy* **32**(Pt3), 193-275

266. Freeman, R., and Kupce, E. (1997) *Nmr in Biomedicine* **10**(8), 372-380

267. Hudson, K. R., Vernallis, A. B., and Heath, J. K. (1996) *Journal of Biological Chemistry* **271**(20), 11971-11978

268. Walker, P. A., Leong, L. E. C., Ng, P. W. P., Tan, S. H., Waller, S., Murphy, D., and Porter, A. G. (1994) *Bio-Technology* **12**(6), 601-605

269. Cohn, E. J., and Edsall, J. T. (1943) *Proteins, Amino Acids and Peptides as Ions and Dipolar Ions*, New York

270. Hwang, T. L., and Shaka, A. J. (1995) *Journal of Magnetic Resonance Series a* **112**(2), 275-279

271. SchulteHerbruggen, T., Briand, J., Meissner, A., and Sorensen, O. W. (1999) *Journal of Magnetic Resonance* **139**(2), 443-446

272. Pearce, K. H., Ultsch, M. H., Kelley, R. F., deVos, A. M., and Wells, J. A. (1996) *Biochemistry* **35**(32), 10300-10307

273. Zhou, M. M., Huang, B. H., Olejniczak, E. T., Meadows, R. P., Shuker, S. B., Miyazaki, M., Trub, T., Shoelson, S. E., and Fesik, S. W. (1996) *Nature Structural Biology* **3**(4), 388-393

274. Morgan, D. A., Rusceth, F. W., and Galli, R. (1976) *Science* , 1007

275. Loughnan, M. S., and Nossal, G. J. V. (1989) *Nature* **340**(6228), 76-79

276. Smith, K. A. (1988) *Science* **240**(4856), 1169-1176

277. Benveniste, E. N., and Merrill, J. E. (1986) *Nature* **321**(6070), 610-613

278. Waldmann, T. A., Goldman, C. K., Robb, R. J., Depper, J. M., Leonard, W. J., Sharrow, S. O., Bongiovanni, K. F., Korsmeyer, S. J., and Greene, W. C. (1984) *Journal of Experimental Medicine* **160**(5), 1450-1466

279. Trinchieri, G., Matsumotokobayashi, M., Clark, S. C., Seehra, J., London, L., and Perussia, B. (1984) *Journal of Experimental Medicine* **160**(4), 1147-1169

280. Henney, C. S., Kuribayashi, K., Kern, D. E., and Gillis, S. (1981) *Nature* **291**(5813), 335-338

281. Herrmann, F., Cannistra, S. A., Levine, H., and Griffin, J. D. (1985) *Journal of Experimental Medicine* **162**(3), 1111-1116

282. Malkovsky, M., Loveland, B., North, M., Asherson, G. L., Gao, L., Ward, P., and Fiers, W. (1987) *Nature* **325**(6101), 262-265

283. Takeshita, T., Asao, H., Ohtani, K., Ishii, N., Kumaki, S., Tanaka, N., Munakata, H., Nakamura, M., and Sugamura, K. (1992) *Science* **257**(5068), 379-382

284. Leonard, W. J., Depper, J. M., Uchiyama, T., Waldmann, T. A., and Greene, W. C. (1982) *Clinical Research* **30**(2), A352-A352

285. Leonard, W. J., Depper, J. M., Crabtree, G. R., Rudikoff, S., Pumphrey, J., Robb, R. J., Kronke, M., Svetlik, P. B., Peffer, N. J., Waldmann, T. A., and Greene, W. C. (1984) *Nature* **311**(5987), 626-631

286. Nikaido, T., Shimizu, A., Ishida, N., Sabe, H., Teshigawara, K., Maeda, M., Uchiyama, T., Yodoi, J., and Honjo, T. (1984) *Nature* **311**(5987), 631-635

287. Sharon, M., Klausner, R. D., Cullen, B. R., Chizzonite, R., and Leonard, W. J. (1986) *Science* **234**(4778), 859-863

288. Tsudo, M., Kozak, R. W., Goldman, C. K., and Waldmann, T. A. (1986) *Proceedings of the National Academy of Sciences of the United States of America* **83**(24), 9694-9698

289. Teshigawara, K., Wang, H. M., Kato, K., and Smith, K. A. (1987) *Journal of Experimental Medicine* **165**(1), 223-238

290. Robb, R. J., Rusk, C. M., Yodoi, J., and Greene, W. C. (1987) *Proceedings of the National Academy of Sciences of the United States of America* **84**(7), 2002-2006

291. Dukovich, M., Wano, Y., Thuy, L. T. B., Katz, P., Cullens, B. R., Kehrl, J. H., and Greene, W. C. (1987) *Nature* **327**(6122), 518-522

292. Tsudo, M., Kitamura, F., and Miyasaka, M. (1989) *Proceedings Of the National Academy Of Sciences Of the United States Of America* **86**(6), 1982-1986

293. Takeshita, T., Goto, Y., Tada, K., Nagata, K., Asao, H., and Sugamura, K. (1989) *Journal Of Experimental Medicine* **169**(4), 1323-1332

294. Satoh, T., Minami, Y., Kono, T., Yamada, K., Kawahara, A., Taniguchi, T., and Kaziro, Y. (1992) *Journal of Biological Chemistry* **267**(35), 25423-25427

295. Merida, I., Williamson, P., Kuziel, W. A., Greene, W. C., and Gaulton, G. N. (1993) *Journal of Biological Chemistry* **268**(9), 6765-6770

296. Williamson, P., Merida, I., Greene, W. C., and Gaulton, G. (1994) *Leukemia* **8**(S1), S 186-S 189

297. Williamson, P., Merida, I., and Gaulton, G. (1994) *Journal of Cellular Biochemistry* (S18D SID), 412-412

298. Jacques, T., Pedro, A. M., and Bertoglio, J. (1996) *Immunology Today* **17**(10), 481-486

299. Leonard, W. J., Noguchi, M., Russell, S. M., and McBride, O. W. (1994) *Immunological Reviews* **138**, 61-86

300. Waldmann, T. A. (1991) *Journal of Biological Chemistry* **266**(5), 2681-2684

301. Miyazaki, T., Maruyama, M., Yamada, G., Hatakeyama, M., and Taniguchi, T. (1991) *Embo Journal* **10**(11), 3191-3197

302. Hatakeyama, M., Kono, T., Kobayashi, N., Kawahara, A., Levin, S. D., Perlmutter, R. M., and Taniguchi, T. (1991) *Science* **252**(5012), 1523-1528

303. Shibuya, H., Yoneyama, M., Nakamura, Y., Harada, H., Hatakeyama, M., Minamoto, S., Kono, T., Doi, T., White, R., and Taniguchi, T. (1990) *Nucleic Acids Research* **18**(13), 3697-3703

304. Balasubramanian, S., Chernovrogan, T., Davis, A. M., Whitehorn, E., Tate, E., Bell, M. P., Zurawski, G., and Barrett, R. W. (1995) *International Immunology* **7**(11), 1839-1849

305. Wu, Z. N., Johnson, K. W., Goldstein, B., Choi, Y., Eaton, S. F., Laue, T. M., and Ciardelli, T. L. (1995) *Journal of Biological Chemistry* **270**(27), 16039-16044

306. Kortt, A. A., Oddie, G. W., Iliades, P., Gruen, L. C., and Hudson, P. J. (1997) *Analytical Biochemistry* **253**(1), 103-111

307. Bowles, M. R., Hall, D. R., Pond, S. M., and Winzor, D. J. (1997) *Analytical Biochemistry* **244**(1), 133-143

308. Kortt, A. A., Gruen, L. C., and Oddie, G. W. (1997) *Journal of Molecular Recognition* **10**(3), 148-158

309. Shi, J. G., Ghirlando, R., Beavil, R. L., Beavil, A. J., Keown, M. B., Young, R. J., Owens, R. J., Sutton, B. J., and Gould, H. J. (1997) *Biochemistry* **36**(8), 2112-2122

310. Toniatti, C., Cabibbo, A., Sporeno, E., Salvati, A. L., Cerretani, M., Serafini, S., Lahm, A., Cortese, R., and Ciliberto, G. (1996) *Embo Journal* **15**(11), 2726-2737

311. Cunningham, B. C., and Wells, J. A. (1993) *Journal of Molecular Biology* **234**(3), 554-563

312. Wang, Y. H., Shen, B. J., and Sebald, W. (1997) *Proceedings of the National Academy of Sciences of the United States of America* **94**(5), 1657-1662

313. Johanson, K., Appelbaum, E., Doyle, M., Hensley, P., Zhao, B., Abdelmeguid, S. S., Young, P., Cook, R., Carr, S., Matico, R., Cusimano, D., Dul, E., Angelichio, M., Brooks, I., Winborne, E., McDonnell, P., Morton, T., Bennett, D., Sokoloski, T., McNulty, D., Rosenberg, M., and Chaiken, I. (1995) *Journal of Biological Chemistry* **270**(16), 9459-9471

314. Myszka, D. G., Arulanantham, P. R., Sana, T., Wu, Z. N., Morton, T. A., and Ciardelli, T. L. (1996) *Protein Science* **5**(12), 2468-2478

315. Stockman, B., and Markley, J. (1992) *Current Opinion in Structural Biology* **2**, 52-56

Appendix I: The human OSM

EMBL Code: M27288 (1)

Protein sequence:

```
1-60 GPLGSAAIGS CSKEYRVLLG QLQKQTDLMQ DTSRLLDPYI RIQGLDVPKL REHCRERPGA

61-120 FPSEETLRGL GRRGFLQTLN ATLGCVLHRL ADLEQRLPKA QDLERSGLNI EDLEKLQMAR

121-180 PNILGLRNNI YCMAQLLDNS DTAEPTKAGR GASQPPTPTP ASDAFQRKLE GCRFLHGYHR

181-201 FMHSVGRVFS KWGESPNRSR R
```

Human OSM sequence starts from AAIGS, which is residue number 26 on the sequence published at EMBL. The underlined GPLGS was part of the 3C protease cleavage site (the residue GPL) and the restriction enzyme (*BamH I*) site (residue GS). The C-terminal for the mutants OSM185 and OSM187 are GRVFS and VFSKW respectively.

DNA sequence:

```
   1 GCGGCTATAG    GCAGCTGCTC    GAAAGAGTAC    CGCGTGCTCC    TTGGCCAGCT

  51 CCAGAAGCAG    ACAGATCTCA    TGCAGGACAC    CAGCAGACTC    CTGGACCCCT

 101 ATATACGTAT    CCAAGGCCTG    GATGTTCCTA    AACTGAGAGA    GCACTGCAGG

 151 GAGCGCCCCG    GGGCCTTCCC    CAGTGAGGAG    ACCCTGAGGG    GGCTGGGCAG

 201 GCGGGGCTTC    CTGCAGACCC    TCAATGCCAC    ACTGGGCTGC    GTCCTGCACA

 251 GACTGGCCGA    CTTAGAGCAG    CGCCTCCCCA    AGGCCCAGGA    TTTGGAGAGG

 301 TCTGGGCTGA    ACATCGAGGA    CTTGGAGAAG    CTGCAGATGG    CGAGGCCGAA

 351 CATCCTCGGG    CTCAGGAACA    ACATCTACTG    CATGGCCCAG    CTGCTGGACA

 401 ACTCAGACAC    GGCTGAGCCC    ACGAAGGCTG    GCCGGGGGGC    CTCTCAGCCG

 451 CCCACCCCCA    CCCCTGCCTC    GGATGCTTTT    CAGCGCAAGC    TGGAGGGCTG

 501 CAGGTTCCTG    CATGGCTACC    ATCGCTTCAT    GCACTCAGTG    GGGCGGGTCT

 551 TCAGCAAGTG    GGGGGAGAGC    CCGAACCGGA    GCCGGAGA
```

The DNA sequence contains only the code for OSM. The five residues added on N-terminal were not included.

Appendix II: The human gp130-CHR

EMBL Code: HSIL6GP(2)

Protein sequence:

1-60 GPGSSGLPPE KPKNLSCIVN EGKKMRCEWD GGRETHLETN FTLKSEWATH KFADCKAKRD

61-120 TPTSCTVDYS TVYFVNIEVW VEAENALGKV TSDHINFDPV YKVKPNPPHN LSVINSEELS

121-180 SILKLTWTNP SIKSVIILKY NIQYRTKDAS TWSQIPPEDT ASTRSSFTVQ DLKPFTEYVF

181-201 RIRCMKEDGK GYWSDWSEEA SGITYEDRAA AEQKLISEED LN

Human gp130-CHR sequence starts from SGLPPE, which is residue number 122 on the sequence published at EMBL. At N-terminal the underlined GPGS was part of the 3C protease cleavage site. The underlined residues at C-terminal are those for a spacer (AA) and the *cmyc* tag (AEQKLISEEDLN). The construct design was adapted from reference (3).

DNA sequence:

```
   1 TCAGGCTTGC    CTCCAGAAAA    ACCTAAAAAT    TTGAGTTGCA    TTGTGAACGA

  51 GGGGAAGAAA    ATGAGGTGTG    AGTGGGATGG    TGGAAGGGAA    ACACACTTGG

 101 AGACAAACTT    CACTTTAAAA    TCTGAATGGG    CAACACACAA    GTTTGCTGAT

 151 TGCAAAGCAA    AACGTGACAC    CCCCACCTCA    TGCACTGTTG    ATTATTCTAC

 201 TGTGTATTTT    GTCAACATTG    AAGTCTGGGT    AGAAGCAGAG    AATGCCCTTG

 251 GGAAGGTTAC    ATCAGATCAT    ATCAATTTTG    ATCCTGTATA    TAAAGTGAAG

 301 CCCAATCCGC    CACATAATTT    ATCAGTGATC    AACTCAGAGG    AACTGTCTAG

 351 TATCTTAAAA    TTGACATGGA    CCAACCCAAG    TATTAAGAGT    GTTATAATAC

 401 TAAAATATAA    CATTCAATAT    AGGACCAAAG    ATGCCTCAAC    TTGGAGCCAG

 451 ATTCCTCCTG    AAGACACAGC    ATCCACCCGA    TCTTCATTCA    CTGTCCAAGA

 501 CCTTAAACCT    TTTACAGAAT    ATGTGTTTAG    GATTCGCTGT    ATGAAGGAAG

 551 ATGGTAAGGG    ATACTGGAGT    GACTGGAGTG    AAGAAGCAAG    TGGGATCACC

 601 TATGAAGATA    GA
```

The DNA sequence contains only the code for gp130-CHR (SGLPPE...ITYEDR). The four residues added on N-terminal and the C-terminal *cmyc* tag are not included.

Appendix III: Human IL-2Rβ

EMBL Code: M26062 (4)

Protein sequence:

1-60 GPGSAVNGTS QFTCFYNSRA NISCVWSQDG ALQDTSCQVH AWPDRRRWNQ TCELLPVSQA

61-120 SWACNLILGA PDSQKLTTVD IVTLRVLCRE GVRWRVMAIQ DFKPFENLRL MAPISLQVVH

121-180 VETHRCNISW EISQASHYFE RHLEFEARTL SPGHTWEEAP LLTLKQKQEW ICLETLTPDT

181-232 QYEFQVRVKP LQGEFTTWSP WSQPLAFRTK PAALGKDTAA AEQKLISEED LN

Human IL-2Rβ sequence starts from AVNGTS, which is residue number 27 on the sequence published at EMBL. At N-terminal the underlined GPGS was part of the 3C protease cleavage site. The underlined residues at C-terminal are those for the *cmyc* tag (AEQKLISEEDLN).

DNA sequence:

1	GCGGTGAATG	GCACTTCCCA	GTTCACATGC	TTCTACAACT	CGAGAGCCAA
51	CATCTCCTGT	GTCTGGAGCC	AAGATGGGGC	TCTGCAGGAC	ACTTCCTGCC
101	AAGTCCATGC	CTGGCCGGAC	AGACGGCGGT	GGAACCAAAC	CTGTGAGCTG
151	CTCCCCGTGA	GTCAAGCATC	CTGGGCCTGC	AACCTGATCC	TCGGAGCCCC
201	AGATTCTCAG	AAACTGACCA	CAGTTGACAT	CGTCACCCTG	AGGGTGCTGT
251	GCCGTGAGGG	GGTGCGATGG	AGGGTGATGG	CCATCCAGGA	CTTCAAGCCC
301	TTTGAGAACC	TTCGCCTGAT	GGCCCCCATC	TCCCTCCAAG	TTGTCCACGT
351	GGAGACCCAC	AGATGCAACA	TAAGCTGGGA	AATCTCCCAA	GCCTCCCACT
401	ACTTTGAAAG	ACACCTGGAG	TTCGAGGCCC	GGACGCTGTC	CCCAGGCCAC
451	ACCTGGGAGG	AGGCCCCCCT	GCTGACTCTC	AAGCAGAAGC	AGGAATGGAT
501	CTGCCTGGAG	ACGCTCACCC	CAGACACCCA	GTATGAGTTT	CAGGTGCGGG
551	TCAAGCCTCT	GCAAGGCGAG	TTCACGACCT	GGAGCCCCTG	GAGCCAGCCC
601	CTGGCCTTCA	GGACAAAGCC	TGCAGCCCTT	GGGAAGGACA	CC

The DNA sequence contains only the code for IL-2Rβ (AVNGTS...ALGKDT). The four residues added on N-terminal and the C-terminal *cmyc* tag are not included.

Reference for Appendixes:

1. Rose, T. M., and Bruce, A. G. (1991) *Proceedings of the National Academy of Sciences of the United States of America* **88**(19), 8641-8645

2. Hibi, M., Murakami, M., Saito, M., Hirano, T., Taga, T., and Kishimoto, T. (1990) *Cell* **63**(6), 1149-1157

3. Staunton, D., Hudson, K. R., and Heath, J. K. (1998) *Protein Engineering* **11**(11), 1093-1102

4. Hatakeyama, M., Tsudo, M., Minamoto, S., Kono, T., Doi, T., Miyata, T., Miyasaka, M., and Taniguchi, T. (1989) *Science* **244**(4904), 551-556